ST. LOUIS
MAR 17 19
PUBLIC LIBRARY

JOURNAL OF THE

AERONAUTICAL SCIENCES

VOLUME 25 MARCH, 1958 NUMBER 3

CONTENTS

On Two-Dimensional Panel Flutter ..... Y. C. FUNG 145

Structural and Impact Loads for the Flexible Airplane During Water Landings ..... EDWARD WIDMAYER, JR., AND ROBERT H. SCHWAB 161

The Compressibility Rule for Drag of Airfoil Noses ..... R. T. JONES AND M. D. VAN DYKE 171

On Heat Transfer in Laminar Boundary-Layer Flows of Liquids Having a Very Small Prandtl Number ..... G. W. MORGAN, A. C. PIPKIN, AND W. H. WARNER 173

Buckling of Simply Supported Plates Under Arbitrary Symmetrical Temperature Distributions ..... J. M. KLOSNER AND M. J. FORRAY 181

An Approximate Method of Determining Axisymmetric Inviscid Supersonic Flow Over a Solid Body and Its Wake ..... SIN-I CHENG 185

Incompressible Two-Dimensional Stagnation-Point Flow of an Electrically Conducting Viscous Fluid in the Presence of a Magnetic Field ..... JOSEPH L. NEURINGER AND WILLIAM MCILROY 194

Readers' Forum 199

Published by
INSTITUTE OF THE AERONAUTICAL SCIENCES, INC.

JOURNAL OF THE AERONAUTICAL SCIENCES

Editor: W. R. SEARS
Director, Graduate School of Aeronautical Engineering, Cornell University

Associate Editor: ROBERT R. DEXTER *Managing Editor:* RITA J. TURINO
Editorial Assistant: CAROLINE TAYLOR

Editorial Committee

Aerodynamics and Fluid Mechanics

Holt Ashley
H. Julian Allen
Dean R. Chapman
Francis H. Clauser
Hugh L. Dryden
John C. Evvard
Antonio Ferri
Alexander Flax
Wallace D. Hayes
R. T. Jones
Carl Kaplan
H. W. Liepmann
C. C. Lin
H. F. Ludloff
Harold Luskin
Clark B. Millikan
Henry T. Nagamatsu
H. J. E. Reid
George S. Schairer
G. B. Schubauer
John Stack
Theodore Theodorsen
Arthur N. Tifford
Th. von Kármán

Flight Testing

R. R. Gilruth
Melvin N. Gough
W. L. Howland
W. F. Milliken, Jr.

Rotating Wing Aircraft

F. B. Gustafson
K. H. Hohenemser
Bartram Kelley
R. B. Maloy
Ralph McClarren
R. H. Miller
R. H. Prewitt
Igor I. Sikorsky

Structures

John E. Duberg
R. R. Heldenfels
N. J. Hoff
Samuel Levy
J. F. McBrearty
W. Ramberg
E. E. Sechler
F. R. Shanley
C. R. Strang
S. Timoshenko

Meteorology

C. F. Brooks
D. M. Little
F. W. Reichelderfer
K. C. Spengler

Vibration and Flutter

Lee Arnold
M. A. Biot
R. L. Bisplinghoff
Harold A. Cheilek
I. E. Garrick
Martin Goland

Aircraft Design

W. E. Beall
E. H. Heinemann
Hall L. Hibbard
Richard Hutton
C. L. Johnson
A. A. Kartveli
F. K. Teichmann

Electronics

K. C. Black
M. V. Kiebert, Jr.
David S. Little
Paul Rosenberg
Giles J. Strickroth

Physiologic Problems

H. G. Armstrong
Louis H. Bauer
Robert J. Benford
W. Randolph Lovelace, II
Ross A. MacFarland

Flight Propulsion

William Bollay
George W. Brady
R. P. Kroon
Frank E. Marble
Abe Silverstein
E. S. Taylor

Instruments

Alan G. Binnie
Charles H. Colvin
Frank R. Cook
C. S. Draper
S. G. Eskin
C. F. Savage
R. C. Sylvander

SUBSCRIPTION RATES

JOURNAL OF THE AERONAUTICAL SCIENCES, Published Monthly. United States and Possessions: 1 Year, $15.00; Single Copies, $1.50. Foreign Countries Including Canada (American Currency Rates): 1 Year, $16.00; Single Copies, $1.50.

AERONAUTICAL ENGINEERING REVIEW, Published Monthly. United States and Possessions: 1 Year, $5.00; Single Copies, $0.50. Foreign Countries Including Canada (American Currency Rates): 1 Year, $6.00; Single Copies, $0.50.

Notices of change of address should be sent to the Institute at least 30 days prior to actual change of address.

Manuscripts for publication, proofs, and all correspondence should be addressed to the Editorial Office of the JOURNAL.

Publication Office, 20th and Northampton Sts., Easton, Pa. Correspondence regarding subscriptions may be addressed to the Editorial Office of the JOURNAL OF THE AERONAUTICAL SCIENCES, 2 East 64th Street, New York 21, N.Y.

© *Copyright, 1958, by the Institute of the Aeronautical Sciences, Inc.*

Second-Class Mail Privileges Authorized at Easton, Penna. Acceptance for mailing at a special rate of Postage provided for in the Act of August 24, 1912. Authorized April 29, 1937.

JOURNAL OF THE AERONAUTICAL SCIENCES

VOLUME 25 MARCH, 1958 NUMBER 3

On Two-Dimensional Panel Flutter†

Y. C. FUNG*

California Institute of Technology

SUMMARY

Theory and experiments of the flutter of a buckled plate are discussed. It is shown that an increase in the initial deviation from flatness or a static pressure differential across the plate raises the critical value of the "reduced velocity."

The applicability of the Galerkin method to the linearized problem of flutter of an unbuckled plate has been questioned by several authors. In this paper the flutter condition was formulated in the form of an integral equation and solved numerically by the method of iteration and the method of matrix approximations, thus avoiding the constraint of assumed modes. For a plate (with finite bending rigidity) the results confirm those given by the Galerkin method.

An approximate analysis of the limiting form and amplitude of the flutter motion for a buckled plate is presented.

SYMBOLS

a_m, a_{m_0} $(m = 1, \ldots)$	= Fourier coefficients of series expansions of z_0, z_i, respectively
A_1, A_2	= amplitude of $B_1(\tau)$, $B_2(\tau)$, Eq. (3.4)
b_m $(m = 1, 2, \ldots)$	= Fourier coefficients of z, see Eq. (1.8)
B_m $(m = 1, 2, \ldots)$	= nondimensional Fourier coefficients of z, see Eq. (1.10)
$c(x, \xi)$	= influence function
$C(X, \Xi)$	= dimensionless influence function, Eq. (2.3)
c_m	= normalization factor of Iguchi functions, Eq. (1.30)
D	= $Eh^3/12(1 - \nu^2)$, bending rigidity of plate
E, E', E''	= effective elastic modulus, see Eqs. (1.5) and (1.6)
F_m	= Iguchi functions, Eq. (1.29)
$G(x)$	= kernel of the integral for aerodynamic pressure, Eq. (2.7)
$g(x)$	= kernel of an integral equation, Eq. (2.11)
h	= plate thickness
k	= $\omega L/U$, reduced frequency of flutter
k_m $(m = 1, 2, \ldots)$	= nondimensional Fourier coefficients of the static pressure p, see Eq. (1.9)
k_0	= $\omega_0 L/U$, stiffness parameter
L	= chord length of plate
M	= Mach Number of flow
N_x	= stress resultant in x direction, tension per unit span, tension positive
N_{x_0}	= the value of N_x corresponding to z_0
$-N_{xcr}$	= buckling load per unit span
p	= static pressure differential across the plate, positive force downward
p_a	= aerodynamic pressure induced by the deflection z, acting on the top surface of the plate
p_r	= coefficient of p, see Eq. (1.9)
P_0	= dimensionless static pressure loading coefficient, see Eq. (1.15)
$P(\Xi)$	= dimensionless aerodynamic pressure, Eq. (2.3)
q	= $(1/2)\rho_0 U^2$ = dynamic pressure of flow
Q	= dynamic pressure ratio, see Eq. (1.14)
r	= A_1/A_2, amplitude ratio, Eq. (3.17)
$\mathcal{R}$	= the Routh discriminant
s	= thrust ratio = compressive stress ÷ buckling stress, in a state corresponding to z_0
t	= time
u_2	= increment of distance between spanwise edges
U	= speed of flow at infinity
x	= streamwise coordinate
X	= x/L, dimensionless streamwise coordinate
y	= spanwise coordinate
$z(x, t)$	= vertical deflection, positive up
$z_i(x)$	= the initial, unstressed shape of the plate midsurface
$z_0(x)$	= the deflection surface when thermal expansion or edge displacements have taken place, but no static or

Presented at the Structures Session, National Summer Meeting, IAS, Los Angeles, Calif., June 17–20, 1957, under the title, "On Panel Flutter." This work is available as IAS Preprint No. 749.

Revised and received October 28, 1957.

† This research was supported by the United States Air Force, through the Office of Scientific Research of the Air Research and Development Command.

* Associate Professor. The author is also Consultant, Ramo-Wooldridge Corporation.

The author is grateful to Prof. E. E. Sechler for suggestions in experiments and to Mrs. D. Eaton of C.I.T. and Dr. J. A. Brooks and Dr. W. Frank of The Ramo-Wooldridge Corporation for obtaining numerical results.

aerodynamic pressure acts on the plate

Z = z/L, dimensionless deflection

$\alpha_0, \alpha_1, \ldots \alpha_4$ = coefficients of stability determinant, Eq. (1.22)

α_T = coefficient of linear thermal expansion

δB_m $(m = 1, 2)$ = assumed small perturbation of B_m

ΔT = temperature rise of plate above that of the supports

ϕ_1, ϕ_2 = phase angles, Eq. (3.4)

φ = $\phi_1 - \phi_2$

θ_m $(m = 1, 2)$ = $k\tau + \phi_m$

κ = $Mk/(M^2 - 1)$

λ_{m_0} $(m = 1, 2, \ldots)$ = nondimensional Fourier coefficients of z_i, Eq. (1.10)

λ_m $(m = 1, 2, \ldots)$ = nondimensional Fourier coefficients of z_0, Eq. (1.10)

μ = $\rho_s h/\rho_0 L$ = mass ratio of panel to air, Eq. (1.12)

ν = Poisson's ratio

ρ_0 = density of undisturbed air

ρ_s = density of plate material

τ = dimensionless time, see Eq. (1.13)

ω = circular frequency of flutter

ω_0 = fundamental frequency of free vibration, rad. per sec.

χ = membrane thrust – buckling load ratio, Eq. (1.17)

Introduction

Panel flutter refers to oscillations of a panel (a thin plate, a shell, or a membrane) in a flow, for which the aerodynamic force induced by the motion of the plate plays a decisive part. The oscillations of such panels excited by mechanical or aerodynamic noise, or buffeting, will not be considered here.

That panel flutter can occur in an incompressible fluid is exemplified by the common experience of the flutter of a flag. But as an engineering problem panel flutter seems to become important only in supersonic flight. In particular, large amplitude panel flutter is likely to occur only for panels that are buckled. (The transient aerodynamic heating may be the cause of buckling.) Because of the usual restrained edge conditions, the maximum amplitude of flutter is limited. Therefore, the apparent importance of panel flutter lies in the determination of the fatigue life and allowable stresses of the panel material, and in its influence on the aerodynamic drag.

The analysis of panel flutter naturally finds its precedent in the works of Kelvin[13] and Rayleigh[22] on the problem of the generation of water waves by wind. Similar analysis has been made by Miles[18] on the flutter of infinite plates; by studying progressive waves in a plate which is immersed in a flow. Miles shows that in such a plate a straight-crested progressive wave interacts with the flow in such a way that a critical flow speed exists above which the wave amplitude will diverge with increasing time and below which it damps. Miles[19, 20] also studies such progressive waves in a thin-walled pressurized cylindrical shell of infinite length, under the assumption that the wave length is short in comparison with the radius of the cylinder. Again the possibility of flutter is found.

It is, however, difficult and unreliable to extrapolate the results obtained for infinite plates or cylinders to those of finite dimensions. In the following we shall consider panels with finite chord but infinite span.

The first recognition of panel flutter was due to Jordan,[12] who suggested that a number of early German V-2 failures were due to panel flutter. The first wind-tunnel testing at supersonic speeds was reported by Sylvester and Baker.[25] Analytical studies of the panel flutter problem have been published by Isaacs, Hayes, Miles, Shen, Goland, Luke, Hedgepeth, Budiansky, Leonard, Jordan, Fung, Eisley, Nelson, Cunningham, Ashley, Zartarian, Constant, St. John, and others (see References for articles directly related to the present paper). The literature is marked by a high degree of controversy, resulting from the subtle effects of various simplifying assumptions used by different authors.

The present paper is a summary of some of the results obtained at GALCIT. Several exploratory experiments will be discussed in order to clarify the physical conditions of flutter in transonic and supersonic flows. Relevant theoretical considerations will also be discussed.

(1) Flutter of Curved Plates With Edge Compression in a Supersonic Flow

The flutter of buckled plates has been a subject of many investigations. The least restrictive among references 4, 5, 6, 9, 11, and 17 refers to the following problem. A uniform plate of finite chord but infinite span is perfectly flat in the initial (no-load) condition. It is buckled by edge constraints in the chordwise direction. The buckled plate is then exposed to a supersonic flow on one side and to stagnant air on the other side. Under the assumptions that the flow is two-dimensional, that the plate is uniform, isotropic, elastic, and has either clamped or pinned edges, and that the acoustic pressure in the air underneath the plate is negligible, the theory gives the critical flutter speed as a function of the amplitude of the buckle.

A comparison of the results of such a theory with experiments described in reference 4 shows, however, a significant discrepancy. On examining the experimental conditions versus the assumptions of the theory, it seems apparent that the assumption of perfect flatness of the plate in the initial, no-load condition is the most offensive. Since the critical flutter condition of a buckled plate is sensitive to the mean compressive load (the so-called "membrane" stress) in the plate, and since the compressive load for any given amplitude of deflection is reduced by any initial curvature, it can be expected that the effect of the initial deviation from flatness is to raise the critical flutter speed.

The effect of initial curvature can be investigated by the same method as used in reference 6. Some details of such an analysis are given in reference 7. A brief outline of the analysis and the numerical results will be

presented below. The assumptions listed above are used again, except that the assumption of perfect flatness in the no-load condition is dropped. The plate is shown in Fig. 1. The edges normal to the flow are fixed on a massive structure; the distance between these edges can be changed by a small amount by external means, but is assumed to be unaffected by the variation of the thrust in the plate.

Let $z_i(x)$ be the initial, unstressed shape of the midsurface of the plate. Let $z_0(x)$ be the deflection surface when any thermal expansion or displacement of the spanwise edges has taken place, but no load acts normal to the surface of the plate. Let $z(x, t)$ be the midsurface of the plate during flutter. Considering a strip of unit width, and assuming that the plate is thin and deflections small, we obtain the equations governing z_0 and z (see Symbols)

$$D[\partial^4(z_0 - z_i)/\partial x^4] - N_{x_0}(\partial^2 z_0/\partial x^2) = 0 \quad (1.1)$$

$$D[\partial^4(z - z_0)/\partial x^4] - N_x(\partial^2 z/\partial x^2) + N_{x_0} \times (\partial^2 z_0/\partial x^2) = -p_a - \rho_s h(\partial^2 z/\partial t^2) - p \quad (1.2)$$

The aerodynamic load will be assumed to be of the form[6, 17]

$$p_a(x, t) = (\rho_0 U^2/\sqrt{M^2 - 1})\{[\partial z(x, t)/\partial x] + [(M^2 - 2)/(M^2 - 1)](1/U)[\partial z(x, t)/\partial t] + [1/(M^2 - 1)](1/U)[\partial z(0, t)/\partial t]\} \quad (1.3)$$

This is valid for slow oscillations[24] (downwash velocity $\ll$ speed of flow), if the Mach Number is sufficiently remote from $\sqrt{2}$; and also for higher Mach Numbers when the so-called piston theory[1] becomes applicable (in which case $(M^2 - 1)^{1/2}$ and $(M^2 - 2)/(M^2 - 1)$ should be replaced by M and 1, respectively).

The compressive load $-N_x$ is computed as follows. If u_2 is the increment of the distance between the two spanwise edges, and ΔT is the temperature rise of the plate above that of the supports, then

$$-N_x = (E'h/2L)\int_0^L [(\partial z_i/\partial x)^2 - (\partial z/\partial x)^2] \times dx - (E'h/L)u_2 + E''h\alpha_T\Delta T \quad (1.4)$$

where, if the spanwise stress vanishes,

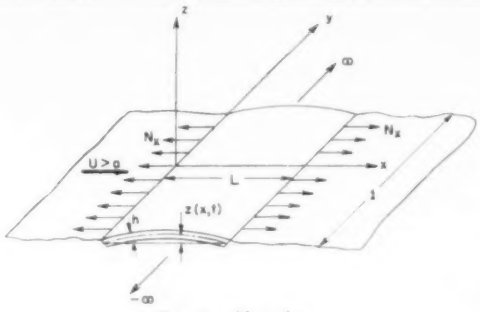

FIG. 1. Notation.

$$E' = E'' = E, \text{ the Young's modulus} \quad (1.5)$$

Whereas, if the spanwise strain vanishes,

$$E' = E/(1 - \nu^2), \quad E'' = E/(1 - \nu) \quad (1.6)$$

Eqs. (1.2), (1.3), and (1.4) are to be solved for the boundary conditions

$$\left.\begin{aligned} z(0, t) &= z(L, t) = 0 \\ (\partial^2 z/\partial x^2)(0, t) &= (\partial^2 z/\partial x^2)(L, t) = 0 \end{aligned}\right\} \quad (1.7a)$$

for pinned edges and

$$\left.\begin{aligned} z(0, t) &= z(L, t) = 0 \\ (\partial z/\partial x)(0, t) &= (\partial z/\partial x)(L, t) = 0 \end{aligned}\right\} \quad (1.7b)$$

for clamped edges.

(1.1) *Approximate Solution by Galerkin's Method for Panel With Pinned Edges*

Let

$$\begin{Bmatrix} z_i \\ z_0 \\ z \end{Bmatrix} = \sum_{m=1}^{N} \begin{Bmatrix} a_{m_0} \\ a_m \\ b_m \end{Bmatrix} L \sin(m\pi x/L) \quad (1.8)$$

$$p = p_0 \sum_{m=1}^{N} k_m \sin(m\pi x/L) \quad (1.9)$$

which satisfy the boundary conditions (1.7a), and

$$-N_{x_{cr}} = \pi^2 D/L^2$$

which is the Euler buckling load of the plate.

Let the following dimensionless parameters be introduced:

$$\begin{Bmatrix} \lambda_{m_0} \\ \lambda_m \\ B_m \end{Bmatrix} = \sqrt{3(1 - \nu^2)E'/E}\,\frac{L}{h}\begin{Bmatrix} a_{m_0} \\ a_m \\ b_m \end{Bmatrix} = m\text{th component of } \begin{Bmatrix} z_i \\ z_0 \\ z \end{Bmatrix} \quad (1.10)$$

$$s = \frac{-N_{x_0}}{(-N_{x_{cr}})} = \frac{\text{compressive load in plate corresponding to } z_0}{\text{Euler buckling load}} \quad (1.11)$$

$$\mu = \text{mass ratio} = \rho_s h/\rho_0 L \quad (1.12)$$

$$\tau = \text{dimensionless time} = Ut/L \quad (1.13)$$

$$Q = \text{dynamic pressure ratio} = (\rho_0 U^2 L^3/D\pi^4\sqrt{M^2 - 1}) \quad (1.14)$$

$$P_0 = \sqrt{3(1 - \nu^2)E'/E}\,(p_0 L^4/\pi^4 Dh) \quad (1.15)$$

The governing equations are reduced by Galerkin's method into

$$B_m\left[\sum_{n=1}^{N} n^2(B_n^2 - \lambda_n^2) + m^2 - s\right] = m^2\lambda_{m_0} - \frac{P_0}{m^2}k_m - \frac{Q}{m^2}\left\{\sum_{n=1}^{N}{}' \frac{2mn[1-(-1)^{m+n}]}{(m+n)(m-n)}B_n + \frac{M^2-2}{M^2-1}\frac{dB_m}{d\tau} + \mu\sqrt{M^2-1}\,\frac{d^2B_m}{d\tau^2}\right\} \quad (m = 1, 2, \ldots, N) \quad (1.16)$$

The symbol Σ' indicates that the term $m = n$ must be excluded.

Numerical results have been obtained for the case of a *two-term approximation*, $N = 2$. In this case we notice that the factor

$$\chi \equiv \lambda_1^2 - B_1^2 + 4(\lambda_2^2 - B_2^2) = [(-N_x)/(-N_{xcr})] - s = \{[(-N_x) - (-N_{x_0})]/(-N_{xcr})\} \quad (1.17)$$

appears in all equations. Hence we write, for $m = 1, 2$,

$$B_1(-\chi + 1 - s) = \lambda_{10} - P_0k_1 + Q\{(8/3)B_2 - [(M^2-2)/(M_2-1)](dB_1/d\tau) - \mu\sqrt{M^2-1}(d^2B_1/d\tau^2)\} \quad (1.18)$$

$$B_2(-\chi + 4 - s) = 4\lambda_{20} - (P_0k_2/4) + (Q/4)\{-(8/3)B_1 - [(M^2-2)/(M^2-1)](dB_2/d\tau) - \mu\sqrt{M^2-1}(d^2B_2/d\tau^2)\} \quad (1.19)$$

At static equilibrium all derivatives with respect to τ vanish. One may then eliminate B_1, B_2 to obtain an equation relating χ and Q. In case $\lambda_{20} = k_2 = 0$, the resulting equation is quadratic in Q^2 and yields simply

$$\frac{16Q^2}{9} = -(4 - s - \chi)(1 - s - \chi) + \frac{(\lambda_{10} - P_0k_1)^2}{2(\lambda_1^2 - \chi)}\left[1 \pm \sqrt{1 + \frac{12(4 - s - \chi)(\lambda_1^2 - \chi)}{(\lambda_{10} - P_0k_1)^2}}\right] \quad (1.20)$$

An example here will clarify the nature of the solution. In Fig. 2 is shown the relationship between the membrane compression ratio χ and the dynamic pressure ratio Q, for the special case of $\lambda_{10} = 1$, $\lambda_{20} = P_0 = 0$, the ordinate being Q^2. The solution depends on the initial compression ratio s. When s is small, one of the roots Q^2 is negative and the other is positive. Both roots tend to infinity asymptotically as χ approaches $\lambda_{10}^2/(1 - s)^2$, at which the plate becomes flat When s is a sufficiently large number, say $s = 0.5$, two curves are shown in the Figure; the lower one can be shown by the method below to be unstable, and the upper one has a peak. No solution exists for Q greater than this relative maximum. It can be shown that the equilibrium configurations corresponding to the front portion of the curve, OA, are stable, whereas those corresponding to AB are unstable.

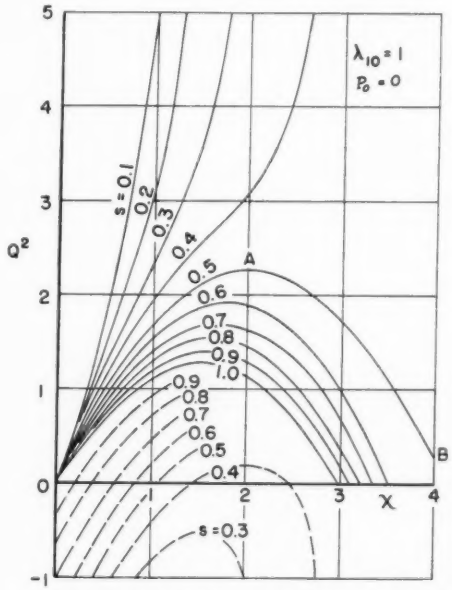

FIG. 2. The square of the dynamic pressure-bending rigidity ratio, Q, vs. the axial thrust ratio χ for $\lambda_{10} = 1$, i. e., for a plate with maximum initial deviation from flatness $\doteq 0.58$ thickness

The stability of the static equilibrium configurations will be defined against infinitesimal perturbations. Let B_1, B_2, χ be the values at a static equilibrium configuration. Consider the variational equations by imposing small perturbations $\delta B_1(\tau)$, $\delta B_2(\tau)$ onto B_1, B_2, respectively. Keeping only linear terms in δB_1, δB_2, we obtain two linear differential equations for δB_1, δB_2. On assuming solutions of the form

$$\delta B_1 \sim e^{\epsilon\tau}, \quad \delta B_2 \sim e^{\epsilon\tau} \quad (1.21)$$

two linear homogeneous equations are obtained. For nontrivial solutions the determinant of these equations must vanish, which may be written as

$$\alpha_4\epsilon^4 + \alpha_3\epsilon^3 + \alpha_2\epsilon^2 + \alpha_1\epsilon + \alpha_0 = 0 \quad (1.22)$$

where

$$\alpha_4 = (M^2 - 1)\mu^2$$

$$\alpha_3 = 2[(M^2 - 2)/\sqrt{M^2 - 1}]\mu$$

$$\alpha_2 = [(M^2 - 2)/(M^2 - 1)]^2 + [(M^2 - 1)^{3/2}/(M^2 - 2)]\mu\alpha_1$$

$$\alpha_1 = (1/Q)[(M^2 - 2)/(M^2 - 1)] \times [17 - 5s - 5\chi + 2B_1^2 + 32B_2^2]$$

$$\alpha_0 = (4/Q^2)\{(16Q^2/9) + (1 - \chi - s)(4 - \chi - s) - 2(1 - \chi - s)(\chi - \lambda_1^2 - 4\lambda_2^2) + 6B_1^2\}$$

The condition of stability of the disturbed motion is that all the roots of Eq. (1.22) must be pseudo-negative (no root has a positive real part). This requires that $\alpha_0, \alpha_1, \ldots, \alpha_4$ and the Routh discriminant $\mathfrak{R}$, have the same sign:

$$\mathfrak{R} = \alpha_1\alpha_2\alpha_3 - \alpha_0\alpha_3^2 - \alpha_4\alpha_1^2 = (M^2 - 1)\mu^2\{\alpha_1^2 + 2[(M^2 - 2)^3/(M^2 - 1)^{7/2}] \times (\alpha_1/\mu) - 4[(M^2 - 2)/(M^2 - 1)]^2\alpha_0\} \quad (1.23)$$

Checking of the conditions of stability for all static equilibrium states can be done numerically. As $\alpha_2 \backsim (M^2 - 2)$, one of the conditions of stability is $M > \sqrt{2}$. When this condition is satisfied, it is generally found that for smaller values of s and λ_{10} the stability is governed by the Routh discriminant, which becomes negative when Q exceeds a certain critical value. For larger values of s and λ_{10}, when the Q vs. χ curve has a relative maximum, the stability is governed by α_0, which becomes negative when χ exceeds the critical value at which Q reaches its maximum.

The critical condition will be expressed by Q_{cr}. It is easy to show that $\sqrt{Q}$ is proportional to the reduced velocity $U/(\omega_0 L)$, and that the inverse of the cubic root of Q, $Q_{cr}^{-1/3}$, is proportional to the thickness of plate required to prevent flutter.

An extreme case is of interest. Consider a slightly warped plate which assumes in the unstressed state the form of a low sinusoidal arch with a center rise

$$La_{1_0} = [h/\sqrt{3(1-\nu^2)E'/E}]\lambda_{10} \doteq 0.58h\lambda_{10} \quad (1.24)$$

We assume

$$|\lambda_{10}| \ll 1, \quad |P_0| \ll 1, \quad \lambda_{20} = k_2 = 0 \quad (1.25)$$

Then it can be shown that, if s is not too close to 1, $M > \sqrt{2}$, and μ is sufficiently large (say, > 20),

$$Q_{cr} \doteq (3/4)\{[(17 - 5s)/4]^2 - (4 - s)(1 - s)\}^{1/2} \quad (1.26)$$

independent of M, μ, P_0 and λ_{10}. $Q_{cr} \doteq 45/16$ when $s = 0$; it decreases as s increases until the expression (1.26) becomes invalid when $s \backsim 0.7$.

Results of calculations based on the equations above can be summarized graphically as follows. In Figs. 3a and 3b is plotted the dynamic pressure ratio Q versus the arch-rise ratio λ_1 for plates that are perfectly flat in the unstressed state. Remember that λ_1 describes the amplitude of the buckle due solely to the movement of the edges. Fig. 3a gives the dividing line between two different states of static equilibrium: above the curve OAB the plate will be blown flat by the wind, below OAB the plate may remain buckled, but of course may also become flat. In Fig. 3b are shown the stability boundaries of the initially flat specimens. A buckled configuration below the curve OAB is stable against infinitesimal perturbations. A flat configuration in the curved-triangular region OCDEAO is also stable against infinitesimal perturbations. In the small area ADE both flat and buckled configurations are stable. Above the curve CDB no static equilibrium is stable.

Fig. 3c shows the stability boundaries for plates that are warped in the unstressed state. The initial deviation from flatness is assumed to be sinusoidal and specified by λ_{10}. For this Figure it is assumed that $P_0 = \lambda_{20} = 0$. The region above each curve is unstable against infinitesimal perturbations. It is seen that the initial deviation from flatness, through its effects on reducing the compressive stress, is beneficial to the prevention of panel flutter.

Fig. 4 gives some calculated values of Q_{cr} for several values of the parameter $P_0 k_1$, with $k_2 = 0$ and $\lambda_{10} = 0.5$ (except that the curve for $P_0 k_1 = 0$ is drawn for $\lambda_{10} = 0$). The effectiveness of the static pressure in raising the flutter boundary is seen. (Note, however, from Eqs. (1.25) and (1.26), $\partial Q_{cr}/\partial P_0 = 0$ when $P_0 = 0$.)

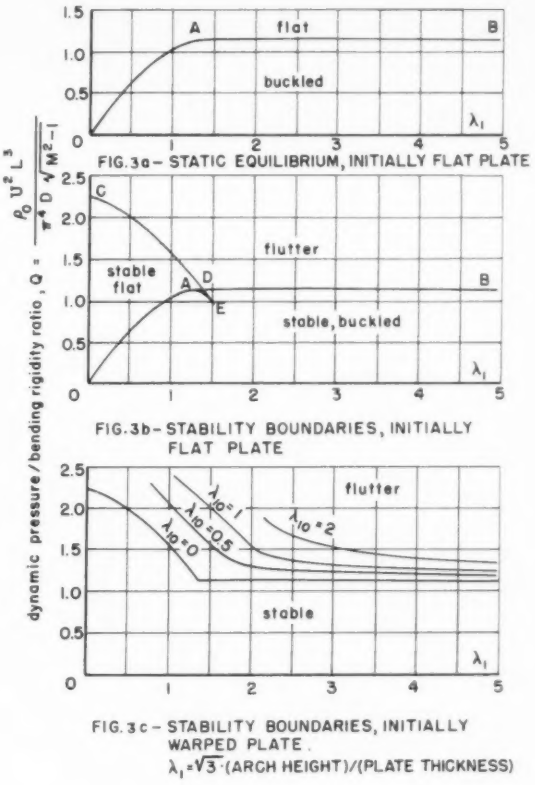

In reference 25, Sylvester and Baker showed experimentally that pressurization is an effective method of raising the reduced velocity of flutter. Fig. 4 is in agreement with this trend, even though it refers to a sinusoidally distributed load,

$$p(x) = [\pi^4 Dh/L^4\sqrt{3(1-\nu^2)E'/E}] \times P_0 k_1 \sin(\pi x/L) \quad (1.27)$$

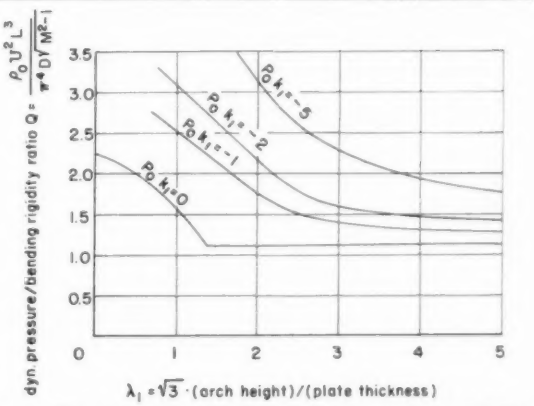
dyn. pressure/bending rigidity ratio $Q = \frac{\rho_0 U^2 L^3}{\pi^4 D \sqrt{M^2-1}}$
$P_0 k_1 = -5$
$P_0 k_1 = -2$
$P_0 k_1 = -1$
$P_0 k_1 = 0$
$\lambda_1 = \sqrt{3}$ · (arch height)/(plate thickness)

FIG. 4. The effect of static pressure differential on the stability boundary.

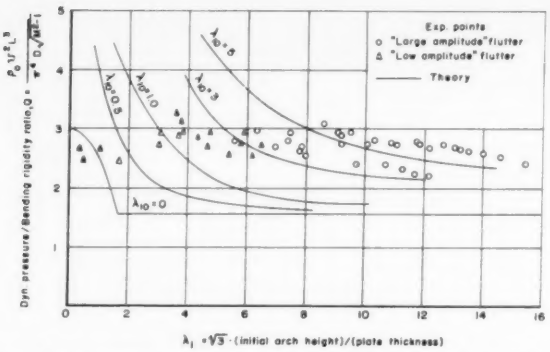

FIG. 5. Comparison of theory and experiment for plates with clamped edges.

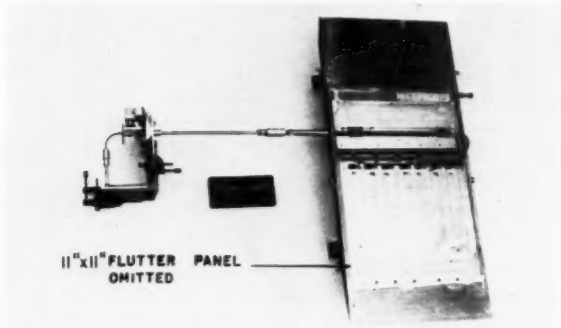

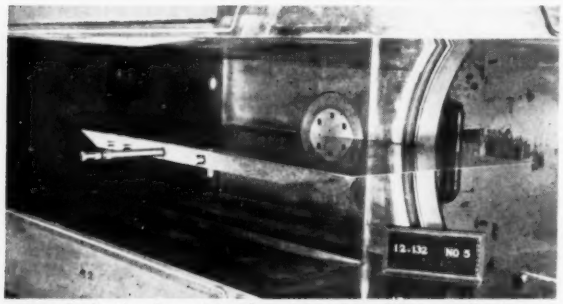

FIG. 6a (*top*). Assembly of model and buckling amplitude control mechanism. FIG. 6b (*bottom*). Installation of the model in the 12-in. tunnel.

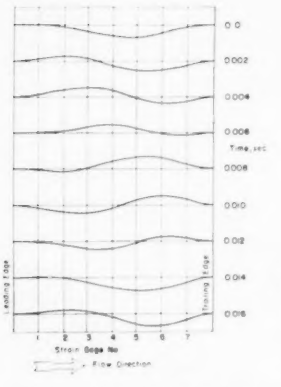

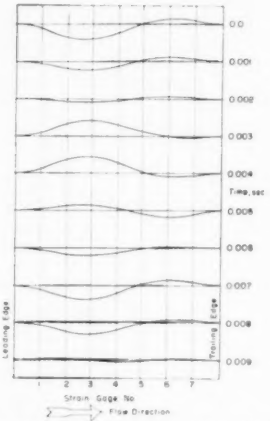

FIG. 7 (*left*). Panel deflection history of a "large amplitude" flutter. FIG. 8 (*right*). Panel deflection history of a "low amplitude" flutter.

for which a negative value of $P_0 k_1$ indicates an excess of pressure underneath the plate (pressurized chamber).

The stability boundaries in Figs. 3 and 4 are practically independent of the mass ratio μ for practical values of μ (say, 20 to 150).

(1.2) *Plates With Clamped Edges*

For plates with clamped edges we use Iguchi functions to describe the deflection surface and the external loading:

$$\begin{Bmatrix} z_i \\ z_0 \\ z \end{Bmatrix} = L \sum_{m=1}^{n} \begin{Bmatrix} a_{m_i} \\ a_m \\ b_m \end{Bmatrix} c_m F_m(X) \tag{1.28}$$

$$p = p_0 \Sigma k_m c_m F_m(X)$$

where

$$F_m(X) = X(X-1)^2 + (-1)^m X^2(X-1) - (1/m\pi)\sin m\pi X \tag{1.29}$$

$$X = x/L$$

and c_m are normalizing factors so chosen that

$$\max_{0 \le X \le 1} c_m F_m(X) = 1 \tag{1.30}$$

The Euler buckling load corresponding to $F_1(X)$ is

$$-N_{x_{cr}} = 41.0631\, D/L^2 \tag{1.31}$$

which must be used in the definition of s. Using the Galerkin method with a two-term approximation, and on setting $E' = E/(1-\nu^2)$, $\nu^2 = 0.1$, the static equilibrium configurations and stability boundaries for $\lambda_{10} = 0.5, 1.0, 3.0, 5.0$; $\lambda_{20} = P_0 = 0$, have been computed in reference 7. Some results are plotted in Fig. 5.

(1.3) *Comparison With Experiments*

In an experiment described by Eisley,[4] a series of 11- by 11-in. aluminum panels, ranging in thickness from 0.025 to 0.051 in., were mounted on the top surface of a wedge-shaped model and tested at Mach Number 2.18 in the JPL 12-in. tunnel. The plate could be buckled from outside the tunnel by moving the plate trailing edge with respect to its leading edge. The onset of flutter was observed. The history of the motion was recorded by strain gages fastened to the lower surface of the plate.

The model is illustrated in Fig. 6. The panel was located near the leading edge to minimize the effects of boundary layer. The leading and trailing edges of the panel were fastened with screws. The side edges were free. The lower surface of the panel was vented to the free stream static pressure by slits along the free edges. A combination screw, wedge, and slide arrangement was used to vary the amplitude of the buckle by moving the trailing edge.

Two distinct types of oscillations were observed. One occurred at small amplitudes of the buckle. It was mostly irregular and of small amplitude. Hence it will be referred to as "low amplitude" type. The other, the "large amplitude" type, was nearly harmonic timewise. An examination of the oscillograph records

showed that, in the large amplitude flutter, the deflection surface changed in such a manner that it resembled traveling waves, whereas in the "low amplitude" oscillations, it appeared to be standing waves. These are shown by the deflection histories in Figs. 7 and 8.

It was most interesting to watch the behavior of the plate in the wind tunnel as one gradually forced the edges of the panel together. In a typical test the tunnel pressure was set at some selected value with the panel in the unbuckled condition. The panel was then buckled and the amplitude was slowly increased. At some point the low amplitude oscillation was observed, mostly irregular but sometimes also nearly harmonic but generally it could be stopped with further increase in the amplitude of buckle. With still further increase of the buckle a point was reached at which large

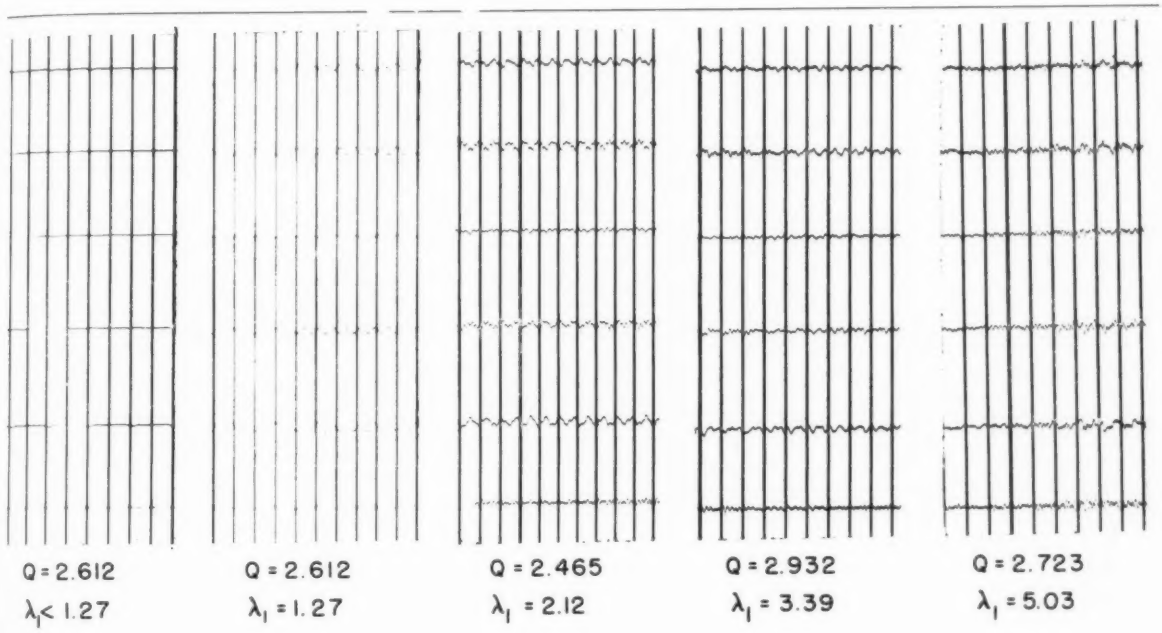

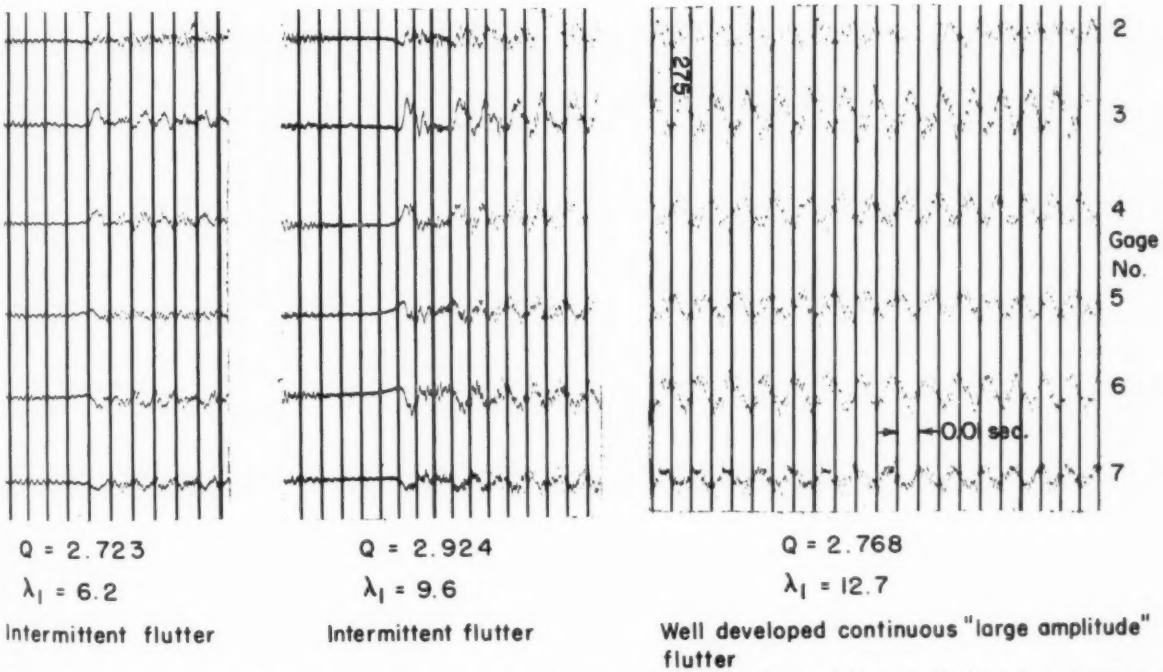

FIG. 9a (*top*). Nonflutter and "low amplitude" flutters, plate thickness 0.031 in., Mach Number 2.18. FIG. 9b (*bottom*). Intermittent and "large amplitude" flutters, plate thickness 0.031 in., Mach Number 2.18.

amplitude flutter occurred. However, at no time was it possible (within mechanical limitations) to stop the large amplitude flutter by further increase in the buckle. In some cases, particularly in those which required very large buckling amplitudes to initiate flutter, no low amplitude oscillation was observed. Such a sequence of events is illustrated in Fig. 9 by the oscillograph records from strain gages attached to the plate.

The test conditions described above were such that the assumptions of the theory presented herein are approximated. In Fig. 5 are shown both the theoretical and the experimental flutter boundaries. (Note that $\lambda_{10} = 1$ corresponds to a sinusoidal deviation from flatness with a maximum deviation approximately equal to 0.58 times the thickness of the plate.) Unfortunately, the actual warping of the test specimens was unknown. It is seen, however, that each experimental point could be explained by a certain amount of initial warping.*

To critically compare experiments and theory, one would have to examine the effects of the simplification introduced by the two-term approximation, of the possible deviation of actual boundary conditions from being clamped, of the influence of the boundary layer, and of the acoustic pressure underneath the plate. Thus many questions remain to be investigated, but the principal features of the problem are now clear. Panel flutter of a buckled plate at a sufficiently high Mach Number may be roughly characterized by a constant critical value of Q, if one were willing to regard the effect of initial warping, buckling amplitude, etc., as secondary influences affecting the scatter of this constant.

(2) Linearized Equations for a Flat Plate and the Galerkin's Method of Solution

The Galerkin method, or the Rayleigh-Ritz method, is widely used in aeroelasticity, but no mathematical foundation has been established for its application to non-self-adjoint eigenvalue problems such as flutter. Recently, doubts were cast over its applicability to the panel flutter problem. Miles,[18] and Goland, Luke, and Constant,[15] using the assumption of small reduced frequency, ($k \ll 1$), have shown that the Galerkin method yields a spurious flutter boundary (one that should not exist) *for a membrane* (without bending stiffness) in a supersonic flow. Ashley and Zartarian[1] have shown the same (also for a membrane), under the assumption that the Mach Number is sufficiently high that the "piston theory" applies. Therefore, it becomes a matter of great interest to see how far the Galerkin method fails. One way to do this is to compare its results with those obtained by a method of proved validity. The method of Laplace transformation, as outlined by Goland and Luke,[8] can be used for this purpose. In the following, however, the iteration method proved by Wielandt[26] and the method of matrix approximation of the integral equation will be used.

(2.1) *Statement of the Problem, Fundamental Equations*

Consider an infinite strip of flat plate, one side of which is exposed to a uniform supersonic flow in the direction of the chord of the strip, whereas the other side is exposed to stagnant air. When not deflected, the plate lies in the x, y plane. Flat solid walls parallel to the uniform flow extend to infinity both in front and in rear of the panel. (See Fig. 1.) The problem is to find whether the plate may flutter.

If flutter exists, the plate will oscillate harmonically without any external excitation other than the interaction of the flow and the plate. It is assumed that the amplitude of oscillation is so small that the elastic and aerodynamic actions can be described by linearized equations. The acoustic pressure beneath the plate will be neglected. The latter has been discussed by Nelson and Cunningham[21] and is expected to be unimportant unless the flutter frequency happens to be near the resonance frequency of the chamber beneath the plate. Since linearity is assumed, a small initial curvature of the plate, or a static pressure acting on the plate, has no effect on the flutter boundary.

Consider a strip of unit span and of chord length L. In the linear range, the elastic behavior of the panel is specified by the influence function which describes the deflection pattern under a unit static lateral load acting at an arbitrary point. Since the condition is two-dimensional, the coordinate y plays no role in the problem. Let $c(x, \xi)$ be the influence function describing the deflection z at x due to a unit load at ξ. Then a load distribution $f(\xi, t)$ yields a deflection surface

$$z(x, t) = \int_S c(x, \xi) f(\xi, t) d\xi \tag{2.1}$$

where S is the domain over which the lateral load acts. The coordinate system is shown in Fig. 1. For the flutter problem it is assumed that the motion is sufficiently slow in comparison with the time of travel of elastic waves in the plate across the chord so that $c(x, \xi)$ is uniquely defined and is independent of the loading rate. In this formulation, the inertia force must be regarded as an exterior force. Hence,

$$f(\xi, t) = -\rho_s h(\partial^2 z / \partial t^2) + p_a(\xi, t) \tag{2.2}$$

where ρ_s is the density of the plate material, h is the plate thickness, and p_a is the aerodynamic load. For a harmonic oscillation, $z(x, t) = z(x)e^{i\omega t}$, the aerodynamic load p_a is also harmonic. To reduce Eq. (2.1) into dimensionless form, let ρ_0 be the density of air at infinity and ω_0 be the fundamental frequency of free vibration of the panel in a vacuum, and define

* Except for two "low amplitude" points. The randomness of the "low amplitude" oscillations is not explained, nor is its stoppage. There remain some doubts as to the possibility of buffeting of the model in the tunnel. Further investigation of the low amplitude flutter is needed.

$$\left.\begin{aligned} &X = x/L, \quad \Xi = \xi/L, \quad Z = z/L \\ &C(X, \Xi) = \rho_a h L \omega_0^2 c(x, \xi) \\ &p_a(\xi, t) = (\rho_0 U^2/2) P(\Xi) e^{i\omega t} \\ &1/\mu = \rho_0 L/\rho_a h = \text{density ratio of air to plate} \\ &k = \omega L/U, \quad k_0 = \omega_0 L/U \end{aligned}\right\} \tag{2.3}$$

Then we have

$$Z(X) = (k^2/k_0^2) \int_0^1 C(X, \Xi) Z(\Xi) d\Xi + (1/2\mu k_0^2) \int_0^1 C(X, \Xi) P(\Xi) d\Xi \tag{2.4}$$

The aerodynamic load is induced by the downwash distribution[16]

$$UW(\Xi) = U[(\partial/\partial\Xi) + ik] Z(\Xi) \tag{2.5}$$

$$\left.\begin{aligned} P(\Xi) &= -\frac{2}{\sqrt{M^2 - 1}} \left\{ W(0) G(\Xi) + \int_0^\Xi G(\Xi - v) \left(\frac{d}{dv} + ik \right) W(v) dv \right\} \\ &= -\frac{2}{\sqrt{M^2 - 1}} \left\{ W(\Xi) + \int_0^\Xi W(v) \left(\frac{\partial}{\partial \Xi} + ik \right) G(\Xi - v) dv \right\} \end{aligned}\right\} \tag{2.6}$$

where

$$G(x) = e^{-i\kappa M x} J_0(\kappa x), \qquad \kappa = Mk(M^2 - 1)^{-1} \tag{2.7}$$

J_0 is the Bessel function of the first kind. Note that when $k = 0$,

$$P(\Xi) = -(2/\sqrt{M^2 - 1}) W(\Xi) = -(2U/\sqrt{M^2 - 1})(dZ/d\Xi)$$

as is expected.

Consider now the integral in the last term of Eq. (2.4); writing the dummy variable as ξ,

$$I = -\frac{\sqrt{M^2 - 1}}{2} \int_0^1 C(X, \xi) P(\xi) d\xi = \int_0^1 C(X, \xi) \left\{ W(\xi) + \int_0^\xi W(v) \left(\frac{\partial}{\partial \xi} + ik \right) G(\xi - v) dv \right\} d\xi \tag{2.8}$$

An interchange of the order of integration of the double integrals gives

$$I = \int_0^1 C(X, \xi) W(\xi) d\xi + \int_0^1 W(v) \left\{ \int_v^1 C(X, \xi) \left(\frac{\partial}{\partial \xi} + ik \right) G(\xi - v) d\xi \right\} dv$$

Integrating by parts, we obtain

$$I = \int_0^1 W(v) C(X, 1) G(1 - v) dv + \int_0^1 W(v) \left\{ \int_v^1 G(\xi - v) \left[-\frac{\partial}{\partial \xi} + ik \right] C(X, \xi) d\xi \right\} dv \tag{2.9}$$

Eqs. (2.8) and (2.9) state in fact the well-known reverse-flow theorem: that the integral over an airfoil of the product of the pressure in the forward flow times the downwash in the reversed flow is the same as that of the product of the pressure in the reversed flow times the downwash in the forward flow. This is recognized if one regards $C(X, \xi) e^{-i\omega t}$ as the downwash in the reversed flow, (X being a parameter).

Returning to Eq. (2.9), substituting Eq. (2.5) for W, and then back to Eq. (2.4), we have, on integrating by parts several times and reducing,

$$\begin{aligned} Z(X) = \frac{-1}{\mu k_0^2 \sqrt{M^2 - 1}} \int_0^1 Z(v) \Bigg\{ & C(X, 1) g(1 - v) + \int_v^1 g(\xi - v) \left[-\frac{\partial}{\partial \xi} + ik \right] C(X, \xi) d\xi + \\ & \left[-\frac{\partial}{\partial v} + ik - \mu k^2 \sqrt{M^2 - 1} \right] C(X, v) \Bigg\} dv - \frac{1}{\mu k_0^2 \sqrt{M^2 - 1}} \Bigg\{ C(X, 1) Z(1) - C(X, 1) G(1) Z(0) + \\ & Z(0) \int_0^1 G(\xi) \left[-\frac{\partial}{\partial \xi} + ik \right] C(X, \xi) d\xi \Bigg\} \end{aligned} \tag{2.10}$$

where

$$\left.\begin{aligned} g(x) &\equiv [(d/dx) + ik] G(x) \\ &= -\kappa e^{-i\kappa M x} [J_1(\kappa x) + (i/M) J_0(\kappa x)] \end{aligned}\right\} \tag{2.11}$$

For plates with pinned or clamped edges,

$$Z(0) = Z(1) = C(X, 1) = 0$$

Hence,

$$\begin{aligned} Z(X) = -\frac{1}{\mu k_0^2 \sqrt{M^2 - 1}} \int_0^1 Z(v) \Bigg\{ & \left[-\frac{\partial}{\partial v} + ik - \sqrt{M^2 - 1}\, k^2 \mu \right] C(X, v) + \\ & \int_v^1 g(\xi - v) \left[-\frac{\partial}{\partial \xi} + ik \right] C(X, \xi) d\xi \Bigg\} dv \end{aligned} \tag{2.12}$$

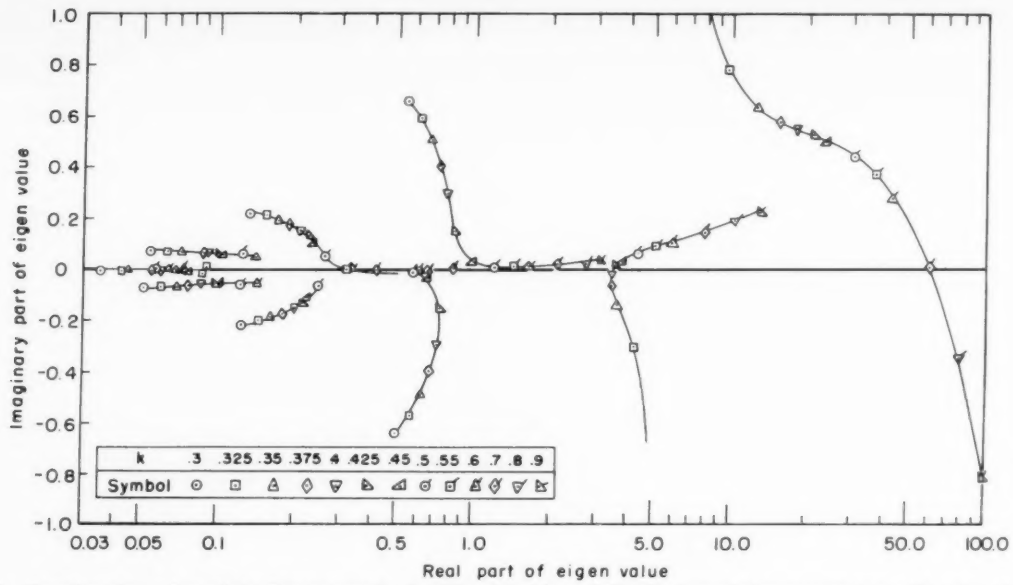

FIG. 10. Complex eigenvalues of the flutter equation for $M = 1.3$, $1/\mu = 0.03$. Each symbol represents a specific value of k. (The loci of the smaller *eiv*'s become complicated at higher values of k and are not shown here.) Real valued *eiv* gives the flutter boundary. $k_0 = \omega_0 L/U = 0.0913366 \cdot \sqrt{\text{R1}}\ eiv$.

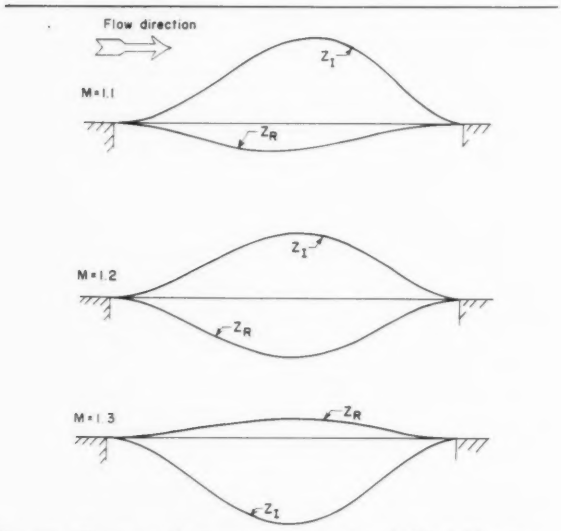

FIG. 11. Flutter mode shapes at low supersonic Mach Numbers.

TABLE I

Comparison of Results of the Present Analysis with Those of the Galerkin's Method

Case Parameters			Eigenvalue k_0 from present analysis		Eigenvalue k_0 from Fig. 3 of Ref. 21 Galerkin's method	
M	$\frac{1}{\mu}$	k	Matrix approximation	Iteration method	4 modes sol.	2 modes sol.
1.3	0.01	0.697	0.685		0.715	0.72
1.3	0.03	0.70054	0.71435		0.745	0.747
1.3	0.05	0.70254	0.73752		0.765	0.767
1.3	0.056581	0.72889		0.74275	0.772	0.772
1.3	0.069778	0.74400		0.75759	0.775	0.775

TABLE II

Flutter Modes at Low Supersonic Mach Numbers

M	$1/\mu$	k	k_0	Z_R	Z_I
1.1	0.102597	0.6559	0.822488	-.0094157	.0154711
				-.0315698	.0585770
				-.563354	.120920
				-.0734332	.196640
				-.0755934	.234865
				-.0618027	.245108
				-.0383118	.206609
				-.0158160	.127740
				-.0031187	.0410662
1.2	0.0227215	0.744000	0.763167	.0191244	.0197330
				.0639772	.0656789
				.115942	.118282
				.157974	.159950
				.177231	.177670
				.166965	.165569
				.129166	.126534
				.0748353	.0723487
				.0232785	.0222116
1.2	0.0708552	0.79685	0.844907	-.0169295	.0169318
				-.0577895	.0587200
				-.106911	.110735
				-.148504	.157326
				-.169211	.183955
				-.161354	.180538
				-.125730	.145147
				-.0729324	.0870067
				-.0225242	.0277275
1.3	0.0565810	0.7316	0.744392	-.0244812	.0052405
				-.0833385	.0180300
				-.153895	.0337257
				-.213730	.0475587
				-.244039	.0552737
				-.233831	.0540422
				-.183664	.0434279
				-.107781	.0261603
				-.0338292	.0084932
1.3	0.0708330	0.744000	0.757629	.0167804	.0173282
				.0577914	.0593487
				.108113	.110286
				.152261	.154091
				.176426	.176900
				.171628	.170268
				.136901	.134179
				.0815998	.0788592
				.0260307	.0246963

2.2) *Solution of the Eigenvalue Problem and Comparison With the Galerkin Method*

It is most convenient to regard Eq. (2.12) as specifying an eigenvalue problem for the functions $Z(X)$ and the eigenvalue k_0^2. k is real-valued since harmonic oscillation is assumed. For each set of specific real-valued k, μ, and M, the kernel of the integral equation is complex-valued. Hence in general the eigenvalue k_0^2 and the function $Z(X)$ are complex. It is necessary to vary the parameters k, μ, and M systematically in order to locate a *real-valued* eigenvalue k_0^2 (a complex-valued k_0^2 has no physical significance). The lack of an existence theorem for such a real-valued eigenvalue is the basic difficulty of our problem.

Eq. (2.12) is already in the most natural form for the application of the iteration method. An arbitrary function Z_0 is assumed. We substitute Z_0 into the integral on the right-hand side, evaluate the integral, and collocate with Z_0 at some point to obtain an approximate eigenvalue k_0^2. The right-hand side may then be designated as Z_1, and the process repeated until it converges. Wielandt[26] has proved that if the integral equation (2.12) has an eigenvalue, that eigenvalue can be obtained by such an iteration procedure, and that the iterated eigenvalue k_0^2 always converges to the one with the largest modulus. Biorthogonality relationships may be used in the iteration procedure to derive successively smaller eigenvalues, and modified formulas can be devised in the case of two or more eigenvalues having the same modulus.

Numerical solution has been obtained with the help of Dr. J. A. Brooks and Dr. W. Frank at the Digital Computing Center of The Ramo-Wooldridge Corporation, on the Univac 1103 machine, for a *plate (with finite bending stiffness) clamped at both the leading and trailing edges*. For such a clamped plate,

$$\omega_0 = [(1.51\pi)^2/L^2]\sqrt{D/\rho_s h}$$

the dimensionless influence function is

$$C(X, \Xi) = [(1.51\pi)^4/6]X^2(1 - \Xi)^2 \times [3(1 - X)\Xi - X(1 - \Xi)] \quad \text{for } (X \leq \Xi)$$

$$= [(1.51\pi)^4/6]\Xi^2(1 - X)^2 \times [3(1 - \Xi)X - \Xi(1 - X)] \quad \text{for } (X \geq \Xi)$$

The function $Z(X)$ was represented first by 10 and then by 20 equal divisions across the chord length. It was found that convergence was readily obtained, but the possibility of having more than one eigenvalue with the same or nearly the same modulus was troublesome. It was found, however, that taking 10 divisions across the chord was sufficient for the problem, for the eigenvalues determined by taking 20 divisions show little difference.

As the program progressed, new machine methods of computation for non-Hermitian matrices became available.[2] The integral equation (2.12) was therefore approximated by a matrix equation, again with $Z(X)$ represented at 10 equal intervals, and the ninth-order matrix equation was solved. The results agree with those obtained by the iteration method.

Some details about the variation of the eigenvalues with the parameters k, M, μ are interesting. In Fig. 10 is shown the variation of all 9 eigenvalues with the reduced frequency k, when $M = 1.3$, $1/\mu = 0.03$. It is seen that when k is small, the eigenvalues occur as nearly conjugate pairs, which accounts for a difficulty with the iteration method.

When sufficient number of cases were solved, the largest real eigenvalue k_0^2 can be obtained by interpolation. The comparison with Nelson and Cunningham's results[21] obtained by the Galerkin method is shown in Table 1.

In this case the Galerkin method appears satisfactory.

There are other solutions confirming the results of the Galerkin analysis for plates. Professor Shen has informed the author that a direct solution of the differential equation for a panel with bending stiffness confirms the Galerkin analysis. Furthermore, William Rodden of North American Aviation and UCLA, working under Professor Miles, has also solved the same problem independently by means of the "aerodynamic influence coefficients," again confirming the Galerkin analysis by a method in which no mode functions is assumed. The special case of static aerodynamic force (high Mach Number) has been confirmed by Hedgepeth.[10]

(2.3) *Results for Clamped Plates at Low Supersonic Mach Numbers*

The iteration method yields eigenfunctions $Z(x)$ which resemble the observed flutter modes* at low supersonic Mach Numbers. In Table 2, several solutions on the flutter boundary are listed. The eigenfunctions are listed for $X = 0.1, 0.2, \ldots, 0.9$; Z being zero at $X = 0$, and 1. The physical displacement is

$$z(x, t) = \mathrm{Rl}\, LZ(x/L)e^{ik\tau} = LZ_R(x/L)\cos(kU/L)t - LZ_I(x/L)\sin(kU/L)t$$

A few typical flutter modes are shown in Fig. 11. It is seen that the phase shift across the chord is very small.

It is of practical interest to summarize the theoretical results of the linearized problem in the form of minimum panel thickness required to prevent flutter. Since†

$$\frac{1}{\mu}\cdot k_0 = \frac{(1.51\pi)^2}{\sqrt{24(1 - \nu^2)}}\sqrt{\left(\frac{\rho_0}{\rho_s}\right)^3 \frac{E}{q}}$$

each panel material and flight condition specifies a hyperbola which intersects the flutter boundaries on

* The experiments will be discussed in another paper.

† It is of interest to note that for a clamped plate

$$k_0 = \omega_0 L/U = 6.8(\sqrt{E/\rho_s}/U)(h/L)$$

which shows clearly the dependence on the velocity of sound in the plate.

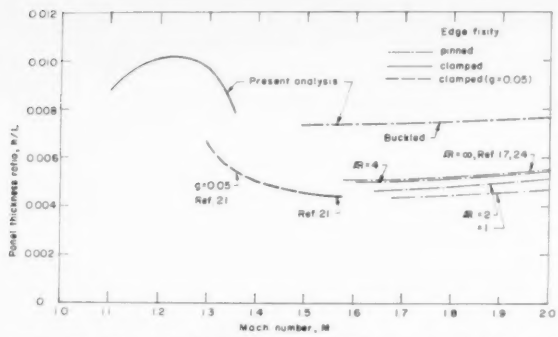

FIG. 12. Theoretical minimum panel thickness required to prevent flutter as a function of Mach Number for aluminum panels in sea-level air; infinite span; two-dimensional flow, except for finite aspect ratio panels which are based on aerodynamic "strip" theory from reference 27.

the $1/\mu$, k_0 plane. This intersection determines the panel thickness ratio. Fig. 12 shows such a summary for aluminum panels in sea-level air. Much extrapolation of available data is needed to sketch such a Figure; hence, the numerical values are rather crude. The region around $M = \sqrt{2}$ requires further investigation. All curves refer to undamped panels with no membrane stress ($N_x = 0$), except the one labeled "buckled," which refers to $\lambda_{1_0} = 0$, and $\lambda_1 > 1.5$; and another labeled $g = 0.05$, where g denotes the usual structural damping coefficient.

(3) Limiting Amplitudes of Flutter

The previous studies are concerned with the determination of flutter conditions under an arbitrary *infinitesimal* disturbance. For a nonlinear system, it is possible that a structure stable with respect to infinitesimal disturbances may still flutter under some *finite* disturbances. Furthermore, experiments show that the amplitude of panel flutter does not grow indefinitely, but rather a limiting cycle is developed.

The possible occurrence of limiting cycles is suggested by Eqs. (1.2) and (1.4) in which the term $N_x\partial^2 z/\partial x^2$ represents the elastic restoring force contributed by the membrane tension N_x. If N_x is positive it tends to flatten the plate, if N_x is negative it tends to buckle the plate. From Eq. (1.4) it is clear that under suitable conditions N_x becomes negative when $|z|$ is small, but N_x always becomes positive when $|z|$ is sufficiently large. Thus, the influence of the nonlinear term becomes increasingly strong in limiting the amplitude of flutter.

Let us consider the case of plates with *pinned edges* and again use the two-term approximation together with the simplified aerodynamic expression, Eq. (1.3). The governing equations are therefore [see Eqs. (1.17)-(1.19)]:

$$\left.\begin{aligned}\mu\sqrt{M^2-1}(d^2B_1/d\tau^2)+[(M^2-2)/(M^2-1)]\times\\ (dB_1/d\tau)+(B_1/Q)(-\chi+1-s)-\\ (8/3)B_2-(1/Q)(\lambda_{10}-P_0k_1)=0\\ \mu\sqrt{M^2-1}(d^2B_2/d\tau^2)+[(M^2-2)/(M^2-1)]\times\\ (dB_2/d\tau)+(4B_2/Q)(-\chi+4-s)+\\ (8/3)B_1-(4/Q)[4\lambda_{20}-(P_0/4)k_2]=0\end{aligned}\right\} \quad (3.1)$$

$$\chi = \lambda_1^2 - B_1^2 + 4(\lambda_2^2 - B_2^2) \quad (3.2)$$

with the motion described by

$$\left.\begin{aligned} z &= [h/\sqrt{3(1-\nu^2)E'/E}]\times\\ &\quad [B_1(\tau)\sin(\pi x/L)+B_2(\tau)\sin(2\pi x/L)]\\ z_0 &= [h/\sqrt{3(1-\nu^2)E'/E}]\times\\ &\quad [\lambda_1\sin(\pi x/L)+\lambda_2\sin(2\pi x/L)]\end{aligned}\right\} \quad (3.3)$$

Even these drastically simplified equations are too complicated for a complete solution. We shall attempt only a first approximation under the assumption that flutter motion exists and is essentially a sinusoidal function of time (as suggested by experiments). The following analysis, first outlined in reference 6, follows the well-known Kryloff and Bogoliuboff[14] procedure. Some numerical results obtained recently will be discussed below.

Let us assume that

$$\left.\begin{aligned} B_1 &= A_1\sin(k\tau+\phi_1) = A_1\sin\theta_1, \quad \theta_1 = k\tau+\phi_1\\ B_2 &= A_2\sin(k\tau+\phi_2) = A_2\sin\theta_2, \quad \theta_2 = k\tau+\phi_2\end{aligned}\right\} \quad (3.4)$$

where $A_1(\tau)$, $A_2(\tau)$, $\phi_1(\tau)$, $\phi_2(\tau)$ are slowly varying functions of time. The second-order differential equations (3.1) can be transformed into a set of first-order differential equations for A_1, A_2, ϕ_1, ϕ_2. Differentiation of Eqs. (3.4) gives

$$(dB_1/d\tau) = A_1k\cos\theta_1 + (dA_1/d\tau)\sin\theta_1 + A_1(d\phi_1/d\tau)\cos\theta_1$$

If we impose the condition

$$(dA_1/d\tau)\sin\theta_1 + (d\phi_1/d\tau)A_1\cos\theta_1 = 0 \quad (3.5)$$

then

$$dB_1/d\tau = A_1k\cos\theta_1 \quad (3.6)$$

$$d^2B_1/d\tau^2 = -A_1k^2\sin\theta_1 + (dA_1/d\tau)k\times\cos\theta_1 - (d\phi_1/d\tau)A_1k\sin\theta_1 \quad (3.7)$$

The first of Eqs. (3.1) then becomes

$$\mu\sqrt{M^2-1}\,[k(dA_1/d\tau)\cos\theta_1 - (d\phi_1/d\tau)A_1k\sin\theta_1 - A_1k^2\sin\theta_1] + [(M^2-2)/(M_2-1)]A_1k\cos\theta_1 + (A_1/Q)\sin\theta_1(-\chi+1-s) - (8/3)A_2\sin\theta_2 - (1/Q)(\lambda_{10}-P_0k_1) = 0 \quad (3.8)$$

From Eqs. (3.5) and (3.8), we obtain

$$\left.\begin{aligned}\mu\sqrt{M^2-1}\,k(dA_1/d\tau) &= \cos\theta_1 f_1(A_1, A_2, \phi_1, \phi_2, k\tau)\\ \mu\sqrt{M^2-1}\,kA_1(d\phi_1/d\tau) &= -\sin\theta_1 f_1(\ldots)\end{aligned}\right\} \quad (3.9)$$

where

$$f_1(\ldots) = \sqrt{M^2-1}\,\mu k^2 A_1 \sin\theta_1 - [(M^2-2)/(M^2-1)]A_1 k\cos\theta_1 - (A_1/Q)\sin\theta_1(-\chi+1-s) + (8/3)A_2\sin\theta_2 + (1/Q)(\lambda_{1_0}-P_0 k_1) \quad (3.10)$$

Similarly,

$$\left.\begin{aligned}\mu\sqrt{M^2-1}\,k(dA_2/d\tau) &= \cos\theta_2 f_2(\ldots)\\ \mu\sqrt{M^2-1}\,kA_2(d\phi_2/d\tau) &= -\sin\theta_2 f_2(\ldots)\end{aligned}\right\} \quad (3.11)$$

where

$$f_2(\ldots) = \sqrt{M^2-1}\,\mu k^2 A_2\sin\theta_2 - [(M^2-2)/(M^2-1)]A_2 k\cos\theta_2 - [4(-\chi+4-s)Q]A_2\sin\theta_2 - (8/3)A_1\sin\theta_1 + (4/Q)[4\lambda_{2_0} - (P_0/4)k_2] \quad (3.12)$$

The right-hand sides of Eqs. (3.9) and (3.11) admit, with respect to θ, a period 2π. If they were averaged over a period, we obtain the average values $dA_1/d\tau$, etc. For steady oscillations, these average values must all vanish. Hence, we obtain the following necessary conditions for steady oscillations:

$$\int_0^{2\pi} f_1(\ldots)\begin{matrix}\cos\\ \sin\end{matrix}\theta_1 d\theta_1 = 0, \qquad \int_0^{2\pi} f_2(\ldots)\begin{matrix}\cos\\ \sin\end{matrix}\theta_2 d\theta_2 = 0 \quad (3.13)$$

On substituting Eqs. (3.4) into Eqs. (3.2) and (3.13) and performing the integration, we obtain

$$\left.\begin{aligned}&-[(M^2-2)/(M^2-1)]kA_1 + (1/Q)A_1A_2^2\sin 2\varphi - (8/3)A_2\sin\varphi = 0\\ &-[(M^2-2)/(M^2-1)]kA_2 - (1/Q)A_2A_1^2\sin 2\varphi - (8/3)A_1\sin\varphi = 0\\ &\sqrt{M^2-1}\,\mu k^2A_1 + (A_1/Q)[\lambda_1^2 + 4\lambda_2^2 - 1 + s - (3/4)A_1^2 - 2A_2^2 - A_2^2\cos 2\varphi] + (8/3)A_2\cos\varphi = 0\\ &\sqrt{M^2-1}\,\mu k^2A_2 + (A_2/Q)[4\lambda_1^2 + 16\lambda_2^2 - 16 + 4s - 2A_1^2 - A_1^2\cos 2\varphi - 12A_2^2] - (8/3)A_1\cos\varphi = 0\end{aligned}\right\} \quad (3.14)$$

where

$$\varphi = \theta_1 - \theta_2 = \phi_1 - \phi_2 \quad (3.15)$$

These equations are to be solved for A_1, A_2, φ, and k for a given set of constants M, μ, Q, and λ_1. An obvious solution is the trivial one $A_1 = A_2 = 0$. It is also easy to see that if $A_1 = 0$, then $A_2 = 0$, and vice versa. In other words, a flutter mode of finite amplitude is never a purely first or second mode of free vibration in vacua. Hence only the case $A_1A_2 \neq 0$ needs consideration. When this is the case, Eqs. (3.14) may be rearranged as

$$\left.\begin{aligned}&Q = -(3/4)\cos\varphi\, A_1^2[(r^2+1)/r(r^2-1)]\\ &3\lambda_1^2 - 3(1-s) = 12 + A_1^2\{(5/4) + [1-(1/r^2)]\cos 2\varphi + (10/r^2)\} + (8Q/3)[r+(1/r)]\cos\varphi\\ &\sqrt{M^2-1}\,\mu k^2 = (1/Q)\{-\lambda_1^2 + 1 - s + A_1^2[(3/4) + (2/r^2) + (\cos 2\varphi/r^2)]\} - (8/3)(\cos\varphi/r)\\ &[(M^2-2)/(M^2-1)] = -(16/3)(\sin\varphi/k)[r/(r^2+1)]\end{aligned}\right\} \quad (3.16)$$

where, for simplicity, we have set

$$\lambda_2 = 0, \qquad r = A_1/A_2 \quad (3.17)$$

In the form (3.16), it is easy to solve the inverse problem of calculating λ_1, k, Q, and M from assigned values of $\sqrt{M^2-1}\,\mu$, A_1, A_2, and φ. From a survey of such results the direct problem can be solved by interpolation.

(3.1) *Buckled Flat Plates*

The flutter motion of initially flat plates has been computed, and the results at $M = 2$ are presented in Figs. 13, 14, and 15. Diagrams for other Mach Numbers and mass ratios are quite similar—an example at $M = 1.3$ is shown in Fig. 16. In these Figures it is assumed that

$$\lambda_{10} = \lambda_{20} = P_0 = 0, \quad s = 1 \quad (3.18)$$

In other words, no initial warping and lateral load other than the aerodynamic pressure is allowed. The calculations were made on a digital computer by assuming various values of φ, A_1, and r and computing Q, λ_1^2, k^2, M^2 according to Eqs. (3.16). Since only real, positive values of Q, λ_1^2, k^2 have physical meaning, many combinations of φ, A_1, r are not admissible. Without loss of generality we may let $A_1 > 0$, $A_2 > 0$, $r > 0$. In order that Q may be positive, we must have $|\varphi| > \pi/2$ if $r > 1$, $|\varphi| < \pi/2$ if $r < 1$. Note that $\sqrt{M^2-1}\,\mu$ enters only in the step of obtaining k and M, and that the sign of φ affects only the Mach Number.

Figs. 13 and 16 show the contours of the phase angle difference φ between the two assumed modes of Eqs. (3.3), [see also Eqs. (3.4) and (3.15)], and the contours of the amplitude of the antisymmetric mode, A_2. The plot is made on the (Q, λ_1) plane with λ_1 written as $\sqrt{3}\times$ (initial arch height)/(plate thickness) when the assumption of vanishing spanwise strain is made—i.e., when $E' = E/(1-\nu^2)$. It is remarkable that the map for $M = 1.5$ appears similar to that for $M = 2.0$. Here we emphasize that the $M = 1.3$ map is valid only in the region where $k \ll 1$.

The mass ratio slightly affects the quantitative disposition of the contours, but not their general character.

Fig. 14 shows the contours of the amplitude ratio A_1/A_2 of the two assumed modes. It is seen that over most of the (Q, λ_1) plane the ratio A_1/A_2 is large. For sufficiently large values of Q, the larger the λ_1 the smaller is the second mode in comparison with the first. Only in the smaller λ_1 region is A_2 approaching A_1 in magnitude.

Fig. 15 shows the contours for the reduced frequency k. It is seen that for any given value of Q, k increases as λ_1 increases.

From these Figures we may expect the following behavior if a plate is forced to buckle in a supersonic flow. As λ_1 gradually increases, the flutter motion, if it occurs at all, will first have a small reduced frequency, an amplitude ratio A_1/A_2 not much greater than 1, and a phase shift φ not far from $-180°$. As the edges are further compressed, so that λ_1 becomes

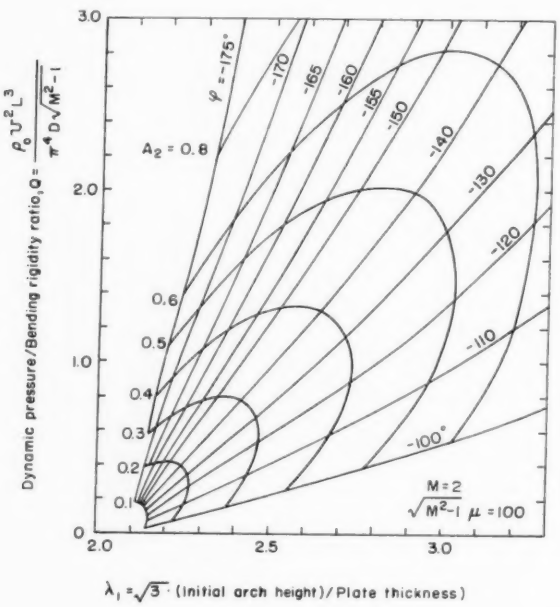

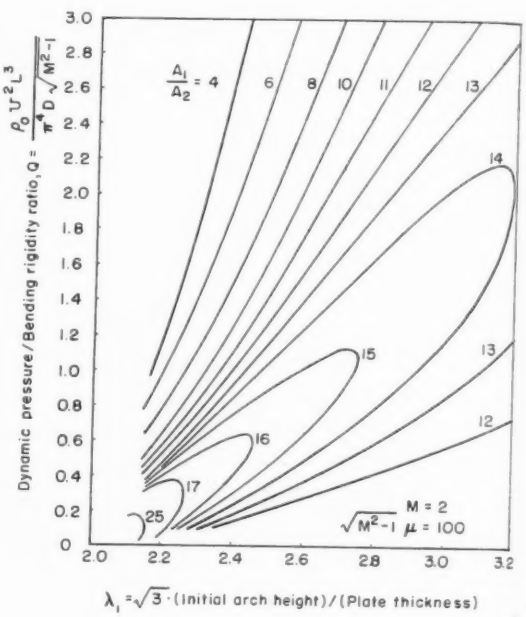

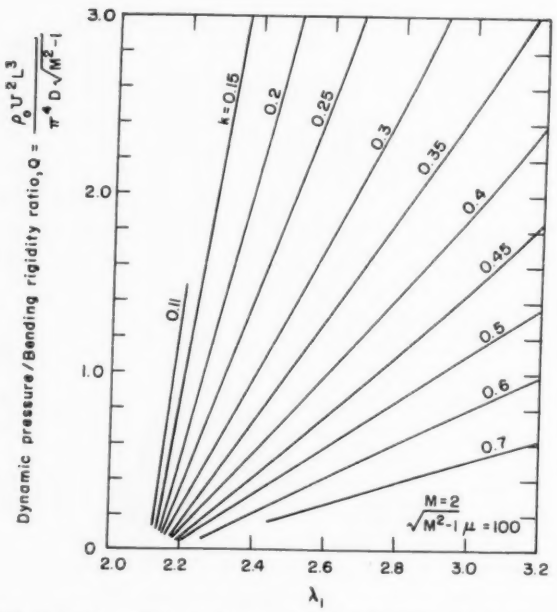

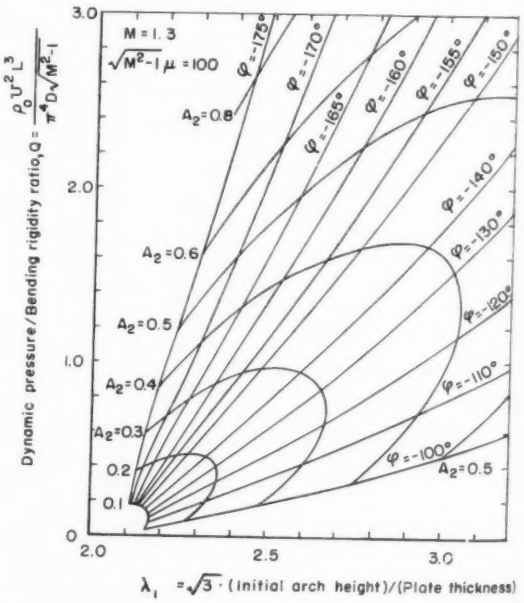

FIG. 13 (*top*). Contours of phase shift φ and amplitude of the second mode A_2. $M = 2.0$, $\sqrt{M^2-1}\,\mu = 100$. FIG. 15 (*bottom*). Contours of the reduced frequency $k = \omega L/U$. Mach Number = 2.0, mass ratio $\sqrt{M^2-1}\,\mu = 100$.

FIG. 14 (*top*). Contours of the amplitude ratio A_1/A_2. $M = 2.0$, $\sqrt{M^2-1}\,\mu = 100$. FIG. 16 (*bottom*). Contours of phase shift φ and amplitude of the second mode A_2. $M = 1.3$, $\sqrt{M^2-1}\,\mu = 100$.

larger, the flutter motion will have higher reduced frequency, more predominant first mode, and a larger phase shift toward 90° between the two modes.

These Figures also throw some light on the flutter in the Mach Number range from 1 to $\sqrt{2}$. In this range the linearized supersonic aerodynamics dictates instability at small reduced frequency due to negative aerodynamic damping. The limiting cycle analysis shows that if flutter occurs at small values of Q, the flutter motion will have a large A_1/A_2 ratio—i.e., the deflection will consist of a predominant first mode.

Unfortunately, at the present time a dearth of experimental data precludes any attempt at an evaluation of the accuracy of the foregoing analysis.

(3.2) *Relation With Stability Boundary*

If we compare the stability boundary labeled $\lambda_{1_0} = 0$ in Fig. 3 with the flutter maps of Figs. 13 through 15, we see that the stability boundary divides each flutter map into two regions. In the region below the stability boundary, there exists a stable static equilibrium configuration; in the region above that boundary, no such stable static equilibrium configuration exists. It is plausible that, in the latter case, any disturbance away from the condition $B_{1,2} = dB_{1,2}/d\tau = 0$ will cause a motion which ultimately will approach the limit cycle. On the other hand, when a stable equilibrium configuration does exist, a small disturbance about the static equilibrium will cause a damped motion converging toward the equilibrium point, but a larger disturbance may cause certain large deviation from the equilibrium point and a motion which ultimately converges onto a limit cycle. It appears that the wind-tunnel experiments described earlier, in which no external disturbances other than those inherent in the flow were imposed, satisfied the qualification of "small" disturbances and thus revealed the infinitesimal stability boundary.

(3.3) *Numerical Integration of the Differential Equations*

In order to verify that the approximation (3.4) is a reasonable one for the differential equations (3.1), numerical integrations of (3.1) were carried out for several values of Q, taking as initial conditions the values of A_1, A_2, φ, k given by the approximate solution (3.16) and shown in the Figures above. Two typical sets of curves are given in Fig. 17. The solutions given by Eqs. (3.16) for these two cases are

(a) $Q = 2.03$ $\quad \lambda_1 = 2.93$
$A_1/A_2 = 14$ $\quad A_2 = 0.6$
$\varphi = 140°$ $\quad k = 0.378$
$M = 1.95$

(b) $Q = 0.524$ $\quad \lambda_1 = 2.99$
$A_1/A_2 = 11.0$ $\quad A_2 = 0.6$
$\varphi = 100°$ $\quad k = 0.679$
$M = 2.08$

From Fig. 17 it is seen that the sinusoidal-variation assumption is reasonable for B_1, but not for B_2; and

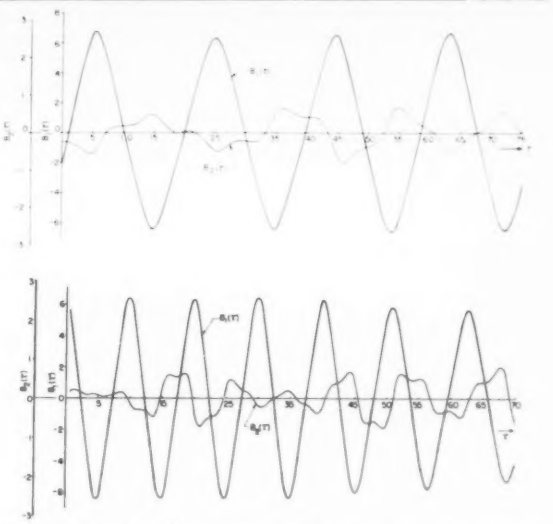

FIG. 17. Solutions from numerical integration (*top*—case a, *bottom*—case b).

that in both examples B_1 predominates. Difficulties were encountered when the numerical integration was continued further; it seems that the rounding-off error and the stability of the solution tend to disturb the cyclic motion into a transient one. It seems remarkable that nearly sinusoidal oscillation exists even for $Q = 0.524$, which lies well below the stability boundary —i.e., in the stable regime—with respect to infinitesimal disturbances.

CONCLUDING REMARKS

In the present article we have shown some finer details about the nature of flutter of buckled plates in a two-dimensional flow. It appears that any relief of the compressive load in the plate, whether it be due to initial curvature, or pressurization, or support elasticity, or temperature differential or edge movements, will be beneficial to the prevention of flutter. An approximate method is demonstrated for the calculation of the limiting form and amplitude of the flutter motion, although the accuracy of this method remains to be evaluated.

The Galerkin method is shown to give satisfactory results for plates with finite bending stiffness. The difficulty of the Galerkin method with the membrane is of course a difficulty in the question of convergence and of relying upon a crude approximation to settle the question of *existence* of a real eigenvalue. We may recall a famous remark by Richard Courant[3] concerning the spectacular success of Walter Ritz in inventing a method which now bears his name: "The first success attained by Ritz depends largely on his good fortune in attacking the seemingly more difficult problem (of the free vibration in vacua) of the plate rather than that of the membrane." Courant has suggested a method to "sensitize" the variational integral to improve the convergence, through the addition of terms of higher order, which vanish for the actual solution, to the

original variational expression. We find that a similar improvement can be achieved by deriving the variational equation through the complementary energy theorem as outlined by Reissner.[23] But then in both cases the calculation required for the membrane becomes even more laborious than that for the plate.

References

[1] Ashley, H., and Zartarian, G., *Piston Theory—A New Aerodynamic Tool for the Aeroelastician*, Journal of the Aeronautical Sciences, Vol. 23, No. 12, pp. 1109–1118, December, 1956.

[2] Brooks, J. A., Levin, E., Frank, W. L., and Tarnove, I., *Eigenvalue Problems in Modern Industry. I. Survey of Physical Origin and Mathematical Formulation. II. Computing Techniques for Matrices*, Proc. Joint NYU-IBM Symposium on Digital Computation in the Aircraft Industry, January 28–31, 1957. Available at the Research Division, New York University, N.Y.

[3] Courant, R., *Variation Methods for the Solution of Problems of Equilibrium and Vibrations*, Bulletin Am. Math. Soc., Vol. 49, pp. 1–23, 1943.

[4] Eisley, J. G., *The Flutter of a Two-Dimensional Buckled Plate with Clamped Edges in a Supersonic Flow*, Ph.D. Thesis, Guggenheim Aeronautical Laboratory, California Institute of Technology, July, 1956. Published as AF OSR TN 56-296.

[5] Fung, Y. C., *The Static Stability of a Two-Dimensional Curved Panel in a Supersonic Flow, with an Application to Panel Flutter*, Journal of the Aeronautical Sciences, Vol. 21, No. 8, pp. 555–565, August, 1954. *Errata:* The coefficients of the last terms in Eqs. (38) and (41) in this reference should be 2 instead of 4. The off-diagonal terms in Eq. (42) should be reduced by one half. The corrected Q_{rr} curve then approaches that of Fig. 3a of the present article. See details in reference 6.

[6] Fung, Y. C., *The Flutter of a Buckled Plate in a Supersonic Flow*, Report OSR TN 55-237, Guggenheim Aeronautical Laboratory, California Institute of Technology, July, 1955.

[7] Fung, Y. C., *Flutter of Curved Plates with Edge Compression in a Supersonic Flow*, Proceedings of the Midwest Conference on Fluid and Solid Mechanics, Ann Arbor, Mich. April 1, 2, 1957. Published as OSR TN 57-187.

[8] Goland, M., and Luke, Y. L., *An Exact Solution for Two-Dimensional Linear Panel Flutter at Supersonic Speeds*, Readers' Forum, Journal of the Aeronautical Sciences, Vol. 21, No. 4, p. 275, April, 1954. See also Shen, S. F., *Remarks on "An Exact Solution for Two-Dimensional Linear Panel Flutter at Supersonic Speeds,"* Readers' Forum, Journal of the Aeronautical Sciences, Vol. 22, No. 9, p. 656, September, 1955.

[9] Hayes, W., *A Buckled Plate in a Supersonic Stream*, Report AL-1029, North American Aviation, Inc., May 10, 1950.

[10] Hedgepeth, J. M., *On the Flutter of Panels at High Mach Numbers*, Readers' Forum, Journal of the Aeronautical Sciences, Vol. 23, No. 6, p. 609, June, 1956.

[11] Isaacs, R. P., *Transtability Flutter of Supersonic Aircraft Panels*, Report P-101, The Rand Corporation, Santa Monica, Calif., July, 1949.

[12] Jordan, P. F., *The Physical Nature of Panel Flutter*, Aero Digest, pp. 34–38, February, 1956.

[13] Thomson, William (Lord Kelvin), *The Influence of Wind on Waves in Water Supposed Frictionless* (Letter of August 16, 1871, to Professor Tait), Mathematical and Physical Papers, Vol. 4, pp. 76–83.

[14] Kryloff, N., and Bogoliuboff, N., *Introduction to Nonlinear Mechanics* (free translation by Lefschetz), Princeton University Press, 1947.

[15] Luke, Y. L., Goland, M., and Constant, P., *Panel Flutter at Supersonic Speeds*, Progress Report (AF 33(616)-2897), Midwest Research Institute, June, 1955.

[16] Miles, J. W., *The Aerodynamic Forces on an Oscillating Airfoil at Supersonic Speeds*, Journal of the Aeronautical Sciences, Vol. 14, No. 6, pp. 351–358, June, 1947.

[17] Miles, J. W., *Dynamic Chordwise Stability at Supersonic Speeds*, Report AL-1140, North American Aviation, Inc., October 18, 1950.

[18] Miles, J. W., *On the Aerodynamic Stability of Thin Panels*, Journal of the Aeronautical Sciences, Vol. 23, No. 8, pp. 771–780, August, 1956. See also Leonard, Robert W., and Hedgepeth, John M., *On the Flutter of Infinitely Long Panels on Many Supports*, Readers' Forum, Journal of the Aeronautical Sciences, Vol. 24, No. 5, p. 381, May, 1957.

[19] Miles, J. W., *Supersonic Flutter of a Cylindrical Shell. I. General Theory*, Report No. AM 5-2, August, 1955. *II. Pressurization and Internal Fluid Effects*, Report No. AM 5-11, November, 1955. *III. Aerolotropic Shell*, Report No. AM 5-12, December, 1955. *IV. Effects of Nonuniform Steady Flow*, Report No. AM 5-16, December, 1955. The Ramo-Wooldridge Corp., Inglewood, Calif.

[20] Miles, J. W., *Supersonic Flutter of a Cylindrical Shell*, Journal of the Aeronautical Sciences, Vol. 24, No. 2, pp. 107–118, February, 1957.

[21] Nelson, H. C., and Cunningham, H. J., *Theoretical Investigation of Flutter of Two-Dimensional Flat Panels with One Surface Exposed to Supersonic Potential Flow*, NACA Report 1280, 1956.

[22] Strutt, John William (Lord Rayleigh), *On the Instability of Jets*, Proc. London Math. Soc., Vol. 10, pp. 4–13, 1879. Also in Scientific Papers, Vol. 1, pp. 361–371. See also Lamb, Hydrodynamics, p. 374.

[23] Reissner, E., *Complementary Energy Procedure for Flutter Calculations*, Readers' Forum, Journal of the Aeronautical Sciences, Vol. 16, No. 5, p. 316, May, 1949. See also van de Vooren, A. I., and Greidanus, J. H., *Complementary Energy Method in Vibration Analysis*, Readers' Forum, Journal of the Aeronautical Sciences, Vol. 17, No. 7, p. 454, July, 1950, and Libby, Paul A., and Sauer, Robert C., *Comparison of the Rayleigh-Ritz and Complementary Energy Methods in Vibration Analysis*, Readers' Forum, Journal of the Aeronautical Sciences, Vol. 16, No. 11, p. 700, November, 1949.

[24] Shen, S. F., *Flutter of a Two-Dimensional Simply Supported Uniform Panel in a Supersonic Stream*, ONR Contract No. N5ori-07833, Department of Aeronautical Engineering, Massachusetts Institute of Technology, August 6, 1952.

[25] Sylvester, M. A., and Baker, J. E., *Some Experimental Studies of Panel Flutter at Mach Number 1.3*, NACA TN 3914, 1957.

[26] Wielandt, H., *Contributions to the Mathematical Treatment of Complex Eigenvalue Problems*, Aerodynamische Versuchsanstalt, AVA B 43/J/21, AVA B 44/J/21, AVA B 44/J/38, AVA B 44/J/19, Goettingen, 1944. AAF Translation TS-1510, TS-904, TS-976, Air Materiel Command, Wright Field, Dayton, Ohio, 1948.

[27] Eisley, J. G., *The Flutter of Simply Supported Plates in a Supersonic Flow*, Ph.D. Thesis, California Institute of Technology, July, 1955. Published as AF OSR TN 55-236.

Structural and Impact Loads for the Flexible Airplane During Water Landings

EDWARD WIDMAYER, JR.* AND ROBERT H. SCHWAB*

The Martin Company

Summary

A method for calculating structural loads due to water landing impact has been developed. The results of this method have, for the most part, been substantiated by the results of an experimental program in which both the hull bottom loads and the acceleration response of the M-270 airplane were measured. Past research has shown that the impact loads are dependent on rate-of-descent, trim angle, landing speed, hull shape, and degree of flexibility of the entire airplane. The method presented herein includes the above factors and emphasizes the dependency of the hydrodynamic loads on the flexible airplane response. Calculations are made for both a rigid and a flexible airplane and are compared with the experimental results. In using modern computing methods it was found that continuous trim variations and load input at several stations were possible.

Symbols

A	= acceleration
a_n	= coefficient of nth vibratory mode
b_x	= distance in x direction from mass center of airplane to mass station, positive aft
C	= wetted width of hull
C_p	= pressure coefficient
D	= viscous damping coefficient
e	= base of Naperion logarithm
F_s	= hydrodynamic force acting through step of airplane normal to keel, positive down
G	= structural damping coefficient
g	= acceleration due to gravity
Z_t	= draft of hull after chine immersion
Z_c	= draft of hull at chine immersion
l_k	= wetted length of hull measured from step
m	= mass considered to act at a given airplane station
M_s	= hydrodynamic moment about step, positive nose up
M_w	= virtual mass of water
P_{ave}, P_{max}	= hydrodynamic pressures
t	= time
V_h	= forward speed
V_n	= speed normal to keel
x	= coordinate in fore and aft direction of airplane
y	= coordinate in span direction
z	= coordinate in direction normal to keel
Δ	= hydrodynamic force associated with dynamic pressure, positive down
μ	= Wagner's function for spray thickness
ρ	= density of water
φ	= slope of deformed structure
ω_n	= circular frequency of nth mode
τ	= trim angle, positive nose up

Superscripts and Subscripts

$(\ddot{}), (\dot{})$	= time derivations
c	= at chine or chine immersion
ave	= average
max	= maximum
s	= at step
0	= initial condition
n, r, s	= modal designation
n	= normal
h	= horizontal

Presented at the Aeroelasticity—II Session, Twenty-Fifth Annual Meeting, IAS, New York, January 28-31, 1957.

* Group Engineer, Dynamics Section.

Introduction

THE SUBJECT MATTER of this paper forms a small portion of the results of a research program initiated by the Bureau of Aeronautics to study loads developed during impact of water landings. (See references 1 and 2.) It is felt that the results of this work represent a significant advance in the treatment of the landing impact problem and form a base from which analytical treatment may be extended to cover landings in any type of sea. Historically, the water landing impact problem has been separated into two distinct parts: the determination of the maximum water loads, and the determination of the transient structural loads arising from the structural response to these water loads.[3] This separation of the generation of water loads from the structural response has been long recognized as an artificial device, and a method of including the influence of wing structural flexibility on the water loads has been given in reference 4.

For relatively rigid seaplanes, the transient structural loads determined from the maximum water loads generally have been sufficient for engineering purposes. However, for more flexible seaplanes a formulation of the impact problem that allows the full interaction of the hydrodynamic forces and the dynamic response of the elastic seaplane is desired. Since the dynamic response of an elastic seaplane is a function of rate-of-load application as well as the peak value of the load, the formulation of the impact problem should permit rapid solution for a wide parametric variation of initial landing conditions.

An analytical method of treating the step landing impact problem in smooth water is developed. It gives in "closed" form the simultaneous determination of both the water loads and the transient structural loads. In solving the resulting equations of motion, a procedure using an electronic analog computer has been developed which permits the rapid solution of the landing problem for a large range of initial landing conditions. Solutions of the impact problem obtained for the M-270 seaplane, considered as being completely rigid and as being completely flexible, for a

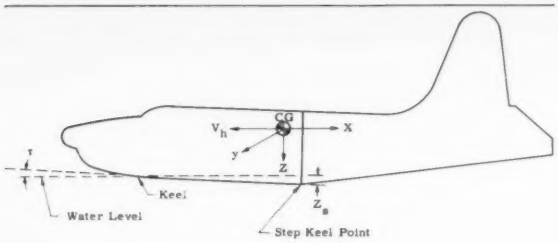

FIG. 1. Airplane coordinate system.

range of landing conditions are presented and discussed.

The experimental program for the M-270 airplane is briefly discussed. While this program includes extensive experimental measurements of hull bottom pressures, loads, and structural response, only those results directly applicable to this paper are presented. These experimental results are compared with the results of the theoretical analysis. These comparisons are discussed with respect to both the time variation and the maximum values of the various parameters.

THEORETICAL LANDING LOADS ANALYSIS

The airplane coordinate system is shown in Fig. 1. The displacement of any point in the elastic structure is considered to be represented by the sum of the displacements of that point in each mode of vibration including the zero frequency modes. This may be expressed as follows:

$$Z(x, y) = b(x) + a_n Z_n(x, y) \tag{1}$$

The selection of the modal shapes necessary to approximate the structure during impact accurately is governed largely by the vibratory characteristics of the structure and by the time variation of the applied forces. Bases for the inclusion of a sufficient number of modes have been discussed in previous literature on dynamic response and, therefore, will not be discussed here. For the purpose of this paper the displacement of an airplane element in the elastic case is represented by the contributions of the first four flexural airplane modes in conjunction with rigid body translation and rotation. The displacement of an airplane element in the rigid body case is represented by rigid body translation and rotation.

The hydrodynamic forces and moments generated during a step landing are given by Eqs. (2) and (3).

$$F_s = -\Delta - M_w(Z_s - 0.65 l_k \ddot{\tau}) \tag{2}$$

$$M_s = -F_s(0.65 l_k) \tag{3}$$

The theoretical development of Eqs. (2) and (3) is discussed in detail in references 1 and 2 and will not be treated here. However, the results of the theory necessary for a solution to the equations of motion are discussed below.

The term Δ is associated with effects of the dynamic pressure and is given in Eq. (4).

$$\Delta = \rho V_n |V_n| \int_0^{l_k} C_p C(dl_k) \tag{4}$$

where

$$V_n = \dot{Z}_s + V_h \sin \tau - 0.65 l_k \dot{\tau}$$

In this expression the influence of the vertical velocity of the wetted surface is obtained from contributions of $\dot{Z}$ and $\dot{\tau}$. The distance $0.65 l_k$ is assumed to be the location of the center of pressure of the wetted surface from the step of the keel. The effect of planning forces is reflected in the contributions of $V_h \sin \tau$.

The functions C_p and C have discontinuities at the point of chine immersion. The wetted width, C, varies with draft until the chines are immersed, and for further increase in draft, C is assumed to be constant. Prior to chine immersion, C_p is given by the following equation:

$$C_p = \frac{P_{ave}}{P_{max}} \frac{1}{\sin^2 \tau + \mu^2 \cos^2 \tau + (Z_c - C)^2 \sin^2 \tau}$$

After chine immersion, C_p is given by

$$C_p = \frac{P_{ave}}{P_{max}} \frac{1}{\sin^2 \tau [1 + (Z_c - C)^2 + (Z_1 - C)]^2}$$

In these expressions for C_p the quantity P_{ave}/P_{max} is a function of the draft. Knowing the variation C_p, C, and l_k as a function of Z_s for a given value of τ, the integral $\int_0^{l_k} C_p C(dl_k)$ could be evaluated.

The second term in Eq. (2) is associated with the forces given by

$$M_w = \rho \int_0^{l_k} C^2 dl_k$$

These are the well-known "apparent mass" effects. With the variation of C with Z_s known, $\int_0^{l_k} C^2 dl_k$ may be evaluated for a given τ.

The moment about the step is taken as that due to the water force acting through the center of pressure.

The hydrodynamic forces acting on a section of the hull are complicated by variations in trim, complex form factors, chine-immersions effects, and three-dimensional flow. The treatment of these parameters may be made by any rationally acceptable methods of analysis (cf. reference 2 or 5). It is important that rational expressions for force and moment in terms of the parameters of the dynamic problem be available.

In the actual evaluation of the above integrals, it was convenient to utilize digital machine computational methods. The integrals were evaluated for τ equal to 3°, 6°, and 9° for the range of Z_s expected to be encountered by the airplane, and the results were shown in graphical form. It was then found to be possible to approximate the curves for constant τ with analytic expressions in which Z_s and τ appeared as simple functions. Further, it was found that the family of curves was adequately given when the value

of τ was permitted to vary. Consequently, when the simple analytic expressions for the integrals are substituted into the equation for the hydrodynamic force, the restriction of the landing conditions to constant values of trim is no longer necessary to the solution of the landing impact problem.

The expressions for the $\int_0^{l_k} C_p C dl_k$ and $\int_0^{l_k} C^2 dl_k$ were found to be as follows for the M-270 airplane:

$$\left.\begin{aligned} 0 < Z_s < 0.2Z_c \qquad & \int_0^{l_k} C_p C dl_k = \frac{4.59 - 12.0\tau}{\tau} Z \\ 0.2 < Z_s < Z_c \qquad & \int_0^{l_k} C_p C dl_k = \frac{1.31 - 2.2\tau}{\tau} (e^{2Z} - 0.82) \\ Z_c < Z \qquad & \int_0^{l_k} C_p C dl_k = \frac{-87.1 + 94.5e^{-3.3(Z-1)} + 40.1 - 34.2e^{-1.88(Z-1)}}{\tau} \end{aligned}\right\} \tag{5}$$

and

$$\left.\begin{aligned} 0 < Z_s < Z_c \qquad & \pi\rho \int_0^{l_k} C^2 dl_k = (17.8/\tau) Z (Z^2 + 0.1435) \\ Z_c < Z \qquad & \pi\rho \int_0^{l_k} C^2 dl_k = (76.8\ \tau)(Z - 0.735) \end{aligned}\right\} \tag{5a}$$

In the present problem, these expressions gave excellent approximations of the integrals for values of Z_s up to 36 in. and gave reasonable agreement for values of Z_s in excess of 36 in. It should be noted that for that portion of the landing most important to the airplane response—i.e., during the build-up to maximum force—these analytical expressions are most valid.

The forces arising from the explicit variation of trim in Eq. (2) include a component due to the dynamic pressure and a component due to the virtual mass. In the force due to dynamic pressure, V_n has components of velocity arising from both the trim and the rate of pitch of the airplane. During the early portions of impact the contribution due to the instantaneous trim does not vary appreciably. However, the contribution due to the rate of change in trim, $\dot{\tau}$, in those cases where there is large wetted length, may become important. The component of force due to the acceleration of the "virtual" mass of water is affected by the angular acceleration. In those cases where the wetted length is long and the pitching acceleration is large, the effect of this acceleration on the forces is appreciable.

In permitting trim variation, it was necessary to determine the centroid of the pressure distribution acting on the bottom. For the high-beam loaded hull where chine immersion occurs early in impact, the center of pressure is taken at 65 per cent of the instantaneous value of the wetted length. The factors on which the selection of $0.65l_k$ is based are discussed in reference 2. The location of the pressure centroid is of importance for landings at low initial values of trim where the wetted length may be expected to exceed four times the beam of the hull.

Equations of Motion

The equations of motion relating the behavior of the airplane to the hydrodynamic forces encountered during impact may be derived with any of usual procedures of this type of analysis. The following equations are obtained:

$$\left.\begin{aligned} -Z_0 + (F_s \textstyle\sum m) &= 0 \\ -\tau + \frac{F_s b_s + M_s}{\sum m\, b^2_{(x)}} &= 0 \\ -Z_n - g\omega_n \dot{Z}_n - \omega_n{}^2 Z_n + \frac{(a_n)_s F_s + \phi_s M_s}{\sum (a_n)^2 m} &= 0 \end{aligned}\right\} \qquad n = 1, 2, 3, 4 \tag{6}$$

when the initial values of $\dot{Z}_s$, τ, and V_n are given, Eqs. (6) may then be solved for the $Z_s(t)$, $\tau(t)$, $F_s(t)$, and $M_s(t)$. In addition, the acceleration at any mass station may be obtained by the use of the following relation:

$$\ddot{Z}_{(x\,y)} = a_0 \ddot{Z}_0 + b_{(x)}\, \ddot{\tau} + \sum_1^n a(x_1 y)_n \ddot{Z}_n$$

With these quantities known, the impact forces and structural response are determined, and the distribution of load over the structure may be studied.

From an examination of Eqs. (6), it can be seen that the equations are nonlinear functions of Z, $\dot{Z}$, $\ddot{Z}$, and τ. Previously, when it was sufficient to treat the landing problem as the rigid body, the translatory response to the hydrodynamic forcing function solutions was obtained either by a step-by-step integration or by use of an analog computer. The inclusion of additional degrees of freedom has increased the complexity of the problem and has made the analog solution attractive.

The solution to Eqs. (6) has been obtained readily by using an electronic analog computer. The left-hand side of Eqs. (6), giving the forces arising within the structure, presents no difficulty in machine programing. The use of a simple analytical expression for the hydrodynamic force and moments, while requiring additional machines, may also be readily programed. Continuous records of hydrodynamic forces and mo-

ments, displacement and structural accelerations, shears, and bending moments may then be obtained.

Experimental Program

A test program was initiated to obtain experimental data for correlation with theoretical hull bottom water loads and airplane accelerations during landing impact of the M-270 airplane.

Instrumentation for the tests consisted of a total of 49 transducers, which included 13 accelerometers, 20 flush-type pressure transducers, and 16 strain gages. The distribution of transducers in the airplane is shown in Fig. 2. The output of the transducers was recorded on oscillographs.

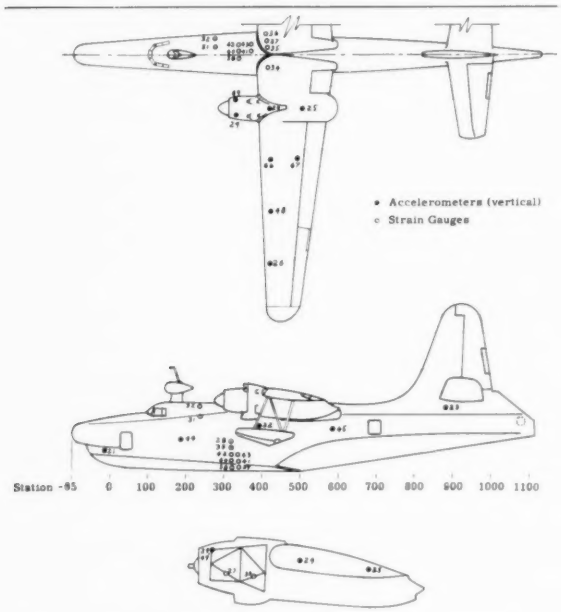

Fig. 2. Location of instrumentation on aircraft structure.

Cable No.	Item	Location
21	accelerometer	hull sta. 18, w.l. 49½, ℄ of ship
22	accelerometer	hull sta. 396, w.l. 130, ℄ of ship
23	accelerometer	hull sta. 885, w.l. 160, ℄ of ship
24	accelerometer	l. wing sta. 147.5, front spar
25	accelerometer	l. wing sta. 147.5, rear spar
26	accelerometer	l. wing sta. 600, front spar
27	strain gage	engine mount tube, center of tube
28	strain gage	vertical shear, hull sta. 328, web of floor frame
29	accelerometer	engine mount, l.h. forward
30	strain gage	engine mount tube, center of tube
31	strain gage	sta. 236, center of longeron, r.h. side
32	strain gage	sta. 236, walkway stringer, r.h. side
33	strain gage	hull sta. 328, ℄ top chord floor frame
34	strain gage	hull sta. 386, center of longeron, l.h. side
35	strain gage	hull sta. 386, walkway stringer, r.h. side
36	strain gage	hull sta. 386, outboard face of longeron, r.h. side
37	strain gage	hull sta. 386, inboard face of longeron, r.h. side
38	strain gage	top of keel former, sta. 321
39	strain gage	hull bottom midway between S-0 and S-1, sta. 338½
40	strain gage	top of S-0 at ℄ of vertical stiffener to stringer attached at sta. 328
41	strain gage	top of S-0 at ℄ of vertical stiffener between sta. 328 and 350
42	strain gage	top of S-2 at ℄ of vertical stiffener at sta. 328
43	strain gage	top of S-2 at ℄ of vertical stiffener between sta. 328 and 350
44	accelerometer	℄ hull, sta. 180
45	accelerometer	℄ hull, sta. 574
46	accelerometer	l. wing, sta. 300, front spar
47	accelerometer	l. wing, sta. 300, rear spar
48	accelerometer	l. wing, sta. 450, front spar
49	accelerometer	engine mount, l.h. forward

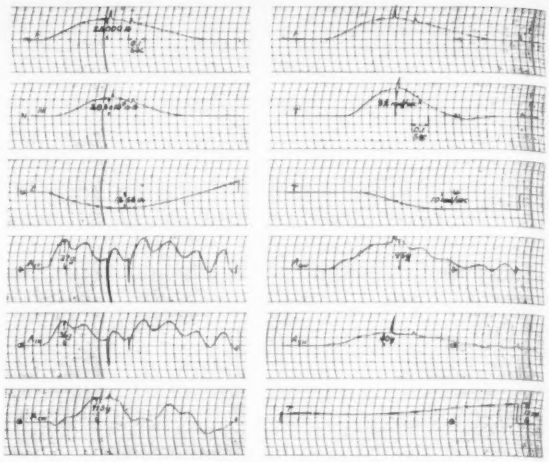

Fig. 3a. REAC solutions to impact problem—flexible case. $V_x = 185$ ft. per sec., $\tau_0 = 3°$, $\dot{Z}_0 = 4$ ft. per sec.

The most difficult quantity to measure—the rate of descent—proved to be, perhaps, the most important. Attempts to use doppler radar were unreliable over anything but a glassy smooth sea. Consequently, a photo-theodolite system was installed at the landing range. The rate of descent could be obtained with reasonable accuracy from motion picture film of each landing trial.

The range of parameters investigated was limited by the structural strength of portions of the airframe and by the handling characteristics of the aircraft. The strength of the engine mount structure (limit load factor of 4.5) placed a limitation on the maximum rate of descent obtainable. Also, it was found difficult to obtain high trim angles at high rates of descent and to obtain low trim angles at low rates of descent. However, the flights were performed within these limits and all possibilities were exploited.

Solutions of the equations of motion for hydrodynamic impact have been obtained and are presented in Tables 1 and 2 and Figs. 3a to 3e. The solutions, as obtained from the analog computer, are in the form of the time variation of the quantities being studied. These data have been reduced to the form of peak values and are reported in terms of the conditions existing at the time of peak values. Oscillograms of landings are also presented, which representatively illustrate variations of hydrodynamic force and moment, motions of the aircraft, and the acceleration response of the aircraft having significance in the structural dynamics problem.

Discussion

It is a well-known result that the response of a simple mechanical system to suddenly applied forces is a func-

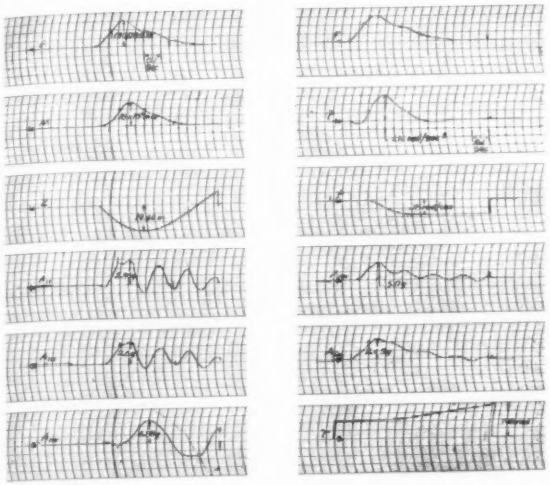

FIG. 3b. REAC solutions to impact problem—flexible case. V_x = 185 ft. per sec., τ_0 = 6°, $\dot{Z}_0$ = 12 ft. per sec.

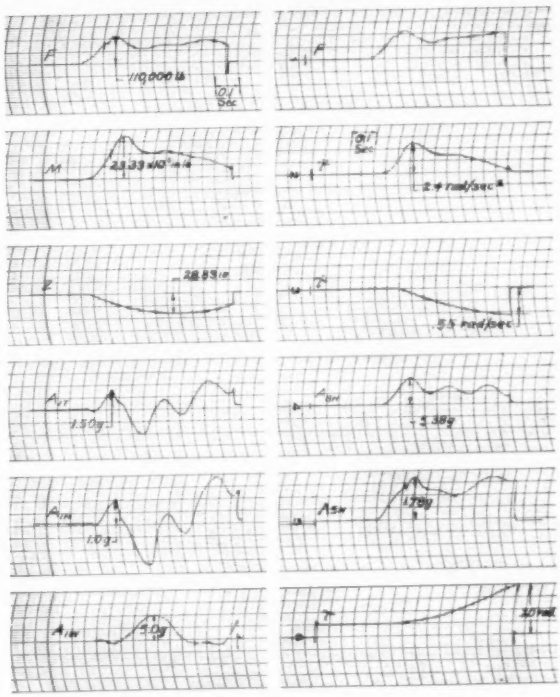

FIG. 3d. REAC solutions to impact problem—flexible case. V_x = 185 ft. per sec., τ_0 = 3°, $\dot{Z}_0$ = 12 ft. per sec.

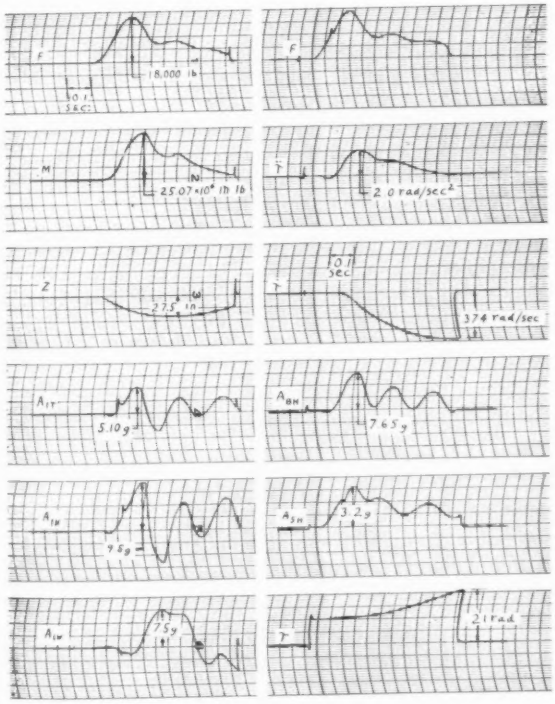

FIG. 3c. REAC solutions to impact problem—flexible case. V_x = 160 ft. per sec., τ_0 = 6°, $\dot{Z}_0$ = 12 ft. per sec.

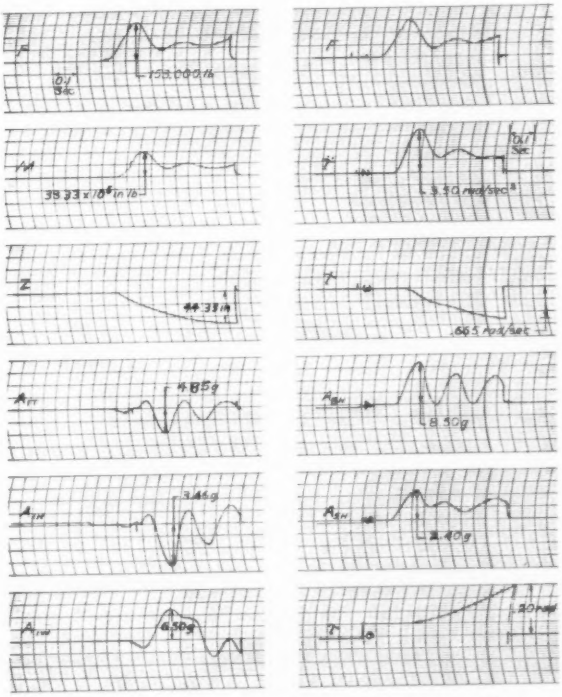

FIG. 3e. REAC solutions to impact problem—flexible case. V_x = 160 ft. per sec., τ_0 = 3°, $\dot{Z}_0$ = 16 ft. per sec.

tion of the time rate of force application and the indicial admittance of the system; thus,

$$x(t) = F_{(s)}A_{(t)} + \int_0^t (dF/dt_1)A(t - t_1)dt_1$$

The response of a mechanical system also may be expressed in terms of the response of each normal vibratory mode to the harmonics of the force. In either approach to the problem, the rate of force application or the harmonic content of the force, in conjunction with the frequency spectrum of the system, has an important bearing on the response of the system. For aircraft of high rigidity, that is, having a fundamental frequency well above $1/4t_{max}$ cycles per sec. (this is the frequency of a harmonic function which will peak at t_{max}) of the impact forcing function, the most severe distributed structural loads are generally obtained in the hardest impact condition. For the flexible aircraft having a frequency close to or within the frequency of $1/4t_{max}$, it is possible for maximum local loads to be ob-

TABLE 1
Analytical Data for the Flexible Airplane

V_x	τ_0	Z_0	F(lb)	M(in.-lb)	Z(in)	r(rad)	$\dot{r}$	$\ddot{r}$	$A_{1H}(\delta)$	A_{5H}	A_{8H}	A_{1W}	A_{1T}	$Z_{at}F_{max}$	$T_{F_{max}}$	Landing No.
185	3	4	25,000	3.83×10^6	12.67	.12	.10	.32	.31	.40	.95	.775	.37	12.0	.34	1
		8	64,000	13.0×10^6	19.67	.20	.32	1.28	.875	1.2	2.75	3.15	.95	12.0	.20	2
		12	110,000	23.33×10^6	28.33	.20	.55	2.4	1.00	1.78	5.38	5.00	1.50	13.33	.125	3
	6	4	31,000	2.13×10^6	10.16	.09	.031	.06	.68	.55	.70	1.07	.76	10.0	.325	4
		8	90,000	9.33×10^6	15.33	.14	.06	.48	1.38	1.6	2.40	4.0	1.63	15.33	.225	5
		12	150,000	18.0×10^6	19.66	.198	.18	1.16	2.60	2.45	5.0	6.88	2.95	16.67	.15	6
.160	3	4	23,500	3.83×10^6	13.73	.138	.115	.36	.28	.42	.90	.688	.33	13.33	.45	7
		8	60,000	12.0×10^6	21.73	.198	.346	1.24	.875	1.10	2.56	2.90	1.00	15.33	.20	8
		12	104,000	21.33×10^6	32.0	.215	.565	2.26	1.05	.170	5.20	4.50	1.00	16.67	.125	9
		16	153,000	33.33×10^6	44.33	.20	.665	3.50	3.46	2.40	8.50	6.50	4.85	16.67	.10	10
	6	4	28,500	53.33×10^6	11.33	.09	.017	.048	.575	.49	.635	.95	.65	11.00	.325	11
		8	83,000	9.13×10^6	17.07	.148	.084	.52	1.32	1.48	2.40	3.66	1.60	15.33	.20	12
		12	130,000	16.33×10^6	21.73	.21	.22	1.16	2.08	2.30	4.15	6.0	2.60	18.0	.15	13
		16	180,000	25.07×10^6	27.5	.21	.374	2.0	9.5	3.2	7.65	7.5	5.10	20.83	.125	14
	9	4	31,000	1.47×10^6	10.27	.12	.25	.11	.80	.55	.56	1.05	.85	10.0	.325	15
		8	83,000	5.93×10^6	16.27	.135	.038	.16	1.70	1.50	1.75	3.55	1.87	16.0	.225	16
		12	135,000	11.83×10^6	20.67	.173	.04	.43	2.94	2.35	3.60	6.20	3.20	17.33	.16	17
		16	185,000	18.53×10^6	26.67	.20	.14	.94	4.88	3.04	6.5	7.0	6.0	24.0	.15	18
135	3	4	23,400	4.1×10^6	14.67	.15	.133	.36	.24	.39	.85	.69	.28	14.0	.40	19
		8	55,000	11.13×10^6	25.33	.21	.36	1.12	.80	.90	2.25	2.80	.90	16.0	.20	20
		12	95,000	20.33×10^6	39.17	.20	.525	2.05	.55	1.45	4.6	4.15	.75	14.17	.125	21
		16	140,000	31.67×10^6	53.33	.21	.60	3.25	3.5	2.20	7.88	6.0	4.5	16.67	.10	22
	6	4	26,000	2.13×10^6	12.27	.105	.009	.072	.50	.45	.75	.83	.57	12.00	.35	23
		8	72,000	8.53×10^6	18.67	.17	.11	.52	1.15	1.30	2.2	3.33	1.35	17.33	.25	24
		12	120,000	16.4×10^6	23.33	.20	.25	1.12	2.30	1.96	4.15	5.25	2.90	20.00	.175	25
		16	160,000	23.67×10^6	33.33	.20	.40	1.90	3.06	2.70	6.9	6.65	4.25	23.33	.15	26
	9	4	29,200	1.60×10^6	11.87	.13	.051	.086	.65	.51	.525	.95	.69	11.8	.375	27
		8	80,000	6.13×10^6	17.60	.15	.019	.124	1.72	.130	.176	3.2	.196	16.67	.225	28
		12	120,000	11.2×10^6	23.33	.194	.075	.472	2.8	1.92	3.4	5.25	3.10	20.00	.15	29
		16	162,000	17.33×10^6	30.0	.20	.188	.96	3.8	2.64	5.75	6.5	4.70	23.33	.15	30

tained for impacts other than those having the greatest hydrodynamic force. This condition requires that a range or envelope of impact conditions be examined in order to insure that the most severe loads are utilized in the design of the aircraft structure.

Table 1 shows that a variation of t_{max} was obtained with variations in the rate of descent. The range of t_{max} was from approximately 0.10 sec. for the high rates of descent to approximately 0.40 sec. for the low rates of descent. Figs. 3a to 3e present the shape of the force and moment generated in representative landings. The spikes appearing in these curves resulted from switching equations in the REAC and may be disregarded. It may be noted that the general shape of the forces and of the moments are similar for different impact conditions with only t_{max} changing. Also, it may be seen that some delay in the generation of the moment with respect to the generation of the force was experienced. This delay is caused by the hydrodynamic center of pressure being close to the airplane center of gravity for short wetted lengths. As the wetted lengths become greater, the moment increases at a

TABLE 2
Analytical Data for the Rigid Airplane

V_x	τ_0	Z_0	F(lb)	M(in.-lb)	Z(in)	τ(rad)	$\dot{\tau}$	$\ddot{\tau}$	$A_{1H}(8)$	A_{5H}	A_{8H}	A_{1W}	A_{1T}	$Z_{at}F_{max}$	$T_{F_{max}}$	Landing No.
185	3	4	25,600	3.93×10^6	12.93	.12	.099	.32	.20	.45	.85	.45	.20	12.0	.35	31
		8	68,000	13.67×10^6	20.0	.205	.33	1.304	.74	1.225	2.74	1.25	.75	16.33	.20	32
		12	115,000	23.6×10^6	30.0	.205	.575	2.40	.52	1.97	4.75	1.97	.52	18.33	.14	33
	6	4	32,600	2.27×10^6	10.33	.09	.028	.06	.595	.58	.60	.575	.60	10.0	.30	34
		8	98,000	10.0×10^6	16.0	.14	.063	.504	1.21	1.70	.565	1.70	1.25	15.33	.20	35
		12	157,000	18.67×10^6	21.0	.18	.188	1.184	1.65	2.76	4.00	2.8	1.60	18.33	.15	36
160	3	4	23,800	4.08×10^6	14.33	.13	.115	.376	.166	.45	.87	.46	.18	13.87	.42	37
		8	61,200	12.33×10^6	22.67	.205	.34	1.20	.720	1.10	2.46	.112	.72	16.00	.20	38
		12	102,000	21.33×10^6	33.33	.195	.55	2.20	.45	1.8	4.2	1.82	.45	18.33	.15	39
		16	148,000	32.67×10^6	46.67	.20	.665	3.36	.63	2.6	6.4	2.76	.63	18.33	.10	40
	6	4	29,800	2.27×10^6	11.33	.20	.012	.048	.50	.53	.59	.55	.51	11.33	.35	41
		8	88,000	9.33×10^6	17.60	.15	.083	.524	1.03	1.54	2.18	1.52	1.05	17.00	.225	42
		12	138,000	17.07×10^6	22.67	.21	.218	1.15	1.48	2.4	3.66	2.46	1.48	18.66	.15	43
		16	190,000	25.07×10^6	29.0	.222	.36	1.9	1.90	3.36	5.50	3.36	1.90	17.66	.10	44
	9	4	33,000	1.53×10^6	10.4	.124	.061	.11	.73	.60	.495	.60	.74	10.33	.30	45
		8	91,000	6.53×10^6	16.4	.14	.033	.16	1.60	1.59	1.64	.163	1.62	16.0	.225	46
		12	143,000	12.67×10^6	21.2	.177	.046	.452	2.30	2.56	2.94	2.60	2.32	19.73	.175	47
		16	190,000	18.67×10^6	26.67	.196	.147	.912	3.00	3.44	4.35	3.48	2.96	21.67	.125	48
135	3	4	24,000	4.23×10^6	15.73	.122	.13	.384	.16	.40	.84	.45	.16	14.67	.40	49
		8	56,000	11.33×10^6	26.67	.20	.354	1.12	.675	.95	2.22	1.03	.70	16.67	.20	50
		12	92,000	19.73×10^6	41.0	.20	.52	2.0	.41	1.60	3.84	1.72	.44	18.33	.125	51
		16	138,000	30.00×10^6	56.0	.195	.60	3.06	.60	2.34	5.85	2.46	.60	16.67	.10	52
	6	4	27,400	2.33×10^6	12.67	.11	.009	.072	.425	.485	.57	.50	.425	12.33	.35	53
		8	74,000	8.67×10^6	19.07	.155	.11	.54	.85	1.35	.194	.138	.85	18.0	.225	54
		12	120,000	14.93×10^6	25.33	.195	.246	1.088	1.26	2.10	3.2	2.20	1.25	8.33	.125	55
		16	165,000	22.4×10^6	33.33	21	.40	1.76	1.66	2.96	4.75	3.04	1.74	18.33	.10	56
	9	4	30,600	1.57×10^6	11.60	.13	.05	.084	.64	.54	.475	.55	.65	11.67	.35	57
		8	80,000	6.067×10^6	18.27	.15	.018	.126	1.33	1.42	1.52	1.42	1.36	17.73	.25	58
		12	120,000	11.2×10^6	23.73	.185	.078	.496	1.90	2.20	2.60	2.26	1.90	19.33	.15	59
		16	164,000	16.67×10^6	30.00	.197	.19	.936	2.44	2.96	3.75	3.00	2.42	22.67	.125	60

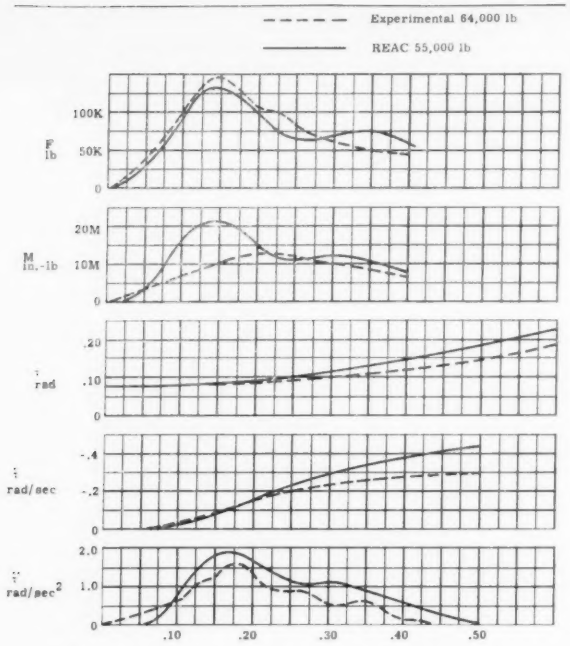

FIG. 4. Experimental vs. REAC; flight 29, landing 4.

greater rate and reaches a maximum at approximately the same instant as the force. Consequently, the loads induced by both the force and the moment must be considered in the landing analysis.

Figs. 3a to 3c show that the frequencies excited in the structure are a function of t_{max} and, hence, the rate of loading. In case 3a, the hull may be seen to respond at both 140 cycles per min. and at 390 cycles per min., the first and third modes of vibration. In case 3b it may be noted for the shorter t_{max} that the hull responds principally in the second vibratory mode at 354 cycles per min. In case 3c having t_{max} of 0.1 sec. the hull response was at 510 cycles per min. which is between the third and fourth modal frequencies.

The maximum accelerations at various locations on the airplane are given in Table 1 for each landing condition, while actual shears and moments were not obtained in this analysis. (The shear and moment distributions as a function of time could have been obtained with the equipment available, but the data obtained illustrate the point.) It may be seen that the maximum positive or negative accelerations were not necessarily obtained at the impact having the maximum force. For instance, the maximum positive bow and wing tip acceleration were obtained for landing 2, while the maximum positive stern and stabilizer tip accelerations and the maximum negative bow acceleration were obtained for landing 10. In landing 18, having the maximum force only, maximum negative accelerations were obtained at the wing tip, the stern, and the center of gravity. These results indicate that even for the rather rigid M-270 airplane an envelope of landing impacts would be necessary for accurate estimation of the landing loads.

A comparison of the maximum forces obtained for the flexible airplane analysis with the maximum forces obtained for the rigid airplane analysis affords an opportunity to study the influence of flexibility on the hydrodynamic loads. Comparing column 7 of Table 1 with column 7 of Table 2, it may be seen that in most instances the maximum forces for the flexible airplane were less than the maximum force for the rigid airplane for the same initial conditions. For the amount of flexibility present in the M-270 airplane, the maximum reduction in force was approximately 7 per cent. For more flexible airplanes, particularly if considerable weight is carried in the wings, it is conceivable that larger reductions in applied force might be obtained. This interaction between the response of the airplane and the hydrodynamic force, and the resulting reduction in applied load may have an important effect on the distributed loading experienced by the aircraft.

In regard to the influence of flexibility on the hydrodynamic moment, no definite trend is exhibited by the data. Since the moment depends among other things on the force and wetted length, there is the possibility of compensating variations in both factors for the rigid airplane case. For more flexible airplanes, appreciable changes in pitching moment may be obtained. When such information becomes available more definite conclusions may be made on the influence of flexibility on the pitching moment.

At this point, some comment on the assumptions and neglected quantities is in order. First, consider the assumption that the distributed hydrodynamic forces are given entirely in terms of the kinematics of the step. For the M-270 airplane this assumption appears

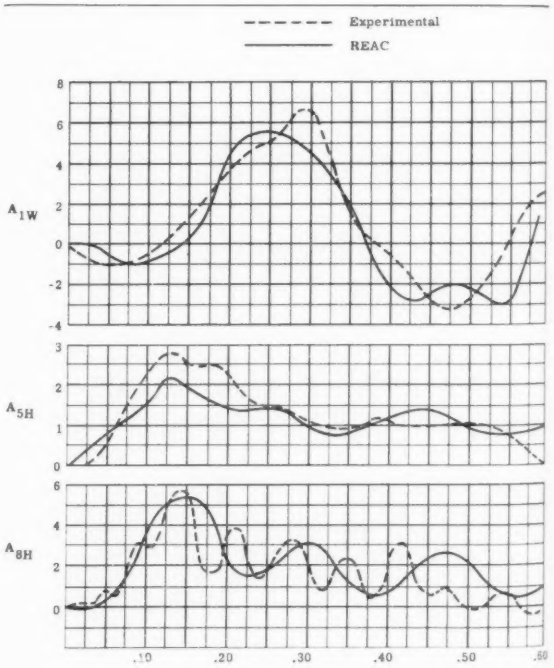

FIG. 5. Experimental vs. REAC; flight 29, landing 4.

valid, since the rigidity of the hull and vibratory modal shapes were such that adequate average values of coefficients could be used. However, for the more flexible hull, it may be necessary to describe the forces in terms of the kinematics of more than one hull station. The use of many hull stations, analogous to aerodynamic strip theory, would permit more accurate application of shape factors and of local kinematics. However, the increase in number of hull stations is accompanied by an increase in computational difficulty and for analog methods may exceed the available machine capacities.

Second, in the formulation of the hydrodynamic forces and moments two quantities have been considered as negligible. These quantities are buoyant force and moment and pitching moment due to water resistance to forward motion of the airplane. In addition, it has been assumed that the weight of the airplane is equal to the lift for the duration of impact. Some consideration of the effect of loss of lift in landing impact has been given in reference 6. The work of this reference, while treating the problem only approximately, indicates that some account for the effects of lift variation may be required. For impacts of long duration or for flexible highly coupled lifting surfaces, the lift variation might enter appreciably into the dynamics of the landing.

As landing impact becomes more critical in determining the design loads for aircraft structure (in addition to the hull bottom) and as more powerful computational methods are used, these forces may be included in the analysis.

Comparison of Experimental and Theoretical Data

Briefly reviewing, the landing impact analysis was performed for symmetric step landings in smooth water. Among the major assumptions of the analysis is that the only hydrodynamic forces acting on the airplane would be approximated by an analytical expression which is a function of the forebody shape and the kinematics of the step. Also, it was assumed that the dynamical response of the airplane is given by the rigid-body response and the superposition of the response of the first four flexible-airplane modes of vibrations. The vibratory analysis of the airplane was performed for a gross weight of 55,000 lbs. It was found after completion of the vibratory analysis that certain changes in the experimental program required the landing tests to be performed at gross weights of 64,000 lbs. and 71,000 lbs. As a consequence, some correction is to be made in interpreting the comparison of the analytical results with the experimental results. A suggested basis for this correction is in terms of the peak loads that might be expected for the rigid airplane as given in reference 6. The loads in accordance with this correction would vary as the ratio of the gross weights taken to the two-thirds power.

The experimental program was formulated for landings at discrete rates of descent, trim angle, and landing speed. However, in actual practice, it was found that only broad ranges of rate of descent and trim angle could be obtained. The analysis (REAC) is a result of discrete initial conditions; there is no direct correspondence between the analytical and nominal experimental initial conditions. One exception to this was landing 4 of flight 29, where all the initial conditions were duplicated in the REAC solution. Rate of descent ($\dot{Z}_0$) was measured relative to the earth and not the water surface, so that even 1/2 to 1-ft. waves or swells could increase or decrease effective $\dot{Z}_0$. Analytical (REAC) data are compared to experimental trends rather than individual test points for this reason.

The comparison of the time variation of the analyti-

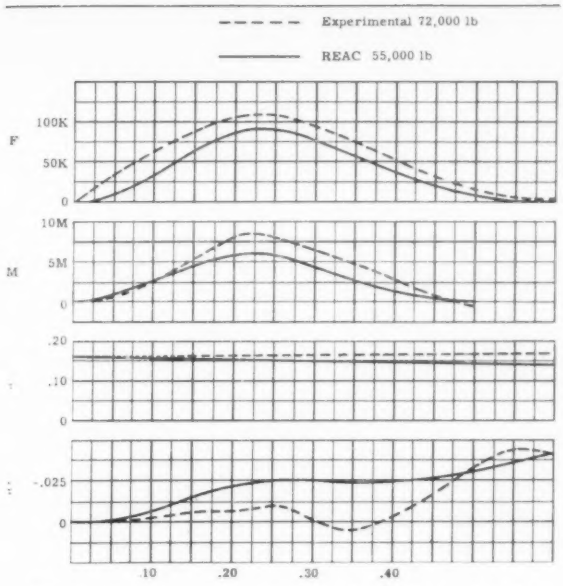

Fig. 6. Experimental vs. REAC; flight 31, landing 8.

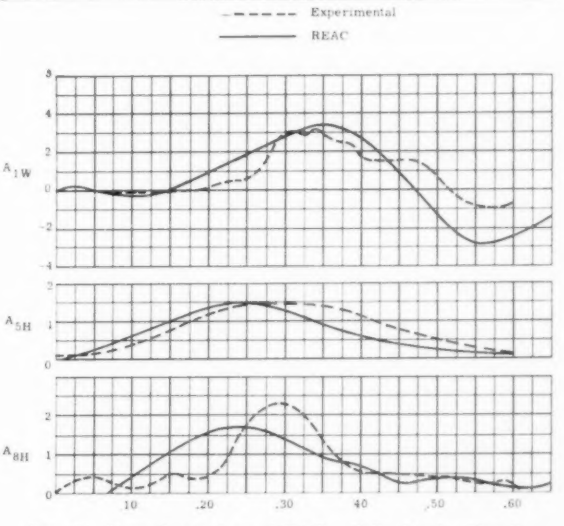

Fig. 7. Experimental vs. REAC; flight 31, landing 8.

cally determined quantities with the experimentally determined quantities for two landings may be made in Figs. 4 through 7. These Figures show the hydrodynamic force, pitching moment, trim pitching velocity, normal accelerations, and, in one instance, the pitching acceleration. In Fig. 4, the analysis was performed for the initial conditions of landing 4, flight 29. This landing represents a rather hard impact, with the variables being of sufficient magnitude that they could be determined with some precision. It is seen that the analytical results are in excellent agreement with the experimental results. The two curves are almost coincident up to t_{max} and are reasonably close after t_{max}. Excellent agreement was also obtained between analytical and experimental results for τ and $\dot{\tau}$ over the greater portion of the impact; some divergence was observed after t_{max} had occurred. In regard to the pitching moment, it may be seen that there is a considerable difference between the curves over the range of time from 0.06 sec. to 0.225 sec. No apparent reason has been found for this discrepancy. The agreement for the pitching acceleration is considered to be good in light of the manner of measurement. The shape of the analytical curve coincides reasonably with the experimental curve and the maximum values are of the same order. A comparison of the analytical acceleration response of the structure as depicted at three stations with the measured response at those stations is shown in Fig. 5. The experimental acceleration response is seen to be predicted quite well by the analytical response. The absence of the higher harmonic content in the analytical response may be attributed to using only four vibratory modes in the structural representation. As may be seen, this harmonic contribution while adding some distortion to the response does not materially affect the correlation between experiment and analysis.

Landing 8 of flight 31 for a gross weight of 72,000 lbs. also offers an opportunity to compare analytical and experimental results. Referring to Fig. 6, again it may be seen that the shape of the experimental curves for both the force and moment is given by the analytical curves. Applying the previously suggested correction for gross weight, the comparable magnitude for the experimental force for the 72,000-lb. airplane corrected to 55,000 lbs. is given by 84 per cent of the magnitude. This reduction brings the experimental force magnitude into excellent agreement with the analytical force magnitude, particularly at the maximum values. The application of the correction to the moments also tends to bring the moment magnitudes into agreement with the analytical moment magnitude. The τ variation for the analytical impact is in agreement also with that of the experiment. Comparison of the pitching velocities showed little or no agreement, and no comparison of pitching accelerations was attempted.

The structural acceleration response for the 72,000-lb. airplane may be seen in Fig. 7. Recalling that the difference in gross weights of the airplane is achieved by the addition of concentrated weights in the hull about the airplane center of gravity, it is to be expected that the vibratory characteristics of the hull would be greatly influenced, and the wing to a lesser degree, by the presence of these weights. Comparing the experimental acceleration response of the 72,000-lb. airplane with the calculated response for the 55,000-lb. airplane, it may be seen that this occurs. The shape and magnitude of the calculated center of gravity and wing tip accelerations are in reasonable agreement with the experimental accelerations. The experimental bow accelerations, apparently showing the influence of the added hull weight, are seen to behave somewhat differently from the calculated accelerations. In light of the above discussion, it is felt that where some basis for comparison with the heavy airplane existed, the analytical results are in agreement with the experimental results.

Figs. 3a to 3d present the maximum values of force and of structural acceleration from the analysis as a function of rate of descent for the different initial trim angles and forward speeds. For purposes of comparison, experimental values having approximately the same initial trim angles and forward speeds are also shown against rate of descent. The analytical results for the structural response of the structure are in good agreement with the experimental data. Reduction of experimental data for the hydrodynamic force was not done for all landings. However, at a forward speed of 160 ft. per sec., the agreement between the analytically predicted force and the experimentally determined force is good in trend and magnitude.

The above comparisons of experimental data with analytical data have shown that the analytically determined results have described accurately the landing impact conditions. The correlation of hydrodynamic forces and moments has indicated that the representation of these forces and moments in the equations of motion has been substantiated. The structural response as given by the equation of motion agrees very well with the actual structural response of the airplane, and indicates that the flexibility of the airplane was adequately represented by the flexible modes of the analysis. The response of the rigid airplane in pitch given in the analysis was in agreement with the experimental observed response. In light of this, it is believed that the hydrodynamic step impact and the dynamic response for the flexible seaplane may be accurately given by the method of analysis presented in this paper.

Conclusions and Recommendations

A theoretical method of computing the dynamical impact landing, including the effects of structural flexibility and continuous trim variation, has been developed in "closed" form. This method, utilizing an electronic analog computer, permits rapid study of a wide range of initial conditions for the impact problem.

The dynamic acceleration response of the M-270

(*Continued on page 216*)

The Compressibility Rule for Drag of Airfoil Noses

R. T. JONES* AND M. D. VAN DYKE*

Ames Aeronautical Laboratory, NACA

SUMMARY

It is shown that the drag of any semi-infinite airfoil section in purely subsonic inviscid flow follows precisely the Prandtl-Glauert compressibility rule. The result for the parabola has application to leading-edge corrections in thin airfoil theory.

INTRODUCTION

SEMI-INFINITE BODIES have long been used to represent the noses of elongated aerodynamic shapes. This role assumes increased importance in compressible flow, because the approximate linearized theory must usually be employed, and it breaks down in the neighborhood of stagnation points.[1] It can be corrected, however, if the flow is known past a simple semi-infinite shape (such as a parabola) that matches the actual body near its nose.[2] Except in incompressible flow, the semi-infinite shape itself cannot be treated exactly, but only by another approximation such as the Janzen-Rayleigh method. However, it is shown in the present paper that for the drag itself the effect of compressibility is known exactly.

DRAG OF A PARABOLA IN SUBSONIC FLOW

As discussed by Prandtl and Tietjens,[3] the drag of a semi-infinite body in inviscid flow is understood to be the limit of the pressure drag on a finite section isolated by a transverse slit into which the surrounding pressure penetrates (see Fig. 1). With this definition, the drag (per unit span) of an infinite parabolic cylinder in incompressible flow along its axis is πR times the dynamic pressure, R being the nose radius.

As the free-stream Mach Number increases to any value short of unity, the entire flow field remains subsonic and hence free of shock waves, because a parabola exerts only a retarding influence on the flow. Local pressures do not, of course, follow the Prandtl-Glauert compressibility rule even approximately near the stagnation point. Nevertheless, the particular weighted average of surface pressures that yields the drag does obey that rule exactly. Thus, at any free-stream Mach Number M less than unity, the drag is

$$D = (1/2)\rho U^2 (\pi R/\sqrt{1 - M^2}) \qquad (1)$$

The proof can be based on consideration of any thin airfoil (say, a symmetrical Joukowski section) of thickness τ. If the leading edge is analytic, it has a nose radius proportional to τ^2. Now suppose the airfoil divided into a short nose section of length τ and a remaining tail section (see Fig. 2), and consider the contribution of each to the total drag. The drag vanishes as τ approaches zero, but the drag coefficient remains finite if referred to a length of order τ^2, such as the nose radius. The nose section disappears in the same limit; but if it is magnified so that its nose radius remains constant, it approaches an infinite parabola.

Over the rear section the slope is uniformly small, so that the linearized theory becomes exact in the limit, giving a drag coefficient proportional to $(1 - M^2)^{-(1/2)}$. Over the nose section linearized theory cannot be applied. However, if the flow is purely subsonic, the total drag is zero according to Theodorsen's extension to subsonic flow of d'Alembert's paradox.[4] Hence the drag of the nose also varies as $(1 - M^2)^{-(1/2)}$.

The same compressibility rule holds for the well-known leading-edge suction force associated with angle of attack. This is clear from a repetition of the preceding argument with the airfoil considered to have an angle of attack α that tends to zero in proportion to the thickness τ. In the limit we obtain asymmetric flow past an infinite parabola (see Fig. 3). One cannot speak of the angle of attack, because the slope of all streamlines tends toward zero far upstream, decaying finally like $[s_0/(-x)]^{1/2}$ where s_0 is some characteristic length. However, one can instead characterize the degree of asymmetry of the flow field far upstream by specifying this parameter s_0 in the dimensionless form s_0/R. (In the limiting process just envisioned, the

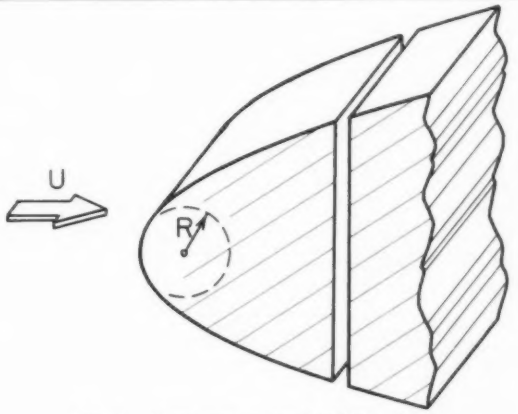

FIG. 1. Flow past a semi-infinite airfoil.

Received December 27, 1956. Revised and received August 20, 1957.

* Aeronautical Research Engineer.

We are indebted to P. A. Lagerstrom for a number of illuminating comments and to Isao Imai for helpful discussions.

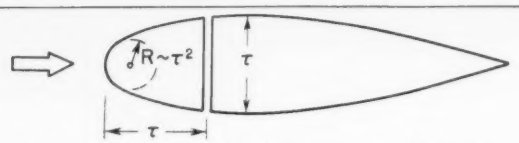

FIG. 2. Division of airfoil into nose and tail sections.

ratio α/τ that was held fixed is proportional to $\sqrt{s_0/R}$.) As indicated in Fig. 3, the stagnation point lies a distance s_0 downstream of the vertex in incompressible flow, but moves nearer the vertex as the Mach Number is increased. Then for a fixed flow pattern far upstream, corresponding to constant s_0, the drag of a parabola is given by

$$D = (1/2)\rho U^2[\pi(R - s_0)/\sqrt{1 - M^2}] \qquad (2)$$

This rule now holds only below the critical Mach Number, which is less than unity for asymmetric flow. At speeds above the critical Mach Number, local supersonic zones appear which undoubtedly terminate in shock waves, and these invalidate the extended d'Alembert paradox on which the argument rests. It may be noted in Eq. (2) that even in nonlinear flow the drag terms are additive.

The rule provides an integral check on detailed approximate solutions. For example, Imai[5] has calculated the Janzen-Rayleigh expansion in powers of M^2 for the surface speed on a parabola in symmetric flow, retaining terms in M^4. Carrying out the complicated integration for the drag gives

$$D/(1/2)\rho U^2\pi R = 1 + (1/2)M^2 + (3/8)M^4 + \ldots \quad (3)$$

This is just the expansion to order M^4 of the Prandtl-Glauert factor $(1 - M^2)^{-(1/2)}$, so that Imai's approximation is in accord with the present rule. Again, Kaplan[6] and others have treated the inclined ellipse by the Janzen-Rayleigh expansion to order M^2, and from that has been extracted the series to M^2 for asymmetric flow past the parabola.[7] Integrating for the drag gives again the compressibility factor $[1 + (1/2)M^2 + \ldots]$. To obtain sufficient accuracy for purposes of correcting compressible thin-airfoil theory for lifting round-nosed wings,[2] this last solution should be extended to include terms in M^4; when that is accomplished the present rule will provide a useful partial check on the formidable calculations involved.

Drag of Other Semi-infinite Bodies

It is clear that the proof given for the parabola will not be invalidated by local changes from parabolic shape near the vertex. Hence any semi-infinite cylinder that approaches a parabola far downstream has (below its critical Mach Number) the drag of that parabola. For example, in Helmholtz' solution for incompressible free-streamline flow past a plate of unit height normal to the stream, the dead-water region far downstream approaches a parabola of nose radius $2/(\pi + 4)$. According to Eq. (1), the dead-water region replaced by a solid body would have a drag of $\pi\rho U^2/(\pi + 4)$, and this is in fact Helmholtz' value for the plate. For the solid body this value would rise with Mach Number as $(1 - M^2)^{-(1/2)}$ until the speed of sound was attained on the surface.

Furthermore, the proof indicates that the rule applies as well to a semi-infinite body that ultimately grows more slowly or more rapidly than a parabola. However, a body has zero drag if it grows more slowly and infinite drag if it grows more rapidly. Hence only the dividing case of a body asymptotic to a parabola provides a significant result.

Similar considerations could be applied to a three-dimensional semi-infinite body—for example, a body of revolution. However, the significant shape that separates axisymmetric bodies of zero and infinite drag has been found by Gurevich[8] to be a peculiar one whose radius varies asymptotically as $x^{1/2}(\ln x)^{-(1/4)}$. As in plane flow, its ultimate form must be the same as that of the dead-water region in axisymmetric free-streamline flow, for which Levinson[9] has indeed found the same form. For a body of noncircular cross section, since the drag depends only on the shape far downstream, where slender body theory becomes accurate, the area rule shows that the drag depends only on the cross-sectional area. Hence, any three-dimensional semi-infinite body having finite drag in subsonic flow grows with cross-sectional area ultimately proportional to $x(\ln x)^{-(1/2)}$.

Application to Subsonic Leading Edges

Thin airfoil theory breaks down near the leading edge of a wing in subsonic flow or in supersonic flow with the edge swept behind the Mach cone. For round edges, the error in pressure is such that the drag can be found correct only by including a leading-edge force associated with the singularity.[1] This force is just the drag of a parabola having the same nose radius, given by Eq. (1). (On swept edges, U and M are to be replaced by their components normal to the edge.) The

(*Continued on page 180*)

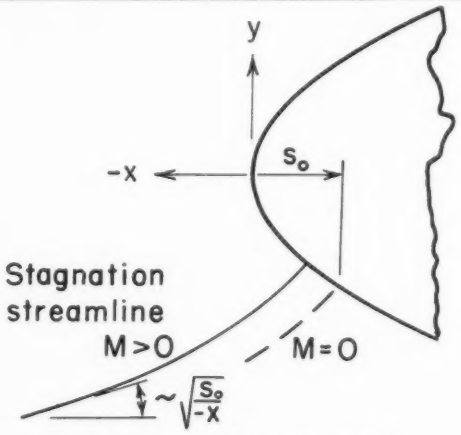

FIG. 3. Asymmetric flow past a parabola.

On Heat Transfer in Laminar Boundary-Layer Flows of Liquids Having a Very Small Prandtl Number†

G. W. MORGAN,* A. C. PIPKIN,** AND W. H. WARNER***
Brown University

SUMMARY

A theoretical study of the heat transfer in plane, incompressible, laminar boundary-layer flows of liquids having a very small Prandtl Number is presented. The analysis is based on the observation that, for very small Prandtl Number, the viscous boundary layer is much narrower than the thermal boundary layer, so that the velocity distribution is essentially potential over most of the thermal layer. A solution is obtained for the first two terms of a series representation for the temperature, for arbitrary potential flow and wall temperature. This general solution is applied to compute the wall temperature gradient for wedge flows with wall temperature varying as a power of the distance from the leading edge, and to compute the recovery temperature for the case of zero heat transfer. The flat plate with constant wall temperature and the insulated flat plate are considered as special cases.

(1) INTRODUCTION

INVESTIGATIONS of the heat transfer in incompressible, laminar boundary layers must usually proceed by means of numerical solutions, due to the complexity of the governing differential equation. Exact solutions in closed form have generally been obtained only when the Prandtl Number σ is equal to one. Analytical results of an asymptotic nature have been obtained for large σ, the approximation being based on the fact that the thermal boundary layer is much narrower than the viscous boundary layer[1, 2] when σ is large. In the present paper we consider the heat-transfer problem for plane boundary-layer flows when σ is very small and obtain the first two terms of a series representation for the quantities of interest. The procedure is based on the fact that the velocity layer is much narrower than the thermal layer when σ is small, so that the velocity field is given essentially by the potential flow solution over the major portion of the thermal layer. This permits a great simplification of the coefficients of the differential equation.

A general solution is obtained for arbitrary potential flow and arbitrary wall temperature in the cooling problem and for arbitrary potential flow in the insulated wall problem. The solutions are given in terms of integrals involving the known velocities and, in the case of the cooling problem, the prescribed wall temperature. The integration is carried out and closed form results are determined for wedge flows, with wall temperature varying as a power of the distance from the leading edge, or with insulated wall.

Fluids having small Prandtl Numbers are, for the most part, liquid metals. The importance of the heat-transfer problem for such liquids is growing rapidly, especially due to the development of nuclear reactor technology. The problem presents many hitherto unsolved questions concerning the physical properties of the flow, such as the extent to which the liquid wets the bounding surface and the appropriate boundary condition for the temperature. These questions are not considered here, the investigation being based on the assumption that the usual boundary conditions apply. It is also assumed that the fluid properties may be considered to be constant.

(2) GENERAL THEORY

The dimensionless energy equation for steady plane flow of a fluid with constant properties expressed in terms of dimensionless coordinates, (x, y), parallel and normal to the boundary, respectively, is

$$\frac{u}{1+Ky}\frac{\partial T}{\partial x}+v\frac{\partial T}{\partial y}=\frac{1}{R\sigma}\left[\frac{1}{(1+Ky)^2}\frac{\partial^2 T}{\partial x^2}+\frac{\partial^2 T}{\partial y^2}-\frac{K'y}{(1+Ky)^3}\frac{\partial T}{\partial x}+\frac{K}{1+Ky}\frac{\partial T}{\partial y}\right]+\frac{U^2}{c_p\Delta TR}\times\left[2\left(\frac{1}{1+Ky}\frac{\partial u}{\partial x}+\frac{Kv}{1+Ky}\right)^2+2\left(\frac{\partial v}{\partial y}\right)^2+\left(\frac{\partial u}{\partial y}+\frac{1}{1+Ky}\frac{\partial v}{\partial x}-\frac{Ku}{1+Ky}\right)^2\right] \quad (2.1)$$

where

$$u=u_1/U,\quad v=v_1/U,\quad T=(T_1-T_\infty)/\Delta T$$
$$x=x_1/L,\quad y=y_1/L,\quad R=UL/\nu$$

U and T_∞ being the constant free-stream velocity and temperature, u_1, v_1 = the velocity components parallel and perpendicular to the wall, T_1 = the temperature, ΔT = a characteristic temperature difference, L = a

Received April 19, 1957.

† The results presented in this paper were obtained in the course of research sponsored by the Office of Naval Research under Contract Nonr 562(07) with Brown University.

* Associate Professor of Applied Mathematics.

** Research Assistant in Applied Mathematics.

*** Formerly, Research Associate in Applied Mathematics. Now, Assistant Professor, Department of Mechanics and Materials, University of Minnesota.

characteristic length, R = the Reynolds Number, σ = the Prandtl Number, ν = the kinematic viscosity, and $K(x)$ = the curvature of the wall.

This equation, together with appropriate boundary conditions, will give rise to a boundary-layer problem provided that the coefficient $R\sigma$ is large. If the thermal layer is thicker than the viscous layer, then u will be of order one in the thermal layer and a stretching of the normal coordinate y by the introduction of a new variable $\xi = (R\sigma)^{1/2}y$ will lead to an equation in which both the convection term $u\,\partial T/\partial x$ and the leading conduction term $\partial^2 T/\partial\xi^2$ are of order one. Hence, using the usual boundary-layer arguments, the thickness of the thermal layer will be of order $(R\sigma)^{-(1/2)}$, which is large compared to $R^{-(1/2)}$, the order of thickness of the viscous layer, whenever $\sigma \ll 1$. Thus, the velocity field will be essentially potential throughout most of the thermal layer, and we therefore write

$$u = u_p + u_c, \quad v = v_p + v_c \tag{2.2}$$

where u_p, v_p are the velocity components of the potential flow solution and u_c, v_c are the corrections which must be added to give the components for the viscous flow. Since we are dealing with a boundary-layer flow, u_c, v_c are taken to be determined approximately by boundary-layer theory.

Since $R\sigma \gg 1$, the thermal layer is very thin compared to a characteristic geometric dimension of the problem and hence the potential velocity components vary only slightly across the width of the thermal layer. We expand them in power series of y about $y = 0$;

$$\left.\begin{aligned} u_p &= u^{(0)}(x) + yu^{(1)}(x) + \ldots \\ v_p &= \qquad\quad yv^{(1)}(x) + \ldots \end{aligned}\right\} \tag{2.3}$$

$v^{(0)}(x)$ being zero since the potential flow satisfies the condition of zero normal velocity at the boundary. Since the potential flow satisfies the continuity equation

$$(\partial u_p/\partial x) + (\partial v_p/\partial y) = 0 \tag{2.4}$$

we have $u^{(0)\prime} = -v^{(1)}$, so that

$$v_p = -yu^{(0)\prime} + \ldots \tag{2.3a}$$

It will be convenient to introduce the variable η, which is the stretched normal coordinate appropriate to the viscous boundary layer; if we set

$$\left.\begin{aligned} \eta &= R^{1/2}y, \quad \tilde{u}_c(x, \eta) = u_c(x, y) \\ \tilde{v}_c(x, \eta) &= R^{1/2}v_c(x, y) \end{aligned}\right\} \tag{2.5}$$

then $\tilde{u}_c$, $\tilde{v}_c$ and η are all of order one in the viscous layer, and $\tilde{u}_c$ vanishes as one leaves the viscous layer.

We now set $$\xi = (R\sigma)^{1/2}y \tag{2.6}$$

substitute Eqs. (2.3), (2.3a), (2.5), and (2.6) in Eq. (2.1), and neglect all terms which have a coefficient $(R\sigma)^{-(1/2)}$ or a higher power thereof. This yields

$$(u^{(0)} + \tilde{u}_c)\,(\partial T/\partial x) + (-\xi u^{(0)\prime} + \sigma^{1/2}\tilde{v}_c) \times (\partial T/\partial\xi) = (\partial^2 T/\partial\xi^2) + (U^2/c_p\Delta T)\,(\partial\tilde{u}_c/\partial\eta)^2 \tag{2.7}$$

We note that to the above order of approximation the potential velocity component parallel to the wall is approximated throughout the thermal layer by its value at the wall (which is also the approximation which arises in the solution of the flow problem), and that the leading term of the potential flow portion of v is taken into account.

Eq. (2.7) together with boundary conditions on T constitute the heat-transfer problem in the boundary layer, the velocity components being assumed known. The problem is prohibitively difficult since the coefficients of the convection terms as well as the nonhomogeneous dissipation term are complicated functions. To simplify the equation we now make use of the fact that the viscous layer is very thin compared to the thermal layer, and that $\tilde{u}_c$ vanishes and $\tilde{v}_c$ approaches a limiting value outside the viscous layer. As usual, because of the linearity of the energy equation, the solution to the cooling problem with dissipation taken into account may be considered to be the sum of two solutions, one being the solution to a cooling problem with dissipation neglected and the other being the solution to a problem in which there is no heat transfer at the wall. It is therefore sufficient to consider those two problems separately, and this will be done in the following to permit a clearer exposition.

(2a) *The Cooling Problem Without Dissipation*

The velocity components being simple functions of ξ outside the viscous layer, but complicated functions within this layer, it is convenient to separate the solution into two components. Outside the viscous layer, let the solution be represented by T_0. To obtain the equation for T_0 we make use of the fact that $\tilde{u}_c(x, \eta)$ vanishes and $\tilde{v}_c(x, \eta)$ is essentially equal to $\tilde{v}_c(x, \infty)$ outside the viscous layer. Hence (omitting the dissipation term) we may write Eq. (2.7) as

$$u^{(0)}\,(\partial T_0/\partial x) + [-\xi u^{(0)\prime} + \sigma^{1/2}\tilde{v}_c(x, \infty)]\,(\partial T_0/\partial\xi) = \partial^2 T_0/\partial\xi^2 \tag{2.8}$$

Let the complete solution be represented as

$$T = T_0(x, \xi) + T_c(x, \eta) \tag{2.9}$$

so that T_c is the correction to T_0 necessary in the viscous layer. Using Eqs. (2.5), (2.7), (2.8), and (2.9), the equation for T_c is

$$(u^{(0)} + \tilde{u}_c)\,(\partial T_c/\partial x) + \tilde{u}_c(\partial T_0/\partial x) + (-\eta u^{(0)\prime} + \tilde{v}_c)\,(\partial T_c/\partial\eta) + \sigma^{1/2}[\tilde{v}_c(x, \eta) - \tilde{v}_c(x, \infty)]\,(\partial T_0/\partial\xi) = \sigma^{-1}\,(\partial^2 T_c/\partial\eta^2) \tag{2.10}$$

The boundary conditions on T are that T assumes a prescribed value $T_w(x)$ on the wall and that the temperature approaches that of the free stream as the normal distance from the wall, ξ, increases. By assumption, T_c vanishes as the viscous layer coordinate η increases. Hence,

$$\left.\begin{aligned} T(x, 0) &= T_0(x, 0) + T_c(x, 0) = T_w(x) \\ T(x, \infty) &= T_0(x, \infty) = 0, \quad T_c(x, \infty) = 0 \end{aligned}\right\} \tag{2.11}$$

Since $\sigma^{1/2}$ is very small, we expand T_0 and T_c in a series of powers of $\sigma^{1/2}$, expecting that the first one or two terms will constitute a good approximation for sufficiently small σ. We note that if terms whose magnitude is of order $\sigma^{1/2}$ relative to the leading terms are to be meaningful while terms of order $(R\sigma)^{-(1/2)}$ have been neglected, we must have $1/R \ll \sigma^2$. Let

$$\left.\begin{aligned} T_0 &= T_0^{(0)} + \sigma^{1/2} T_0^{(1)} + \cdots \\ T_c &= T_c^{(0)} + \sigma^{1/2} T_c^{(1)} + \cdots \end{aligned}\right\}; \tag{2.12}$$

substitute in Eq. (2.8) and equate coefficients of like powers of $\sigma^{1/2}$. This gives

$$u^{(0)}(\partial T_c^{(0)}/\partial x) - \xi u^{(0)\prime} \times (\partial T_0^{(0)}/\partial \xi) = (\partial^2 T_0^{(0)}/\partial \xi^2) \tag{2.13}$$

$$u^{(0)}(\partial T_0^{(n)}/\partial x) - \xi u^{(0)\prime}(\partial T_0^{(n)}/\partial \xi) + \bar{v}_c(x, \infty) \times (\partial T_0^{(n-1)}/\partial \xi) = (\partial^2 T_c^{(n)}/\partial \xi^2) \quad n = 1, 2, \ldots \tag{2.14}$$

In Eq. (2.10), T_0 may be expanded in powers of ξ. If it is assumed that the series converges in some interval $(0, \xi_1)$, it will converge throughout the viscous layer when σ approaches zero, since the value of η corresponding to ξ_1 is $\eta_1 = \sigma^{-(1/2)}\xi_1$. Using $\xi = \sigma^{1/2}\eta$ in the series, we obtain the explicit dependence of T_0 on σ and η in the viscous layer.

The expansions (2.12) are also introduced. Equating coefficients of like powers of $\sigma^{1/2}$, we obtain

$$\left.\begin{aligned} &\partial^2 T_c^{(0)}/\partial \eta^2 = 0, \quad \partial^2 T_c^{(1)}/\partial \eta^2 = 0 \\ &\partial^2 T_c^{(2)}/\partial \eta^2 = (u^{(0)} + \bar{u}_c)(\partial T_c^{(0)}/\partial x) + \\ &(-\eta u^{(0)\prime} + \bar{v}_c)(\partial T_c^{(0)}/\partial \eta) + \bar{u}_c(\partial T_0^{(0)}/\partial x)\big|_{\xi=0} \end{aligned}\right\} \tag{2.15}$$

and more complicated expressions for $\partial^2 T_c^{(n)}/\partial \eta^2$, $n > 2$. Since $T_c^{(n)}$ vanishes as η approaches infinity, so does $\partial T_c^{(n)}/\partial \eta$. These conditions are sufficient to allow direct integration for $T_c^{(n)}$ when $T_c^{(n-2)}$ and $T_0^{(n-2)}$ are known. We see immediately that $T_c^{(0)}$ and $T_c^{(1)}$ are identically zero.

Once we know the value of $T_c^{(n)}$ at the wall, the conditions on $T_0^{(n)}$ are given, using Eq. (2.11):

$$\left.\begin{aligned} T_0^{(0)}(x, 0) &= T_w(x) - T_c^{(0)}(x, 0) = T_w(x) \\ T_0^{(1)}(x, 0) &= -T_c^{(1)}(x, 0) = 0 \\ T_0^{(n)}(x, 0) &= -T_c^{(n)}(x, 0) \qquad (n \geq 1) \\ T_0^{(n)}(x, \infty) &= 0 \qquad (n \geq 0) \end{aligned}\right\} \tag{2.16}$$

The equations for $T_c^{(n)}$ and $T_0^{(n)}$ may be solved in sequence. At each stage the nonhomogeneous terms of the equations and the boundary conditions are completely determined in terms of the solutions already found.

In the following we shall be concerned only with finding the first two terms of the solution, and therefore do not need to be concerned with any $T_c^{(n)}$ equations beyond those given in Eq. (2.15). The equations for $T_0^{(0)}$ and $T_0^{(1)}$ are (2.13) and (2.14), and the boundary conditions are given in Eq. (2.16). The required result is found from Eqs. (2.9), (2.12), and (2.15), with $\xi = (R\sigma)^{1/2}y$ and $\eta = R^{1/2}y$:

$$\left.\frac{\partial T}{\partial y}\right|_{y=0} = (R\sigma)^{1/2}\left.\frac{\partial T_0}{\partial \xi}\right|_{\xi=0} + R^{1/2}\left.\frac{\partial T_c}{\partial \eta}\right|_{\eta=0} = (R\sigma)^{1/2}\left[\sigma^{-(1/2)}\left.\frac{\partial T_c^{(0)}}{\partial \eta}\right|_{\eta=0} + \left(\left.\frac{\partial T_0^{(0)}}{\partial \xi}\right|_{\xi=0} + \left.\frac{\partial T_c^{(1)}}{\partial \eta}\right|_{\eta=0}\right) + \sigma^{1/2}\left(\left.\frac{\partial T_0^{(1)}}{\partial \xi}\right|_{\xi=0} + \left.\frac{\partial T_c^{(2)}}{\partial \eta}\right|_{\eta=0}\right) + 0(\sigma)\right] = (R\sigma)^{1/2}\left[\left.\frac{\partial T_0^{(0)}}{\partial \xi}\right|_{\xi=0} + \sigma^{1/2}\left(\left.\frac{\partial T_0^{(1)}}{\partial \xi}\right|_{\xi=0} - T_w'(x)\int_0^\infty \bar{u}_c d\eta\right) + 0(\sigma)\right] \tag{2.17}$$

It is worth notice that the functional dependence of the result on σ has been determined without actual solution of the equations, and that the leading term is the thermal layer solution for inviscid flow.

A general solution to the order indicated will be given in Section (3).

(2b) *The Insulated Wall, or Thermometer Problem*

The procedure here differs only in detail from that followed in Section (2a). The differences are that the dissipation term is included in the equation for T_c, where ΔT is set equal to U^2/C_p, and that the wall condition is

$$\left.\frac{\partial T}{\partial \xi}\right|_{\xi=0} = 0 \tag{2.18}$$

It is found that $T_0^{(0)}$ vanishes, so that T is of order $\sigma^{1/2}$. It is thus convenient to introduce new variables τ_0, τ_c by the relations

$$T_0 = \sigma^{1/2}\tau_0, \quad T_c = \sigma^{1/2}\tau_c \tag{2.19}$$

so that τ_0 and τ_c are of order one.

The details of the procedure will be omitted; only the final formulation of the problem and the result will be given.

We assume expansions

$$\left.\begin{aligned} \tau_0 &= \tau_0^{(0)} + \sigma^{1/2}\tau_0^{(1)} + \cdots \\ \tau_c &= \tau_c^{(0)} + \sigma^{1/2}\tau_c^{(1)} + \cdots \end{aligned}\right\} \tag{2.20}$$

The equations for $\tau_0^{(0)}$ and $\tau_0^{(n)}$ are the same as those for $T_0^{(0)}$ and $T_0^{(n)}$ in the cooling problem—namely, Eqs. (2.13) and (2.14). The boundary conditions on $\tau_0^{(n)}$ are

$$\left.\begin{aligned}
\left.\frac{\partial \tau_0^{(0)}}{\partial \xi}\right|_{\xi=0} &= -\int_0^\infty \left(\frac{\partial \bar{u}_e}{\partial \eta}\right)^2 d\eta, \quad \tau_0^{(0)}(x, \infty) = 0 \\
\left.\frac{\partial \tau_0^{(1)}}{\partial \xi}\right|_{\xi=0} &= \frac{\partial \tau_0^{(0)}(x, 0)}{\partial x}\int_0^\infty \bar{u}_e d\eta, \quad \tau_0^{(1)}(x, \infty) = 0 \\
\text{and, in general,} \quad \left.\frac{\partial \tau_0^{(n)}}{\partial \xi}\right|_{\xi=0} &= -\left.\frac{\partial \tau_e^{(n+1)}}{\partial \eta}\right|_{\eta=0}, \quad \tau_0^{(n)}(x, \infty) = 0
\end{aligned}\right\} \tag{2.21}$$

The result of interest is the wall temperature.

$$\begin{aligned}
T(x, 0) &= \sigma^{1/2}[\tau_0(x, 0) + \tau_e(x, 0)] \\
&= \sigma^{1/2}\tau_0^{(0)}(x, 0) + \sigma\left[\tau_0^{(1)}(x, 0) - \int_0^\infty \left(\frac{\partial \bar{u}_e}{\partial \eta}\right)^2 \eta d\eta\right] + 0(\sigma^{3/2})
\end{aligned} \tag{2.22}$$

As in the cooling problem, the nature of the dependence of the result on the parameter σ is obtained without solving the equation. The leading term is the solution for inviscid flow, the dissipation appearing as a heat source distribution on the wall.

A general solution for the thermometer problem, for arbitrary potential flow $u^{(0)}(x)$, will be given to the indicated order in Section (4).

(3) Solution of the Cooling Problem

According to our method of approximation, the cooling problem in the absence of dissipation is defined by Eqs. (2.13), (2.14), (2.16), and (2.17). A solution for arbitrary $u^{(0)}(x)$ and $T_w(x)$ will now be determined. Eq. (2.13) may be converted to the one-dimensional heat equation by introduction of new independent variables. Let

$$\left.\begin{aligned}
z &= \int_0^x u^{(0)}(x)dx, \quad \zeta = \xi u^{(0)}(x) \\
T_0^{(j)}(x, \xi) &= \Phi^{(j)}(z, \zeta) \qquad j = 0, 1 \\
T_w(x) &= \Phi_w(z), \quad \frac{\bar{v}_e(x, \infty)}{u^{(0)}(x)} = h(z)
\end{aligned}\right\} \tag{3.1}$$

The equations and boundary conditions become

$$\Phi_z^{(0)} = \Phi_{\zeta\zeta}^{(0)} \tag{3.2}$$

$$\Phi_z^{(1)} = \Phi_{\zeta\zeta}^{(1)} - h(z)\,\Phi_\zeta^{(0)} \tag{3.3}$$

$$\Phi^{(0)}(z, 0) = \Phi_w(z), \quad \Phi^{(0)}(z, \infty) = 0 \tag{3.4}$$

$$\Phi^{(1)}(z, 0) = \Phi^{(1)}(z, \infty) = 0 \tag{3.5}$$

where subscripts z, ζ denote partial differentiation. The desired result can be obtained from Eq. (2.17) by noting that

$$\partial T_0^{(j)}(x, 0)/\partial \xi = u^{(0)}(x)\,\Phi_\zeta^{(j)}(z, 0)$$

To find $\Phi^{(j)}$ we define the Laplace transform with respect to z:

$$\mathfrak{L}\,[\Phi^{(j)}(z, \zeta)] \equiv \varphi^{(j)}(s, \zeta) \equiv \int_0^\infty e^{-sz}\Phi^{(j)}\,dz$$

To transform the equation we shall require to know $\Phi^{(j)}(0, \zeta) = T_0^{(j)}(0, \xi)$. The conditions of the problem demand that $T(0, \xi) = 0$ for all ξ except possibly $\xi = 0$, so that both $T_0^{(0)}(0, \xi)$ and $T_0^{(1)}(0, \xi)$ are zero. At $\xi = 0$, the wall temperature may or may not have a discontinuity depending on whether or not $T_w(0) = 0$. We therefore have

$$\mathfrak{L}\,[\Phi_z^{(j)}(z, \zeta)] = s\varphi^{(j)}(s, \zeta)$$

The equations and boundary conditions become

$$\varphi_{\zeta\zeta}^{(0)} - s\varphi^{(0)} = 0 \tag{3.6}$$

$$\varphi_{\zeta\zeta}^{(1)} - s\varphi^{(1)} = H(s, \zeta) \tag{3.7}$$

where

$$\mathfrak{L}\,[h(z)\,\Phi_\zeta^{(0)}(z, \zeta)] \equiv H(s, \zeta);$$

$$\varphi^{(0)}(s, 0) = \varphi_w(s), \quad \varphi(s, \infty) = 0 \tag{3.8}$$

$$\varphi^{(1)}(s, 0) = \varphi^{(1)}(s, \infty) = 0 \tag{3.9}$$

where $\mathfrak{L}\,[\Phi_w(z)] \equiv \varphi_w(s)$

The solution of Eqs. (3.6) and (3.8) is

$$\varphi^{(0)} = \varphi_w e^{-s^{1/2}\zeta} \tag{3.10}$$

Inversion by convolution yields

$$\Phi^{(0)} = \frac{\zeta}{2\pi^{1/2}}\int_0^z \frac{\Phi_w(z - t)e^{-\zeta^2/4t}}{t^{3/2}}\,dt \tag{3.11}$$

We are interested in $\Phi_\zeta^{(0)}(z, 0)$. If an attempt is made to obtain this function by differentiating Eq. (3.11) and then setting $\zeta = 0$ an integral will be obtained which diverges as a result of the singularity $t^{-3/2}$ at $t = 0$. This is because the process of integration and of letting $\zeta \to 0$ may not be reversed. A different formula may easily be obtained, however, which contains an integral with an integrable singularity. We note that

$$\begin{aligned}
\mathfrak{L}\,[\Phi_\zeta^{(0)}(z, 0)] &= \varphi_\zeta^{(0)}(s, 0) = -s^{1/2}\varphi^{(0)}(s, 0) = -(1/s^{1/2})\,[s\varphi_w(s)] \\
&= -(1/s^{1/2})\{\Phi_w(+0) + \mathfrak{L}[\Phi_w']\}
\end{aligned}$$

where we have written $\Phi_w(+0)$ to avoid an error in case Φ_w has a discontinuity at $z = 0$. Inverting by convolution, we have

$$\Phi_\xi^{(0)}(z, 0) = -\frac{1}{\pi^{1/2}}\left[\frac{\Phi_w(+0)}{z^{1/2}} + \int_0^z \frac{\Phi_w'(z-t)}{t^{1/2}}\,dt\right] \tag{3.12}$$

it being understood that the term $\Phi_w(+0)/z^{1/2}$ is to be omitted whenever $\Phi_w(+0) = T_w(+0) = 0$.

The solution of Eqs. (3.7) and (3.9) for $\varphi^{(1)}$ is

$$\varphi^{(1)} = e^{s^{1/2}\xi}\int_\infty^\xi \frac{He^{-s^{1/2}\xi}}{2s^{1/2}}\,d\xi - e^{-s^{1/2}\xi}\int_\infty^\xi \frac{He^{s^{1/2}\xi}}{2s^{1/2}}\,d\xi + e^{-s^{1/2}\xi}\int_\infty^0 \frac{H(e^{s^{1/2}\xi} - e^{-s^{1/2}\xi})}{2s^{1/2}}\,d\xi \tag{3.13}$$

To obtain $\Phi_\xi^{(1)}(z, 0)$ we note that

$$\varphi_\xi^{(1)}(s, 0) = -\int_0^\infty H(s, \xi)e^{-s^{1/2}\xi}\,d\xi \tag{3.14}$$

Now

$$\Phi_\xi^{(1)}(z, 0) \equiv \mathfrak{L}^{-1}\left[\varphi_\xi^{(1)}(s, 0)\right] = -\mathfrak{L}^{-1}\int_0^\infty H(s, \xi)e^{-s^{1/2}\xi}\,d\xi$$

If we assume that it is permissible to place the inversion operator inside the integral, then, inverting by convolution and recalling the definition of H in Eq. (3.7), we obtain

$$\Phi_\xi^{(1)}(z, 0) = -\int_0^\infty\int_0^z h(z-\omega)\Phi_\lambda^{(0)}(z-\omega, \lambda) \times (\lambda/2\sqrt{\pi\omega^3})\,e^{-\lambda^2/4\omega}\,d\omega d\lambda$$

We now substitute for $\Phi_\xi^{(0)}(z, \xi)$ using Eq. (3.11). Then, again reversing the order of integration so as to integrate first over λ from zero to infinity, and finally transforming the integral over t from zero to $z - \omega$ by integration by parts, we find

$$\Phi_\xi^{(1)}(z, 0) = \frac{\Phi_w(+0)}{\pi z}\int_0^z h(z-\omega)\left(\frac{z-\omega}{\omega}\right)^{1/2} d\omega + \frac{1}{\pi}\int_0^z\int_0^{z-\omega}\left(\frac{t}{\omega}\right)^{1/2} \times \frac{h(z-\omega)\Phi_w'(z-\omega-t)}{t+\omega}\,dtd\omega \tag{3.15}$$

where it is again understood that the first term will vanish whenever $\Phi_w(+0) = 0$.

The functions Φ_w and h can be determined from their definitions (3.1) for any given flow and prescribed wall temperature T_w. The integrals in Eqs. (3.12), (3.15) can then be evaluated in closed form, if possible, or numerically. The integral appearing in Eq. (2.17) depends only on the flow, not on the wall temperature, but will generally have to be evaluated numerically. The results for $\Phi_\xi^{(0)}(z, 0)$ and $\Phi_\xi^{(1)}(z, 0)$ are then used in conjunction with the relation

$$\partial T_0^{(j)}(x, 0)/\partial\xi = u^{(0)}(x)\,\Phi_\xi^{(j)}(z, 0)$$

and the definition (3.1) of z to determine the desired wall temperature gradient from the formula (2.17).

(3a) *The Cooling Problem for $u^{(0)} = x^m$ and $T_w = x^\beta$*

As an example of the application of the general solution obtained above, we compute the wall temperature gradient for wedge flows having the potential velocity component

$$u_1(x, 0) = U x^m, \quad 0 \le m \le 1$$

at the wall, and a wall temperature given by

$$T_1 = T_\infty + \Delta T\, x^\beta, \quad \beta \ge 0$$

Hence,

$$u^{(0)}(x) = x^m, \quad 0 \le m \le 1; \qquad T_w(x) = x^\beta, \quad \beta \ge 0 \tag{3.16}$$

Observe that there is no characteristic length L in this problem, but we may, for convenience, retain the analysis in the previous form, with $L = 1$. From Eq. (3.1)

$$z = [x^{m+1}/(m+1)], \quad \Phi_w(z) = [(m+1)z]^{\beta/(m+1)} \tag{3.17}$$

The zero-order solution may be computed immediately from Eq. (3.12), the integral representing a Beta function. Expressing the latter in terms of Gamma functions, we find, when $\beta \ne 0$, and hence, when $\Phi_w(+0) = 0$,

$$\Phi_\xi^{(0)}(z, 0) = -\frac{\Phi_w(z)}{z^{1/2}}\,\frac{\Gamma\{1 + [\beta/(m+1)]\}}{\Gamma\{(1/2) + [\beta/(m+1)]\}}, \quad \beta \ne 0 \tag{3.18}$$

When $\beta = 0$, Φ_w' vanishes and the integral in Eq. (3.12) vanishes, while $\Phi_w(+0) = 1$, giving

$$\Phi_\xi^{(0)}(z, 0) = -(1/\pi^{1/2}z^{1/2}), \quad \beta = 0 \tag{3.19}$$

As is to be expected, the result (3.18) approaches, when $\beta \to 0$, the result (3.19) for $\beta = 0$. To the zero order of approximation the wall temperature gradient is

$$\frac{\partial T(x, 0)}{\partial y} = -(R\sigma)^{1/2}\frac{x^{\beta+m/2}}{x^{1/2}}\,(m+1)^{1/2} \times \frac{\Gamma\{1 + [\beta/(m+1)]\}}{\Gamma\{(1/2) + [\beta/(m+1)]\}}, \quad \beta \ne 0 \tag{3.20}$$

Specializing to the flat plate with constant wall temperature, we set $m = 0$ and $\beta = 0$. Then

$$\frac{\partial T(x, 0)}{\partial y} = -\frac{(R\sigma)^{1/2}}{(x\pi)^{1/2}}, \quad m = 0, \quad \beta = 0 \tag{3.21}$$

or $$\partial T(x, 0)/\partial y_1 = -(U\sigma/\nu\pi x_1)^{1/2}$$

To determine the first-order approximation we need information about the velocity distribution within the

boundary layer. The boundary-layer solution for the velocity components may be written in terms of the similarity variable γ

$$\left.\begin{aligned} u &\cong u^{(0)} + u_e = x^m f'(\gamma; m) \\ v &\cong -yu^{(0)\prime} + R^{-(1/2)}\bar{v}_e = \\ &\quad -(1/2)R^{-(1/2)}x^{(m-1)/2}[(m+1)f(\gamma; m) + \\ &\qquad (m-1)\,\gamma f'(\gamma; m)] \end{aligned}\right\} \quad (3.22)$$

where

$$\gamma = R^{1/2}x^{(m-1)/2}y, \quad \text{or} \quad \gamma = x^{(m-1)/2}\eta$$

and $f(\gamma; m)$ satisfies the equation and boundary conditions

$$m(f')^2 - [(m+1)/2]ff'' = m + f'''$$

$$f(0) = f'(0) = 0, \quad f'(\infty) = 1$$

The asymptotic behavior of f for large γ is $f \sim \gamma - \alpha$ where α depends only on m.

Now $u_e = x^m[f' - 1]$, so that

$$\int_0^\infty \bar{u}_e(x, \eta)d\eta = x^{(1-m)/2}\int_0^\infty u_e d\gamma = -\alpha x^{(m+1)/2} \quad (3.23)$$

From Eq. (3.22), we find for $\gamma \to \infty$

$$\bar{v}_e(x, \infty) = [\alpha(m+1)/2]\,x^{(m-1)/2} \quad (3.24)$$

and, hence,

$$h(z) = \bar{v}(x, \infty)/u^{(0)}(x) = \alpha(m+1)^{1/2}/2z^{1/2} \quad (3.25)$$

The integrals in Eq. (3.15) must now be computed. When $\beta = 0$ the second integral vanishes since Φ_w is a constant, and $\Phi_w(+0) = 1$. This gives

$$\Phi_\zeta^{(1)}(z, 0) = \alpha(m+1)^{1/2}/\pi z^{1/2}, \quad \beta = 0 \quad (3.26)$$

When $\beta \neq 0$, $\Phi_w(+0) = 0$ and only the second term in Eq. (3.15) remains. It has been possible to evaluate this integral in the special case when $2\beta/(m+1) = n$, where n is a positive integer. The calculation must be omitted to conserve space. The result is

$$\Phi_\zeta^{(1)}(z, 0) = \alpha(m+1)^{(n+1)/2} \times \left\{\frac{\Gamma^2[1 + (n/2)]}{\Gamma^2[(1/2) + (n/2)]} - \frac{n}{2}\right\} z^{(n-1)/2} \quad (3.27)$$

We have not succeeded in establishing that this relation also holds for noninteger values of n—i.e., for arbitrary $2\beta/(m+1)$. It may be noted, however, that if we formally let $\beta \to 0$—i.e., $n \to 0$—in Eq. (3.27) the limiting result agrees with that given by Eq. (3.26) for $\beta = 0$. The wall temperature gradient now becomes

$$\frac{\partial T(x, 0)}{\partial y} = -(R\sigma)^{1/2}\frac{x^{\beta+m/2}}{x^{1/2}}\left((m+1)^{1/2}\frac{\Gamma[1 + (n/2)]}{\Gamma[(1/2) + (n/2)]} - \sigma^{1/2}\alpha\left\{(m+1)\frac{\Gamma^2[1 + (n/2)]}{\Gamma^2[(1/2) + (n/2)]} - \frac{n}{2}\right\}\right) + 0(\sigma^{3/2}) \quad (3.28)$$

For the special case of the flat plate with constant wall temperature we have

$$\partial T(x, 0)/\partial y = -[(R\sigma)^{1/2}/(\pi x)^{1/2}]\,[1 - \sigma^{1/2}(\alpha/\pi^{1/2})] + 0(\sigma^{3/2}) \quad (3.29)$$

Inserting the value 1.721 for α (see reference 3, p. 136), we have

$$-(x/R)^{1/2}\,[\partial T(x, 0)/\partial y] = 0.564\sigma^{1/2} - 0.547\sigma + 0(\sigma^{3/2}). \quad (3.30)$$

The right-hand side of Eq. (3.30) is plotted as a function of σ in Fig. 1. The results computed numerically by E. Pohlhausen[4] are shown, and E. M. Sparrow's approximation[5] based on the Kármán-Pohlhausen method is also given. The present results are in general agreement with Sparrow's at very low σ, with Sparrow's values slightly smaller. Since Sparrow's values for larger σ are also slightly smaller than Pohlhausen's, we may expect that the exact curve should lie higher than Sparrow's throughout the interval. In this special case, the available comparison with Pohlhausen's and Sparrow's computations indicates that our zero-order approximate solution is quite good up to, say, $\sigma = 0.03$ and the first-order solution up to, say, $\sigma = 0.1$. Since no comparisons appear to be available for other cases, the above limits might be taken as a first guess for the range of validity of our general solution.

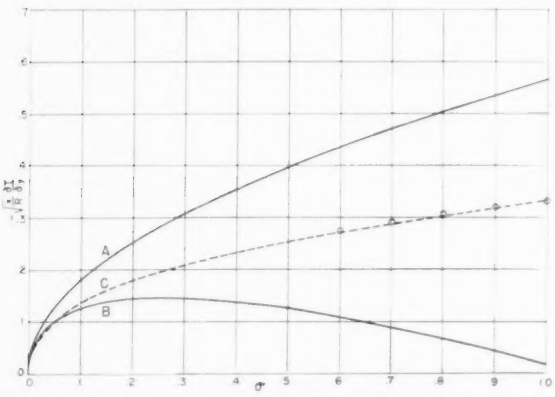

FIG. 1. Wall temperature gradient vs. Prandtl Number in forced convection over a flat plate at constant temperature T_w. $T = (T_1 - T_\infty)/(T_w - T_\infty)$, where T_1 is the temperature and T_∞ the temperature of the free stream; A = first term of series solutions, B = first two terms of series solution, C = Sparrow's result, ⊙ = Pohlhausen's exact results.

It may be of interest to note that the results derived in this Section from the general solution may also be obtained by looking for solutions to the energy equation in terms of the similarity variable γ—i.e., by setting $T_0 = x^\beta\chi(\gamma)$ to obtain an ordinary differential

equation for χ. The boundary conditions to be applied are the same as those for T_0, and the solution when $2\beta \div (m+1)$ is a nonnegative integer is found in terms of Hermite functions. The temperature gradient may then be determined from Eq. (2.17). The results derived by this method agree with those obtained by means of the general solution.

(4) Solution of the Insulated Wall Problem

The differential equations governing this problem are the same as those for the cooling problem, viz., Eqs. (2.13) and (2.14). The boundary conditions are (2.21), and the principal result, the recovery temperature, is to be determined from Eq. (2.22). The method of solution is completely analogous to that employed in the cooling problem. We introduce the new independent variables (z, ζ) by the transformation (3.1) and define

$$\left.\begin{aligned} &\Phi^{(j)}(z,\zeta) \equiv \tau_e{}^{(j)}(x,\xi) \quad (j=0,1)\\ &h(z) \equiv \frac{\bar{v}_e(x,\infty)}{u^{(0)}(x)}, \quad l(z) \equiv \int_0^\infty \bar{u}_e d\eta\\ &D(z) \equiv \frac{1}{u^{(0)}(x)} \int_0^\infty \left(\frac{\partial \bar{u}_e}{\partial \eta}\right)^2 d\eta \end{aligned}\right\} \tag{4.1}$$

The equations to be satisfied by $\Phi^{(j)}$ are the same as those in Section (3)—that is, Eqs. (3.2) and (3.3). The boundary conditions are

$$\Phi_\zeta{}^{(0)}(z,0) = -D(z), \quad \Phi^{(0)}(z,\infty) = 0 \tag{4.2}$$

$$\Phi_\zeta{}^{(1)}(z,0) = l(z)\Phi_z{}^{(0)}(z,0), \quad \Phi^{(1)}(z,\infty) = 0 \tag{4.3}$$

Again solving by using Laplace transforms, we find

$$\Phi^{(0)}(z,0) = \frac{1}{\sqrt{\pi}} \int_0^z \frac{D(z-t)dt}{\sqrt{t}} \tag{4.4}$$

$$\Phi^{(1)}(z,0) = \frac{1}{2\pi} \int_0^z \int_0^\lambda \int_0^\omega \frac{h(\omega)D(t)}{(\lambda - t)^{3/2}(z-\lambda)^{1/2}}\, dt d\omega d\lambda - \frac{1}{\sqrt{\pi}} \int_0^z \frac{\Phi_t{}^{(0)}(t,0)l(t)}{\sqrt{z-t}}\, dt \tag{4.5}$$

(4a) *The Insulated Wall Problem for $u^{(0)} = x^m$*

As an example we apply the general solution to the case $u^{(0)} = x^m$, the wedge flow. In terms of the functions defined in Section (3a) and Eq. (4.1), we have

$$\left.\begin{aligned} h(z) &= \bar{v}_e(x,\infty)/u^{(0)}(x) = \alpha \sqrt{m+1}/2\sqrt{z}\\ l(z) &= \int_0^\infty \bar{u}_e d\eta = -\alpha [(m+1)z]^{1/2}\\ D(z) &= \frac{1}{u^{(0)}(x)} \int_0^\infty \left(\frac{\partial \bar{u}_e}{\partial \eta}\right)^2 d\eta = [(m+1)z]^{[2m/(m+1)]-(1/2)} \int_0^\infty [f''(\gamma;m)]^2 d\gamma \end{aligned}\right\} \tag{4.6}$$

Substitution in Eqs. (4.4) and (4.5) and integration yields

$$\Phi^{(0)}(z,0) = [(m+1)z]^{2m/(m+1)} \frac{\Gamma\{[2m/(m+1)] + (1/2)\}}{\sqrt{m+1}\,\Gamma\{[2m/(m+1)]+1\}} \int_0^\infty [f''(\gamma;m)]^2\, d\gamma \tag{4.7}$$

$$\Phi^{(1)}(z,0) = \alpha[(m+1)z]^{2m/(m+1)} \int_0^\infty [f''(\gamma;m)]^2 d\gamma \tag{4.8}$$

The recovery temperature is given by Eq. (2.22), using Eq. (3.1) and writing $B \equiv 2m/m+1$ for the wedge half-angle in right angles:

$$\frac{T(x,0)}{x^{2m}} = \sigma^{1/2} \frac{\Gamma[B+(1/2)]}{\sqrt{m+1}\,\Gamma(B+1)} \int_0^\infty [f''(\gamma;m)]^2\, d\gamma + \sigma\left[\alpha \int_0^\infty [f''(\gamma;m)]^2\, d\gamma - \int_0^\infty \gamma [f''(\gamma;m)]^2 d\gamma\right] + 0(\sigma^{3/2}) \tag{4.9}$$

The results derived here have been checked at $B = 0, 1/2, 1$ by looking for solutions of the energy equation of the form $T_0 = x^{2m}\chi(\gamma)$.

In the special case of the flat plate, $B = m = 0$, and

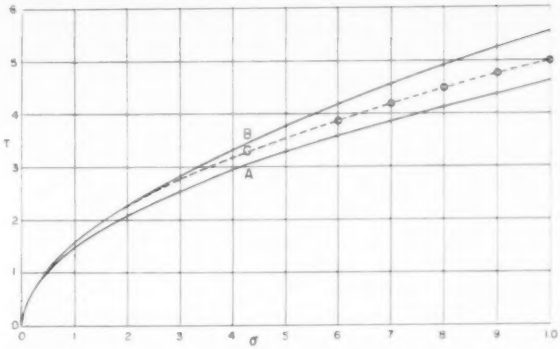

Fig. 2. Recovery factor $T = (T_w - T_\infty)\, C_p/U^2$ vs. Prandtl Number in forced convection over a plate thermometer. T_w is the wall temperature, T_∞ the free-stream temperature; A = first term of series solution, B = first two terms of series solution, C = smooth curve through Pohlhausen's results and low-σ results, and ⊙ = Pohlhausen's exact results.

$$T(x, 0) = \sigma^{1/2}\sqrt{\pi}\int_0^\infty [f''(\gamma; 0)]^2 d\gamma + \sigma\left[\alpha\int_0^\infty [f''(\gamma, 0)]^2 d\gamma - \int_0^\infty \gamma[f''(\gamma; 0)]^2 d\gamma\right] + 0(\sigma^{3/2}) \quad (4.10)$$

The two integrals may be evaluated numerically from known[3] values of $f''(\gamma; 0)$. Using

$$\alpha = 1.721, \quad \int_0^\infty [f''(\gamma; 0)]^2 d\gamma = 0.2607, \quad \int_0^\infty \gamma[f''(\gamma; 0)]^2 = 0.3515 \quad (4.11)$$

we have

$$T(x, 0) = 0.462\sigma^{1/2} + 0.097\sigma + 0(\sigma^{3/2}) \quad (4.12)$$

The right-hand side of this equation is plotted in Fig. 2 and the numerical results by Pohlhausen[4] for $0.6 \leq \sigma \leq 1.0$ are also shown. The smooth curve through Pohlhausen's values and the present low-σ approximation is expected to be an accurate representation of the recovery temperature for the whole interval (0, 1). The apparent range of validity of our zero-order approximation is roughly $\sigma \leq 0.15$, while the first-order solution is good in the range $\sigma \leq 0.30$. As in the cooling problem, we take these limits of validity for the flat plate as a first guess at the limits of validity for the general solution.

The approximation here appears to be valid for much larger σ than the corresponding approximation in the cooling problem. This may be explained by the following reasoning: the accuracy of our method is greater, the smaller the ratio of viscous layer thickness to thermal layer thickness. In the cooling problem, heat enters the fluid only from the wall, producing a thermal layer of some thickness. In the thermometer problem, heat is generated as far away from the wall as the outer edge of the viscous layer, hence the thermal layer is thicker than in the cooling problem by roughly the thickness of the viscous layer. The thickness ratio is thus smaller in the thermometer problem (given R, σ), and the approximation is more accurate.

(5) Conclusion

We have presented a method of solution of the energy equation for laminar forced convection problems with small Prandtl Number. General solutions for very low Prandtl Number were obtained, and these solutions were applied to give specific results for flow over wedges. The results for the flat plate were evaluated numerically and were found to be consistent with existing results, the comparison yielding an indication of the range of validity of our solution.

References

[1] Lighthill, M. J., *Contributions to the Theory of Heat Transfer through a Laminar Boundary Layer*, Proc. Roy. Soc. London, A, Vol. 202, p. 359, 1950.

[2] Morgan, G. W. and Warner, W. H., *On Heat Transfer in Laminar Boundary Layers at High Prandtl Number*, Journal of the Aeronautical Sciences, Vol. 23, No. 10, p. 937, October, 1956.

[3] Goldstein, S., *Modern Developments in Fluid Dynamics*, 1st Ed., Vol. 1, p. 136; Oxford University Press, London, 1938.

[4] Pohlhausen, E., *Der Wärmeaustausch zwischen festen Körpern und Flüssigheiten mit kleiner Reibung und kleiner Wärmeleitung*, ZAMM, Vol. 1, p. 115, 1921.

[5] Sparrow, E. M., *Analysis of Laminar Forced-Convection Heat Transfer in Entrance Region of Flat Rectangular Ducts*, NACA TN 3331, January, 1955.

Compressibility Rule for Drag of Airfoil Noses

(*Continued from page 172*)

derivation of these corrections on the basis of thin airfoil theory was, of course, inadequate since the flow is clearly nonlinear in local regions, but when the derivation is based on the extended d'Alembert paradox the corrections are seen to apply to more realistic fluids provided only that the flow remains of the reversible subsonic type.

References

[1] Jones, Robert T., *Leading-Edge Singularities in Thin-Airfoil Theory*, Journal of the Aeronautical Sciences, Vol. 17, No. 5, pp. 307–310, May, 1950.

[2] Van Dyke, Milton D., *Subsonic Edges in Thin-Wing and Slender-Body Theory*, NACA TN 3343, 1954.

[3] Prandtl, L., and Tietjens, O. G., *Applied Hydro- and Aeromechanics*, McGraw-Hill Book Co., Inc., pp. 118–121, 1934.

[4] Theodorsen, Theodore, *The Reaction on a Body in a Compressible Fluid*, Journal of the Aeronautical Sciences, Vol. 4, No. 6, pp. 239–240, April, 1937.

[5] Imai, Isao, *Application of the M^2-Expansion Method to the Subsonic Flow of a Compressible Fluid Past a Parabolic Cylinder*, Proc. 1st Japan Nat. Cong. Appl. Mech., pp. 349–352, 1952.

[6] Kaplan, Carl, *On the Use of Residue Theory for Treating the Subsonic Flow of a Compressible Fluid*, NACA Rep. 728, 1942.

[7] Van Dyke, Milton D., *Second-Order Subsonic Airfoil Theory Including Edge Effects*, NACA Rep. 1274, pp. 7–8, 1956.

[8] Gurevich, M. I., *Flow Past an Axisymmetrical Semi-Body of Finite Drag*, Prikl. Mat. Mech., Akad. Nauk SSSR, Vol. 11, pp. 97–104, 1947 (Russian, English summary).

[9] Levinson, Norman, *On the Asymptotic Shape of the Cavity Behind an Axially Symmetric Nose Moving Through an Ideal Fluid*, I, Ann. of Math. (2), Vol. 47, pp. 704–730, 1946.

Buckling of Simply Supported Plates Under Arbitrary Symmetrical Temperature Distributions

J. M. KLOSNER* AND M. J. FORRAY**

Polytechnic Institute of Brooklyn and Republic Aviation Corporation

SUMMARY

The plane stress problem for a plate, subjected to an arbitrary symmetrical temperature distribution, is solved for the case where the edges of the plate are assumed to remain straight. The deflection function for the buckled plate is then approximated by the first four terms of a double infinite harmonic series, and the Rayleigh-Ritz procedure is used to determine approximately when initial buckling occurs.

SYMBOLS

A_x, A_y	= effective areas of supporting structure in the x and y directions, respectively
$2a$	= length of plate
$2b$	= width of plate
D	= flexural modulus of rigidity $[D = Et^3/12(1 - \nu^2)]$
E	= average modulus of elasticity of plate material
K_x, K_y	= extensional rigidity parameters in the x and y directions, respectively ($K_x = 1 + 1/\Phi_x$, $K_y = 1 + 1/\Phi_y$)
k_t	= thermal buckling coefficient
N_x, N_y, N_{xy}	= stress resultants
$\bar{T}$	= difference between the average temperature of the supporting structure and room temperature
T_0	= difference between the temperature at the edge of the plate and the average temperature of the supporting structure
T_1	= difference between the temperature at the center of the plate and the plate edges
t	= thickness of plate
α	= coefficient of linear expansion at average temperature of the plate
ν	= Poisson's ratio
Φ_x, Φ_y	= ratios of extensional rigidities of effective area of supporting structure to the skin in the x and y directions, respectively ($\Phi_x = A_x\bar{E}/btE$, $\Phi_y = A_y\bar{E}/atE$)

Bars over letters refer to supporting structure

INTRODUCTION

THE WINGS of an airplane flying at supersonic speeds are aerodynamically heated to high temperatures. In the initial stages of heating the temperature of the skin is nonuniform and higher than the temperature of the supporting interior structures. Buckling of the skin may follow since, for example, the cooler interior structure will prevent the skin from expanding freely.

It is assumed that the supports remain straight, do not deflect transversely, and offer no rotational stiffness. In general, the skin and supporting structure may be composed of different materials, with the result that thermal stresses will be induced when the temperature is raised uniformly. The values of the physical constants are taken to be equal to those existing at the average temperature of the skin and of the effective supporting structure, respectively.

THEORY

The equilibrium conditions of a plane stress problem are satisfied if an Airy stress function, ψ, exists such that the stresses are defined as follows:

$$\sigma_x = \frac{\partial^2\psi}{\partial y^2}, \quad \sigma_y = \frac{\partial^2\psi}{\partial x^2}, \quad \tau_{xy} = -\frac{\partial^2\psi}{\partial x \partial y} \tag{1}$$

For a simply-connected region the compatibility expression[1] for the thermoelastic plane stress problem is

$$\nabla^4\psi = -E\alpha\nabla^2 T \tag{2}$$

The temperature distribution T acting on the plate is assumed to be symmetrical about the centerlines of the plate (Fig. 1) and can be expressed as

$$T = \bar{T} + T_0 + \sum_{s=0}^{\infty}\sum_{t=0}^{\infty} T_{st} \cos(s\pi x/a) \cos(t\pi y/b) \tag{3}$$

where $\bar{T}$ is the difference between the average temperature of the supporting structure and room temperature, and T_0 is the difference between the temperature at the edge of the plate and the average temperature of the supporting structure.

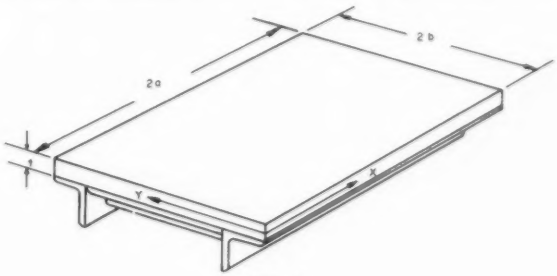

FIG. 1

Received July 11, 1957.

* Research Associate, Polytechnic Institute of Brooklyn.

** Member of Scientific Research Staff, Republic Aviation Corporation.

The stress function

$$\psi = (K_1 y^2/2) + (K_2 x^2/2) + \sum_{s=1}^{\infty} t_{s0} \cos(s\pi x/a) + \sum_{t=1}^{\infty} t_{0t} \cos(t\pi y/b) + \sum_{s=1}^{\infty}\sum_{t=1}^{\infty} t_{st} \cos(s\pi/a)x \times \cos(t\pi/b)y \quad (4)$$

will be shown to satisfy the following conditions: (a) compatibility, [see Eq. (2)], and (b) boundary, in which (1) the edges remain straight, and (2) the average strain along each edge equals the strain in the support—i.e.,

$$\bar{\epsilon}_x = \epsilon_x]_{\text{av.}} = (1/2a)\int_0^{2a} \epsilon_x dx$$

Substituting Eqs. (3) and (4) into Eqs. (2) and (1) results in the following expressions for the stresses:

$$\left.\begin{aligned} \sigma_x &= K_1 - \sum_{t=1}^{\infty} t_{0t}(t\pi/b)^2 \cos(t\pi y/b) - \sum_{s=1}^{\infty}\sum_{t=1}^{\infty} t_{st}(t\pi/b)^2 \cos(s\pi x/a)\cos(t\pi y/b) \\ \sigma_y &= K_2 - \sum_{s=1}^{\infty} t_{s0}(s\pi/a)^2 \cos(s\pi x/a) - \sum_{s=1}^{\infty}\sum_{t=1}^{\infty} t_{st}(s\pi/a)^2 \cos(s\pi x/a)\cos(t\pi/b)y \\ \tau_{xy} &= -\sum_{s=1}^{\infty}\sum_{t=1}^{\infty} t_{st}(s\pi/a)(t\pi/b)\sin(s\pi x/a)\sin(t\pi y/b) \end{aligned}\right\} \quad (5)$$

where

$$\left.\begin{aligned} t_{s0} &= [E\alpha/(s\pi/a)^2]T_{s0} \\ t_{0t} &= [E\alpha/(t\pi/b)^2]T_{0t} \\ t_{st} &= E\alpha T_{st}/[(s\pi/a)^2 + (t\pi/b)^2] \end{aligned}\right\} \quad (6)$$

The linear thermal stress-strain relationship is

$$\left.\begin{aligned} \epsilon_x &= (1/E)(\sigma_x - \nu\sigma_y) + \alpha T \\ \epsilon_y &= (1/E)(\sigma_y - \nu\sigma_x) + \alpha T \end{aligned}\right\} \quad (7)$$

Integration of the stress-strain relation results in the following normal displacement at the edge $x = 2a$:

$$\tilde{u} = (2a/E)[K_1 - \nu K_2 + E\alpha(\bar{T} + T_0 + T_{00})] \quad (8)$$

where $T_{st} = T_{0t}$ when $s = t = 0$ and $\tilde{u}_{x=0} = 0$ is imposed. Similarly,

$$\tilde{v} = (2b/E)[K_2 - \nu K_1 + E\alpha(\bar{T} + T_0 + T_{00})] \quad (9)$$

The resultant forces on any cross section of the plate parallel to the x and y axes are, respectively,

$$\left.\begin{aligned} P_x &= t\int_0^{2b} \sigma_x dy = 2K_1 bt \\ P_y &= t\int_0^{2a} \sigma_y dx = 2K_2 at \end{aligned}\right\} \quad (10)$$

Since there are no external loads acting on the system (plate and supports), the resultant forces in the plate must be equilibrated by the forces acting on the supporting members. Thus the loads acting on the stringers in the x and y directions are

$$\bar{P}_x = -K_1 bt, \quad \bar{P}_y = -K_2 at \quad (11)$$

From Eqs. (8) and (9) it is clear that the displacement of the plate edges depend only upon the constant stresses, K_1 and K_2 and upon the average temperature of the plate, $\bar{T} + T_0 + T_{00}$. The resultant force on any cross section is due to K_1 and K_2 only. Therefore, the nonconstant temperature terms produce stresses which are self-equilibrating. The strain in the plate consists of two parts: (1) a constant strain, due to the average temperature on the plate; and (2) a strain which varies over the plate, but with the restriction that the resultant displacements of the edges of the plate are zero.

The boundary condition for strain compatibility along each edge of the plate is approximated by equating the strain in the supporting members to the average strain of the plate edges. Thus,

$$\bar{\epsilon}_x = \frac{1}{2a}\int_0^{2a} \epsilon_x dx, \quad \bar{\epsilon}_y = \frac{1}{2b}\int_0^{2b} \epsilon_y dy \quad (12)$$

Substituting Eqs. (3), (5), (7), and (11) into Eq. (12) yields

$$K_1 = \frac{[E\alpha(T_0 + T_{00}) + E(\alpha - \bar{\alpha})\bar{T}](\nu + K_y)}{\nu^2 - K_y K_x} \quad (13)$$

$$K_2 = \frac{[E\alpha(T_0 + T_{00}) + E(\alpha - \bar{\alpha})\bar{T}](\nu + K_x)}{\nu^2 - K_y K_x} \quad (14)$$

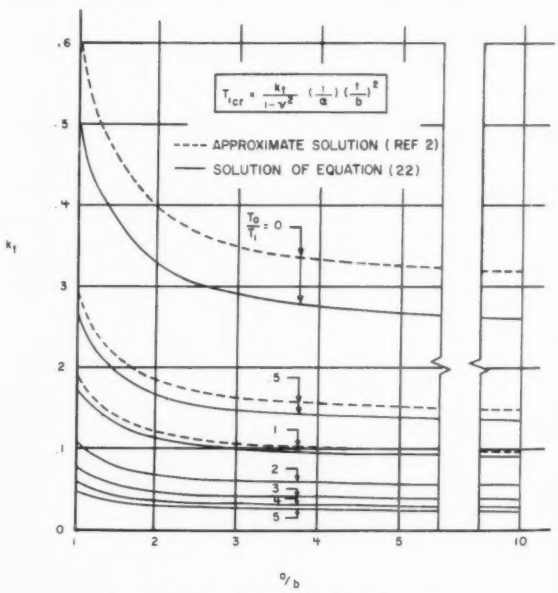

FIG. 2. Thermal buckling coefficient.
$T = T_0 + T_1\{1 - [(x-a)/a]^2\}\{1 - [(y-b)/b]^2\}$,
$\bar{T} = 0$, $K_x = K_y = 1$, $\nu = 0.32$

where $K_x = 1 + (1/\Phi_x)$, $K_y = 1 + (1/\Phi_y)$ (15)

$\Phi_x = A_x\bar{E}/btE$, $\Phi_y = A_y\bar{E}/atE$ (16)

(A_x is equal to the stringer area for a single panel and is equal to 1/2 the area for an interior panel.)

Substituting Eqs. (13), (14), and (6) into Eq. (5) results in the following stresses:

$$\left.\begin{aligned}
\sigma_x &= \frac{[E\alpha(T_0 + T_{00}) + E(\alpha - \bar{\alpha})\bar{T}](\nu + K_y)}{\nu^2 - K_yK_x} - E\alpha\sum_{t=1}^{\infty} T_{0t}\cos\frac{t\pi y}{b} - \\
&\qquad E\alpha\sum_{s=1}^{\infty}\sum_{t=1}^{\infty}\frac{T_{st}}{[(s/t)^2(b/a)^2 + 1]}\cos\frac{s\pi x}{a}\cos\frac{t\pi y}{b} \\
\sigma_y &= \frac{[E\alpha(T_0 + T_{00}) + E(\alpha - \bar{\alpha})\bar{T}](\nu + K_x)}{\nu^2 - K_yK_x} - E\alpha\sum_{s=1}^{\infty} T_{s0}\cos\frac{s\pi x}{a} - \\
&\qquad E\alpha\sum_{s=1}^{\infty}\sum_{t=1}^{\infty}\frac{T_{st}}{[1 + (t/s)^2(a/b)^2]}\cos\frac{s\pi x}{a}\cos\frac{t\pi y}{b} \\
\tau_{xy} &= -E\alpha\sum_{s=1}^{\infty}\sum_{t=1}^{\infty}\frac{T_{st}}{[(s/t)(b/a) + (t/s)(a/b)]}\sin\frac{s\pi x}{a}\sin\frac{t\pi y}{b}
\end{aligned}\right\} \quad (17)$$

Buckling of Plate

The deflection function is approximated by four terms of an infinite series in the form

$$w = \sum_{m=1,3}\sum_{n=1,3} a_{mn}\sin(2\pi/\lambda_m)x\sin(2\pi/\mu_n)y \quad (18)$$

where

$$\lambda_m = 4a/mu, \quad \mu_n = 4b/nv \quad (19)$$

u, v are arbitrary positive integers.

The deflection mode in the x direction, for example, will be symmetrical or antisymmetrical depending upon whether u is odd or even. The problem then is to determine the parameters u, v in such a way as to minimize the load necessary to cause the deformation (18) for each aspect ratio a/b, and each temperature ratio T_0/T_1.

Rayleigh-Ritz Procedure

The total change of energy of the system at buckling is due to (1) the strain energy of bending of the plate, and (2) the total work done by the forces acting in the middle plane of the plate during buckling. The assumption is made that the stresses acting in the middle plane of the plate remain constant during the deflection, and thus the stresses in the supports must also remain constant. Thus the total change of energy is

$$U = \frac{D}{2}\int_0^{2a}\int_0^{2b}\left[\left(\frac{\partial^2 w}{\partial x^2} + \frac{\partial^2 w}{\partial y^2}\right)^2 - 2(1-\nu)\left\{\frac{\partial^2 w}{\partial x^2}\frac{\partial^2 w}{\partial y^2} - \left(\frac{\partial^2 w}{\partial x\partial y}\right)^2\right\}\right]dydx + \frac{1}{2}\int_0^{2a}\int_0^{2b}\left[N_x\left(\frac{\partial w}{\partial x}\right)^2 + N_y\left(\frac{\partial w}{\partial y}\right)^2 + 2N_{xy}\frac{\partial w}{\partial x}\frac{\partial w}{\partial y}\right]dydx \quad (20)$$

Since the total change of energy at buckling must be stationary, then,

$$\partial U/\partial a_{mn} = 0 \qquad (m, n = 1, 3) \quad (21)$$

Substituting Eqs. (17) and (18) into Eqs. (20) and (21) leads to four linear homogeneous simultaneous algebraic equations. The nontrivial solution of these equations leads to the following determinantal equation:

$$\begin{vmatrix} K_{11} & K_{13} & K_{31} & K_{33} \\ L_{11} & L_{13} & L_{31} & L_{33} \\ M_{11} & M_{13} & M_{31} & M_{33} \\ N_{11} & N_{13} & N_{31} & N_{33} \end{vmatrix} = 0 \quad (22)$$

where

$$K_{11} = \frac{1}{192}\left(\frac{b}{a}\right)^3\left[u^2 + v^2\left(\frac{a}{b}\right)^2\right]^2\left(\frac{1}{k_t}\right) + \frac{1}{4\pi^2}u^2\frac{b}{a}\theta_y + \frac{1}{4\pi^2}v^2\frac{a}{b}\theta_x - \frac{1}{3\pi^4}\left[\left(\frac{u}{v}\right)^2\frac{b}{a} + \left(\frac{v}{u}\right)^2\frac{a}{b}\right]$$

$$K_{13} = L_{11} = -\frac{1}{4\pi^2}\frac{u^2v^2t_{(u)}t_{(2v)}}{[u^2(b/a) + 4v^2(a/b)]} + \frac{1}{12\pi^4}\frac{b}{a}\left(\frac{u}{v}\right)^2$$

$$K_{31} = M_{11} = -\frac{1}{4\pi^2}\frac{u^2v^2t_{(2u)(v)}}{[4u^2(b/a) + v^2(a/b)]} + \frac{1}{\pi^2}\frac{u^2v^2t_{(u)(v)}}{[u^2(b/a) + v^2(a/b)]} + \frac{1}{12\pi^4}\frac{a}{b}\left(\frac{v}{u}\right)^2$$

$$K_{33} = N_{11} = -\frac{3}{8\pi^2}\frac{u^2v^2t_{(2u)(v)}}{[4u^2(b/a)+v^2(a/b)]} + \frac{21}{8\pi^2}\frac{u^2v^2t_{(u)(2v)}}{[u^2(b/a)+4v^2(a/b)]}$$

$$L_{13} = \frac{1}{192}\left(\frac{b}{a}\right)^3\left[u^2+9v^2\left(\frac{a}{b}\right)^2\right]^2\left(\frac{1}{k_t}\right) + \frac{1}{4\pi^2}u^2\frac{b}{a}\theta_y + \frac{9}{4\pi^2}v^2\frac{a}{b}\theta_x - \frac{1}{27\pi^4}\left[\frac{b}{a}\left(\frac{u}{v}\right)^2 + 81\frac{a}{b}\left(\frac{v}{u}\right)^2\right]$$

$$L_{31} = M_{13} = \frac{5}{8\pi^2}\frac{u^2v^2t_{(2u)(v)}}{[4u^2(b/a)+v^2(a/b)]} - \frac{1}{\pi^2}\frac{u^2v^2t_{(2u)(2v)}}{[u^2(b/a)+v^2(a/b)]} + \frac{45}{8\pi^2}\frac{u^2v^2t_{(u)(2v)}}{[u^2(b/a)+4v^2(a/b)]}$$

$$L_{33} = N_{13} = -\frac{9}{4\pi^2}\frac{u^2v^2t_{(2u)(3v)}}{[4u^2(b/a)+9v^2(a/b)]} + \frac{9}{\pi^2}\frac{u^2v^2t_{(u)(3v)}}{[u^2(b/a)+9v^2(a/b)]} + \frac{3}{4\pi^4}\left(\frac{a}{b}\right)\left(\frac{v}{u}\right)^2$$

$$M_{31} = \frac{1}{192}\left(\frac{b}{a}\right)^3\left[9u^2+v^2\left(\frac{a}{b}\right)^2\right]^2\left(\frac{1}{k_t}\right) + \frac{9}{4\pi^2}u^2\left(\frac{b}{a}\right)\theta_y + \frac{1}{4\pi^2}v^2\frac{a}{b}\theta_x - \frac{3}{\pi^4}\left[\frac{b}{a}\left(\frac{u}{v}\right)^2 + \frac{1}{81}\frac{a}{b}\left(\frac{v}{u}\right)^2\right]$$

$$M_{33} = N_{31} = -\frac{9}{4\pi^2}\frac{u^2v^2t_{(3u)(2v)}}{[9u^2(b/a)+4v^2(a/b)]} + \frac{3}{4\pi^4}\frac{b}{a}\left(\frac{u}{v}\right)^2$$

$$N_{33} = \frac{27}{64}\left(\frac{b}{a}\right)^3\left[u^2+v^2\left(\frac{a}{b}\right)^2\right]^2\left(\frac{1}{k_t}\right) + \frac{9}{4\pi^2}u^2\frac{b}{a}\theta_y + \frac{9v^2}{4\pi^2}\frac{a}{b}\theta_x - \frac{1}{3\pi^4}\left[\frac{b}{a}\left(\frac{u}{v}\right)^2 + \frac{a}{b}\left(\frac{v}{u}\right)^2\right] \quad (23)$$

where

$$\theta_t = \left\{\frac{T_0+T_{t0}}{T_1} + \left[1-\frac{\bar{\alpha}}{\alpha}\right]\frac{\bar{T}}{T_1}\right\}\left[\frac{(\nu+K_i)}{(\nu^2-K_yK_x)}\right] \quad (i = x, y) \quad (24)$$

and

$$t_{(mu)(nv)} = \frac{1}{ab}\int_0^a\int_0^b T(x,y)\times \cos\frac{mu\pi}{a}x\cos\frac{nv\pi}{b}y\,dydx \quad (25)$$

$$k_t = (1-\nu^2)((b/t)^2\alpha T_{1_cR} \quad (26)$$

Conclusions

The determinantal equation (22) is easily solved for the unknown k_t where u and v may be any positive integers. The smallest value for the temperature is the critical value. The critical value for the temperature corresponds to $u = v = 1$ in all cases for which the stiffnesses of the supporting structure are the same in the x and y directions. This result is consistent with the exact solution for the case of a plate under a uniform temperature (see reference 2).

For the purposes of determining the effect of the nonuniformity of temperature, calculations were performed for the case of a parabolic temperature variation on the plate—i.e.,

$$T = T_0 + T_1\{1-[(x-a)/a]^2\}\{1-[(y-b)/b]^2\} \quad (27)$$

where $\bar{T} = 0$, $K_x = K_y = 1$

The results are presented in Fig. 2. Comparing the two sets of curves of Fig. 2, we observe that accurate results can be obtained if it is assumed that the plate is subjected to a uniform temperature equal to the average temperature of the plate, only for $T_0/T_1 \geq 2$. For $T_0/T_1 < 2$, the effect of the self-equilibrating stress distribution is quite important and the results given in this note are significant. It should be noted that as the stiffnesses of the supports decrease, the greater will be the discrepancy between the two solutions. Of course, in the most severe case where there are no supports ($K_x = K_y = \infty$) then the use of the average value has no significance.

References

[1] Timoshenko, S., and Goodier, J. N., *Theory of Elasticity*; McGraw-Hill Book Co., Inc., New York, 1951.

[2] Timoshenko, S., *Theory of Elastic Stability*, pp. 333; McGraw-Hill Book Co., Inc., New York, 1936.

[3] Gossard, M. L., Seide, P., and Roberts, W. M., *Thermal Buckling of Plates*, NACA TN 2771, August, 1952.

An Approximate Method of Determining Axisymmetric Inviscid Supersonic Flow Over a Solid Body and Its Wake†

SIN-I CHENG*

Avco Manufacturing Corporation

SUMMARY

A simple approximate method is advanced for the determination of a supersonic inviscid axisymmetric flow field over a pointed nose solid body of revolution and over its wake. This method is equally applicable to flow fields with diverging streamlines in the front end of the body and to flow fields with converging streamlines at the rear end of the body and over the wake. The method gives good results for problems with *local* values of the hypersonic parameter $M\varphi$ not larger than 0(1). The effect of rotationality is included. Accuracy of this approximate method is tested for ogive cylinders.

In the approximate calculation, the tangent cone approximation is adopted in the nose region and continued with the present method. The surface pressure coefficient over the front end of the ogive as calculated from (1) "complete characteristic calculations," (2) the present approximation, and (3) other approximations is shown in Fig. 3 for comparison. The present result agrees remarkably well with the "complete characteristic solution." It is also demonstrated that the present results are insensitive to the uncertain factors in the approximate calculation. The time required for calculating a pressure curve as shown in Fig. 3 is approximately two to three hours at most.

There is no "complete characteristic solution" in the region with converging streamlines available for comparison. Neither is there any known approximate scheme proposed for this region. The present method is thus not tested for its accuracy in such regions. From its analytic foundation, the present method is expected to be valid in flow regions with either converging or diverging streamlines. Direct comparison, if possible, is certainly more desirable.

Eggers and Savin[4] showed that in axisymmetric hypersonic flow, the local variation is essentially planar. The present method indicates that such is the case with *local* hypersonic parameter $M\varphi > 1$, but for the lower hypersonic range with the *local* hypersonic parameter $M\varphi \lesssim 1$, the deviation is rather significant.

The simplicity of the present approximate scheme is preserved for body shapes involving discontinuous slopes.

(1) INTRODUCTION

THE METHOD of characteristics for the determination of the inviscid supersonic flow field over a solid body has been extensively developed and is well known. It is usually carried out stepwise partly graphically and partly numerically. It is capable of providing an accurate numerical solution of a specific problem under usual circumstances and is often considered as the "exact" solution. The method is, however, tedious and not convenient for many purposes. We would like to have a fast method of calculating the desired flow property in a restricted region, appropriate for the specific purpose, even if it is less accurate.

The small perturbation theory with or without higher order corrections will often serve this purpose. This is especially true for the planar supersonic flow over a thin airfoil. The most convenient aspect of the approximate result is that the static pressure at a given point is a function only of the local streamline inclination φ up to the order of φ^2. Higher order corrections in different forms are comparatively simple. For the planar flow problems, the differential form of the Prandtl-Meyer relation can be extensively used to evaluate the local changes of flow properties without serious error. The situation of supersonic flow over a slender body of revolution is unfortunately considerably more complicated. The static pressure at a given point on the surface of a smooth pointed body is no longer determined by the local streamline deflection even to the first order but is dependent extensively on the upstream geometry. Neither is the local change of the static pressure simply determined by the local change of the streamline deflection.

If there is a sudden change of the slope of the meridian curve of the body, the linearized solution of the flow field downstream of the slope discontinuity becomes quite complicated. Higher order approximations are even more so.[1] The dependence of the flow field at a given point on the details of the upstream geometry is an essential feature of the axisymmetric problem. This aspect makes it difficult to study an isolated portion of the downstream flow field without referring to the details of the upstream conditions.

There are several other approximate methods relating the local static pressure and the local streamline deflection which may be applied to axisymmetric problems under certain circumstances—for example, the various forms of Newtonian approximation, those of the tangent-cone approximations, and the shock expansion methods.[2] The relative accuracy of these methods has been evaluated.[3] The shock expansion methods take into account the effect of the upstream geometry, while the others are purely local. A weak feature common to all these approximate methods is that they are applicable only in the nose region. There is, as yet, no approximate method available for the de-

Received March 22, 1957.

† The conclusions presented in this paper were obtained in the course of research conducted for the Research and Advanced Development Division, Avco Manufacturing Corporation.

* Consultant. Also Associate Professor, Aeronautical Engineering Department, Princeton University.

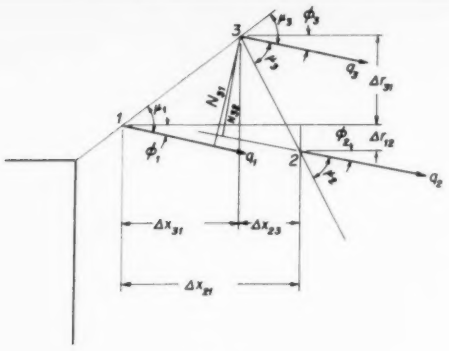

FIG. 1.

termination of the inviscid supersonic flow field with converging streamlines downstream of the maximum cross section of the body. The shock expansion method will give an answer, but its accuracy is doubtful. If one is not willing to use the method of characteristics and/or the approximate method of Lighthill, etc., one must develop some new approximate method for such problems as the determination of the static pressure over the effective wake boundary of the body. It cannot be expected that the approximate method can do away with the overall effect of the upstream geometry in general, like the tangent-cone approximation for the flow in nose region. It is hoped, however, that some overall parameter may be introduced to represent the integrated effect. To have some feeling for such a parameter, the problem with nonuniform inflow over a slender body was first investigated with the method of singularities. With this in mind, the method of characteristics is linearized and then developed into a simple treatment of the supersonic flow field over axisymmetric body and wake. For details of the development and the sample computations, see reference 9.

(2) The Approximate Method—Formulation and Discussion

Let us consider the elementary characteristic net 1–3–2 in a meridian section as shown in Fig. 1 where x is the distance along the axis of symmetry and r is the radial distance from the axis. 1–3 is the positive family characteristics or Mach line, and 3–2 is the negative family characteristics. q is the local flow speed and φ is the angle between the local velocity vector and the axis, measured positive if the streamline is directed away from the axis (negative as shown in Fig. 1). Denote the Mach angle by μ, the flow Mach Number by M with $\beta^2 = M^2 - 1 = \cot^2 \mu$. Also let ν be the angle through which a sonic stream will have to turn in a planar isentropic flow to reach the local Mach Number M—i.e., the Prandtl-Meyer angle given as

$$\nu = [(\gamma+1)/(\gamma-1)]^{+1/2} \tan^{-1} \{[(\gamma-1) \div (\gamma+1)](M^2-1)\}^{1/2} - \tan^{-1}(M^2-1)^{1/2}$$

for gases with constant specific heat ratio γ. The functions ν, μ, β are all tabulated.[6]

Let $\Delta\varphi_{31} = \varphi_3 - \varphi_1$, etc., then the characteristic relations valid along 13 and 32, respectively, may be written as

$$\left.\begin{aligned} \beta_1(\Delta q_{31}/q_1) &= \Delta\varphi_{31} + [\sin\mu_1 \sin\varphi_1 \div \cos(\mu_1+\varphi_1)](\Delta x_{31}/r_1) - \sin\mu\cos\mu\Delta S_{31} \\ \beta_2(\Delta q_{23}/q_2) &= -\Delta\varphi_{23} + [\sin\mu_2 \sin\varphi_2 \div \cos(\mu_2+\varphi_2)](\Delta X_{23}/r_2) - \sin\mu\cos\mu\Delta S_{23} \end{aligned}\right\} \quad (1)$$

provided that r is not zero and that neither of the two Mach lines are normal to the axis. Here S is the entropy of the gas normalized in proper units.

Let us consider the local flow field in which the flow deflection angle varies along the positive family Mach line according to the power law

$$\varphi(r)/\varphi(r_0) = (r_0/r)^{1/s} \quad (2)$$

where s is some constant which will vary throughout the flow field. Large values of s mean small variation of φ. This representation of the variation of φ is appropriate only when $\varphi(r_0) \neq 0$. Assuming Eq. (2) is locally valid, we have

$$\Delta\varphi_{31} = -(\varphi/s)(\Delta r_{31}/r) \quad (3)$$

Through some algebraic manipulations with the characteristic relations (1) and the relation (3) and some geometric identities, assuming locally straight Mach lines for a small net 1–3–2, there is obtained

$$\Delta\nu_{21} = \beta\frac{\Delta q_{21}}{q} = -\Delta\varphi_{21} + \frac{\Delta x_{21}}{r}\left[\frac{\sin\mu\sin\varphi\cos\varphi}{\cos\mu} - \frac{\varphi}{s}\frac{\sin(\mu+\varphi)\sin(\mu-\varphi)}{\cos\mu\sin\mu}\right] - \frac{\Delta r_{21}}{r}\frac{\varphi}{s} \times \frac{\sin(\mu+\varphi)\cos(\mu-\varphi)}{\sin\mu\cos\mu} - \sin\mu\cos\mu S_\psi\Delta\psi_{21} \quad (4)$$

where S_ψ is the local entropy gradient across the streamline in the units of γR for ideal gas, ψ being the stream function. Quantities without subscripts mean the average value over the net.

We shall investigate the possible simplifications of Eq. (4) under varying circumstances.

For ordinary supersonic flows over an unyawed slender body of revolution, the following conditions are satisfied:

$$|\varphi/\mu| << 1, \quad \sin\varphi \cong \varphi, \quad \cos\varphi \cong 1 \quad (5)$$

The first condition in Eq. (5) is the same as $|M\varphi| << 1$, which is the well-known basic requirement of the linearized supersonic flow analysis. There is some difference, however; the $M\varphi$ here is the local value, not the product of the undisturbed stream Mach Number and the semi-nose angle of the body. This local condition is usually less restrictive. Under conditions (5), the relation (4) becomes

$$\Delta\nu_{21} = -\Delta\varphi_{21} + [1-(1/s)]\varphi(\Delta x_{21}/\beta r) - (\varphi/s)(\Delta r_{21}/r) - [\beta/(1+\beta^2)]S_\psi\Delta\psi_{21} \quad (6)$$

which will enable us to determine ν_2 if φ_2 is known at

point 2, provided also that we know the values of s and S_ψ at point 1 and that β is not too small (the flow is not in the upper transonic range).

The physical origin of the four terms on the right-hand side of Eq. (6) is quite clear; the middle two are the axisymmetric corrections. It may also be noted that with $S_\psi = 0$ for isentropic flow, the relation (6) with $s = 2$ reduces to the result obtained by a source distribution along the axis with nonuniform inflow.

For flows with large Mach Numbers φ and μ may be of comparable magnitude and the local value of the hypersonic parameter $M\varphi$ becomes of the order of unity or larger. Practical situations are usually such that both μ and φ are small, so that

$$\left.\begin{aligned} &|\varphi/\mu| \simeq 0(1), \\ &\sin\varphi \cong \varphi, \quad \sin\mu \cong \mu, \quad \cos\varphi \cong \cos\mu \cong 1 \end{aligned}\right\} \tag{7}$$

Then Eq. (4) becomes

$$\begin{aligned} \Delta\nu_{21} = {} & -\Delta\varphi_{21} + [1 - (1/s)]\varphi(\Delta x_{21}/\beta r) - \\ & (\varphi/s)(\Delta r_{21}/r) - [\beta^2(1+\beta^2)S_\psi\Delta\psi_{21}] + \\ & (\varphi/s)(\beta\varphi/r)(\varphi\Delta x_{21} - \Delta r_{21}) \end{aligned} \tag{8}$$

The last term in Eq. (8) is an additive correction to relation (6) due to the hypersonic effect $|\beta\varphi| \gtrsim 0\,(1)$. It is interesting to note that this correction vanishes if the path line 21 is a streamline with $\varphi = \Delta r/\Delta x$. Thus, for the evaluation of the pressure on the surface of the solid body, which is a streamline itself, Eqs. (6) and (8) become identical and the entropy gradient term also drops out as $\Delta\psi_{21} = 0$. While there is little difficulty in carrying these two terms along if we are interested in the flow properties at points not on the same streamline, the following development will be concerned mostly with the particular cases with the path line 2–1 either coinciding with or not deviating significantly from the streamline. For such cases, the equation

$$\begin{aligned} \Delta\nu_{21} = {} & -\Delta\varphi_{21} + [1 - (1/s)]\varphi(\Delta x_{21}/\beta r) - \\ & (\varphi/s)(\Delta r_{21}/r) \end{aligned} \tag{9}$$

may be used throughout the supersonic-hypersonic range.

Before considering these equations any further, we have to get some idea as to the initial magnitude of $1/s$ and its variation throughout the downstream field. $1/s$ is the parameter representing the extent of the local axisymmetric correction on the planar contribution $-\Delta\varphi$ for the determination of the local change of flow speed. It also represents the integrated effect of the axisymmetry and rotationality upstream of the given point as reflected in the local variation of stream deflection along the positive family Mach line. Therefore, $1/s$ must represent some integrated property of the upstream geometry and must vary from point to point.

The supersonic flow field over a pointed, smooth contoured axisymmetric body at zero lift is well known. We can evaluate $1/s = -\partial(\ln r)/\partial(\ln r)$ along the positive family Mach line from the solution with some representative geometrical shape. We find that the linearized slender body theory gives

$$1 - (1/s) = 0[\beta r/(x - \beta r)] = 0(\beta\varphi) \ll 1 \tag{10}$$

If we take the Taylor-Maccoll solution over an unyawed cone and evaluate at the cone surface where $\varphi = \Omega$ we have

$$1/s = (\tan\Omega/\Omega)[1/(1 + \beta\tan\Omega)] \tag{11}$$

which is valid for values of Ω and β not necessarily small. In the limit of $|\beta\Omega| \ll 1$, this result agrees with that from slender body theory. Calculations show that the value of $1/s$ is usually between 0.5 to 0.7, and decreases toward the shock (receding from the solid surface). Furthermore, it may be shown that for a particular type of nonuniform inflow over a blunt section, the linearized (isentropic) supersonic flow theory will lead to a constant value of $1/s = 1/2$. On the other hand, at the point where a streamline becomes parallel to the axis, s must vanish in a definite manner as is obvious from relation (2) if the flow field is locally regular. This last aspect certainly indicates that the functional form of (2) is inappropriate under this circumstance.

Consider (Fig. 2) two neighboring points 1–2 and denote the positive family Mach line through 1 and that through 2 by 1–3–5 and 2–4. Let 32 and 54 be the negative family Mach lines through 3 and 5, respectively. Then write down the characteristic relations along 24, 32, 35, and 54, with both φ and μ sufficiently small to have their sines given approximately by their angles

$$\Delta\nu = \mp\Delta\varphi + \varphi(\Delta x/\beta r) - [\beta/(1+\beta^2)]S_\psi\Delta\psi \tag{12}$$

Introduce the definitions

$$\left.\begin{aligned} \Delta\varphi_{53} &= -(\varphi_3/s_3)(\Delta r_{53}/r) \\ \Delta\varphi_{42} &= -(\varphi_2/s_2)(\Delta r_{42}/r) \end{aligned}\right\} \tag{13}$$

and eliminate ν's. Then take the limit that $4 \to 2$ and $5 \to 3$. After dropping higher order small terms and letting

$$\kappa = [1 - (2/s)]\varphi \tag{14}$$

we obtain

$$\begin{aligned} (\partial\kappa/\partial x)_p = {} & (\partial\kappa/\partial r)_+^{\,} [(\mu^2 - \varphi^2)/2\mu] + \\ & [(\mu + \varphi)/2\mu]\varphi_+^{\,} + [(\kappa - \varphi)/2](1/r) \times \\ & {}_+^{\,}[(\mu^2 - \varphi^2)/2\mu] - [(\mu - \varphi)/2\mu]\varphi_+^{\,} \end{aligned} \tag{15}$$

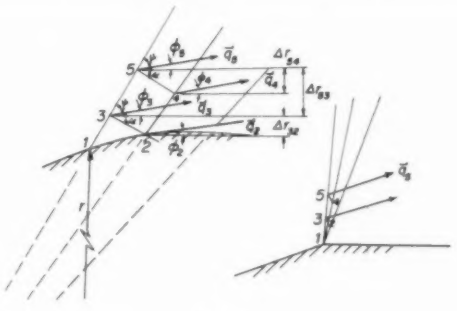

FIG. 2.

where subscript p indicates differentiation along the path 2–1 and subscript $+$ indicates differentiation along a positive family Mach line. From this relation, we can infer that the fractional variation of κ is of the order of μ or of φ if both of them are sufficiently small. Accordingly, a rough approximation will be taken that

$$\kappa = [1 - (2/s)]\varphi = \text{constant} \tag{16}$$

This relation is not in contradiction with the previous observation that $s = 2$ represents a stationary value of s in a particular linearized isentropic supersonic flow field.

The simple relation (16) certainly cannot be a valid approximation in the immediate vicinity of $\varphi = 0$ because the postulated variation of φ in the form of relation (2) loses its significance. s must vanish as φ approaches zero if the relation (2) implies a nonuniform stream. In this respect, the rough approximation (16) is at least qualitatively compatible in requiring s to vanish with φ if κ is a nonzero constant. In fact, if we adopt for this region a more reasonable description of the φ variation along the Mach line, in terms of a parameter k, as

$$\varphi = \varphi_1 + k_1[(r - r_1)/r_1] \tag{17}$$

we obtain a relation identical with Eq. (15) with κ replaced by k. This indicates that it may be feasible to adopt the limiting definition

$$\lim_{\varphi \to 0} [-(\varphi/s)] = \lim_{\varphi \to 0} \kappa = k \tag{18}$$

and let relation (16) be approximately valid even when the streamline locally becomes parallel to the axis of symmetry.

It cannot be overemphasized here that Eq. (16) must be regarded more as an empirical relation selected for convenience rather than analytical consequence even if $[\partial(\ln \kappa)/\partial r]_+$ is, at its maximum, $0(\varphi)$. In practical applications, neither μ nor φ is sufficiently small to warrant the order of magnitude. Consequently, reasonable numerical accuracy can be expected only when the axisymmetric contributions (involving φ/s) may be considered as corrections to the planar contribution.

Eq. (9) may be written, for $\Delta\varphi_{21} \neq 0$ and $\varphi \neq 0$, as

$$\Delta\nu_{21} = -\Delta\varphi_{21}\left(1 - (k_p\varphi/\beta r)\left\{1 - [(1 + \beta\varphi)/s]\right\}\right) \tag{19}$$

where k_p is the local radius of curvature of the streamline through point 1, the second term being the ratio of the axisymmetric contribution to the planar contribution in the determination of $\Delta\nu$. Regardless of the magnitude of $\beta\varphi$, the factor $\varphi[1 - (1 + \beta\varphi/s)]$ is $0(\kappa)$, under the restriction (16), which is determined by the initial value of κ. According to the approximate scheme proposed later for a pointed nose body, the tangent cone approximation will be used with

$$|\kappa_0| = |\varphi_0(\beta_0\varphi_0 - 1)/(1 + \beta_0\varphi_0)| < |\varphi_0|$$

Thus, $k_p\varphi_0/\beta\varphi_0(r/\varphi_0)$ determines the relative importance of the axisymmetric correction. It is then apparent that, for a curved convex body where $k_p\varphi_0/(r/\varphi_0)$ is usually less than unity, the axisymmetric correction is relatively unimportant when $\beta\varphi_0$ becomes large. This is in agreement with the result of Eggers and Savin[4] that axisymmetric hypersonic flows are locally planar to the first approximation. The present result indicates, however, that $\beta\varphi_0 = 1$ does not seem to be large enough. Later calculations do indicate the importance of the axisymmetric correction.

Over a conical or even cylindrical portion of a body of revolution the local planar contributions vanish identically and the axisymmetric contributions predominate. Therefore, an approximate description of the axisymmetric effect in terms of the variation of a gross parameter is not likely to be a valid approximate scheme. For lack of anything better, it is proposed that the following variation of k in relation (17) may serve as a rough approximation:

$$k = k_0 \exp\left\{[1 - (2n/\beta r)][(x - x_0)/4\beta r]\right\} \tag{20}$$

where $k_0 = \kappa_0/2$ evaluated at the station x_0 where the cylinder portion begins. The constant n will be selected that the undisturbed free-stream pressure may be approximately reached at the far downstream end if the cylinder should extend to downstream infinity. In the case of a conical portion, the selection of n will be based on the presumption that in the limit of very large x, the surface pressure must approach the Taylor-Maccoll value.

Having selected the law of variation of the parameter, and relation (16) or (20) for their respective range of application, we may look upon Eq. (9) as a differential equation for $\nu(x)$ if $\varphi(x)$ and $r(x)$ are prescribed. β is a known function of ν. It is considered more consistent, however, to adopt the following approximation:

$$\nu - \nu_0 = -(\varphi - \varphi_0) + \frac{1}{2\bar{\beta}}\int_{x_0}^{x} (\kappa_0 + \varphi) \times \frac{dx}{r} + \frac{1}{2}\int_{x_0}^{x} (\kappa_0 - \varphi)\varphi\,\frac{dx}{r} \tag{21}$$

where $\bar{\beta}$ is taken to be some average value of β between the initial station x_0 and that at the station x.

For a pointed nose curved body, the following procedure of approximate calculation is proposed.

(1) The initial value of $\kappa_0 = \varphi_0[1 - (2/s_0)]$ will be evaluated at some convenient upstream station with the tangent cone approximation as

$$\kappa_0 = \varphi_0[1 - (2/s_0)] = \varphi_0 - 2\tan\varphi_0/(1 + \beta\tan\varphi_0) \tag{22}$$

(2) Estimate the value of $\beta_{2\,\text{dim.}}(x)$ at the station x neglecting the axisymmetric contributions, and compute

$$\bar{\beta} = [\beta_0 + \beta_{2\,\text{dim.}}(x)]/2 \tag{23}$$

(3) Then carry out the integrals as indicated in (21) with the known function $r(x)$ and $\varphi(x) = dr/dx$ if $r(x)$ is taken as a streamline. Then $\nu(x)$ is obtained, from which we obtain the corrected value of $\beta(x)$. A new average value of $\bar{\beta}$ may be obtained by replacing

$\beta_{2\,\text{dim.}}(x)$ in Eq. (23) with the corrected value of $\beta(x)$ and the process repeated, if circumstances so require. Sample calculations show that this is quite unnecessary.

For arbitrary body shapes, the integrals in Eq. (21) must be evaluated numerically. The following form of Eq. (21) is probably more convenient:

$$\left.\begin{aligned} \nu - \nu_0 = &-(\varphi - \varphi_0) + (1/2\bar{\beta})I_0 - \\ &(1/2)I_2 + [(1/\bar{\beta}) + \kappa_0] \ln [r(x)/r(x)_0] \end{aligned}\right\} \quad (21a)$$

where

$$I_0 = \int_{x_0}^{x} \frac{dx}{r(x)} \quad \text{and} \quad I_2 = \int_{x_0}^{x} \varphi^2 \frac{dx}{r(x)}$$

are purely the geometrical properties of the body shape that determine the axisymmetric corrections for flow properties on the body surface according to the present approximate scheme.

For a cylindrical or conical portion of the body, relation (20) will be adopted, giving explicitly

$$\nu - \nu_0 = \left\{4k_0/[(2n/\beta r) - 1]\right\} \times \left(1 - \exp\left\{-[(2n/\beta r) - 1][(x - x_0)/\beta r]\right\}\right) \quad (24)$$

where subscript 0 indicates the station where the conical or cylinder portion begins. The value of n is determined by

$$\nu_\infty - \nu_0 = 4k_0/[(2n/\beta r) - 1] \quad (25)$$

with the value of ν_∞ taken from the appropriate downstream asymptotic value of ν for an infinitely extended conical or cylinder body.

As a final remark, the above specific selections of semiempirical rules are made primarily for the purpose of simplicity and convenience, not with the purpose of giving results in best agreement with the exact solutions available. The accuracy of the results obtained with the above scheme, the effects of the uncertainties, and the arbitrariness in the selection of the mean values are reported in the next section.

(3) Accuracy of the Integral Method and Other Practical Considerations

We shall consider the complete characteristic calculation of the inviscid flow of an axisymmetric body, including the effects of a curved shock wave at the nose, of the wave interactions at the shock, and of the entropy gradient across the streamlines as the "exact inviscid solution." The deviations of the pressure coefficients, $(p - p_e)/p_e$, as evaluated from different approximate methods, from the values given by the "exact inviscid solution" will be considered as the errors of the approximate methods. The body shapes selected for detailed investigation are ogive cylinders. As previously noted, the results in the cylindrical portion will serve as a very critical test of the present approximation because we expect analytically that the prsent approximation is likely to be the least accurate. The present author fails to find any "complete characteristic solutions" for the flow field with negative flow deflection

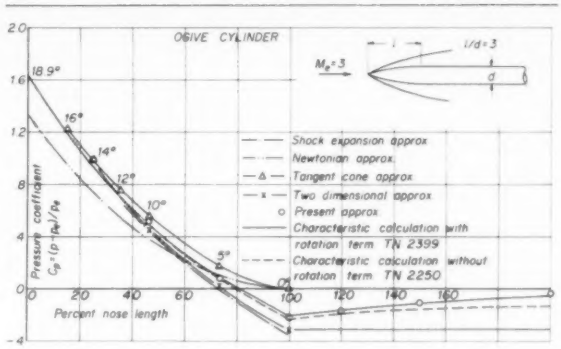

FIG. 3.

(toward the axis of symmetry) such as about the downstream half of the body of revolution of a circular arc—i.e., biconvex body.

Charts and tables in reference 6 are extensively used both for the conical shock solution and for the isentropic planar relations. Linear interpolation of the tabulated isentropic relations is found necessary in order to maintain the slide rule accuracy of three significant figures throughout the calculation. Accordingly, two decimals in the pressure coefficient calculated from the present integral method are considered as correct in the curves reported herein. The result of the characteristic calculation as is available to the present author are in the form of curves of similar scale as reproduced in the graphs of this report. Accordingly, no attempt has been made to improve the accuracy of the present calculation under the integral scheme.

In Fig. 3 the results of a sample calculation are summarized. The body under consideration is an ogive cylinder of slenderness ratio $l/d = 3$ where d is the diameter of the cylinder and l the axial length of the ogive nose. The flight Mach Number is $M_e = 3$. The ordinary hypersonic similarity parameter $M_e/(l/d)$ is unity. The ordinate in the curve is the pressure coefficient expressed as the excess static pressure $p - p_e$ over the undisturbed free-stream static pressure p_e. The abscissa is the axial distance downstream of the nose in per cent of nose length l of the ogive. Thus, 100 on the abscissa indicates the station where the ogive joins with the cylinder with discontinuous radius of curvature, but with continuous slope. The angle marking each set of computed points is the angle representing the arc length along the meridian section from the local point to the point of 100 per cent nose length where the cylinder begins.

The triangles represent the pressure coefficients as calculated from the tangent cone approximation. The curve joining these triangles should pass through the point, $c_p = (p - p_e)/p_e = 1.64$, at the nose $x = 0$ and the point $c_p = (p - p_e)/p_e = 0$ at $x = 100$. Beyond this point, $x > 100$, the tangent cone approximation, if extrapolated, would give a zero pressure coefficient along the surface of the cylinder. Starting from the 14° station—roughly 25 per cent from the nose, where the tangent cone approximation is taken for the determina-

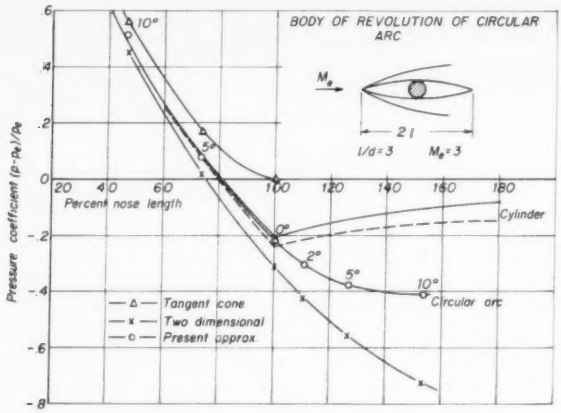

FIG. 4.

tion of the initial values—the pressure coefficients at different downstream stations were also determined, based on the extreme assumption that the flow field downstream of the 14° station is planar, governed by the Prandtl-Meyer relation. These points are represented by × up to the 0° station ($x = 100$). This two-dimensional approximation gives a pressure coefficient over the entire length of the cylinder which is the same as that at 0° station. The dotted curve is taken from reference 7, which is the result of a characteristic calculation without rotation term in the characteristic relation. The solid curve is taken from reference 5 which is a result of a characteristic calculation, with rotation term in the characteristic relation taken into account. Superposed on the graphs are the two c_p curves as determined from the uncorrected Newtonian approximation and from the shock expansion method. The Newtonian approximation results in an underestimate of c_p near the nose and gives a zero pressure coefficient at the maximum diameter point ($x = 100$)—that is, a local overestimate of c_p. The Newtonian c_p curve crosses the characteristic c_p curves in the upstream region. Clearly, it cannot be expected to serve as a good approximation in the flow regions with negative deflection angles locally. The shock expansion method gives a very good approximation near the nose, slightly underestimating the c_p consistently. But toward the downstream region, say near the maximum diameter point ($x = 100$), the c_p curve obtained from the shock expansion method agrees well with the locally planar curve but deviates further away from the "complete characteristic solution." Therefore, we cannot expect the shock expansion method to give a better than planar approximation for flow fields with negative deflection angle, further downstream.

The results of the present integral approximation with initial station 14° where the tangent cone approximation is adopted, and with $\bar{\beta}$ evaluated as the arithmetic mean according to Eq. (23) are represented by ⊙. The cylinder portion $x > 100$ was calculated with Eq. (24) and $n = 5/4$, selected to have approximately the downstream asymptotic behavior of the zero pressure coefficient along the cylinder surface based on Eq. (25). No curve is drawn to joint these points because such a curve would be too close to and hardly distinguishable from the solid curve representing the results of the "complete characteristic calculation."

It might seem that the good agreement could be due to the overestimate of the initial pressure coefficient at the initial station under the tangent cone approximation. If the correct pressure coefficient from the characteristic calculation were used as the initial value, the present approximate results would be displaced to lower values of c_p all the way downstream. This is not so because, when the initial pressure is taken from the characteristic calculation, the value of $1/s$, and therefore κ_0, should also be evaluated from the results of a characteristic calculation locally, not from the tangent cone approximation. Whether a consistent use of the results of the characteristic calculation in evaluating the initial values will permit the present integral approximation to give as good an agreement as is indicated here is open to question and is not to be resolved here. What seems to be the important question is the possibility that the good agreement might just be an accident of the particular choice of the initial station or other uncertain factors in the present approximate scheme. We shall, therefore, look into these aspects.

It is natural to expect that the errors committed by these uncertainties will be magnified and become more significant in regions further downstream of the $x = 100$ point. To avoid the added complication and uncertainty of the cylinder portion, the pressure coefficient c_p over the body of revolution of the circular arc as a continuation of the nose ogive is calculated with the present method even though there is no complete characteristic solution for such a biconvex body available for comparison. The results of the present approxi-

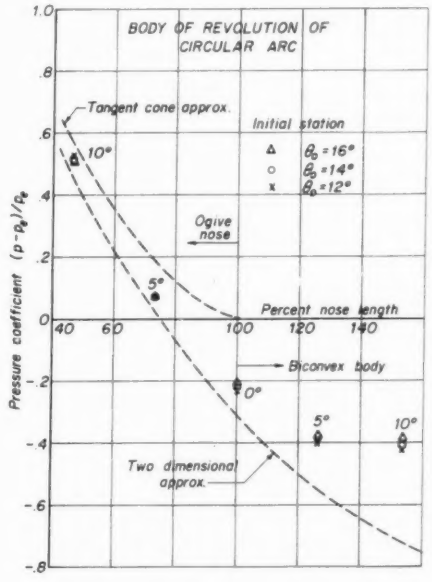

FIG. 5.

mate calculation are plotted in Fig. 4 with a slightly enlarged ordinate. The result of the present calculation shows a strong tendency of the c_p curve to flatten out in the downstream half of the body because of the three-dimensional effect. The differences among the two-dimensional approximation, the tangent cone approximation, and the present result become large. As expected on physical grounds, the recompression due to three-dimensional effects is milder in the present case of a continuous arc than in the case of a cylinder.

The effect of different initial stations in starting the present approximate solution is shown in Fig. 5 for the case of a body of revolution of a circular arc. Three sets of calculations were made with initial stations at 16°, 14°, and 12°. The values of κ_0 are different for different initial stations, and the values of $\bar{\beta}$ are also different at a given value of x in the calculations with different initial stations. It is clear from Fig. 5 that the calculated results based on the present approximate method is not sensitive to the choice of the initial station. The divergence of the results with different initial stations is somewhat irregular, but the magnitude of the divergence lies mostly in the third significant figure of the calculation. This is considerably smaller than the difference between the present result and the tangent cone or the two-dimensional approximation, especially in the flow region with negative flow deflection where no results from characteristic calculation are available. For the ogive nose portion, the variation is within the two bounds of characteristic calculations, closer to the one including the rotation term. It is, therefore, inferred that the effect of an arbitrary selection of the initial station in starting the present approximation within a reasonable range is of little consequence. Clearly, one should not and will not select the station too far downstream where the tangent cone approximation is excessively off. In fact, if one should select the initial station at $x = 100$, the present methods would also predict zero pressure coefficient all the way on the ensuing cylinder body. Even under this extreme case, the present method still gives, on the downstream half of the body of revolution of a circular arc, a pressure coefficient converging toward the "correct values" determined with the proper selection of the initial station.

Comparison of the three sets of results seems to indicate that better agreement with the rotation-characteristic solution is obtained with the initial station taken further upstream. The solution with the initial station of 16° seems to be the closest to the result of characteristic calculation. (The nose half angle is 18.9°.) But it should be emphatically brought out that the difference is so small that such an inference cannot be justified with the slide rule accuracy of the present calculation. Difficulties will certainly be encountered if one should try to start directly from the nose where $r = 0$. It seems that the upstream limit of selecting the initial station depends very much on the numerical accuracy of the calculation. For engineering purposes, there appears to be no difficulty in selecting a reasonable initial position.

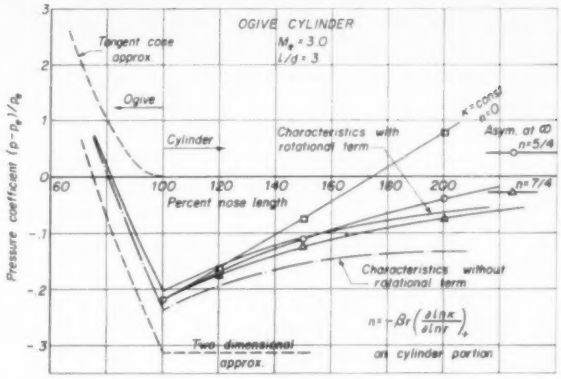

FIG. 6.

Let us now investigate the effect of the different ways of determining $\bar{\beta}$. The previous calculations for C_p over the body of revolution of the circular arc are repeated with all three initial stations when the mean $\bar{\beta}$ is taken as the geometric mean of β_1 and $\beta_{2\,\mathrm{dim.}}(x)$

$$\bar{\beta} = [\beta_1 \cdot \beta_{2\,\mathrm{dim.}}(x)]^{1/2}$$

instead of the arithmetic mean given previously as Eq. (23). The difference of c_p at a given station calculated with the two different ways of taking $\bar{\beta}$ is completely overshadowed by the numerical accuracy of a 12-in. slide rule for practically all the points calculated. There are several instances where deviations may appear in the third significant figure. The arithmetic mean of β^2 defined as

$$\bar{\beta}^2 = [\beta_1^2 + \beta_{2\,\mathrm{dim.}^2}(x)]/2$$

has also been tried with insignificant effect. The step by step integration with the immediately preceding point as the initial station has also been carried out. The values of c_p so determined are still insignificant in the graph presented here. The difference seems to be bigger than that between the different averaging schemes and tend toward the characteristic solution without rotation terms. It is difficult to resolve whether this is due to the accumulation of inaccuracies of the calculation at successive points, or due to the self-compensation of different errors when average $\bar{\beta}$ is taken. The important thing, for the time being, is that any of these schemes will give substantially the same result. Since the arithmetic mean can be handled more easily, the scheme as indicated by Eq. (23) may be adopted in general.

Let us consider the arbitrariness of the selection of n for the calculation on the cylinder portion. The physical meaning of n is indicated by $n = -\beta r(\partial \ln \kappa/\partial \ln r)_+$ along the positive family characteristic line. Calculated results on the cylinder portion of the ogive cylinder shown in Fig. 3 are exemplified in Fig. 6 for three different values of $n = 0$, $5/4$, and $7/4$, indicated by lines joining points marked □, ⊙, and △, respectively. The case of $n = 0$ represents a flow over the cylinder with the flow deflection taking a constant value over the

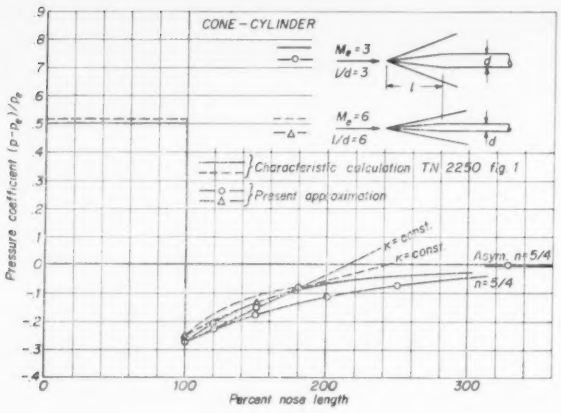

FIG. 7.

entire flow field downstream of the Mach cone at the shoulder $x = 100$. This situation contradicts either the initial condition at $x = 100$ or the boundary condition on the cylindrical surface. Therefore, the calculated result over the cylinder with $n = 0$ cannot be expected as a satisfactory approximation in the overall picture. Some finite value of n must be selected. In the sample calculations for the ogive cylinder combination, as shown in Fig. 6, both the results with $n = 5/4$ and $n = 7/4$ give a satisfactory approximation to the characteristic solution with rotation terms up to one nose length downstream. The calculation was made with Eq. (24) and the asymptotic values of c_p in the far downstream region are also shown in Fig. 6. The asymptotic value of c_p with $n = 5/4$ is slightly positive and that with $n = 7/4$ is slightly negative, both fairly close to zero as they should be in the very far downstream region. The curve of c_p as calculated with $n = 7/4$ as a function of x is nearly parallel to that of the characteristic calculation. Thus, for this particular example, $n = 7/4$ seems to give a better approximation than $n = 5/4$, even though $n = 5/4$ seems to give a smaller absolute deviation from the characteristic solution in the region with $x < 200$ per cent. This observation certainly cannot be extrapolated to other body shapes. What is important is that either of the results with $n = 5/4$ and $n = 7/4$, as suggested by the rough approximation, relation (25), may be adopted without serious error. This aspect cannot be confidently extrapolated to cylinder bodies whose nose shapes are quite different from an ogive. For illustrative purposes, the cone-cylinder combination has been investigated. The results are presented in Fig. 7. Within one nose length of the cylinder body, the calculated results using $n = 0$ and $n = 5/4$ may all be considered as fair approximations. The result with $n = 0$ seems to give the least absolute deviation. It is, therefore, difficult even to make an intelligent guess as to what value of n should be taken in order to get reasonable approximations over the cylinders with arbitrary nose for common engineering problems. If one is willing to accept the cone-cylinder as an extreme configuration, and tolerate an error in static pressure by 10 per cent, it really does not matter what values of n one takes, especially if guided by a rule such as Eq. (25).

As an additional example, the same ogive cylinder combination flying at $M_e = 6$ has also been analyzed, with the results given in Fig. 8. The scale for the pressure coefficient c_p in this plot is much coarser than that in Fig. 3, for example. While graphically, the agreement between the present approximate solution and the characteristic solution with rotation terms in the characteristic relations appear to be equally good, as is shown in Fig. 3 for $M_e = 3$, the deviation of the actual magnitude is considerably larger in the higher Mach Number case. There are several other aspects that are worth mentioning concerning this specific example. First, the rotation term in the characteristic relation representing the effect of the entropy gradient across streamlines appears to be very important in the characteristic calculation. The error in neglecting this term is considerably bigger than that of any of the approximate methods. This important part of the effect of rotationality in determining the surface pressure is accounted for in a general fashion in the present approximate method by the parameter κ. Second, the two-dimensional approximation becomes very good at Mach Number $M_e = 6$ ($k = 2$) but not nearly so good at $M_e = 3$ ($k = 1$). This is in agreement with the observations made previously in this report [see Eq. (19)].

The foregoing numerical evidence of the accuracy of the present approximate method when applied to an ogive body is quite encouraging, especially in view of the insensitivity of the results of the present approximation toward uncertainties implicit in the method. Further numerical evidence as to the accuracy of the present method compared with the complete characteristic calculations when applied to other pointed bodies and for results in regions of negative flow deflection is extremely desirable, if the applicability of the present approximate scheme is to be carefully explored. The agreement as shown in Fig. 3 may not be obtained for other pointed bodies. Ordinary engineering practice, however, will tolerate errors considerably larger than

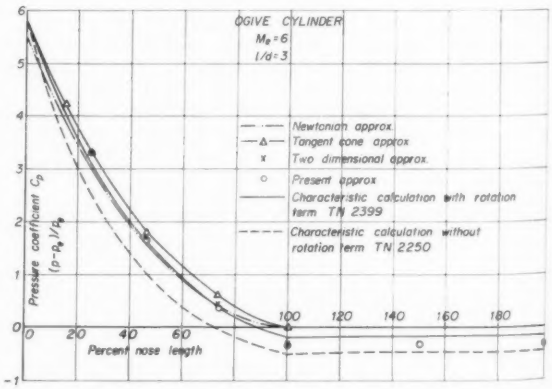

FIG. 8.

those indicated in Fig. 3. Hence, some extrapolation in applying the present scheme to pointed bodies similar to an ogive may be permitted. The advantage of the present approximate method lies primarily in its simplicity, as compared with the characteristic method, and in the fact that the surface pressure can be determined without carrying along the flow field in its vicinity or even the pressure at intermediate points. Most important of all, the previous investigation justifies the introduction of an overall parameter $\kappa = [1 - (2/s)]\varphi$ to represent the integrated effect of the upstream geometry in evaluating the axisymmetric corrections. This makes it possible to study the downstream portion of a flow field without referring to the details of the upstream configuration. Thus, the major object of the present investigation is achieved.*

Conclusions

The approximate method developed analytically and investigated numerically in this report is shown to be very satisfactory for pointed ogive bodies and may be applied with reasonable assurance to other curved, pointed nose convex bodies with axisymmetric inviscid flow fields, in flow regions with streamlines either diverging from or converging toward the axis of symmetry. The result of the approximate method is insensitive to the arbitrary factors implicit in the method.

For an axisymmetric flow field over prolonged conical or cylindrical portions, an alternate formulation is provided, which may be considered as a fair engineering approximation.

Calculations indicate that a locally planar approximation is good at relatively large values of the hypersonic similarity parameter, say $M\varphi \geq 2$, but that the axisymmetric correction is quite significant at $M\varphi \leq 1$. An inference from the analytic formulation of the present method is that the axisymmetric correction is likely to be more significant at the lower values of the hypersonic similarity parameters.

The integrated effect of the detailed configuration upstream of a given station on the inviscid flow field in the downstream region may be represented by an overall parameter $\kappa = [1 - (2/s)]\varphi$. With the introduction of this parameter it is possible to study an isolated portion of an axisymmetric flow field in the downstream region without referring to the details of the upstream configurations.

* The author was informed of reference 8 after the present manuscript had been completed. In this reference a second-order correction to the shock expansion method is introduced. Like the original shock expansion method, it will depend on the details of the upstream geometry.

References

[1] Sears, W. R. (Ed.), *General Theory of High Speed Aerodynamics;* (Vol. VI of "High Speed Aerodynamics and Jet Propulsion"), Sears, W. R , "Small Perturbation Theory," Section C, pp. 61–121; Heaslet, Max A., and Lomax, Harvard, "Supersonic and Transonic Small Perturbation Theory," Section D, pp. 122–344; Lighthill, M. J., "Higher Approximations," Section E, pp. 345–489; Princeton University Press, Princeton, N. J., 1954.

[2] Eggers, A. J., Jr. and Syvertson, C. A., *Inviscid Flow About Airfoils at High Supersonic Speeds*, NACA TN 2646, 1952.

[3] Ehert, Dorris M., *Accuracy of Approximate Methods for Predicting Pressures on Pointed Nonlifting Bodies of Revolution in Supersonic Flow*, NACA TN 2764, 1952.

[4] Eggers, A. J., Jr., and Savin, R. C., *Approximate Methods for Calculating the Flow About Nonlifting Bodies of Revolution at High Supersonic Speeds*, NACA TN 2579, 1951.

[5] Rossow, V. J., *Applicability of the Hypersonic Similarity Rule to Pressure Distributions Which Include the Effects of Rotation for Bodies of Revolution at Zero Angle of Attack*, NACA TN 2399, 1951.

[6] Staff, Ames Laboratory, NACA, *Equations, Tables and Charts for Compressible Flow*, NACA TR 1135, 1953.

[7] Ehert, D. M., Rossow, V. J. and Stevens, V. I., *An Analysis of the Applicability of the Hypersonic Similarity Law to the Study of Flow About Bodies of Revolution at Zero Angle of Attack*, NACA TN 2250, 1950.

[8] Syvertson, C. A. and Dennis, D. H., *A Second-Order Shock Expansion Method Applicable to Bodies of Revolution Near Zero Lift*, NACA TN 3527, 1956.

[9] Cheng, S. I., *An Approximate Method of Determining Axisymmetric Inviscid Flow Over Solid Body and Wake*, Aerodynamics Technical Report No. 3, Research and Advanced Development Division, Avco Manufacturing Corporation, 1956.

Third U.S. National Congress of Applied Mechanics

Brown University, June 11–14, 1958

The congress program, which is to be distributed in May, will feature over 100 papers in Applied Mechanics, including mechanics of rigid bodies, mechanics of deformable solids, mechanics of fluids and gases, thermodynamics, and heat transfer. In addition, there will be four general lectures by leading authorities.

To reduce the cost of attending the symposium to the utmost, the following all-inclusive living arrangement is offered. This covers rooms in the new West Quadrangle of Brown University and all meals from Breakfast on Wednesday, June 11, through Luncheon on Saturday, June 14, but *not* the Banquet on Thursday night ($5.00). The rates will be $24.00 for each of two persons sharing a room, or $30.00 for a person occupying a single room. Rooms will be available without additional charge for Tuesday night and Saturday night.

Registration Fees: Advance Registration on or before June 7, $4.00. Registration on June 8 or later, $6.00. Please make checks payable to: *Applied Mechanics Congress*, not to any person.

Requests for copies of the program and letters concerning advance registration should be addressed to Miss E. M. Addison, Box F, Brown University, Providence 12, R.I. In registering, please indicate number of persons in party and family relationship, desire for single rooms or willingness to share rooms, estimated arrival and departure times, and need for parking space.

Incompressible Two-Dimensional Stagnation-Point Flow of an Electrically Conducting Viscous Fluid in the Presence of a Magnetic Field

JOSEPH L. NEURINGER* AND WILLIAM McILROY**

Republic Aviation Corporation

SUMMARY

When a blunt body moves through the atmosphere at high hypersonic speeds, there exists a cap of ionized gas between the detached shock and the nose of the body. It was considered possible that, by impressing a magnetic field out of the nose of the body and into the conducting gas, some beneficial effects could be derived from this region. In order to demonstrate this fact theoretically, consideration was given to the well-known problem of the two-dimensional stagnation-point flow on an infinite flat plate, modified in two ways: (1) the fluid was assumed incompressible but conducting, and (2) impressed on the fluid was an external parallel magnetic field normal to the plate. From the resulting analysis of the hydromagnetic interaction, it appears that a considerable reduction in skin friction may be possible with reasonable values of the applied magnetic intensity and electrical conductivity of the fluid.

The reduction in shear stress at the wall is found to be a function of a nondimensional parameter $h^2(0)/\gamma$ defined in the text.

SYMBOLS

Rational m. k. s. system is used throughout

$\boldsymbol{E}^*$	= electric intensity
$\boldsymbol{H}^*$	= magnetic intensity
$\boldsymbol{B}^*$	= magnetic induction
$\boldsymbol{J}^*$	= current density
σ	= fluid conductivity
δ	= charge density
μ_e	= magnetic permeability
ϵ	= dielectric constant
$\boldsymbol{q}^*$	= fluid velocity
P^*	= fluid pressure
ρ_0	= fluid density
μ	= coefficient of viscosity
ν	= coefficient of kinematic viscosity
x^*, y^*	= coordinates
b, b_0	= parameters (dimensions sec.$^{-1}$)
η	= $1/\mu_e\sigma$
γ	= η/ν
U^*, V^*	= velocity components in x^* and y^* directions, respectively
H_x^*, H_y^*	= magnetic intensity components in x^* and y^* directions, respectively
$u(y)$, $h(y)$, $P_1(y)$, $P_2(y)$	= dimensionless functions of the dimensionless y coordinate (see Analysis)
∇^*	= gradient
$\boldsymbol{i}, \boldsymbol{j}$	= unit vectors

The starred quantities are dimensional, the unstarred nondimensional

Received June 14, 1957. Presented at the Aerodynamics Session, Twenty-Sixth Annual Meeting, IAS, New York, January 27–30, 1958.

* Associate Scientist, Scientific Research Staff.

** Specialist Engineer, Scientific Research Staff.

The writers wish to express their appreciation to Dr. Theodore Theodorsen and Alfred Kunen of Scientific Research and Robert Sanator of the Aerodynamics Department for many critical and stimulating discussions during the preparation of this paper. Thanks are also extended to Julius Port of the Analogue Computing Section for his interest and cooperation in obtaining solutions.

INTRODUCTION

HIGH-SPEED RE-ENTRY MISSILES, especially those in the intercontinental class, re-enter the earth's atmosphere at such tremendous speeds that the gas behind the shock may become highly dissociated and ionized. Ionization renders the gas electrically conducting and hence capable of being affected by electromagnetic fields. The name given to the study of the interaction of an electrically conducting moving fluid in the presence of magnetic fields is magnetohydrodynamics. In its simplest terms, the interaction may be described as follows. The motion of the conducting fluid in the magnetic field induces electric currents in the fluid, thereby modifying the field; at the same time, the flow in the magnetic field produces mechanical forces which in turn modify the motion.

Up until the present, magnetohydrodynamics was virtually the sole concern of the geophysicist and the astrophysicist, since the fluid in the earth's interior, and the gases in and around celestial bodies and in interstellar space, are already highly ionized and capable of interacting with the magnetic fields of these bodies. However, now that the gases behind the shock are conducting, the subject becomes of interest to the missile aerodynamicist.

One of the chief problems associated with the reentry of an intercontinental ballistic missile is that of convective heating. However, since the gas near the stagnation region is conducting, the question may be raised as to whether the flow in this region can be sufficiently influenced magnetohydrodynamically so as to effectively reduce the heat transfer. In this report, we will not be concerned with the more complex problem of heat transfer, but rather with skin friction. If, as is usually the case, reduced skin friction implies reduced heat transfer, then a marked reduction in skin friction hydromagnetically should also have the same favorable effect on heat transfer.

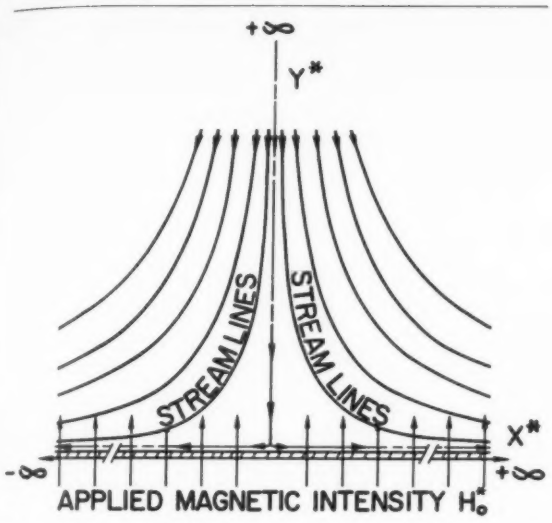

FIG. 1. Stagnation flow of an ionized gas on an infinite plate in presence of a magnetic field.

In order to demonstrate the interaction, we choose to consider what perhaps is the simplest of the stagnation flow problems, the well-known two-dimensional stagnation-point flow on an infinite plate, modified in two ways: (1) the fluid is assumed incompressible but conducting, and (2) impressed on the fluid is an external parallel magnetic field normal to the plate, Fig. 1. We wish to determine the flow in the vicinity of the stagnation point with particular emphasis on skin friction.

The Magnetohydrodynamic Equations

(a) The Electromagnetic Equations

Assuming μ_e and ϵ constant in the conducting fluid, Maxwell's equations in the rational m. k. s. system become

$$\nabla^* \mathbf{x} \boldsymbol{E}^* = -(\partial \boldsymbol{B}^*/\partial t) \tag{1}$$

$$\nabla^* \cdot \boldsymbol{E}^* = \delta/\epsilon \tag{2}$$

$$\nabla^* \cdot \boldsymbol{B}^* = 0 \tag{3}$$

$$\nabla^* \mathbf{x} \boldsymbol{H}^* = \boldsymbol{J}^* + \epsilon(\partial \boldsymbol{E}^*/\partial t) \tag{4}$$

where $\boldsymbol{B}^* = \mu_e \boldsymbol{H}^*$. The most general expression for $\boldsymbol{J}^*$ in a homogeneous isotropic medium is

$$\boldsymbol{J}^* = \sigma \boldsymbol{E}^* + \sigma(\boldsymbol{q}^* \mathbf{x} \boldsymbol{B}^*) + \delta \boldsymbol{q}^* \tag{5}$$

where the terms on the right represent, respectively, the conduction current, the induction current, and the convection current. The last term of the right-hand side of Eq. (4) represents the displacement current. It can be shown,[1] by dimensional and order of magnitude arguments, that the displacement current and convection currents are negligible compared with the conduction and induction currents, and they are therefore neglected in the analysis.

Taking the curl of Eqs. (5), using Eqs. (1) and (4), and remembering that $\boldsymbol{B}^* = \mu_e \boldsymbol{H}^*$, Eq. (5) becomes

$$\nabla^* \mathbf{x} (\nabla^* \mathbf{x} \boldsymbol{H}^*) = -\sigma\mu_e(\partial \boldsymbol{H}^*/\partial t) + \sigma\mu_e \nabla^* \mathbf{x} (\boldsymbol{q}^* \mathbf{x} \boldsymbol{H}^*) \tag{6}$$

Expanding the vectors $\nabla^* \mathbf{x} (\nabla^* \mathbf{x} \boldsymbol{H}^*)$ and $\nabla^* \mathbf{x} (\boldsymbol{q}^* \mathbf{x} \boldsymbol{H}^*)$ and remembering that $\nabla^* \cdot \boldsymbol{q}^* = 0$ (incompressibility) and $\nabla^* \cdot \boldsymbol{H}^* = 0$ (Eq. 3), Eq. (6) becomes, in steady state,

$$(\boldsymbol{q}^* \cdot \nabla^*)\boldsymbol{H}^* - (\boldsymbol{H}^* \cdot \nabla^*)\boldsymbol{q}^* = \eta \nabla^{*2} \boldsymbol{H}^* \tag{7}$$

where the Laplacian operator acts on each component of $\boldsymbol{H}^*$ and $\eta = 1/\sigma\mu_e$.

It is seen that, as far as the electromagnetic equations are concerned, the interaction with the moving conducting fluid is represented by the current induction term in Eq. (5) or the two terms on the left-hand side of Eq. (7).

(b) Flow Equations

The equations of continuity and momentum for an incompressible magnetohydrodynamically interacting fluid in steady motion are

$$\nabla^* \cdot \boldsymbol{q}^* = 0 \tag{8}$$

$$(\boldsymbol{q}^* \cdot \nabla^*)\boldsymbol{q}^* = -(1/\rho_e)\nabla^* P^* + (\mu_e/\rho_0)(\boldsymbol{J}^* \mathbf{x} \boldsymbol{H}^*) + \nu \nabla^{*2} \boldsymbol{q}^* \tag{9a}$$

where the interaction term $\mu_e(\boldsymbol{J}^* \mathbf{x} \boldsymbol{H}^*)$, represents the ponderomotive force per unit volume exerted by the magnetic field on the fluid.

Substituting for $\boldsymbol{J}^*$ in Eq. (9a) from Eq. (4), we obtain

$$(\boldsymbol{q}^* \cdot \nabla^*)\boldsymbol{q}^* = -(1/\rho_0)\nabla^* P^* + (\mu_e/\rho_0)(\nabla^* \mathbf{x} \boldsymbol{H}^*) \mathbf{x} \boldsymbol{H}^* + \nu \nabla^{*2} \boldsymbol{q}^* \tag{9}$$

Analysis

(a) Stagnation Flow Equations

Considering now the two-dimensional stagnation flow problem, introduce the dimensionless variables

$$x = x^*(b/\nu)^{1/2}, \quad y = y^*(b/\nu)^{1/2}, \quad \boldsymbol{q} = \boldsymbol{q}^*/(b\nu)^{1/2},$$
$$P = P^*/(\rho_0 b\nu), \quad \boldsymbol{H} = (\boldsymbol{H}^*/H_0^*)(\mu_e H_0^{*2}/\rho_0 b\nu)^{1/2}$$

where H_0^* represents the magnitude of the applied field, and b a parameter, of dimensions sec.$^{-1}$, whose significance will be discussed later.

In component form, Eqs. (9) and (7) become

$$U(\partial U/\partial x) + V(\partial U/\partial y) = -(\partial P/\partial x) - H_y[(\partial H_y/\partial x) - (\partial H_x/\partial y)] + [(\partial^2 U/\partial x^2) + (\partial^2 U/\partial y^2)] \tag{10}$$

$$U(\partial V/\partial x) + V(\partial V/\partial y) = -(\partial P/\partial y) + H_x[(\partial H_y/\partial x) - (\partial H_x/\partial y)] + [(\partial^2 V/\partial x^2) + (\partial^2 V/\partial y^2)] \tag{11}$$

$$U(\partial H_x/\partial x) + V(\partial H_x/\partial y) - H_x(\partial U/\partial x) - H_y(\partial U/\partial y) = \gamma[(\partial^2 H_x/\partial x^2) + (\partial^2 H_y/\partial y^2)] \tag{12}$$

$$U(\partial H_y/\partial x) + V(\partial H_y/\partial y) - H_x(\partial V/\partial x) - H_y(\partial V/\partial y) = \gamma[(\partial^2 H_y/\partial x^2) + (\partial^2 H_y/\partial y^2)] \tag{13}$$

where

$$\boldsymbol{q} = U\boldsymbol{i} + V\boldsymbol{j}, \quad \boldsymbol{H} = H_x\boldsymbol{i} + H_y\boldsymbol{j}, \quad \gamma = \eta/\nu$$

Continuity and Eq. (3) yield the auxiliary equations

$$(\partial U/\partial x) + (\partial V/\partial y) = 0; \qquad (\partial H_x/\partial x) + (\partial H_y/\partial y) = 0 \quad (14)$$

Since, (1) the x components of both $\boldsymbol{q}$ and $\boldsymbol{H}$ are antisymmetric with respect to x, (2) the y components are symmetric, and (3) both $\boldsymbol{q}$ and $\boldsymbol{H}$ are divergenceless, we seek a solution of the system of Eqs. (10) to (14) of the form

$$\left.\begin{aligned} U &= u'(y)x, \quad H_x = h'(y)x \\ V &= -u(y), \quad H_y = -h(y) \\ P &= P_0 - P_1(y) - P_2(y)x^2 \end{aligned}\right\} \quad (15)$$

where the prime denotes differentiation with respect to y, and $u(y)$, $h(y)$, $P_1(y)$, $P_2(y)$ are functions of y to be determined. P_0 represents the dimensionless stagnation pressure. The odd powers of x are missing from the P expression because of symmetry with respect to x.

Substituting Eqs. (15) into the system (10) to (13) and equating coefficients of like powers of x, we obtain from Eq. (10),

$$u'^2 - uu'' = 2P_2 - hh'' + u''' \quad (16)$$

from Eq. (11),

$$uu' = P_1' - u'' \quad (17)$$

$$P_2' = h'h'' \quad (18)$$

from Eq. (12),

$$hu'' - uh'' = \gamma h''' \quad (19)$$

from Eq. (13),

$$uh' - u'h = -\gamma h'' \quad (20)$$

Integrating Eq. (18) we obtain

$$P_2 = (h'^2/2) + C \quad (21)$$

where C is the integration constant to be evaluated.

(b) *Boundary Conditions*

The velocity conditions at the plate require

$$u(0) = u'(0) = 0$$

The total magnetic field at the wall is the vector sum of the applied and induced fields, the latter resulting from the induced current distribution in the fluid. This distribution depends on the solution and is therefore unknown. However, for the purpose of calculating the effect of the interaction on the flow field, the induced field at the wall is neglected in comparison with the applied field. The magnetic field components at the wall thus become

$$h(0) = -(\mu_e H_0^{*2}/\rho_0 b\nu)^{1/2}, \quad h'(0) = 0$$

h being obtained from the transformation to dimensionless variables.

As in the field free case, the conditions for P_1 and P_2 at the wall are determined by integrating the inviscid momentum equation along the wall streamline and comparing the result obtained with the expression for P assumed in Eq. (15).

Returning to Eq. (9), neglecting the viscous term, and expanding $(\boldsymbol{q}^*\cdot\nabla^*)\boldsymbol{q}^*$, we obtain

$$\nabla^*[P^* + (1/2)\rho_0 q^{*2}] = \rho_0[\boldsymbol{q}^* \times (\nabla^* \times \boldsymbol{q}^*)] + \mu_e(\nabla^* \times \boldsymbol{H}^*) \times \boldsymbol{H}^*$$

Integrating along the wall streamline from $x^* = 0$ to $x^* = x^*$, and remembering that the velocity components are zero at the stagnation point and the vertical component of $\boldsymbol{q}^*$ is zero at the wall, the above expression becomes

$$P^*(x^*, 0) = P_0^*(0, 0) - (\rho_0/2)U^{*2}(x^*, 0) + \rho_0 \int_0^{x^*} [\boldsymbol{q}^* \times (\nabla^* \times \boldsymbol{q}^*)]\cdot\boldsymbol{i}\, dx^* + \mu_e \int_0^{x^*} [(\nabla^* \times \boldsymbol{H}^*) \times \boldsymbol{H}^*]\cdot\boldsymbol{i}\, dx^* \quad (22)$$

The first integral on the right-hand side is identically zero. Expanding the last integral, we obtain

$$P^*(x^*, 0) = P_0^*(0, 0) - (\rho_0/2)U^{*2}(x^*, 0) + \mu_e \int_0^{x^*} H_y^*[(\partial H_x^*/\partial y^*) - (\partial H_y^*/\partial x^*)]dx^* \quad (23)$$

We assume the velocity components of the inviscid magnetohydrodynamic flow are given by $U^* = bx^*$, $V^* = -by^*$ since these forms are the simplest representation satisfying both continuity and symmetry. It is seen that the parameter, b, introduced in the dimensionalization, has the same significance as in the field free case.[2] In dimensionless form, these become $U = x$, $V = -y$. In nondimensional form Eq. (23) becomes

$$P(x, 0) = P_0(0, 0) - (1/2)x^2 + \int_0^x H_y[(\partial H_x/\partial y) - (\partial H_y/\partial x)]dx \quad (24)$$

Again, the components of $\boldsymbol{H}$ are of the form assumed in Eq. (15)—i.e.,

$$H_x = h'(y)x, \quad H_y = -h(y)$$

Hence, Eq. (24) reduces to

$$P(x, 0) = P_0(0, 0) - (1/2)x^2 - h(0)\int_0^x h''(0)x\, dx$$

or

$$P(x, 0) = P_0(0, 0) - (1/2)[1 + h(0)h''(0)]x^2$$

Now, in the inviscid flow, Eq. (20) is still valid, and since $u = 0$ and $u' = 1$ at the wall, $\gamma h''(0) = h(0)$. The above expression for the pressure finally becomes

$$P(x, 0) = P_0(0, 0) - (1/2)\{1 + [h^2(0)/\gamma]\}x^2$$

When this is compared with the expression assumed for P in Eq. (15), the wall conditions

TABLE 1

γ	10^5		2×10^5		5×10^5		10^6	
$h(0)$	$u''(0)$	τ/τ_0	$u''(0)$	τ/τ_0	$u''(0)$	τ/τ_0	$u''(0)$	τ/τ_0
0	1.2326	1.000	1.2326	1.000	1.2326	1.000	1.2326	1.000
-100	1.2742	0.961	1.2492	0.977	1.2382	0.988	1.2354	0.996
-200	1.3818	0.873	1.3094	0.925	1.2640	0.970	1.2470	0.982
-300	1.5554	0.779	1.4062	0.863				
-350	1.6566	0.738			1.3270	0.913	1.2820	0.954
-400	1.7680	0.700	1.5256	0.795				
-450	1.8868	0.668						
-500			1.6698	0.737	1.4220	0.852	1.3310	0.913
-600			1.8282	0.685				
-650					1.5418	0.790	1.3948	0.868
-800					1.6788	0.735	1.4746	0.828
-900					1.7790	0.702		

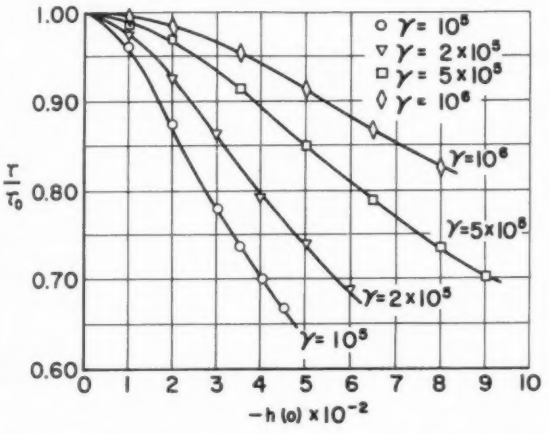

FIG. 2. Shear stress ratio versus parameter $h(0)$ for various values of γ.

$$P_1(0) = 0, \quad P_2(0) = (1/2)\{1 + [h^2(0)/\gamma]\}$$

are obtained.

For the boundary condition at large distances from the wall, we require that the horizontal velocity component approach asymptotically the assumed inviscid form—i. e., $U = x$. This requires $u' = 1$ as y approaches infinity.

Returning to Eq. (21), and using the condition that $h' = 0$ at the wall, the constant $C = (1/2)\{1 + [h^2(0)/\gamma]\}$.

Substituting for P_2 in Eq. (16), we obtain

$$u''' + uu'' - u'^2 + \{1 + [h^2(0)/\gamma]\} + h'^2 - hh'' = 0 \quad (25)$$

and Eq. (20), $\gamma h'' + uh' - u'h = 0$ (20)

It is seen that the derivative equation of (20) yields Eq. (19); hence, a solution involving Eqs. (25) and (20) automatically satisfies Eq. (19). Once u and h are obtained from Eqs. (25) and (20), P_1 and P_2 can be obtained from Eqs. (17) and (18), respectively.

(c) *Recapitulation*

In summary, we need to solve the following system of equations:

$$u''' + uu'' - u'^2 + \{1 + [h^2(0)/\gamma]\} + h'^2 - hh'' = 0 \quad (25)$$

$$\gamma h'' + uh' - u'h = 0 \quad (20)$$

subject to the conditions;

At $y = 0$,
$u = u' = h' = 0, \quad h = -(\mu_e H_0^{*2}/\rho_0 b\nu)^{1/2}$

At $y = \infty$, $u' = 1$

It is noted that when the applied $h = 0$, the equations uncouple and Eq. (25) reduces identically to the corresponding field free equation.

SOLUTION AND DISCUSSION

The pressure expressions at the wall with and without a field are, respectively,

$$P^*(x^*, 0) = P_0^*(0, 0) - (1/2)\rho_0 b^2\{1 + [h^2(0)/\gamma]\}x^{*2}$$
$$P^*(x^*, 0) = P_0^*(0, 0) - (1/2)\rho_0 b_0^2 x^{*2}$$

The assertion is now made that the nature of the hydromagnetic force (regarded as a strong magnetic "viscosity" tending to destroy the motion across the lines of force[3]) and the character of the interaction are such as to transform, by the application of the magnetic field, an initial infinite two-dimensional inviscid field free flow whose velocity components are characterized by the parameter, b_0, to a flow whose velocity components are characterized by the parameter, b, the pressure distribution at the wall remaining essentially unaltered. Hence, comparing the above expressions, we have

$$b = b_0\{1 + [h^2(0)/\gamma]\}^{-(1/2)} \quad (26)$$

Now the shear stress, τ, at the wall is given by

$$\tau = \mu(\partial U^*/\partial y^*)_{y^*=0} = \mu(\partial U^*/\partial y)_{y=0}(\partial y/\partial y^*) = \rho_0\nu^{1/2}b^{3/2}u''(0)x^*$$

Comparing wall shears, with and without the field,

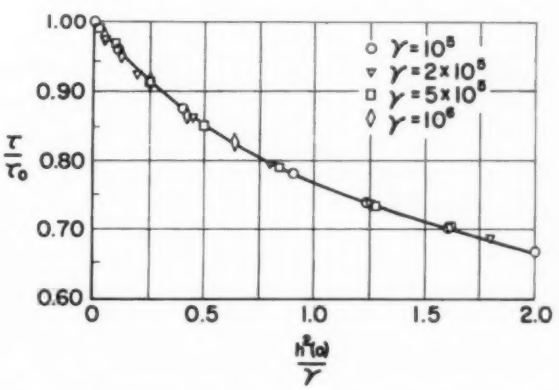

FIG. 3. Relationship between the shear stress ratio and the parameter $[h^2(0)/\gamma]$.

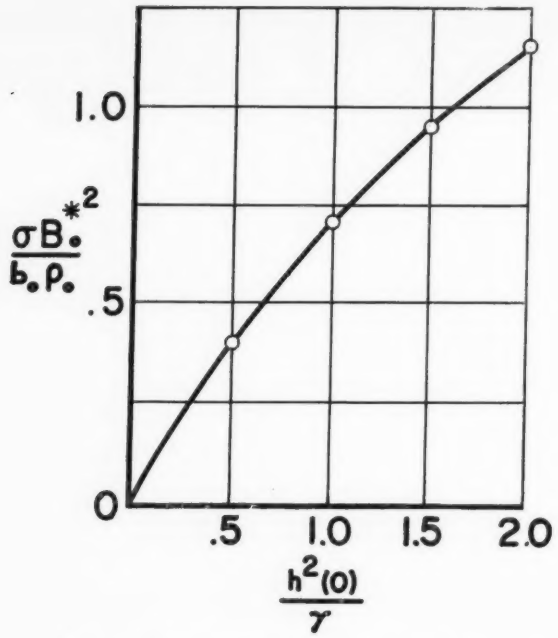

FIG. 4. Parameter $(\sigma B_0^{*2}/b_0\rho_0)$ versus $h^2(0)/\gamma$.

yields

$$(\tau/\tau_0) = [u''(0)/u_0''(0)](b/b_0)^{3/2} = [u''(0)/u_0''(0)]\{1 + [h^2(0)/\gamma]\}^{-3/4} \quad (27)$$

where $$u_0''(0) = 1.2326$$

The solution of the system (25) and (20) was obtained on an analog computer and the results for $u''(0)$ for various values of $h(0)$ and γ are shown in Table 1. Curves for the shear stress ratio, according to Eq. (27), are shown in Fig. 2. If the shear stress ratio is plotted as a function of the parameter, $h^2(0)/\gamma$, then the curves of Fig. 2 transform into the single universal curve represented in Fig. 3. The parameter $h^2(0)/\gamma$, in terms of the field free flow parameter, b_0, and dimensional quantities, is given by

$$\frac{h^2(0)}{\gamma} = \frac{2}{[1 + (4b_0^2\rho_0^2/B_0^{*4}\sigma^2)]^{1/2} - 1} \quad (28)$$

where $$B_0^* = \mu_e H_0^*$$

The relation between $h^2(0)/\gamma$ and the more fundamental parameter, $\sigma B_0^{*2}/b_0\rho_0$, is shown in Fig. 4.

It is seen from Fig. 3 and Eq. (28) that the reduction in shear stress, for a given field free flow, depends on both the applied field and the fluid conductivity. This reduction depends much more strongly on the impressed field than on the fluid conductivity.

Physically the magnetohydrodynamic interaction may be described as follows. At the wall, where the fluid velocity is zero, the induction is zero. As the horizontal velocity component increases further away from the wall, the induced currents increase and consequently the ponderomotive force, $\mu_e(\boldsymbol{J}^* \times \boldsymbol{H}^*)$ increases. This force, whose direction is opposite to the direction of the horizontal flow and therefore opposes the motion, conspires in the steady state to give a horizontal velocity component smaller in magnitude than would exist if the impressed field were absent. The net effect is a reduction in the velocity gradient at the wall.

To illustrate the orders of magnitude involved, consider the case $h^2(0)/\gamma = 1.6$. This, according to Fig. 3, corresponds to a 30 per cent reduction in wall shear stress. Using Eq. (28), and the following values for ρ_0, b_0, and σ which, for the re-entry problem, appear reasonable—$\rho_0 \simeq 1.6 \times 10^{-3}$kg./m.^{3}, $b_0 \simeq 5 \times 10^3$ sec.$^{-1}$, $\sigma \simeq 250$ mhos/m.; B_0^* becomes $\simeq 0.18$ webs/m.^{2} or 1,800 gauss.

Conclusion

By considering the two-dimensional stagnation-point flow of an infinite plate in a conducting fluid upon which is impressed an external parallel magnetic field normal to the plate, it has been demonstrated theoretically that a considerable reduction of wall shear stress can be effected. The percentage reduction depends markedly on the strength of the applied field and the conductivity of the fluid. It appears that it may be possible to utilize the natural ionization existing in the shock layer of a high speed re-entry missile to reduce the skin friction magnetically.

It is interesting to speculate on the effect of the magnetohydrodynamic interaction on heat transfer. As was pointed out in the Introduction, if reduced skin friction implies reduced heat transfer, (Reynolds' analogy), then a reduction in skin friction hydromagnetically should also have the same favorable effect on heat transfer. The situation here, however, is not as obvious as it seems, for it must be remarked that besides viscous there is Joulian dissipation. The Joulian heating, which increases with increasing distance from the wall, may more than offset some favorable thermomechanical analogy which might be in operation.

Further, it is interesting to conjecture on the effect of the interaction on transition to turbulence. It is well known[3] that the magnetic lines of force pervading the fluid give it a certain degree of rigidity so that the onset or growth of any random motions would be inhibited; also, the fact that the velocity gradient is reduced may perhaps have some favorable effect on transition.

Finally, it must be emphasized that the potentialities of this interesting new field of magnetohydrodynamics and its practical application to hypersonics will require much careful experimentation in addition to theoretical studies similar to that of this paper.

References

[1] Elsasser, Walter M., *Hydromagnetic Dynamo Theory*, Reviews of Modern Physics, Vol. 28, No. 2, pp. 135–163, April, 1953.

[2] Schlichting, Hermann, *Boundary Layer Theory*, pp. 70–73, McGraw-Hill Book Company, Inc., New York, 1955.

[3] Cowling, T. G., *Magnetohydrodynamics*, Interscience Publishers, Inc., New York, 1957.

Readers' Forum

BRIEF REPORTS of investigations in the aeronautical sciences and discussions of papers published in the JOURNAL are presented in this special department. Entries must be restricted to a maximum of 1,300 words or the equivalent of one JOURNAL page including formulas and illustrations. Publication is completed as soon as possible after receipt of the material. The Editorial Committee does not hold itself responsible for the opinions expressed by the correspondents.

Contents

Comments on "The Rotational Field Behind a Curved Shock Wave Calculated by the Method of Flux Analysis" ..... E. S. LOVE 199

Author's Reply ..... SHIGEO UCHIDA 200

Flows in Partly Dissociated Gases ..... HANS-JOACHIM METZDORF 200

On Axisymmetric Thermal Stresses in Thin Shells of Revolution ..... G. D. GALLETLY 201

On the Electric Tank Method for Study of Centrifugal Machines ..... SYŌGO MATSUNAGA 202

Lift and Rolling Moment on a Slender Wing-Body Combination With a Deflected Tip Control ..... JOHN F. CLARKE 203

Experiments on Chemical Kinetics in a Supersonic Nozzle ..... PETER P. WEGENER, JACK E. MARTE, AND CARL THIELE 205

Approximate Solution for Slightly Yawed n-Power Bodies at Hypersonic Speeds ..... ROBERT W. TRUITT 206

Buckling of a Simply Supported Rectangular Plate Under Compression Reacted by Shear ..... VICTOR I. WEINGARTEN 207

A Note on the Expressions for the Local Heat-Transfer Coefficient ..... RICHARD R. GOLD 208

On the Generalized Prandtl Relation ..... RUDI S. ONG 209

Further Comments on Diffuser Instability ..... W. C. RANDELS 210

A Test of the Uniqueness of Solutions for Problems of Nonsteady Flow Under Given Boundary Conditions ..... J. ALTENHOFF 210

Inelastic Combined Thermal and Applied Stresses in Skin-Stringer Aircraft Structure ..... B. E. GATEWOOD 212

A Special Case of Swirling Viscous Flow ..... DENNIS G. MABEY 212

Subsonic Lift Response to Penetration of a Sharp-Edged Gust Moving at Supersonic Speed ..... E. KRASNOFF 214

A Remark on the Optimum Design of Round Tubing ..... WILLIAM L. POESCH 215

On Optimum Nose Shapes for Missiles in the Superaerodynamic Region ..... DAVID H. DENNIS 216

Comments on "The Rotational Field Behind a Curved Shock Wave Calculated by the Method of Flux Analysis"

E. S. Love

Supervisory Aeronautical Research Engineer, Langley Aeronautical Laboratory, NACA, Langley Field, Va.

September 30, 1957

UCHIDA AND YASUHARA[1] have presented a means for calculating the rotational flow field behind a curved shock. In their evaluation of the effect of rotation and the validity of the characteristic relation employed, application was first made to the flow about a semiconvex airfoil. Calculations were made of the shock shape and of the pressure distribution over the airfoil (Figs. 10 and 12[1]) and were compared with experimental results designated as being those of Ferri.[2] The almost exact agreement between the calculated and the experimental results led to the conclusion[1] that the relation as developed "will be valid as a formula for giving corrections of effects caused by rotation as shown in the example of semiconvex airfoils." Examination of this excellent agreement between the theory and experiment has, however, revealed some disturbing features which, as they stand, do not lend support to the above conclusion.

The airfoil considered was two-dimensional semiconvex, 8.8 per cent thick with leading-edge and trailing-edge angles of 20°, and was at zero angle of attack with $M = 2.13$. For these conditions, the pressure coefficient C_p at the leading edge must be about 0.6 and the initial shock angle must be about 49.6°. However, reference 1 shows a theoretical value of C_p at the leading edge of about 0.85 and an initial shock angle of about 58°; further, these theoretical values are shown to be in agreement with Ferri's experimental results, thus implying that the experimental results contain errors that are identical with the deviations of the theoretical results from the correct values. Since this represents an unusual occurrence, a check was made of Ferri's original

Contributors Please Note

Readers' Forum items must be confined to the equivalent of one page in the *Journal*. Contributions that exceed this limit will be returned to the authors for condensation and rewrite. To avoid inconvenience and delay, please adhere to the following specifications:

(1) Five, double-spaced, typewritten, manuscript pages ($8\frac{1}{2}$ by 11 in.), including wide margins, formulas, and headings equal one printed page.

(2) For every illustration, deduct at least one-half or as much as one manuscript page, depending on the size of the illustration.

work where the pressures are both tabulated[2] and plotted.[2, 3] This check revealed that the experimental points contained in Fig. 12[1] are incorrect. Ferri has confirmed this in a private communication in which he suspects that ". . . the authors (of reference 1) misprinted the scale of the C_p coefficient. All the (experimental) values must be divided by 1.5 since the scale of q in my original paper corresponds to 15 divisions in place of 10; this is probably the source of the error." Thus, the theoretical results of reference 1 and the correct experimental results[2] do not agree. Moreover, division by 1.5 would still leave discrepancies between the experimental values in Fig. 12[1] and those obtained from the tabulations in reference 2 that are too large to be attributed to plotting accuracy. For example, the first experimental point in Fig. 12[1] would be about 0.41 instead of the correct value of about 0.46. Further, there remains unexplained the almost 10° error in shock angle at the leading edge and its supposed agreement with Ferri's results, which in fact does not occur.

In a search for an explanation of these discrepancies, the writer noted that the values of pressure coefficient and the shock angle at the leading edge obtained in reference 1 would be correct if the airfoil were at $\alpha = -4°$. However, this explanation is unsatisfactory since C_p at the 50 per cent chord would not be essentially zero at $\alpha = -4°$. Further, reference 2 presents no pressures for this airfoil at $\alpha = -4°$ and $M = 2.13$.

Some clarification of the errors in the theoretical pressures and shock shape and of the errors introduced in the use of Ferri's experimental results is needed, since these errors tend to cast doubt upon parts of the paper[1] which may otherwise be correct.

REFERENCES

[1] Uchida, Shigeo, and Yasuhara, Michiru, *The Rotational Field Behind a Curved Shock Wave Calculated by the Method of Flux Analysis*, Journal of the Aeronautical Sciences, Vol. 23, No. 9, pp. 830–845, September, 1956.

[2] Ferri, Antonio, *Experimental Results With Airfoils Tested in the High-Speed Tunnel at Guidonia*, Atti di Guidonia No. 17, September 20, 1939. (Available as NACA TM 946, July, 1940.)

[3] Ferri, Antonio, *Elements of Aerodynamics of Supersonic Flows*; The Macmillan Co., New York, 1949.

Authors' Reply

Shigeo Uchida
Professor of Fluid Dynamics, Nagoya University, Nagoya, Japan

November 7, 1957

THE AUTHORS APPRECIATE Love's comments on parts of reference 1 because slight but clear mistakes were found in Fig. 12.[1]

The application of the Flux-Analysis Method to the 8.8 per cent semiconvex airfoil was for the Mach Number $M_1 = 1.85$, not $M_1 = 2.13$ as given in reference 1. The pressure coefficient C_p at the leading edge is, therefore, about 0.815 and the initial shock angle is about 62.0°. These are almost satisfied by the original figure in reference 1.

The calculation was compared with Ferri's experiment given by Fig. 13 of reference 2, multiplying original values by 3/4 instead of 2/3. Incorrectness of the description of the experimental data was caused by this. In order to show the accurate result, a corrected figure for the original Fig. 12[1] is presented here. The full line is not altered from the original one excepting the part near the leading edge which was not exact in the tracer's work. The chain line shows the 0th order approximation calculated by the shock-expansion method with nonreflecting characteristics. The broken line is an analytical curve given by Ferri[2] which is coincident with the curve of shock expansion in the region of $0.5 \leqq x/l \leqq 1.0$. The reason for the deviation of these curves in the foresection is not clear to the present writer.

Since the effect of rotation diminishes the pressure coefficient as shown in the figure, better results of successive approximations will be expected if the start of the present calculation is based on Ferri's analysis.

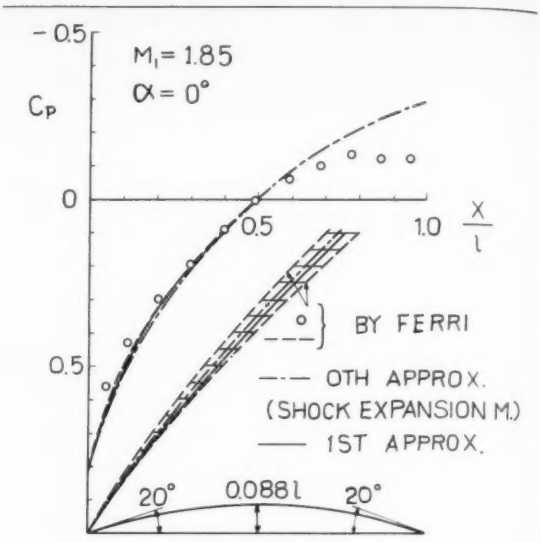

FIG. 12. (Revised).

Errata for reference 1:

(1) Change $M_1 = 2.13$ to $M_1 = 1.85$ on page 838 and in Figs. 10 and 12.

(2) Replace Fig. 12 with the revised Fig. 12.

(3) Change scale $y_1/d = 0, 2, 4, \ldots, 10, 12, 14$ to $y_1/d = 0, .2, .4, \ldots, 1.0, 1.2, 1.4$ in Fig. 17.

Flows in Partly Dissociated Gases†

Hans-Joachim Metzdorf*
Institut für Theoretische Physik der Freien Universitat Berlin, Berlin, Germany

October 17, 1957

THE SOLUTION of the laminar boundary-layer equations given by L. Moore[1] for a compressible medium with variable properties under the consideration of dissociation requires a correction, since next to the possible influence of nonbalanced state of dissociation the diffusion effects have not been considered. As the dissociation energy E_D in the range of temperature of partial dissociation is much greater than the internal and translational energy of the molecules and atoms, one must expect that the diffusion introduces a large influence on the heat-flow vector q_σ.

It is, therefore, suggested here that the following system of equations be considered for treatment of the flows of partly dissociated biatomic gases:

$$dn_1/dt = -n_1 v_{\sigma,\sigma} + r_1 - d_{1\sigma,\sigma} \tag{1a}$$

$$dn_2/dt = -n_2 v_{\sigma,\sigma} + r_2 - d_{2\sigma,\sigma} \tag{1b}$$

$$\rho(dv_\nu/dt) = -p_{,\nu} + (\mu \Pi_{\nu\sigma})_{,\sigma} \tag{2}$$

$$\rho(du/dt) + p v_{\sigma,\sigma} = \mu v_{\rho,\sigma} \Pi_{\rho\sigma} - q_{\sigma,\sigma} \tag{3}$$

$$p = (n_1 + n_2)kT \tag{4}$$

† The research discussed in this paper was sponsored by The Glenn L. Martin Company, Baltimore 3, Md. A detailed report was published by the company in May, 1956.

* I would like to express thanks to Prof. Dr. Ludwig for his constant encouragement and clear discussions during this work. Further thanks and gratitude are owed to the Bundesversicherungsanstalt, the Firma AEG-Turbinenfabrik, and specially to Messrs. Giese, Luhnau, and Dr. Nasitta.

with $\Pi_{\rho\sigma} = v_{\rho,\sigma} + v_{\sigma,\rho} - (2/3)v_{\tau,\tau}\delta_{\rho\sigma}$

where $\phi_{\nu_1 \ldots \nu_m,\nu} = (\partial/\partial x_\nu)\phi_{\nu_1 \ldots \nu_m}$

and $(d/dt)\phi_{\nu_1 \ldots \nu_m} = (\partial/\partial t)\phi_{\nu_1 \ldots \nu_m} + v_\nu \phi_{\nu_1 \ldots \nu_m,\nu}$

Similar to the style of the relativity theory, we are to sum over the double indices wherever they enter. The symbols used in the above equations are:

- v_ν = the three components ($\nu = 1, 2, 3$) of the flows velocities,
- q_ν = components of the vector of the heat-flow density,
- $d_{1\nu}, d_{2\nu}$ = components of the diffusion flow of atoms and molecules respectively,
- n_1, n_2 = number of atoms and molecules per unit volume, respectively,
- ρ = density,
- r_1, r_2 = change of n_1 and n_2 per unit time due to dissociation and recombination,
- μ = viscosity,
- λ = heat conductivity of gas without considering dissociation and diffusion,
- p = hydrostatic pressure,
- T = absolute temperature,
- k = Boltzmann constant,
- $\bar{\epsilon}$ = average internal energy of a molecule,
- E_D = dissociation energy,
- $\delta_{\mu\nu}$ = 1 for $\mu = \nu$, otherwise 0.
- m_1, m_2 = masses of an atom and a molecule, respectively,
- k_T = coefficient of thermal diffusion,
- k_1, k_2 = coefficients of reaction rate, which can be calculated from the cross section of the molecules for dissociation reaction,
- K = temperature-dependent constant of law of mass action: $n_2 = Kn_1^2$ (valid for equilibrium).

We are to substitute:

$$u = (1/\rho)\{(3/2)kTn_1 + [(3/2)kT + \bar{\epsilon}]n_2 + (1/2)E_D n_1\}$$

and $$r_1 = (k_1 n_1 + k_2 n_2)(n_2 - Kn_1^2)$$

$$r_2 = -(m_1/m_2)r_1$$

For the heat flow we are to use approximately:

$$q_\sigma = -\lambda T_{,\sigma} + (5/2)kT(d_{1\sigma} + d_{2\sigma}) + pk_T[(1/n_1)d_{1\sigma} - (1/n_2)d_{2\sigma}] + d_{1\sigma}(E_D/2) + d_{2\sigma}\bar{\epsilon}$$

The diffusion flow possesses, in the same approximation, the form:

$$d_{1\sigma} = -(m_2 n^2/\rho)\, D_{12}[d_{12\sigma} + k_T(\log T)_{,\sigma}]$$
$$d_{2\sigma} = (m_1 n^2/\rho) D_{12}[d_{12\sigma} + k_T(\log T)_{,\sigma}]$$

with

$$d_{12\sigma} = [n_1/(n_1 + n_2)]_{,\sigma} + [n_1 n_2(m_2 - m_1)/(n_1 + n_2)\rho]\ (\log p)_{,\sigma}$$

If we treat the problem of a stationary laminar boundary layer as Moore has done along a tangentially extended infinite flat plate, under the simple assumption that the dissociation equilibrium appears only momentarily and that we can set $k_T = 0$ without introducing large error, then the system (1) to (4) reduces to the usual boundary-layer equations for the flat plate. Only the coefficient $\bar{\lambda}$ ($q_\sigma = -\bar{\lambda}T_{,\sigma}$) and the specific heat c_p possess high maxima in the range of temperature of partial dissociation. If c_{pu} is the specific heat of the mixture without consideration of the dissociation and c_{pD} the part caused by dissociation, we get:

$$c_p = c_{pu} + c_{pD}$$

and $$\bar{\lambda} = \lambda + \rho D_{12} c_{pD}$$

with

$$c_{pD} = (n^2/\rho^2)m_1[n_1/(n_1 + n_2)]_{,T}\,[E_D + (5/2)kT - \bar{\epsilon}]$$

The heat conductivity, viscosity, etc. for pure nitrogen subjected to a pressure of $p = 3.10^8$ g. cm.$^{-1}$ sec.$^{-2}$ has been calculated under the consideration of experimental data and certain assumptions. As a result it came out that $\mu\rho$ shows a wave nature only by a small amount about an average value in a range of temperature from 3,500°K. to 7,500°K. It increases sharply, however, with decreasing temperature and reaches, at 1,000°K., nearly 200 per cent of the average value. It appears that the assumption $\mu\rho$ = constant, which had simplified the solution of the boundary layer equation, is not justified.

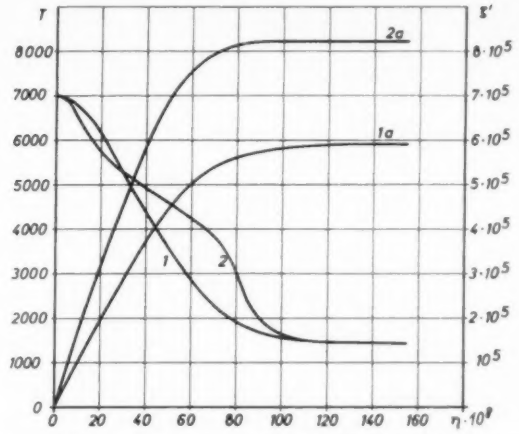

FIG. 1. The 1 and 2 curves show the temperature in the boundary layer depending on $\eta = (1/\sqrt{x})\int_0^y \rho(x,y^*)dy^*$ without and with consideration of diffusion, respectively. The 1a and 2a curves represent the corresponding velocity profiles ξ' cm.sec. [1]

According to a procedure similar to Dorodnizyn's method the boundary-layer equations have been reduced to a system of ordinary differential equations. The coefficients concerned are given in table form.

With the help of an electronic digital computer, the equations for the case of an isolated plate have been solved for special boundary conditions, once with and then without the consideration of the influence of diffusion on the heat conductivity. In the second case, the boundary values have been chosen in such a way that the temperature of the wall and the nuclear flow take the same value as in the first case (see Fig. 1).

REFERENCE

[1] Moore, L. L., *A Solution of the Laminar Boundary-Layer Equations for a Compressible Fluid with Variable Properties, Including Dissociation*, Journal of the Aeronautical Sciences, Vol. 19, No. 8, p. 505, August, 1952.

On Axisymmetric Thermal Stresses in Thin Shells of Revolution

G. D. Galletly
Mechanical and Electrical Engineering Department, Shell Development Company, Emeryville, Calif.
October 21, 1957

IN THEIR RECENT BOOK on thermal stresses,[1] Melan and Parkus give two coupled linear ordinary differential equations for calculating the stresses in a thin shell of revolution due to axisymmetric temperature distributions. Since these equations may be, or may have been, used for calculating thermal stresses in shells of varying wall thickness, the purpose of this note is to call attention to an apparent error in them. Only for shells of constant wall thickness will their equations yield correct results.

The notation used by Melan and Parkus will also be employed herein except that a prime will be used to indicate differentiation with respect to ϕ.

With the radial displacement, w, measured positive outward, the angle of rotation of a tangent to a meridian, χ, is given by

$$\chi = (1/r_1)\,(v - w') \tag{1}$$

In Eq. (1) χ is positive when the positive semitangent turns inward. The displacement along the meridian, v, is positive when directed in the direction of increasing ϕ.

The horizontal displacement, u, (considered positive outward) is related to v and w by

$$u = w \sin \phi + v \cos \phi \tag{2}$$

From Eqs. (1) and (2) we find

$$\chi = (1/r_1 \sin \phi)\,(u \cot \phi - u') - (\cot \phi/r_1)\,(v \cot \phi - v') \tag{3}$$

From Timoshenko,[2] we have

$$v \cot \phi - v' = r_2\,\epsilon_{\theta\theta} - r_1\,\epsilon_{\phi\phi} \tag{4}$$

The horizontal displacement, u, is also given by

$$u = r_2 \sin \phi\,\epsilon_{\theta\theta} \tag{5}$$

Now it can be shown that

$$r_2' = r_1\,(1 - r_2/r_1) \cot \phi \tag{6}$$

Using Eqs. (5) and (6) it will be found that

$$u \cot \phi - u' = (r_2 - r_1) \cos \phi \epsilon_{\theta\theta} - r_2 \sin \phi\,(\epsilon_{\theta\theta})' \tag{7}$$

Hence, from Eqs. (3), (4) and (7), we obtain

$$\chi = (\epsilon_{\phi\phi} - \epsilon_{\theta\theta}) \cot \phi - (r_2/r_1)\,(\epsilon_{\theta\theta})' \tag{8}$$

Eq. (8) is the compatibility equation relating the middle surface strains, $\epsilon_{\phi\phi}$ and $\epsilon_{\theta\theta}$, and the rotation of the meridional tangent, χ.

Utilizing Eq. (8), and proceeding in the manner outlined in reference 1, yields the following differential equations:

$$\chi'' + [(r_1/r_2)\,(r_2/r_1)' + \cot \phi + (3\delta'/\delta)]\chi' - \{[(r_1/r_2) \cot \phi]^2 + (\mu r_1/r_2)\,[1 - (3\delta'/\delta) \cot \phi]\}\chi = -(\delta^2 r_1^2/4Kr_2)Q + \alpha(1 + \mu)r_1[(3\delta'/\delta)\tau + \tau'] \tag{9}$$

$$Q'' + [(r_1/r_2)\,(r_2/r_1)' + \cot \phi - (\delta'/\delta)]Q' - \{[(r_1/r_2) \cot \phi]^2 - (\mu r_1/r_2)\,[1 + (\delta'/\delta) \cot \phi]\}\,Q = (4E/\delta)r_1[(r_1/r_2)\,\chi + \alpha\,T_0'] \tag{10}$$

The left-hand sides of Eqs. (9) and (10) agree with those given in Timoshenko* for shells of revolution subjected to axisymmetric edge bending loads. The right-hand sides of the equations agree in essence with those given by Melan and Parkus; however, the above right-hand sides are simpler. The simplification occurs as a result of using Eq. (6).

It will be seen that the left-hand side of Eq. (10) differs from the corresponding expression given by Melan and Parkus. The author believes that they introduce an error here by using the following compatibility equation:

$$\chi = [\epsilon_{\phi\phi} - (r_2/r_1)\epsilon_{\theta\theta}] \cot \phi - (1/r_1)\,(r_2\epsilon_{\theta\theta})' \tag{11}$$

The author believes Eq. (8) is the correct compatibility equation and not Eq. (11).

Denoting the value of χ given by Eq. (8) by $\bar{\chi}$, then Eq. (11) gives

$$\chi = \bar{\chi} - (2v/r_1) \cot^2 \phi \tag{12}$$

Usually, the tangential displacement, v, is small for shell problems and the error will probably not be important in many cases. However, near the apex of the shell (nose of a missile) $\cot \phi$ becomes very large. The error may be of importance in this region; however, as v will be quite small near the apex, it is difficult to make definite statements even for this case. Resort will probably have to be made to numerical comparisons of specific examples. Whatever the result of this comparison, it is nevertheless theoretically desirable to use the correct and somewhat simpler equations.

It is to be noted that in the special case of constant wall thickness (which is of importance in practice) the equations given herein coincide with those given by Melan and Parkus.

References

[1] Melan, E., and Parkus, H., *Wärmespannungen*, p. 91; Springer, Vienna, Austria, 1953.

[2] Timoshenko, S., *Theory of Plates and Shells*, p. 371; McGraw-Hill Book Co., Inc., New York, N.Y., 1940.

* See reference 2, p. 456.

On the Electric Tank Method for Study of Centrifugal Machines

Syōgo Matsunaga
University of Osaka Prefecture, Sakai, Osaka, Japan
August 2, 1957

AN APPROXIMATE METHOD for study of nonaxisymmetric flow by the electric tank method is described. With this method, the difference of circulation between blades and the radial thrust of runners will be roughly estimated from observation of the streamlines around the blades. The absolute flow in runners is decomposed into three potential flows—viz., discharge flow caused by the centrifugal force, the displacement flow itself, and circulation around the blade. These flows are combined in the electric tank so as to fulfill the boundary conditions on the casing wall automatically.

The streamlines of the fluid flow through the blade wheel are caused by the centrifugal force acting on the fluid. The velocity q_n is the velocity caused by the partial discharge quantity Q_n as shown in Fig. 1. The total flow quantity $\sum_n Q_n$ distributed along the circle around the eye of the pump gives rise to sum $\sum_n q_n$. The streamlines caused by centrifugal force acting on the fluid must satisfy the boundary condition of the blade surface, so a distribution of doublets on the blade surface must be added.

The velocity V_s in Fig. 1 is the velocity caused by the distributed doublets. The local strength of the doublet distribution must be chosen so as to satisfy the condition that the vector direction of v_B be coincident with the tangent line of the blade curve, where v_B is the vector sum of V_s and $\sum_n q_n$.

When the distribution of Q_n is given, the distribution of doublets on the blade will be known, and then the velocity distribution

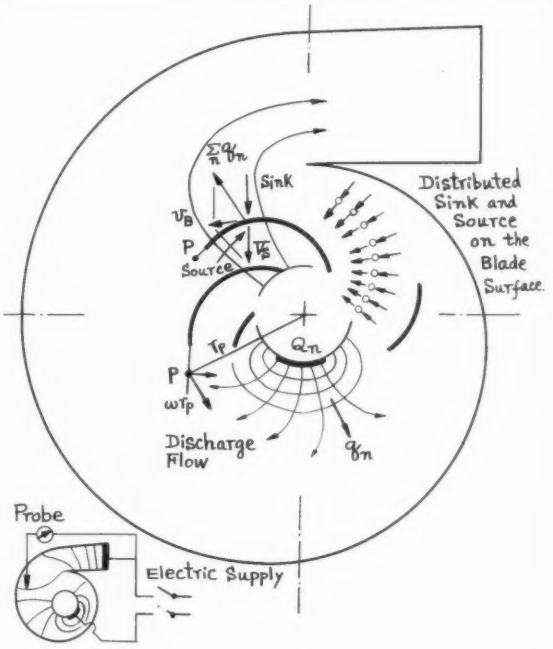

FIG. 1.

in the pump can be determined. The author considered the point P on the extension line of the blade near its edge (Fig. 1).

The velocity V is caused by the centrifugal force acting on the fluid, and its component V_n is perpendicular to the extension line of the blade (Fig. 3).

The electric tank method for study of the fluid flow caused by the rotating displacement at the point P is shown in Fig. 2, where a voltage difference added on the upper and lower surface of each blade represents a distribution of doublets of approximately constant strength. This approximation will be useful for the point near the blade edge. The streamlines caused by the rotating displacement of the blade can be obtained as the curves perpendicular to the equipotential lines. Using the normal velocity component $r\omega \cdot \cos\beta$ normal to the blade surface to determine the relation between applied voltage and fluid velocities, the velocity V_p at the point P can be determined by the streamline, and hence the normal component, V_{pn}.

The velocity v at the point P caused by the circulation is obtained by the method shown in the lower part of Fig. 3. The velocity v_n is the velocity component of v normal to the extension line of the blade curve. The velocity v' at the point P on the extension line of blade curve of one blade is caused by the circulation around another blade. v_n' is the component normal to the extension line of the blade curve.

The fluid flow must go smoothly along the blade curve at the exit of the bladed wheel, and this condition can be written as follows: the velocity component normal to the extension curve of the blade must be zero at the point P. The relations can be written at the point P of blade A as follows,

$$(V_n)_A + (V_{pn})_A + (v_n)_A + (\omega r_p \cdot \cos\beta_p)_A + (v_n')_{B\to A} + (v_n')_{C\to A} + (v_n')_{D\to A} + \ldots = 0$$

The sign of each term must be determined by the flow direction, where $(\ )_A$ shows the value at the point P of blade A, and, for example, $(\ )_{B\to A}$ shows the value caused by the circulation Γ_B around the blade B on the point P of the blade A. The values of $(v_n)_A$, $(v_n')_{B\to A}$, $(v_n')_{C\to A}$, etc. are functions of the circulations Γ_A, Γ_B, Γ_C, etc., having unknown magnitude. This relation between $(v_n)_A$ and Γ_A etc. can be obtained by the electric tank method.

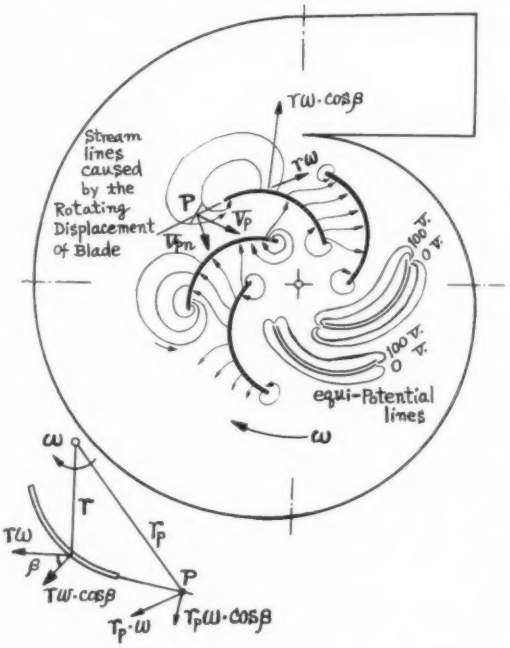

FIG. 2.

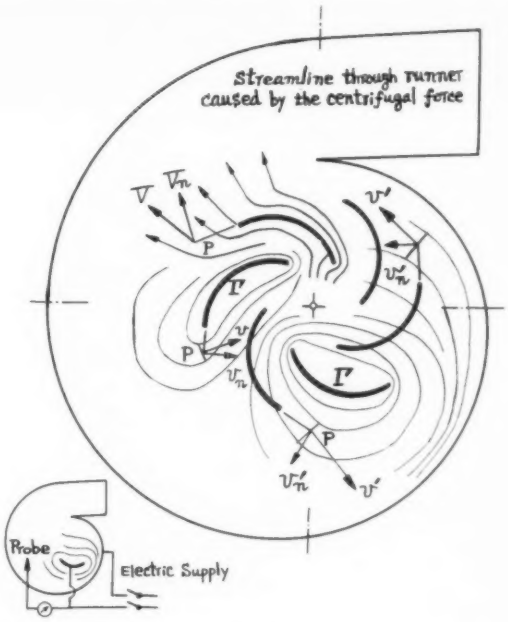

FIG. 3.

The above equation for blade A contains the unknown variables Γ_A, Γ_B, Γ_C, etc., and similar equations can be obtained for blades B, C, D etc., respectively. The unknown circulations Γ_A, Γ_B, Γ_C, etc., can be obtained by the solution of the group of equations mentioned above. It will be noticed that the interferences of the circulations around the blades are not considered because of the experimental difficulty of the electric tank method.

Lift and Rolling Moment on a Slender Wing-Body Combination With a Deflected Tip Control

John F. Clarke
English Electric Co. Ltd., Guided Weapons Division, Luton, Bedfordshire, England
October 24, 1957

SUMMARY

Lift and rolling moment acting on a wing-body combination with a single deflected wing-tip control have been calculated on the basis of the slender body approximation.

INTRODUCTION

THE MUTUAL INTERFERENCE between the components of a wing-body tip-control configuration of small aspect ratio may be significant at Mach Numbers up to low supersonic values. Some estimate of this interference can, in this case, be obtained from a slender body theory. We may take the configuration sketched in Fig. 1 as a fundamental element of such a system—i.e., the outboard section ($y_1 < y < y_2$) of a flat plate wing on a circular cross-section body (radius a) is deflected through an angle α. The wing body is at zero angle of attack to a main stream of velocity U.

Ward[1] gives results for the wing body at angle of attack while Mirels[2] has dealt with the case of both wings deflected on a body at zero angle of attack. Superposition of these results on those to be given below will allow very general solutions to be built up within the framework of the slender body approximation.

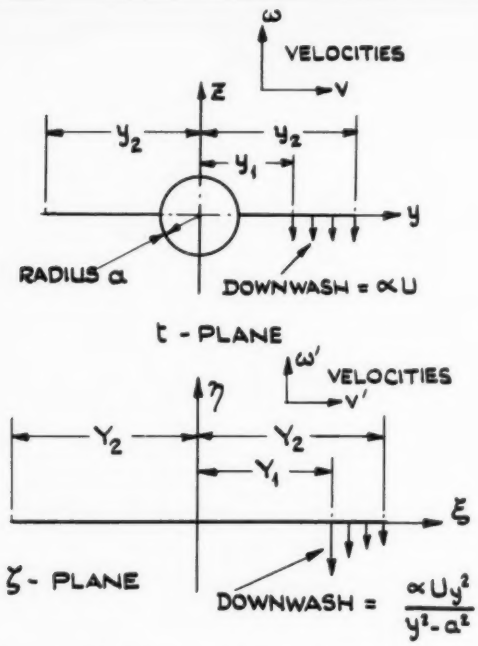

FIG. 1. Physical and transformed plane configurations.

RESULTS

The physical cross-flow plane (t plane) is transformed into the ζ plane by writing $\zeta = t + a^2 t^{-1}$, (see Fig. 1). The velocity field in the ζ plane can be shown to be given generally[3] by

$$v' - iw' = \left(-1/\pi \sqrt{Y_2^2 - \zeta^2}\right) \int_{-Y_2}^{Y_2} W(\xi') \left[\sqrt{Y_2^2 - \xi'^2}/(\zeta - \xi')\right] d\xi' \tag{1}$$

where $Y_2 = y_2 + a^2 y_2^{-1}$, $\zeta = \xi + i\eta$, and $W(\xi)$ is the downwash distribution between $-Y_2 < \xi < Y_2$. In the present case

$$\left.\begin{aligned} W(\xi) &= 0; \quad -Y_2 < \xi < Y_1; \quad \eta = 0 \\ W(\xi) &= (-\alpha U/2)\left[1 + \left(\xi/\sqrt{\xi^2 - 4a^2}\right)\right]; \\ & \qquad Y_1 < \xi < Y_2; \quad \eta = 0 \end{aligned}\right\} \tag{2}$$

and $Y_1 = y_1 + a^2 y_1^{-1}$.

Ward[1] has shown that the complex normal force F acting on a slender body of any cross section is

$$F = 2\pi\rho_\infty U a_1 + \rho_\infty U^2 (d/dx)\,[t_y(x) S(x)] \tag{3}$$

where ρ_∞ is undisturbed stream density, S is body cross-sectional area at station x and $t_y = y_y + iz_y$ is the (complex) co-ordinate of the body's center of area at station x. The coefficient a_1 is derived from the expansion,[1]

$$\Omega = \varphi + i\psi = a_0(x) \log_e t + b(x) + \sum_{n=1}^{\infty} a_n(x) t^{-n}$$

where φ is the velocity potential of the fluid motion created by the slender body. $a_0(x) = US'/2\pi$ for all body shapes (the dash indicating differentiation with respect to x). Using similar (momentum) methods we may show the rolling moment L to be

$$L = \Re\, 2\pi\rho_\infty U a_2 i - \rho_\infty U^2 (d/dx)\,[y_y z_y S + I] \tag{4}$$

where I is the product moment of body cross section taken about axes Gy', Gz' parallel to Oy, Oz and passing through the center of area G. For the body shape treated here $I = 0$; also $t_y = 0$ since the body is at zero angle of attack. We may find a_1, a_2 directly from series expansion of Eq. (1) in inverse powers of ζ, using the relation $\zeta = t + a^2 t^{-1}$. It is found from Eqs. (3) and (4) that (N B. $F = Y + iZ$),

$$Y = 0; \quad Z = 2\alpha q \int_{Y_1}^{Y_2} f(\xi')\, d\xi' \tag{5}$$

$$L(\alpha) = -\alpha q \int_{Y_1}^{Y_2} f(\xi')\, \xi'\, d\xi' \tag{6}$$

where q is dynamic pressure, $\rho_\infty U^2/2$, and $L(\alpha)$ is the rolling moment due to control deflection α. The function $f(\xi) = [1 + \xi(\xi^2 - 4a^2)^{-1/2}](Y_2^2 - \xi^2)^{1/2}$.

Eq. (5) can be integrated in terms of simple functions and yields

$$Z/\alpha q = Y_2^2[(\pi/2) - \sin^{-1}(Y_1/Y_2)] + (Y_2^2 - 4a^2) \sin^{-1}\sqrt{(Y_2^2 - Y_1^2)/(Y_2^2 - 4a^2)} - \sqrt{Y_2^2 - Y_1^2}\left[Y_1 + \sqrt{Y_1^2 - 4a^2}\right] \tag{7}$$

Noting that $\pi - \sin^{-1}(2a/y_2) = 2\cot^{-1}(a/y_2)$, Eq. (7) simplifies in the case of the single all-moving wing ($Y_1 = 2a$) and gives a value precisely half that found by Mirels[2] for both wings deflected. (Presumably the term in parentheses multiplying $\cot^{-1}(a/y_2)$ in reference (2) should be squared. It can then be shown that Dugan's result[4] is identical with Mirels'.)

Eq. (6) is rather more complicated but can be reduced to Legendre elliptic integrals of the first and second kinds plus simple functions. Then

$$-3L(\alpha)/\alpha q = (Y_2^2 - Y_1^2)^{3/2} + Y_1^{-1}(Y_2^2 - Y_1^2 - 8a^2)\sqrt{Y_1^2 - 4a^2}\sqrt{Y_2^2 - Y_1^2} + 4a^2 Y_2[K(k) - F(\theta, k)] + Y_2(Y_2^2 - 8a^2)[E(k) - E(\theta, k)] \tag{8}$$

where $F(\theta, k)$ and $K(k)$ are incomplete and complete elliptic integrals of the first kind, respectively, and similarly $E(\theta, k)$ and $E(k)$ are second kind integrals. The angle θ is given by $k \sin\vartheta = (1 - 4a^2 Y_1^{-2})^{1/2}$ and k is the modulus, $k^2 = 1 - 4a^2 Y_2^{-2}$. Some values of $-L(\alpha)/\alpha q y_2^3$ are plotted versus (a/y_2) in Fig. 2. The rolling moment produced by deflecting an all-moving wing is maximum when $(a/y_2) \simeq 0.3$.

The rolling moment $L(p)$ due to rolling at angular velocity p can be found by similar methods to those used for $L(\alpha)$. The result is

$$-(2U/qp)L(p) = Y_2^4 \cot^{-1}(a/y_2) - 4\pi a^4 + a(Y_2^2 - 8a^2)\sqrt{Y_2^2 - 4a^2} \tag{9}$$

Values of $-UL(p)/qpy_2^4$ are plotted in Fig. 2. Equilibrium roll rate is achieved when $L(\alpha) = L(p)$ and Eqs. (8) and (9) may be used to define a rolling effectiveness parameter $\beta = py_2/\alpha U$.

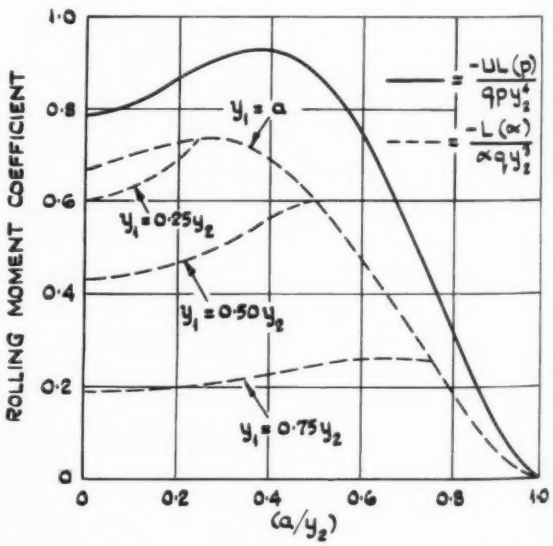

FIG. 2. Rolling moment coefficients versus (body radius/semi-span) ratio.

Values of β can be found from Fig. 2; and $\beta = 0.5$ when $(a/y_2) = 1.0$.

Slender body results are often useful in the form of ratios expressing the interference effect of the body. Since extensive information exists on tip controls fixed to the wing alone (reference 5, for example) we may define the ratio $L(\alpha)/L(\alpha)_0$ where $L(\alpha)_0 = -(2/3)\alpha q(y_2^2 - y_1^2)^{3/2}$, the rolling moment produced by an equivalent wing-control system without a body. This ratio is greater than one for all $(a/y_2) \gtrsim 0.9$, but tends to zero as $(a/y_2) \to 1.0$. Setting $y_1 = a$ as $a \to y_2$, results because $L(\alpha) \to 0$ as $(y_2 - a)^2$ while $L(\alpha)_0 \to 0$ as $(y_2 - a)^{3/2}$. The physical explanation is that the induced loading on the body is unable to contribute to L while the carry-over onto the wing with no body present has a favorable influence on rolling moment.

References

1. Ward, G. N., *Supersonic Flow Past Slender Pointed Bodies*, Quart. Jour. Mech. & App. Math., Vol. II, Part 1, 1949.
2. Mirels, H., *Lift Effectiveness of Slender Wings on Cylindrical Bodies*, Journal of the Aeronautical Sciences, Readers' Forum, Vol. 20, No. 7, pp. 504, 505, July, 1953.
3. Sears, W. R., *General Theory of High Speed Aerodynamics*, Vol. VI, Heaslet, Max A., and Lomax, Harvard, "Supersonic and Transonic Small Perturbation Theory, Section D.12; O.U.P., 1955.
4. Dugan, D. W., *Gap Effect on Slender Wing-Body Interference*, Journal of the Aeronautical Sciences, Readers' Forum, Vol. 21, No. 1, pp. 57, 58, January, 1954.
5. Mangler, K. W., and Thomas, H. H. B. M., *All-Moving Wing-Tip Controls at Subsonic, Sonic and Supersonic Speeds*, Aero. Report 2499, R.A.E. Farnborough, England, July, 1953.

Experiments on Chemical Kinetics in a Supersonic Nozzle*

Peter P. Wegener, Jack E. Marte, and Carl Thiele
Jet Propulsion Laboratory, California Institute of Technology, Pasadena, Calif.

October 31, 1957

SEVERAL MODERN TECHNIQUES in fluid dynamics have recently been applied to determine the rate and mechanism of fast chemical reactions.[1] Also, aerodynamicists have become interested in flows with chemical reactions and, in particular, those flows where relaxation effects become apparent. A new method for measuring fast, homogeneous gas reactions in a steady-state supersonic nozzle[2] will be described, and observations will be shown where a reaction is lagging with respect to chemical equilibrium throughout a steady-state flow field. The present experiment concerns the measurement of the rate of recombination of nitrogen dioxide into tetroxide, a reaction which was chosen because the properties of both species are well-known in chemical equilibrium.[3] The reacting species are carried in small concentration in dry nitrogen, and this mixture is passed through a supersonic nozzle. The process under investigation may be written as

$$N_2 + N_2O_4 \underset{k_R}{\overset{k_D}{\rightleftharpoons}} N_2 + 2\,NO_2 \qquad (1)$$

where k_D and k_R represent the rate constants for the dissociation and recombination reaction, respectively. Nitrogen is stored in a reservoir to permit continuous operation of a 2 by 3 cm. nozzle at $M = 1.9$ for about 1 hour. The reacting species are carefully prepared, metered, and added to the nitrogen, and the gas mixture is passed through an electric heater and fed into a screened settling chamber at 2 atm. total pressure and 400°K. temperature. For small reactant concentration, the N_2O_4 is fully dissociated into NO_2 in the supply. The ensuing expansion through the nozzle to $M = 1.9$ proceeds practically unaffected by the recombination reaction caused by the isentropic temperature drop. This is because the heat of reaction released in the flow is a negligible fraction of the stagnation enthalpy of the mixture at such low reactant concentration. This fact was experimentally verified, and, from a pressure calibration of the nozzle, the Mach Number and all thermodynamic parameters in the flow field are known.

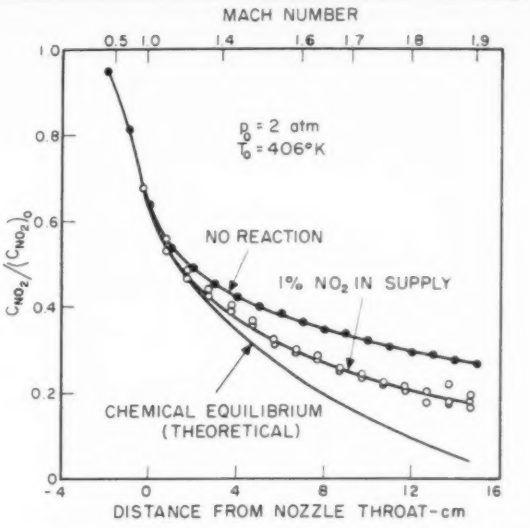

FIG. 1. Concentration of nitrogen dioxide mixed with nitrogen in a supersonic nozzle.

The concentration of nitrogen dioxide as a function of Mach Number, if no reaction takes place, can be computed from

$$C_{XO_2}/(C_{XO_2})_0 = \{1 + [(\gamma - 1)/2]M^2\}^{1/(1-\gamma)} \qquad (2)$$

where the subscript 0 denotes supply conditions, $\gamma = \gamma_{N_2} = 1.400$, and $C_{XO_2} = p_{XO_2}/RT$. Conversely, assuming that the recombination occurs infinitely fast, taking advantage of the fact that the stagnation enthalpy of the mixture remains unchanged during the expansion and making minor simplifying assumptions, it can be shown[2] that the concentration of NO_2 as a function of Mach Number is given by

$$\frac{C_{XO_2}}{(C_{XO_2})_0} = \left(\left\{1 + \frac{8\varphi p_0 F^{\gamma/(1-\gamma)}}{\exp\,[B - (A/T_0)F]}\right\}^{1/2} - 1\right) \times \frac{F}{4p_0\varphi} \exp\left(B - \frac{A}{T_0}F\right) \qquad (3)$$

where $F = 1 + [(\gamma - 1)/2]M^2$

p_0(atm) = supply pressure
T_0(°K.) = supply temperature
φ = volumetric fraction of NO_2 in supply
A = 6747, B = 20.72 (from experimental results on the equilibrium constant as a function of temperature)

Local concentrations of NO_2 determined from Eqs. (2) and (3) are shown in Fig. 1 as a function of distance along the continuously diverging nozzle. In Eq. (2) the experimentally observed Mach Number was used, and this result is, of course, independent of supply concentration. The theoretical concentration for chemical equilibrium computed from Eq. (3) is shown for the single admixture of 1 per cent NO_2 by volume in the supply. Also shown in the figure are observed NO_2 concentrations determined from several independent experiments. The experimental concentration was measured by optical absorption using a beam of near monochromatic light centering around 4,400Å, a wavelength which is strongly absorbed by the

* This work presents one phase of research carried out at the Jet Propulsion Laboratory, California Institute of Technology, under joint sponsorship of the Department of the Army, Ordnance Corps, and the Department of the Air Force.

brown NO_2, while N_2O_4 is transparent.[3] This light beam was passed through the nozzle center plane at right angles to the flow, and it was received by a battery-driven photomultiplier tube. The optical system could be moved along the flow during the experiment, and the incident and transmitted light intensities were determined. The concentration was finally computed from Beer's law by the use of a molar extinction coefficient previously determined with a similar optical system.[4]

Fig. 1 shows the interesting experimental fact that, in this experiment where the flow undergoes a cooling rate of the order of $10^5 < dT/dt(°K./sec.) < 10^6$, the net recombination reaction is not rapid enough to permit chemical equilibrium to be established during the entire expansion in contrast to Feldmann's[5] observations on air. Since all flow parameters are well-known at every Mach Number and since it is possible to observe concentration accurately in a steady-state system, it is evident that the rate of the reaction may now be computed. As a first attempt to determine k_R, it will be assumed that for Eq. (1) the net rate of concentration of NO_2 is given by

$$dC_{NO_2}/dt = 2k_D C_{N_2O_4} C_{N_2} - 2k_R C_{NO_2}^2 C_{N_2} \quad (4)$$

Without any further assumptions, k_R or k_D may be computed from the experimental data and Eq. (4), remembering that $K_c = k_D/k_R$, where K_c is the known equilibrium constant.[3] It was found that for $220 < T(°K.) < 300$ the recombination rate constant is independent of temperature and in the range $0.007 < \varphi < 0.013$, it is independent of concentration within the measuring accuracy. The average value obtained from 28 experiments is $k_R = 2 \times 10^{14}$ (cm.^{6} mole^{-2} sec.$^{-1}$), and it is known within about 70 per cent. Finally, in this temperature range general agreement is found with the dissociation rate measured by Carrington and Davidson[6] who used a shock-tube technique.

References

[1] The Study of Fast Reactions. Discussions of the Faraday Society No. 17; The Aberdeen University Press, Ltd., Aberdeen, G. B., 1954.

[2] Wegener, P. P., *Study of Fast Chemical Rate Processes in Supersonic Flow*, Bulletin APS, Series II, Vol. 1, No. 7, p. B7, November, 1956.

[3] Gray, P., and Yoffe, A. D., *The Reactivity and Structure of Nitrogen Dioxide*, Chem. Rev., Vol. 55, No. 6, pp. 1069–1155, December, 1955.

[4] Rosser, W. A., and Wise, H., *The Gas-Phase Oxidation of Ammonia by Nitrogen Dioxide*, Jet Propulsion Laboratory, California Institute of Technology, Progress Report, No. 20-273, September, 1955.

[5] Feldmann, S., *The Chemical Kinetics of Air at High Temperatures: a Problem in Hypersonic Aerodynamics*, 1957 Heat Transfer and Fluid Mechanics Institute, Preprints of Papers, pp. 173–192, June, 1957.

[6] Carrington, T., and Davidson, N., *Shock Waves in Chemical Kinetics: the Rate of Dissociation of N_2O_4*. J. Phys. Chem. Vol. 57, No. 4, pp. 418–427, April, 1953.

Approximate Solution for Slightly Yawed *n*-Power Bodies at Hypersonic Speeds

Robert W. Truitt

Professor of Aeronautical Engineering, Virginia Polytechnic Institute, Blacksburg, Va.

October 24, 1957

A STUDY OF THE results of references 1 and 2 suggests that, neglecting centrifugal forces, a reasonable approximation for the pressure distribution over a general slender body at finite hypersonic speeds and small angle of attack may be written as

$$C_p = 2\{1 + \lambda[(1 + N)/4]\} (\cos\alpha \sin\theta - \sin\alpha \cos\theta \sin\beta)^2 \quad (1)$$

In Eq. (1), $\lambda = (\gamma - 1)/(\gamma + 1)$, $N = (2f/M_\infty)^2/\lambda$, γ = ratio of specific heats, f = fineness ratio, M_∞ = Mach Number, α = angle of attack, θ = angle between local tangent to a meridian and the longitudinal body axis, and β = angular position of a point on the body surface.[1] For the special case of $M_\infty/f \to \infty (\gamma \to 1)$, Eq. (1) reduces to the expression for C_p derived in reference 1 where centrifugal forces and real-gas effects were neglected. On the other hand, when $\alpha \to 0$ Eq. (1) reduces to the equivalent C_p value given in reference 2 for slender conical surfaces at finite hypersonic speeds ($N < 2$ or 3).

Solution for *n*-Power Body

Perhaps the most suitable type body of revolution at hypersonic speeds is the n-power body, of fineness ratio $f = L/d$, with meridian section shape given by[2,3]

$$y/(d/2) = (x/L)^n \quad (2)$$

where L = length and d = diameter of the body. The advantages of the n-power body are twofold: (a) With or without centrifugal force effects, Eq. (2) is a reasonable approximation to the correct minimum-foredrag shape ($n = 3/4$ when centrifugal forces are neglected[3] and $n = 2/3$ when centrifugal forces are considered[2,3]); and (b) the blunt nose of the n-power body is appropriate from the point of view of aerodynamic heating.

It is in order to discuss the applicability of Eq. (1) in the region of the blunt nose of the n-power body—i.e., at $\theta = \pi/2$. For the case when $\alpha \to 0$ and $M_\infty/f \to \infty (\gamma \to 1)$, Eq. (1) is a satisfactory approximation since it reduces to the Newtonian impact value; for finite hypersonic speeds, however, Eq. (1) overpredicts the stagnation pressure coefficient. Nevertheless, the error in net drag at finite hypersonic speeds, due to this overprediction at the nose, is quite small since these high pressures act on a relatively small area of large slope near the nose. For the case of small angle of attack and $N < 2$ or 3, Eq. (1) should be a reasonable approximation for the n-power body pressure distribution.

Following the method of reference 1, Eq. (1) was applied (tangent-cone approximation) to the n-power body type. The expressions thus derived for the normal- and chord-force coefficients are, respectively,

$$C_N = (2Kn/f^{2n}) \sin 2\alpha \int_0^f \{x\, dx/[(n/2f^n)^2 + x^{2-2n}]\}^{\frac{1}{2}} \quad (3)$$

and

$$C_c = K\Big(|1 - (3/2)\sin^2\alpha|(n^3/f^{4n}) \times \int_0^f \{x^{2n-1}\, dx/[(n/2f^n)^2 + x^{2-2n}]\}^{\frac{1}{2}} + \sin^2\alpha\Big) \quad (4)$$

where $K = 1 + \lambda(1 + N)/4$ and x is in per cent of the body diameter—i.e., C_N and C_c are based on the maximum cross-sectional area. In Eqs. (3) and (4), the maximum body diameter was taken as unity and thus the fineness ratio $f = L$. The solutions for Eqs. (3) and (4) can be written in the general forms

$$C_N = K k_1 \sin 2\alpha \quad (5)$$

and

$$C_c = K[k_2 + k_3 \sin^2\alpha] \quad (6)$$

Table 1 contains the results of the integration of Eqs. (5) and (6) for a fineness ratio $f = 3$ and a series of values of n.

Since the results in Table 1 do not take into account centrifugal-force effects, the minimum-drag body corresponds to $n = 3/4$, as previously found in reference 3.

Centrifugal-Force Corrections

Cole,[2] taking into account centrifugal forces, derived an expression for the drag coefficient of n-power bodies for the special case of zero angle of attack and $N = 0$. A comparison of Cole's

Table 1
($f = 3$, Without Centrifugal-Force Effects)

n	k_1	k_2	k_3
0.6	0.975	0.0540	0.919
2/3	0.992	0.0474	0.929
0.7	0.997	0.0464	0.930
3/4	0.996	0.0457	0.932
0.8	0.994	0.0467	0.930
0.9	0.990	0.0503	0.925

TABLE 2
($f = 3$, With Centrifugal-Force Effects)

n	$C k_2$	$C k_3$
0.6	0.0400	0.680
2/3	0.0372	0.730
0.7	0.0374	0.751
3/4	0.0390	0.787
0.8	0.0416	0.828
0.9	0.0478	0.878

results with those in Table 1 suggests the use of an approximate centrifugal-force correction, C, in Eq. (6):

$$C_c = K[C k_2 + C k_3 \sin^2 \alpha] \quad (7)$$

where, for the range of $n(0.6 \leq n < 1)$, $C = 0.32 + 0.7n$. Table 2 contains the results of Table 1 corrected for centrifugal force. For small angle of attack, there is no corresponding centrifugal-force correction for the normal-force coefficient, Eq. (5).

For the special case of $\alpha = 0°$, $K = 1$ ($C_{c\alpha=0} \equiv C_D$), Eq. (7) and Table 2 reduce, of course, to Cole's original values for drag coefficient. In any case, based on the present approximate analysis, Eq. (7) and Table 2 show that for any Mach Number ($N < 2$ or 3) the minimum-drag body corresponds to $n = 2/3$.

The final expressions for the lift and drag coefficient for the n-power body, fineness ratio $f = 3$, are

$$C_L = K[k_1 \sin 2\alpha \cos \alpha - \sin \alpha (C k_2 + C k_3 \sin^2 \alpha)] \quad (8)$$

$$C_D = K[k_1 \sin 2\alpha \sin \alpha + \cos \alpha (C k_2 + C k_3 \sin^2 \alpha)] \quad (9)$$

For the case of $\alpha = 0°$,

$$C_D = K C k_2 \quad (10)$$

and it is seen that when $M_\infty/f \to \infty (K \to 1)$, the error in neglecting the centrifugal-force correction is appreciable—i.e., the error is 15 per cent for $n = 3/4$ and over 20 per cent for $n = 2/3$. On the other hand, for finite Mach Numbers, the product KC approaches unity and, therefore, the drag coefficient predicted by impact theory ($C_D = k_2$) would tend to be correct (for $\alpha = 0°$). For example, when $f = 3$, the product $KC \approx 1$ for the following combinations of Mach Number and n: (1) $n = 3/4$ and $N = 3$ ($K = 1.167$) and (2) $n = 0.8$ and $N = 2$ ($K = 1.125$). It would appear, therefore, that one should expect Newtonian impact theory predictions of pressure-drag coefficients (for $\alpha \to 0°$) to agree rather well with experiment for certain combinations of body shape and Mach Number—i.e., when $KC \approx 1$.

REFERENCES

[1] Grimminger, G., Williams, E. P., and Young, G. B. W., *Lift on Inclined Bodies of Revolution in Hypersonic Flow*, Journal of the Aeronautical Sciences, Vol. 17, No. 11, pp. 657–690, November, 1950.

[2] Cole, J. D., *Newtonian Flow Theory for Slender Bodies*, USAF, Project Rand, RM-1633, February 13, 1956.

[3] Eggers, A. J., Jr., Resnikoff, Meyer M., and Dennis, David H., *Bodies of Revolution Having Minimum Drag at High Supersonic Airspeeds*, NACA TN 3666, 1956.

Buckling of a Simply Supported Rectangular Plate Under Compression Reacted by Shear

Victor I. Weingarten

Structures Research Engineer, Northrop Aircraft, Inc., Hawthorne, Calif.

October 28, 1957

SUMMARY

The energy method was used in order to find the critical buckling load of a simply supported rectangular plate under compression reacted by shear. The plate here considered is assumed to follow the classical small-deflection theory. One point was checked by the method of finite differences. Results are presented graphically.

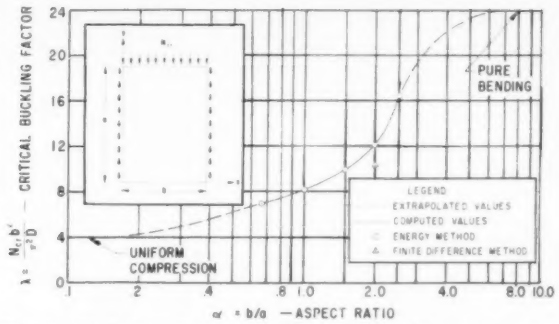

FIG. 1. Variation of critical buckling factor with aspect ratio.

SYMBOLS

x, y	= rectangular coordinates
a, b	= lateral dimensions of plate (Fig. 1)
w	= transverse deflection of plate
h	= thickness of plate
D	= $Eh^3/12(1-\mu^2)$ = bending stiffness of plate
α	= b/a
λ	= $N_{cr} b^2/\pi^2 D$
μ	= Poisson's ratio
m, n r, s p, q a	= positive integers
N_{cr}	= critical compressive buckling load
V	= strain energy of bending
T	= work produced by external forces
N_x, N_y	= normal forces per unit length of sections of a plate perpendicular to x- and y-directions, respectively
N_{xy}	= shear force in direction of y axis per unit length of section of a plate perpendicular to x axis

SOLUTION OF THE PROBLEM

A SIMPLY SUPPORTED rectangular plate (Fig. 1), is considered, along whose sides $x = 0$ and $x = b$ shear reacts a uniformly distributed compressive force applied at $y = a$. The compressive force at any interior point is assumed by the equation

$$N_y = N_{cr}(y/a) \quad (1)$$

The deflection of the buckled plate simply supported on all sides is taken in the form of the double trigonometric series,

$$w = \sum_{m=1}^{\infty} \sum_{n=1}^{\infty} a_{mn} \sin (m\pi y/a) \sin (n\pi x/b) \quad (2)$$

The energy method will be used to calculate the critical value of the compressive force N_{cr}. The strain energy of bending is given by the equation.[1]

$$\Delta V = (1/2)D \int_0^a \int_0^b \{[(\partial^2 w/\partial x^2) + (\partial^2 w/\partial y^2)]^2 - 2(1-\mu)[(\partial^2 w/\partial x^2)(\partial^2 w/\partial y^2) - (\partial^2 w/\partial x \partial y)^2]\} dy\, dx \quad (3)$$

Substituting Eq. (2) into Eq. (3) and integrating we obtain:[1]

$$\Delta V = (\pi^4 ab/8) D \sum_{m=1}^{\infty} \sum_{n=1}^{\infty} a_{mn}^2 [(m^2/a^2) + (n^2/b^2)]^2 \quad (4)$$

The work done by external forces during buckling of the plate is

$$\Delta T = (1/2) \int_0^a \int_0^b (N_{cr}\, y/a)(\partial w/\partial y)^2 dy\, dx \quad (5)$$

Substituting Eq. (2) into Eq. (5) and noting that

$$\int_0^b y \cos (r\pi y/b) \cos (s\pi y/b)\, dy = b^2/4 \quad \text{for } r = s$$

$$\int_0^b y \cos (r\pi y/b) \cos (s\pi y/b)\, dy = 0 \quad \text{for } r \neq s$$

$r \pm s$ is an even number.

$$\int_0^b y \cos (r\pi y/b) \cos (s\pi y/b)\, dy = -(2b^2/\pi^2)[(r^2+s^2)/(r^2-s^2)^2] \quad \text{for } r \neq s$$

$p \pm s$ is an odd number. We obtain the following equation:

$$\Delta T = (N_{cr}\, b/4a)\left(\sum_{n=1}^{\infty}\sum_{m=1}^{\infty} a_{mn}{}^2\,(m\pi/a)^2\,(a^2/4) - \sum_{m=1}^{\infty}\sum_{n=1}^{\infty}\sum_{p}^{\infty} a_{mn}a_{pn}(m\pi/a)\,(p\pi/a)\times \left\{(2a^2/\pi^2)\,[(m^2+p^2)/(m^2-p^2)^2]\right\}\right) \quad (6)$$

$m \neq p$, $m \pm p$ is an odd number.

In order to simplify computation, the general expression, Eq. (2), is reduced to

$$w = \sin(\pi x/b)\sum_{m=1}^{\infty} a_{m1}\sin(m\pi y/a) \quad (7)$$

which is equivalent to the assumption that the plate buckles into a half wave in the x direction. Letting the strain energy of bending equal the work produced by the external forces in conjunction with Eq. (7) we obtain

$$a_{m1}\left\{\left[(b^2/a^2)\,m^2+1\right]^2 - (N_{cr}\,b^4/2\,a^2\,\pi^2 D)\,m^2\right\} + (2\,N_{cr}\,b^4/a^2\,\pi^4 D)\sum_{p}^{\infty} a_{p1}\,mp\left[(m^2+p^2)/(m^2-p^2)^2\right] = 0 \quad (8)$$

$m \neq p$, $m \pm p$ is an odd number.

By letting $\alpha = b/a$ and $\lambda = (N_{cr}\,b^2/\pi^2 D)$ and writing Eq. (8) for three equations we obtain

$$\left[(\alpha^2+1)^2 - (\alpha^2/2)\,\lambda\right]a_{11} + \left[(20\alpha^2/9\pi^2)\lambda\right]a_{21} = 0$$

$$\left[(20\alpha^2/9\pi^2)\lambda\right]a_{11} + \left[(4\alpha^2+1)^2 - 2\alpha^2\lambda\right]a_{31} + \left[(60\alpha^2/9\pi^2)\lambda\right]a_{21} = 0$$

$$\left[(60\alpha^2/9\pi^2)\lambda\right]a_{21} + \left[(9\alpha^2+1)^2 - (9/2)\alpha^2\lambda\right]a_{31} = 0$$

Equating the determinate of these equations to zero, an equation for calculating the three term approximation is obtained which has been found to be sufficiently accurate for this problem.

A plot of α versus λ is found in Fig. 1 extrapolated to the limiting cases:

Case 1: $\alpha \to \infty$ Approaches a plate under pure bending $\lambda = 23.9$ (reference 1)

Case 2: $\alpha \to 0$ Approaches a plate under uniform compression $\lambda = 4$ (reference 1)

For an aspect ratio of $\alpha = 2$ a finite difference solution was performed using 21 interior points. The biharmonic Eq. (9):

$$(\partial^4\phi/\partial x^4) + 2\,(\partial^4\phi/\partial x^2\partial y^2) + (\partial^4\phi/\partial y^4) = 0 \text{ (reference 2)} \quad (9)$$

was solved in finite difference form using the appropriate boundary conditions in order to determine the stress distribution throughout the plate. The buckling equation.[1]

$$(\partial^4 w/\partial x^4) + 2(\partial^4 w/\partial x^2\partial y^2) + (\partial^4 w/\partial y^4) = (1/D)\,[N_x(\partial^2 w/\partial x^2) + N_y(\partial^2 w/\partial y^2) + 2\,N_{xy}(\partial^2 w/\partial x\partial y)] \quad (10)$$

was then solved in finite difference form which determined the critical buckling load. A comparison of the finite difference solution with the energy solution showed a difference of 15 per cent. The finite difference solution has been found, in previous papers, to be a lower limit of the critical buckling load.[3, 4]

The energy solution always gives an answer above the true buckling load. The true solution is therefore somewhere between the two.

Since the energy solution assumes a stress distribution to equal $N_{cr}\,y/a$ and the finite difference techniques calculate the stress distribution, this might further account for the 15 per cent difference of the two answers. This error will become small for lower values of α since the stress distribution will approach the linear variation assumption.

References

[1] Timoshenko, S., *Theory of Elastic Stability*, 1st Ed., pp. 315, 324, 329, 355; McGraw-Hill Book Co., Inc., N.Y., 1936.

[2] Timoshenko, S., and Goodier, J. N., *Theory of Elasticity*, 2nd Ed., p. 26; McGraw-Hill Book Co., Inc., N.Y., 1951.

[3] Weingarten, V. I., *The Buckling of Triangular or Skew Plates*, Journal of the Aeronautical Sciences, Readers' Forum, Vol. 24, No. 5, p. 384, May 1957.

[4] Weingarten, V. I., *Method of Determining the Critical Buckling Stress of Oblique and Triangular Plates*, Northrop Aircraft Report NAI-57-164.

A Note on the Expressions for the Local Heat-Transfer Coefficient

Richard R. Gold

Member of Technical Staff, Aerodynamics Department, Hughes Aircraft Company, Culver City, Calif.

October 28, 1957

A GREAT DEAL of effort has been put forth on establishing the expressions for the local heat-transfer coefficients in laminar and turbulent flow. Several surveys on the subject[1, 2, 3] present an extensive picture of the problem along with the assumptions made in the various theories for incompressible as well as compressible flow. The remarks of this note will be restricted to the case of an isothermal flat plate at zero angle of attack. The standard transformations[2] provide the corresponding expressions for the cone.

For the case of laminar incompressible flow, the following generally accepted result of Pohlhausen is used:

$$Nu_L = 0.332\,Re^{1/2}Pr^{1/3} \quad (1)$$

Frequently used results for laminar compressible flow are those of Chapman and Rubesin, and Van Driest.

Using Blasius' equation for the turbulent skin friction and Reynolds' analogy, where S = Reynolds' analogy factor = $Pr^{-2/3}$, the local Nusselt number for turbulent incompressible flow is given by

$$Nu_T = 0.0296\,Re^{4/5}Pr^{1/3} \quad (2)$$

A widely used expression for compressible flow is due to Van Driest.

Various authors have attempted to apply the incompressible heat-transfer relations to compressible flow by evaluating the fluid properties at some reference temperature. The success of this concept has been illustrated by Eckert[2] for both laminar and turbulent flow.

In keeping with this idea consider* the variation of the local heat-transfer coefficient as indicated through Eq. (1). This equation reduces to

$$h_L = 0.332\,(\rho u/Rx)_\delta{}^{1/2}\,F(T) \quad (3)$$

where all the temperature-dependent quantities have been collected into the single term

$$F(T) = (k\,Pr^{1/3}/\sqrt{\mu T})\text{ (B.t.u./sec. ft. °F.)}\times \text{(ft.}^2\text{/lb. sec. °R.)}^{1/2} \quad (4)$$

The subscript δ refers to conditions at the outer edge of the boundary layer while the subscripts L and T refer to laminar and turbulent flow. Using the results of the standard gas tables along with those of reference 4 to evaluate $F(T)$ independently, it can be shown that $F(T)$ is approximately constant in the range $100 \leq T \leq 2000$°R. This approximate value is $F(T) = 0.000256$, in which case Eq. (3) reduces to

$$h_L = 2.0579 \times 10^{-6}\,(\rho u/x)_\delta{}^{1/2}\text{ (B.t.u./ft.}^2\text{ °F. sec.)} \quad (5)$$

This result is within the accuracy maintained in the analysis of Eckert, for example, where the validity of using the constant-property solution for the compressible case is shown. As a result, one can observe that, within the accuracy of our knowledge of the variation of the fluid properties with temperature, the assump-

* This approach was used by A. E. Bryson, C. P. Stensgaard, Jr., and J. M. Bozajian as early as 1952 based on reference 5.

tion that h_L is independent of the choice of reference temperature, indeed that it is actually independent of temperature, is reasonable. For ease of use, the resultant simplified expression for h_L, given by Eq. (5), can be reduced to the form of a nomograph by standard methods. It is interesting to note that if the frequently used expressions for the variation of viscosity and conductivity with temperature, namely Pr = constant, $\mu \sim K \sim T$, are applied to the function F one would obtain: $F(T)$ = constant. Experimental verification of the above has been obtained from reference 3 where the laminar expressions of Pohlhausen, Chapman and Rubesin, and Eq. (5) are compared with test data. Further verification has been obtained from existing flight-test data on cones of various sizes covering a wide range of Mach Number, Reynolds' Number, and ratio of wall temperature to temperature outside the boundary layer. The results of this correlation indicate that Eq. (5) predicts the test data reasonably well. The results of Eq. (5) are in excellent agreement with the values predicted by Pohlhausen's expression, as would be expected, and are in good agreement with the values predicted by the expression of Chapman and Rubesin, and Van Driest. The data include an appreciable amount of scatter at times in addition to several points lying in the transition region, which accounts for some of the disparity with theory. As a result of the above discussion, it may be stated that h_L is independent of temperature for all practical purposes and the resultant simplified expression for h_L can be conveniently represented by a simple nomograph.

A similar reasoning can be applied to the case of turbulent compressible flow in which case the results serve to justify the analysis of Eckert and present a calculation simplifying expression based on his equations. We will use the analysis of Eckert outlined in reference 2. The experimental calculations examined in the present investigation have generally been in the range $Re_\delta \leq 40 \times 10^6$ in which case the constant value $S = 1.18$ suggested in the literature is used. A theoretical correlation with experimental data using Blasius' incompressible expression gave good results in this range. As a result, this expression is used instead of the several expressions suggested by Eckert for turbulent incompressible flow. In order to simplify the calculation of the heat-transfer quantities from Eckert's analysis, the temperature dependent terms have once again been collected into a single term in the expression for the local turbulent heat-transfer coefficient. The resultant expression is given by

$$\left.\begin{aligned} h_T &= 0.0349\ [(pux)_\delta^{0.8}/xR^{0.8}]G(T^*) \\ G(T^*) &= [k\ Pr/(\mu T^*)^{0.8}]\ \text{(B.t.u./sec. ft. °F.)} \times \\ &\qquad \text{(ft.}^2\text{/lb. sec. °R.)}^{0.8} \end{aligned}\right\} \quad (6)$$

where T^* is Eckert's reference temperature. Using the aforementioned variation as a guide, namely, $\mu \sim K \sim T$, one obtains $G(T^*) \sim T^{*-0.6}$ and applying the previously mentioned data one obtains, with adequate accuracy,

$$G(T^*) = 0.113\ T^{*-0.6}, \quad 150 \leq T \leq 2000°\text{R},$$

such that

$$h_T = 10.25 \times 10^{-6}[(pux)_\delta^{0.8}/xT^{*0.6}] \quad (7)$$

Eq. (7) can also be conveniently represented by a nomograph. Various experimental results of flight-test data which were described above indicate that Eq. (7) predicts the test data generally within 10 per cent, and, in several instances, this figure rises to 15–20 per cent. It is of interest to note that the results of Eq. (7) are conservative. For comparison purposes the well-known expression of Van Driest was used to predict the same test data. The results of this correlation were similar to those obtained using Eq. (7) except that the results of Van Driest were nonconservative. Eq. (7) generally overpredicted the test data while Van Driest's expression gave values which were generally low. As a result, the analysis of Eckert seems justified.

References

[1] Kaye, J., *Survey of Friction Coefficients, Recovery Factors, and Heat-Transfer Coefficients for Supersonic Flow*, Journal of the Aeronautical Sciences, Vol. 21, No. 2, pp. 117–129, February, 1954.

[2] Eckert, E. R. G., *Survey on Heat Transfer at High Speeds*, WADC TR 54-70, April, 1954.

[3] Decoursin, D. G., Bradfield, W. S., and Sheppard, J. J., *Aerodynamic Heating and Heat Transfer Phenomena at Mach Numbers 2.7 through 5.7*, WADC TR 53-379, February, 1954.

[4] Tribus, M., and Boelter, L. M. K., *An Investigation of Aircraft Heaters II —Properties of Gases*, NACA A.R.R. W-9, 1942.

[5] Johnson, H. A., Rubesin, M. W., Sauer, F. M., Slack, E. G., Possner, L., *A Design Manual for Determining the Thermal Characteristics of High Speed Aircraft*, AAF TR 5632, September, 1947.

On the Generalized Prandtl Relation

Rudi S. Ong

Assistant Professor, Department of Aeronautical Engineering, University of Michigan, Ann Arbor, Mich.

October 28, 1957

Consider a four-dimensional Euclidean space-time manifold, E_4. The time variable will be denoted by t, and the space variables by x^λ, $\lambda = 1, 2, 3$. In particular, we assume that the space variables are Cartesian and define ∞^1 Euclidean three spaces E_3 in E_4.

The tensor formulation of the hydrodynamical equations in these coordinate systems has the form:

$$(\partial/\partial t)\ (\rho v_\lambda) + \nabla_\mu(\rho v^\mu v_\lambda + p\delta^\mu_\lambda) = 0 \quad (1)$$

$$(\partial\rho/\partial t) + \nabla_\mu(\rho v^\mu) = 0 \quad (2)$$

$$(\partial/\partial t)\ \{\rho[(q^2/2) + e]\} + \nabla_\mu\{\rho v^\mu[(q^2/2) + h]\} = 0 \quad (3)$$

δ^α_α is the usual notation for the Kronecker delta, and ρ, v_λ, q, e, p, and h denote the density, component of velocity, magnitude of the velocity, internal energy, pressure, and enthalpy, respectively.

Eq. (1) is equivalent to the Eulerian equations of motion for compressible nonviscous fluids in the absence of body forces; Eq. (2) is the equation of continuity; and Eq. (3) is the energy relation.

The hypersurface (or lower-dimensional manifold) in space time along which discontinuities occur will be denoted by

$$\overset{j}{\phi}(t, x^\lambda) = {}^jk \quad \text{where the } {}^jk \text{ are constants} \quad (4)$$

If Eq. (4) consists of only one equation ($j = 0$), then the discontinuity manifold defines a hypersurface. If the system consists of more than one equation, then the equations define a manifold of lower dimension. In any case, the vector fields for the various types of j, $\partial\overset{j}{\phi}/\partial t$, $\partial\overset{j}{\phi}/\partial x^\lambda$, determine vectors normal to the discontinuity manifold. Furthermore, the unit normal vectors of this manifold are determined by

$$\left.\begin{aligned} n_t &= (\partial\phi/\partial t)/[(\partial\phi/\partial t)^2 + g^{\lambda\mu}(\partial\phi/\partial x^\lambda)\ (\partial\phi/\partial x^\mu)] \\ n_\lambda &= (\partial\phi/\partial x^\lambda)/[(\partial\phi/\partial t)^2 + g^{\lambda\mu}(\partial\phi/\partial x^\lambda)\ (\partial\phi/\partial x^\mu)] \end{aligned}\right\} \quad (5)$$

where $g^{\alpha\beta}$ is the metric tensor.

In the case where the discontinuity manifold is a shock wave, the values of ρ, v_λ, e, p, and h and their space-time derivatives are assumed to be continuous, while in crossing the discontinuity manifold these values are discontinuous.

Let $\overline{\rho v_\lambda}$ denote the jump in the value of ρv_λ across the shock discontinuity, $\overline{\rho v^\mu v_\lambda}$ the jump in the value of $\overline{\rho v^\mu v_\lambda}$, etc. Then by means of the integral forms of Eqs. (1), (2), and (3), the following jump relations corresponding to Eqs. (1), (2), and (3) may be obtained[1]

$$(\partial\phi/\partial t)\ \overline{\rho v_\lambda} + (\partial\phi/\partial x^\mu)\ (\overline{\rho v^\mu v_\lambda} + \delta_\lambda{}^\mu\bar{p}) = 0 \quad (6)$$

$$(\partial\phi/\partial t)\bar{\rho} + (\partial\phi/\partial x^\mu)\overline{\rho v^\mu} = 0 \quad (7)$$

$$(\partial\phi/\partial t)\ [\overline{(\rho q^2/2)} + \overline{\rho e}] + (\partial\phi/\partial x^\mu)\ [\overline{(\rho q^2 v^\mu/2)} + \overline{\rho h v^\mu}] = 0 \quad (8)$$

Let the subscripts 1 and 2 indicate values on the sides of the

shock wave, then

$$\overline{\alpha\beta} = (\alpha\beta)_2 - (\alpha\beta)_1 = (\alpha_2 - \alpha_1)(\beta_2 - \beta_1) + \alpha_1\beta_2 + \alpha_2\beta_1 - 2\alpha_1\beta_1$$

Upon simplifying the right hand side of the above, the jump may be expressed in the form

$$\overline{\alpha\beta} = \bar{\alpha}\bar{\beta} + \alpha_1\bar{\beta} + \beta_1\bar{\alpha}$$

Hence,

$$\overline{\rho v_\lambda} = \bar{\rho}\bar{v}_\lambda + \rho_1\bar{v}_\lambda + v_{\lambda_1}\bar{\rho}$$

$$\overline{\rho v^\mu v_\lambda} = \overline{\rho v^\mu}\,\bar{v}_\lambda + \rho_1\bar{v}_1{}^\mu\bar{v}_\lambda + v_{\lambda_1}\overline{\rho v^\mu} \quad \text{etc.}$$

Expanding Eq. (6) in this manner the following equation is obtained:

$$(\partial\phi/\partial t)(\bar{\rho}\bar{v}_\lambda + \rho_1\bar{v}_\lambda + \bar{\rho}v_{\lambda_1}) + (\partial\phi/\partial x^\mu)[\overline{\rho v^\mu}\bar{v}_\lambda + (\rho v^\mu)_1\bar{v}_\lambda + \overline{\rho v^\mu}\,v_{\lambda_1}] + \bar{p}\,\partial\phi/\partial x^\lambda = 0$$

Assume now that $\bar{p} = c^2\bar{\rho}$ where c^2 is the "velocity of sound." Then using Eq. (7), the above equation may be reduced to

$$\rho_1\bar{v}_\lambda[(\partial\phi/\partial t) + v_1{}^\mu(\partial\phi/\partial x^\mu) + c^2\bar{\rho}(\partial\phi/\partial x^\lambda)] = 0$$

Solving for $\bar{\rho}$,

$$\bar{\rho} = -\{\rho_1\bar{v}_\lambda[(\partial\phi/\partial t) + v_1{}^\mu(\partial\phi/\partial x^\mu)]/c^2(\partial\phi/\partial x^\lambda)\} \qquad (9)$$

Expanding Eq. (7) the following equation is obtained:

$$(\partial\phi/\partial t)\bar{\rho} + (\partial\phi/\partial x^\mu)(\overline{\bar{\rho}v^\mu} + \rho_1\bar{v}^\mu + \bar{\rho}\,v_1{}^\mu) = 0$$

or $$\bar{\rho}[(\partial\phi/\partial t) + (\bar{v}^\mu + v_1{}^\mu)(\partial\phi/\partial x^\mu)] + \rho_1\bar{v}^\mu(\partial\phi/\partial x^\mu) = 0$$

Substituting the value of $\bar{\rho}$ from Eq. (9) into the last equation yields

$$-\frac{\rho_1\bar{v}_\lambda[(\partial\phi/\partial t) + v_1{}^\mu(\partial\phi/\partial x^\mu)][(\partial\phi/\partial t) + (\bar{v}^\mu + v_1{}^\mu)(\partial\phi/\partial x^\mu)]}{c^2(\partial\phi/\partial x^\lambda)} + \rho_1\bar{v}^\mu(\partial\phi/\partial x^\mu) = 0$$

or $$\bar{v}_\lambda[(\partial\phi/\partial t) + v^\alpha(\partial\phi/\partial x^\alpha)]_1[(\partial\phi/\partial t) + v^\beta(\partial\phi/\partial x^\beta)]_2 - c^2\overline{v^\mu}(\partial\phi/\partial x^\mu)(\partial\phi/\partial x^\lambda) = 0 \qquad (10)$$

Since the tangential component of velocity is continuous across a shock discontinuity,

$$\bar{v}_\lambda = \bar{v}^\mu(\partial\phi/\partial x^\mu)(\partial\phi/\partial x^\lambda)/g^{\alpha\beta}(\partial\phi/\partial x^\alpha)(\partial\phi/\partial x^\beta)$$

Thus Eq. (10) becomes

$$\bar{v}_\lambda\{[(\partial\phi/\partial t) + v^\alpha(\partial\phi/\partial x^\alpha)]_1[(\partial\phi/\partial t) + v^\beta(\partial\phi/\partial x^\beta)]_2 - c^2g^{\alpha\beta}(\partial\phi/\partial x^\alpha)(\partial\phi/\partial x^\beta)\} = 0$$

Since by hypothesis $\bar{v}_\lambda \neq 0$,

$$[(\partial\phi/\partial t) + v^\alpha(\partial\phi/\partial x^\alpha)]_1[(\partial\phi/\partial t) + v^\beta(\partial\phi/\partial x^\beta)]_2 - c^2g^{\alpha\beta}(\partial\phi/\partial x^\alpha)(\partial\phi/\partial x^\beta) = 0 \qquad (11)$$

Expressing this equation in terms of n_t, n_λ, as defined by Eqs. (5), yields the following equation:

$$(n_t + v^\lambda n_\lambda)_1(n_t + v^\mu n_\mu)_2 = c^2$$

This is the generalized Prandtl relation.

REFERENCES

[1] Coburn, N., *Discontinuities in Compressible Fluid Flow*, Math. Mag., Vol. 27, No. 5, May-June, 1954.

[2] Coburn, N., *Vector and Tensor Analysis*, pp. 270–280; Macmillan Company, New York, 1955.

Further Comments on Diffuser Instability

W. C. Randels

Missiles Systems Division, Lockheed Aircraft Corp., Sunnyvale, Calif.

December 3, 1957

I HAVE FOLLOWED, with much pleasure, the spirited polemics of Dailey[1] and Trimpi[2] on the subject of diffuser "buzz."

In view of the obvious satisfaction derived by the antagonists, it seems almost cruel to point out that the whole thing can be explained by a classical theorem on compressor surge which may be found in standard textbooks[3–7] on rotating machinery.

REFERENCES

[1] Dailey, C. L., *Supersonic Diffuser Instability*, Journal of the Aeronautical Sciences, Vol. 22, No. 11, pp. 733–749, November, 1955; Vol. 24, No. 1, p. 70, January, 1957; Vol. 24, No. 11, p. 846, November, 1957.

[2] Trimpi, R. L., *Comments on "Supersonic Diffuser Instability,"* Journal of the Aeronautical Sciences, Readers' Forum, Vol. 23, No. 6, pp. 611, 612, June, 1956; Vol. 24, No. 11, pp. 845, 846, November, 1957.

[3] Kearton, W. J., *Turbo Blowers and Compressors*, p. 147; Sir Isaac Pitman & Sons, London, 1926.

[4] Stepanoff, A. J., *Centrifugal and Axial Flow Pumps*, p. 296; John Wiley & Sons, New York, 1948.

[5] Vincent, E. T., *The Theory and Design of Gas Turbines and Jet Engines*, p. 290; McGraw-Hill Book Co., Inc., New York, 1950.

[6] Sorenson, H. A., *Gas Turbines*, p. 269; Ronald Press Co., New York, 1951.

[7] Keenan, J. G., *The Elementary Theory of Gas Turbines and Jet Propulsion*, p. 75; Oxford Press, Oxford, 1946.

A Test of the Uniqueness of Solutions for Problems of Nonsteady Flow Under Given Boundary Conditions*

J. Altenhoff

Research Staff, General Motors Corp., Detroit, Mich.

November 4, 1957

THE STEADY STATE which is approached by a flow system, from given space-like initial states and under given time-like periodic boundary conditions, is generally postulated, for lack of a rigorous proof,[1] to be uniquely determined by the boundary conditions and independent of the initial state—i.e., independent of the transient processes through which it is established. Even in the absence of viscosity, when the approach to periodicity can be expected to be asymptotic, the existence of a uniquely determined final steady state, regarded in this case as a limiting state, is usually taken for granted.

These postulates stem from physical intuition and have also derived at least qualitative support from the experimental observation of the behavior of periodic-flow devices under controlled boundary conditions.

This note concerns an investigation, the results of which provide further evidence of the uniqueness of the final steady state under given boundary conditions. The object of this investigation was to determine, by the method of characteristics,[2] the final steady state or limiting state which would be approached by a particularly simple, inviscid, and isentropic flow system under given boundary conditions from various randomly chosen initial states.

The system chosen for the analysis consisted of a tube filled with and surrounded by air, open at one end and closed at the other end by a piston oscillating with simple harmonic motion

* The author wishes to thank Dr. J. V. Foa, Rensselaer Polytechnic Institute and Dr. R. Davies, Research Staff, General Motors Corp. for their guidance and assistance in preparing this note.

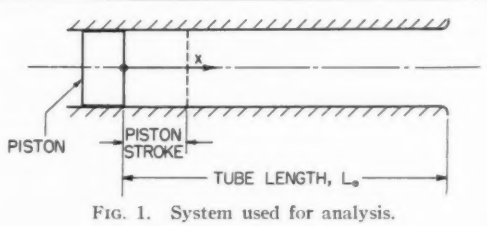

FIG. 1. System used for analysis.

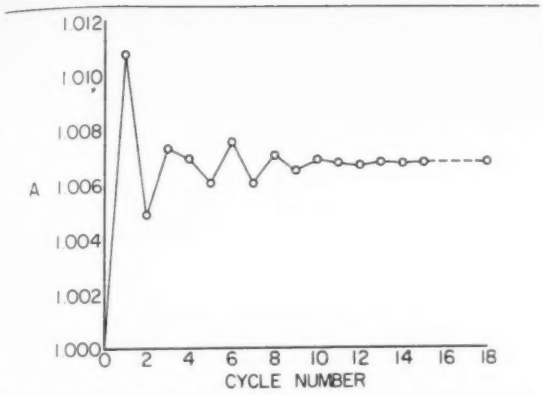

FIG. 2. Values of A at $\xi = 0.1$ at the end of each cycle (Run 1).

(Fig. 1). The piston oscillation frequency, the ratio of piston stroke to tube length, and the temperature of the air in the tube were so chosen as to avoid the formation of shock waves, and the tube diameter was assumed to be large enough to make it permissible to neglect boundary-layer effects. The open end of the tube was assumed to be flared so that inflow would be nearly isentropic.

In all the cases analyzed, the piston oscillation frequency was assumed to be 4000 cycles per min. and the ratio of piston stroke to tube length was assumed to be 0.25. The following initial conditions were considered:

(1) $A = 1.0$, $U = 0$ for $0 \leqq \xi \leqq 1.0$
(2) $A = 1.01$, $U = 0$ for $0 \leqq \xi \leqq 1.0$
(3) $A = 0.989$, $U = 0$ for $0 \leqq \xi \leqq 1.0$
(4) $A = 1.0$ for $0 \leqq \xi \leqq 1.0$, $U = 0.001\ (1 - \xi)$
(5) $A = 1.01$ for $0.5 < \xi \leqq 1.0$, $A = 0.989$ for $0 \leqq \xi < 0.5$, $U = 0$ for $0 \leqq \xi \leqq 1.0$
(6) Same A as (5) but $U = 0.025$ for $0 \leqq \xi \leqq 1.0$

where $\xi = x/L_0$, and A and U are the ratios of the local speed of sound and of the local particle velocity, respectively, to a reference speed of sound.

The calculations were carried out on an IBM model 704 digital computer.

The distribution of state and flow parameters along the tube was calculated at the end of each cycle, and the absence of significant changes in this distribution from one cycle to the next was interpreted in each case as indicating the establishment of the final steady state. The validity of this interpretation was verified in each case by carrying the computation further, for several cycles, to check for the possibility of a subsequent divergence of the solution (which was, however, never encountered). Table 1 gives the number of cycles required to reach the steady-state condition.

TABLE 1

Run	Cycle at Which Steady State Was Reached
1	11
2	14
3	16
4	11
5	16
6	14

One can illustrate the way in which the solution converges to the steady-state value by means of a curve as shown in Fig. 2 which is for the initial conditions of Run 1. The curve shows the value of A at the end of each cycle and represents the conditions at the location $\xi = 0.1$ along the tube. This value of ξ was selected because the variation of A was greatest at the piston end of the tube.

For the "standard" initial conditions (Run 1), the maximum difference between any two values of A at $\xi = 0.1$ was 0.01077. It was arbitrarily decided that the solution had come sufficiently close to the steady-state value when the change during one cycle was less than 2 per cent of 0.01077. This value was then used as the criterion for convergence for all runs.

The value of A along the length of the tube at the end of various numbers of cycles is shown in Figs. 3 and 4. Fig. 3 illustrates the convergence for Run 1 in which the steady-state condition was reached by the eleventh cycle. Fig. 4 shows the convergence for Run 6, the case that showed the most erratic variation in A. Although the solutions for these two sets of initial conditions differ greatly during the first few cycles, they do eventually converge to the same steady-state value. Likewise for the other cases: the first few cycles may differ considerably, but eventually the solution approaches a steady-state value that is independent of the initial conditions.

In summary, within the accuracy of these computations, the final steady state is the same for all cases considered, independent of the transient processes through which it is established.

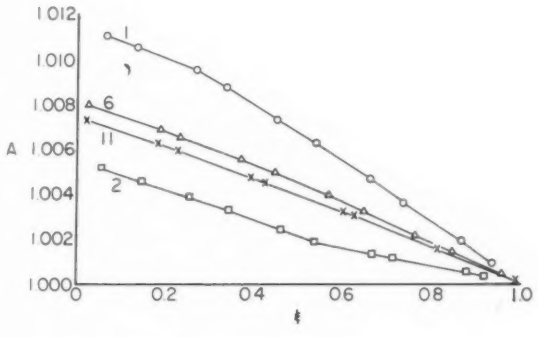

FIG. 3. Variation of A along the tube at the end of various cycles (Run 1).

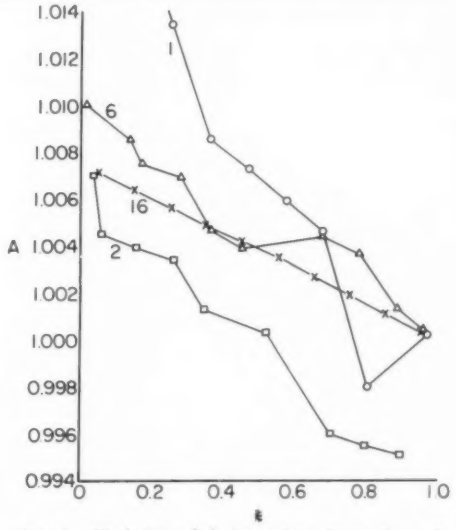

FIG. 4. Variation of A along the tube at the end of various cycles (Run 6).

REFERENCES

[1] R. Courant and K. O. Friedrichs, *Supersonic Flow and Shock Waves*, p. 367; Interscience Publishers, Inc., New York, 1948.

[2] G. Rudinger, *Wave Diagrams for Nonsteady Flow in Ducts;* D. Van Nostrand Company, New York, 1955.

Inelastic Combined Thermal and Applied Stresses in Skin-Stringer Aircraft Structure

B. E. Gatewood

Research Professor, Air Force Institute of Technology, Wright-Patterson AFB, Ohio

November 6, 1957

In CHAPTER 7 of reference 1, procedures involving strain equations and trial-and-error calculations are used to determine inelastic thermal stresses. If the stress-strain curves are represented by approximate equations, it is possible to obtain the inelastic thermal stresses directly from charts, and the procedures for combined applied and thermal stresses can be considerably simplified.

Consider a skin-stringer element in which the skin of area A_s is at the uniform temperature T_s above datum and the stringer of area A_s is at uniform temperature T_b above datum. From Eq. (3-1) of reference 1, the thermal stresses in the skin and stringer are (the skin and stringer restrain each other and there is no bowing or buckling)

$$\left.\begin{aligned} f_s &= -\{E_s(\alpha_s T_s - \alpha_b T_b)/[1 + (A_s E_s/A_b E_b)]\} \\ f_b &= -(A_s/A_b) f_s \end{aligned}\right\} \qquad (1)$$

where α is coefficient of thermal expansion, E is secant modulus, and f is thermal stress.

An approximate equation for the stress-strain curves for various materials is the Ramberg-Osgood equation (see section 6–3 of reference 1 for discussion that $n = 10$ gives a good approximation at various temperatures for various materials)

$$(eE/F_{cy}) = (f/F_{cy})\,[1 + (3/7)\,(f/F_{cy})^{n-1}] \qquad (2)$$

where F_{cy} is the compressive yield stress and E is the elastic modulus. Assume that the stress-strain curve in tension has the same shape as in compression and take the value of n for the skin and stringer stress-strain curves to be the same. Then by using the secant modulus from Eq. (2), Eq. (1) becomes

$$\left.\begin{aligned} (f_s/F_{cys})_{e1} &= (f_s/F_{cys})\,[1 + C_1(f_s/F_{cys})^{n-1}] \\ (f_s/F_{cys})_{e1} &= -\{E_s(\alpha_s T_s - \alpha_b T_b)/ \\ &\qquad F_{cys}[1 + (A_s E_s/A_b E_b)]\} \\ C_1 &= (3/7)\,[1 + (E_s/E_b)\,(A_s/A_b)^n\,(F_{cys}/F_{tyb})^{n-1}]/ \\ &\qquad [1 + (A_s E_s/A_b E_b)] \end{aligned}\right\} \qquad (3)$$

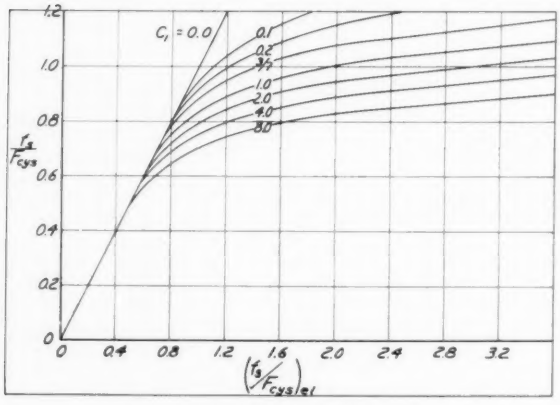

FIG. 1. Inelastic thermal stresses.

where E is the elastic modulus and the skin is taken as the compression member.

For given values of C_1 in Eq. (3) the skin stress f_s/F_{cys} can be graphed against the elastic skin stress $(f_s/F_{cys})_{e1}$. Fig. 1 shows the curves for the case of $n = 10$. If C_1 is larger than values given, the roles of the skin and stringer can be reversed to give a smaller C_1.

Note that the stress-strain curve in Eq. (2) is represented in Fig. 1 by $C_1 = 3/7$ with $(f/F_{cy})_{e1} = eE/F_{cy}$. If during the application of the temperatures $(f_s)_{e1}$ should decrease, then because most materials unload elastically the unloading curves on Fig. 1 will be parallel to the $C_1 = 0$ curve.

For the case in which the skin-stringer element is subjected to a tension or compression force Q, Eq. (1) becomes

$$\left.\begin{aligned} f_s &= [-E_s(\alpha_s T_s - \alpha_b T_b) + (E_s/E_b)\,(Q/A_b)] \div \\ &\qquad [1 + (A_s E_s/A_b E_b)] \\ f_b &= (Q/A_b) - (A_s/A_b) f_s \end{aligned}\right\} \qquad (4)$$

By using Eq. (2) the inelastic stresses for Eq. (4) can be written in the form

$$\left.\begin{aligned} \frac{f_s}{F_{cys}} &= \frac{-E_s(\alpha_s T_s - \alpha_b T_b) + B_1(E_s/E_b)\,(Q/A_b)}{F_{cys}\,[1 + (A_s E_s/A_b E_b)]\,[1 + C_1(f_s/F_{cys})^{n_s-1}]} \\ f_b/F_{tyb} &= (Q/A_b F_{tyb}) - (A_s/A_b)\,(F_{cys}/F_{tyb})\,(f_s/F_{cys}) \\ B_1 &= 1 + (3/7)\,(f_b/F_{tyb})^{n_b-1} \\ C_1 &= \frac{3/7}{1 + (A_s E_s/A_b E_b)} \times \left[1 + \frac{A_s E_s}{A_b E_b}\,\frac{(f_b/F_{tys})^{n_b-1}}{(f_s/F_{cys})^{n_s-1}}\right] \end{aligned}\right\} \qquad (5)$$

where n_s and n_b are the values of n for the skin and stringer, respectively.

Eq. (5) can be solved for the inelastic stresses by a successive approximation process using Fig. 1. The procedure is as follows:

(1) Calculate $(f_s/F_{cys})_{e1}$ and $(f_b/F_{tyb})_{e1}$ from Eq. (4).

(2) Calculate B_1 and C_1 from Eq. (5) using the elastic values.

(3) Calculate a corrected $(f_s/F_{cys})_{e1}$ using B_1 but taking $C_1 = 0$ in Eq. (5).

(4) Use this corrected $(f_s/F_{cys})_{e1}$ and the calculated C_1 to read the inelastic f_s/F_{cys} on Fig. 1. This assumes that $n_s = 10$. For a different n_s, curves similar to Fig. 1 can be constructed from Eq. (3).

(5) With this value of f_s/F_{cys} calculate f_b/F_{tyb} from Eq. (5).

(6) Use these inelastic stresses to calculate a new B_1 and C_1.

(7) Repeat steps 3, 4, and 5.

(8) Repeat the process until the stresses repeat within the desired accuracy.

Note that this process can be used for thermal stresses alone when $n_s \neq n_b$ by taking $B_1 = 0$. Note also that if unloading occurs during the temperature and applied load cycles, $B_1 = 1$ for the stringer unloading and $C_1 = 0$ for the skin unloading.

REFERENCES

[1] Gatewood, B. E., *Thermal Stresses;* McGraw-Hill Book Company, Inc., New York, 1957.

A Special Case of Swirling Viscous Flow

Dennis G. Mabey

Royal Aircraft Establishment, Bedford, England

November 7, 1957

SYMBOLS

r, θ, ϕ	= spherical polar co-ordinates
U, V, W	= velocities in r, θ, ϕ directions
μ	= $\cos\theta$
ν	= kinematic viscosity
R	= characteristic Reynolds Number = $U_a r_a/\nu$ = constant

Subscript

a	= magnitude on jet axis

The prime indicates derivatives with respect to μ.

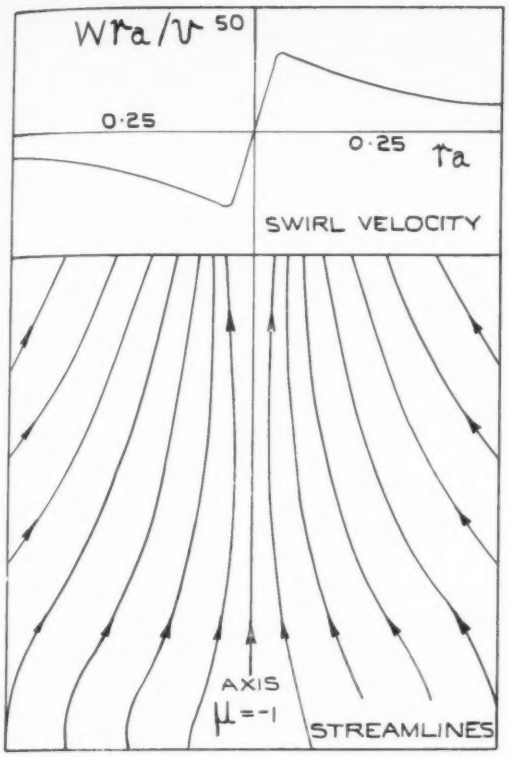

FIG. 1. Type 1 solution, $R = 2.10^3$.

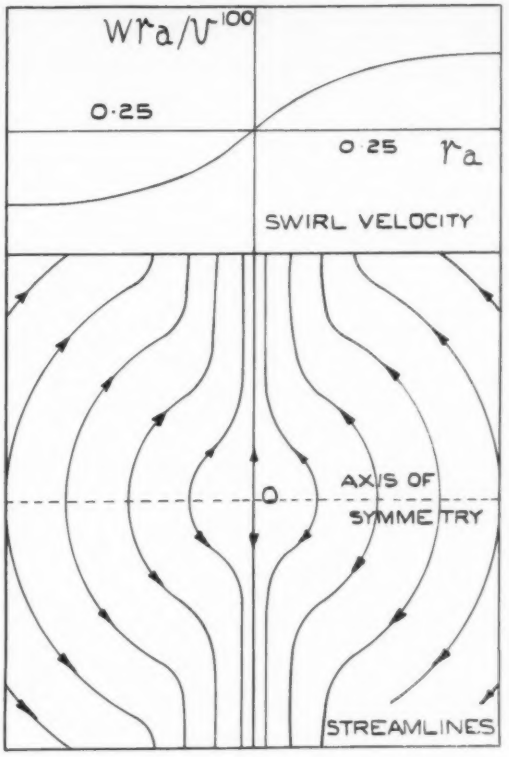

FIG. 2. Type 2 solution, $R = 2.10^3$.

THEORY

AN EXACT SOLUTION has been found to the equations of incompressible viscous flow for axially symmetric motion with swirl.[1] The swirl velocity W is of the form

$$W = -\nu f(\mu)/r(1 - \mu^2)^{1/2} \tag{1}$$

and the stream function is $\psi = \nu r f(\mu)$ as in the earlier solutions without swirl.[2,3,4]

The three equations of motion (reference 5, Eq. 45) then give

$$ff' = (1 - \mu^2)f''' \tag{2}$$

Prof. H. B. Squire remarked to the author that W may be generalized in the form $W = -\nu h(\mu)/r(1 - \mu^2)^{1/2}$. The equations of motion then give

$$fh' = (1 - \mu^2)h''$$

$$2[(1 - \mu^2)f''' - hh'] = (1 - \mu^2)[ff' - (1 - \mu^2)f''']'$$

The simple case considered in Eq. (2) when $h(\mu) \equiv f(\mu)$ corresponds to $W = V$.

It can be shown from the variation of the pitot pressure that Eq. (2) can only describe flows away from the origin, for which $f' \leq 0$. No wall boundary condition ($U = V = W = 0$) can be applied, except in the trivial case when the fluid is quiescent,[6,7] since the solution represents a jet mixing process. The relevant boundary condition is the characteristic Reynolds Number of the jet R, and, to illustrate the two types of solution, the appropriate boundary-layer solutions are now given.

TYPES OF SOLUTION

Formally the Type 1 solution represents a source vortex along the $\mu = 1$ axis and a force applied at the origin (as discussed in reference 2). The boundary conditions are:

$$f(-1) = 0, \quad f'(-1) = (ur/\nu)_{-1} = -R$$

When $R \gg 1$, then f tends to a limit when $\mu \doteq -1$. The boundary-layer solution is

$$f = -4R(1 + \mu)/[4 + R(1 + \mu)]$$

and the potential flow solution is $f = -4$, which gives circular streamlines in the inflow.

The Type 2 solution represents a radial jet in the plane $\mu = 0$ combined with a pair of source-vortices along the $\mu = \pm 1$ axes. The boundary conditions are:

$$f(0) = 0, \quad f'(0) = (ur/\nu)_0 = -R$$

When $R \gg 1$, then f tends to a limit when $\mu \ll 1$. The boundary-layer solution is

$$f = -(2R)^{1/2} \tanh [(R/2)^{1/2}\, \mu]$$

Both types of solution can be obtained numerically for $R > 0$ without making the boundary-layer approximations. (Note that for an air jet with a speed of 300 ft./sec., 1 ft. from the orifice, $R = 2.10^6$.)

TYPES OF FLOW

The Type 1 and Type 2 solutions are radically different. The Type 1 solution represents a small jet along the $\mu = -1$ axis with swirl in the inflow about the jet axis. Fig. 1 shows the streamlines of the motion for $R = 2.10^3$. The angular width of a jet may be specified as the angle θ between the half-velocity cone $\mu = \mu_1$, on which $U(\mu_1)r_a/\nu = 0.5U_a r_a/\nu$, and the jet axis. For the Type 1 solution $\theta_1 = 1.82/(R)^{1/2}$. Along a line $r\mu = r_a$ normal to the jet axis, the maximum swirl velocity is $0.71\nu(R)^{1/2} \div r_a$ (see Fig. 1).

The Type 2 solution represents a radial jet in the plane $\mu = 0$ with swirl (about the axes $\mu = \pm 1$) which is equal and opposite on both sides of the jet. Fig. 2 shows the streamlines of the motion for $R = 2.10^3$. For the Type 2 solution the half-velocity cone is $\theta_1 = 1.25/(R)^{1/2}$. Along a line $r(1 - \mu^2)^{1/2} = r_a$ normal to the jet axis, the swirl velocity attains a constant value of $\nu(2R)^{1/2}/r_a$ (see Fig. 2).

The streamlines close to the jet axis diverge for the Type 1 solution and are parallel for the Type 2 solution as shown in Figs. 1 and 2.

References

[1] Mabey, D. G., M.Sc. Thesis, University of London, 1955.

[2] Squire, H. B., *The Round Laminar Jet*, Quart. Journ. Mech. and Appl. Math., Vol. IV, Part 3, p. 321, September, 1951.

[3] Squire, H. B., *Some Viscous Flow Problems: (I) Jet emerging from a hole in a plane wall*, Phil. Mag. Ser. 7, Vol. 43 (1952) p. 942.

[4] Görtler and Tollmien, (Ed.), *50 Jahre Grenzschichtforschung*, Squire, H. B., "Radial Jets," pp. 47–54; Braunschweig, 1955.

[5] Howarth, L., (Ed.), *Modern Developments in Fluid Dynamics*, Vol. I "Oxford Engineering Science Series," Oxford University Press, Oxford; p. 104, 1953.

[6] Morgan, A., *On a Class of Laminar Viscous Flows Within One or Two Boundary Cones*, Aero. Quart., p. 225, July, 1956.

[7] Beran, M., *A Note on Laminar Axially Symmetric Jets*, Quart. Appl. Maths., p. 213, July, 1956.

Subsonic Lift Response to Penetration of a Sharp-Edged Gust Moving at Supersonic Speed*

E. Krasnoff

Staff Engineer, Allied Research Associates, Inc., Boston, Mass.

November 20, 1957

Introduction

Interest in the problem of the penetration (by a wing) of a moving sharp-edged gust has recently been stimulated because of its application to the blast wave penetration problem. The relation of a moving sharp-edged gust to a blast wave is discussed in reference 1 which includes calculations of lift response functions for the following cases: airfoils in both incompressible and supersonic flow; wide delta and rectangular wings in supersonic flow; and very narrow delta wings in both compressible and incompressible flow. However, the only lift response functions that have been calculated for subsonic, compressible, two-dimensional flow are those associated with a sudden change in airfoil angle of attack (infinite gust front velocity). Results of these calculations are included in references 2 through 6.

* The author wishes to express his appreciation to the Aircraft Laboratory, Wright Air Development Center, USAF, for permission to publish this note.

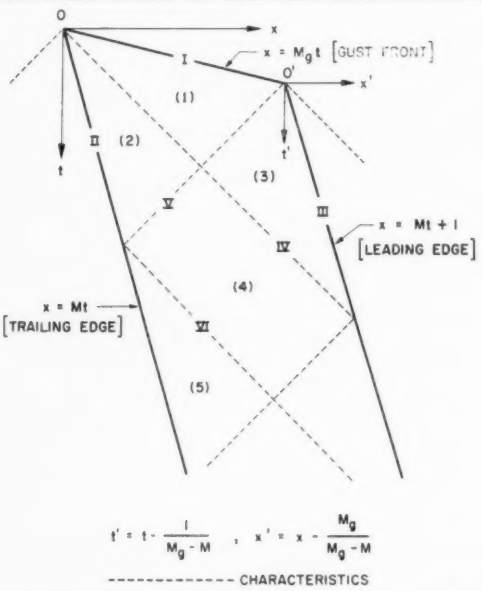

Fig. 1. Representation of the airfoil-gust penetration problem in the x, t plane.

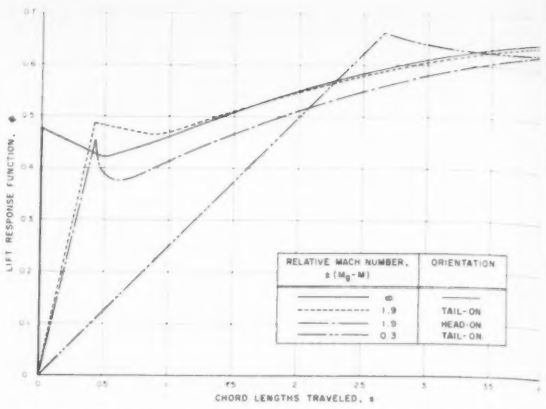

Fig. 2. Typical lift response functions for an airfoil Mach Number of 0.8.

The purpose of this note is to present lift response functions for an airfoil moving at subsonic speed corresponding to penetration of a sharp-edged gust moving at finite supersonic speed. Linearized airfoil theory is employed and calculations are carried out for periods of time somewhat exceeding the time required for the airfoil to be completely immersed in the uniform gust field. Both head-on and tail-on (gust front overtaking the airfoil) orientations are considered and the general results are specialized to the case of infinite gust front velocity.

Discussion

The representation of an airfoil moving at subsonic speed being overtaken from the rear by a sharp-edged gust moving at supersonic speed is depicted in the x, t plane (plane of the airfoil) shown in Fig. 1. Here the space dimension, X, has been nondimensionalized by the chord of the airfoil, c, and the time, T, by a_0/c, where a_0 is the sound speed in the homentropic flow field. That is, $X/c = x$ and $a_0T/c = t$. M and M_g are the Mach Numbers of the airfoil and gust front respectively, taken positive in the positive x direction.

Calculation of the Lift Response Functions

It is well-known (see, e.g., reference 7) that the boundary value problem posed by compressible nonstationary airfoil theory is analogous to that of supersonic finite wing theory, the governing partial differential equation in each case being the wave equation. Thus the techniques of supersonic wing theory (in particular those of references 8 and 9) were employed to compute the pressure coefficients in the five regions indicated in Fig. 1. The lift coefficient was then obtained as a function of time by integrating the pressure coefficients over the chord of the airfoil. All computations are discussed in some detail in reference 7.

The following notation is introduced:

$$\phi = C_L/C_L(\infty), \quad \delta_1 = 2|M_g| \sqrt{1 - M^2}/\pi M \sqrt{M_g^2 - 1} \quad (1)$$

where $C_L(\infty) = 2\pi\alpha_g/\sqrt{1 - M^2}$, the steady-state value of the lift coefficient, C_L, attained as t approaches infinity. The results are presented below.

For the tail-on case

$$0 \leq t \leq 1/(M_g - M): \quad \phi = \delta_1 t \sqrt{(M_g - 1)(M_g - M)} \quad (2)$$

and, during the analogous time interval for the head-on case ($M_g < -1$),

$$0 \leq t' \leq -1/(M_g - M): \quad \phi = \delta_1 t' (M_g - M) \sqrt{(M_g + 1)(M_g - M)}/M_g \quad (3)$$

The lift response functions during the remaining time intervals for which computations have been performed are presented below. The upper (lower) sign refers to the tail-on (head-on) orientation. In specifying the time interval, the upper (lower) symbol refers to the tail-on (head-on) orientation

$$\pm\frac{1}{M_v - M} \leq \begin{Bmatrix} t \\ t' \end{Bmatrix} \leq \frac{M_v + 1}{(1 + M)(M_v - M)},$$

$$0 \leq \begin{Bmatrix} t' \\ t \end{Bmatrix} \leq \frac{1}{1 + M}: \phi = \delta_1 \left\{ 1 + t'(M_v - M) \times \left[1 \mp \frac{\sqrt{(M_v - M)(M_v + 1)}}{M_v} \right] + t\left[M - M_v \pm \sqrt{(M_v - M)(M_v - 1)} \right] \right\} \quad (4)$$

$$\frac{M_v + 1}{(1 + M)(M_v - M)} \leq \begin{Bmatrix} t \\ t' \end{Bmatrix} \leq \frac{1}{1 - M},$$

$$\frac{1}{1 + M} \leq \begin{Bmatrix} t' \\ t \end{Bmatrix} \leq \frac{M_v - 1}{(1 - M)(M_v - M)}:$$

$$\phi = \delta_1 \left\{ 1 + \frac{K}{\pi}\sqrt{t'^2 - (Mt' - 1)^2} - t\left[(M_v - M) \mp \sqrt{(M_v - M)(M_v - 1)}\right] + t'(M_v - M) \times \left(1 - K\frac{1 + M}{M}\right) + \frac{Kt'}{\pi M}(M_v - M)(1 + M)\cos^{-1}\frac{1 - Mt'}{t'} + \frac{K}{\pi\sqrt{1 - M^2}}\left[1 - \frac{M_v}{M}\frac{1 - M^2}{M_v - M} - (1 - M^2)t'\right] \times \cosh^{-1}\left[(1 - M^2)t' + M\right] \mp \frac{K}{\pi}\frac{M_v}{M}\frac{1 + M}{M_v - M}\sqrt{\frac{M_v - 1}{M_v + 1}} \times \left[(M_v - M)t' + 1\right]\cos^{-1}\left[\frac{M_v(1 - Mt') + t'}{(M_v - M)t' + 1}\right] \right\} \quad (5)$$

where $K = M\sqrt{(M_v - M)(M_v + 1)}/|M_v|(1 + M)$ (6)

Indicial Lift Response Functions

The lift response functions corresponding to a sudden change in angle of attack (infinite gust front velocity) can be obtained from Eqs. (1) through (6) by performing a limiting process in a straightforward manner. In view of Eq. (2) or (3), the first time interval shrinks to zero and the lift instantly becomes

$$\phi = \delta_1 \quad (7)$$

where now

$$\delta_1 = 2\sqrt{1 - M^2}/\pi M \quad (8)$$

[see Eq. (1)]. From Eqs. (4), (5), and (6) there results

$$0 \leq t \leq [1/(1 + M)]: \quad \phi = \delta_1[1 - (1 - M)t] \quad (9)$$

$$\frac{1}{1 + M} \leq t \leq \frac{1}{1 - M}: \quad \phi = \delta_1 \left\{ 1 + \frac{1 + 2M}{\pi(1 + M)} \times \sqrt{t^2 - (Mt - 1)^2} - (1 - M)t + \frac{M}{\pi(1 + M)\sqrt{1 - M^2}} \times \left[1 - \frac{1 - M^2}{M} - (1 - M^2)t \right] \cosh^{-1}\left[(1 - M^2)t + M\right] + \frac{(1 - M)t - 1}{\pi}\cos^{-1}\frac{1 - Mt}{t} \right\} \quad (10)$$

Numerical Results

Representative numerical results are presented in Fig. 2 for an airfoil Mach Number of 0.8 and a wide range of gust front velocities. The abscissa is specified in terms of chord lengths traveled, s, which is determined from the time by

$$s = Mt = UT/c \quad (11)$$

A complete set of numerical results is presented in reference 7 for an airfoil Mach Number range from 0.5 to 0.9. Reference 7 also includes a discussion of methods of approximating the lift response functions for large values of time. These methods are based on the premise that the asymptotic behavior of the indicial lift response function in compressible flow is the same as that in incompressible flow. The validity of this premise is discussed in reference 2 where it is also shown that the distribution of pressure over the airfoil chord attains the steady-state distribution after only several chord lengths traveled for the case of infinite gust front velocity.

References

[1] Drischler, J. A., and Diederick, F. W., *Lift and Moment Responses to Penetration of Sharp-Edged Traveling Gusts, with Application to Penetration of Weak Blast Waves*, NACA TN 3956, May, 1957.

[2] Lomax, H., et al, *Two- and Three-Dimensional Unsteady Lift Problems in High Speed Flight*, NACA Report 1077, 1952.

[3] Drischler, J. A., *Calculation and Compilation of the Unsteady Lift Functions for a Rigid Wing Subjected to Sinusoidal Gusts and Sinusoidal Sinking Oscillations*, NACA TN 3748, October, 1956.

[4] Mazelsky, B., and Drischler, J. A., *Numerical Determination of Indicial Lift and Moment Functions for a Two-Dimensional Sinking and Pitching Airfoil at Mach Numbers 0.5 and 0.6*, NACA TN 2739, July, 1952.

[5] Mazelsky, B., *Numerical Determination of the Indicial Lift of a Two-Dimensional Sinking Airfoil at Subsonic Mach Numbers from Oscillatory Lift Coefficients with Calculations for Mach Number 0.7*, NACA TN 2563, 1951.

[6] Laitone, E. V., *Non-Steady Motion of an Airfoil by Indicial Response Method*, Hughes Aircraft Company, Report No. B-A-1-1, December 17, 1952. (Confidential, title unclassified.)

[7] Smiley, R., and Krasnoff, E., WADC TR 57-594. To be published.

[8] Evvard, J. C., *Use of Source Distributions for Evaluating Theoretical Aerodynamics of Thin Finite Wings at Supersonic Speeds*, NACA Report 951, 1950.

[9] Goodman, T. R., *The Lift Distribution on Conical and Nonconical Flow Regions of Thin Finite Wings in a Supersonic Stream*, Journal of the Aeronautical Sciences, Vol. 16, No. 6, pp. 365–374, June, 1949.

A Remark on the Optimum Design of Round Tubing

William L. Poesch

Graduate Student, College of Engineering, University of California, Los Angeles, Calif.

December 2, 1957

THIS NOTE presents experimental verification of a previously published theory on the optimum design of round tubular columns in axial compression.[1]

This investigation was directed toward the analytical determination of the optimum diameter/thickness ratio of a pin-ended tubular column using an experimentally obtained optimum structural index. This ratio was compared with the actual ratio of

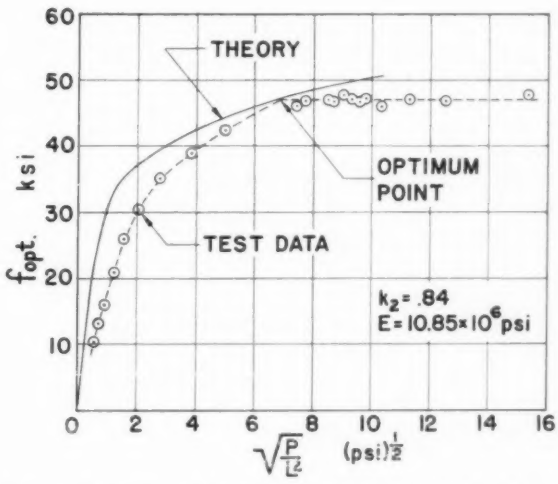

FIG. 1. Optimum (maximum) stress for round tubular column of 2024-T3 aluminum.

diameter and thickness of the specimens to obtain a measure of the accuracy of the theory.

Twenty-one test specimens with lengths varying from 4.0 to 89.0 inches were utilized in the tests. The material, 2024-T3 aluminum alloy, and a D/t ratio of 70.5 were used throughout the experiment.

For convenience, two relations from reference 1 are shown below:

$$(D/t)_{\text{optimum}} = 2[k_2^2 E/\pi(P/L^2)]^{1/3} \quad (1)$$

$$P/L^2 = 8f^3_{\text{optimum}}/k_2\pi E_t^{3/2}E^{1/2} \quad (2)$$

Eq. (1) gives the optimum cross section for a given material and structural index. Eq. (2) was used to plot the optimum stress versus structural index curve shown in Fig. 1. Note that to plot this curve, it is only necessary to have the material properties. These were obtained from compression tests on the column material.

After data on the buckling or crippling load had been obtained for each column, it was possible to plot the test data as shown in Fig. 1. As the length was varied, the test points approached the optimum curve and then broke away again. The optimum point was obtained as $(P/L^2)^{1/2} = 6.9$.

Substituting the experimentally obtained optimum structural index into Eq. (1), an optimum D/t ratio of 74.2 was obtained. An error of 5.25 per cent resulted when this value was compared with the actual D/t ratio of the specimens. A value of 0.84 was used for k_2 in Eqs. (1) and (2), on the basis of experimental data previously obtained at the University of California at Los Angeles, Calif.[2]

References

[1] Shanley, F. R., *Principles of Structural Design for Minimum Weight*, Journal of the Aeronautical Sciences, Vol. 16, No. 3, pp. 133–149, March, 1949.

[2] Needham, R. A., *Compression Tests of Round Tubes*, Memorandum Report to F. R. Shanley, Univ. of California, College of Engineering, Los Angeles, Calif., July 18, 1954.

On Optimum Nose Shapes for Missiles in the Superaerodynamic Region

David H. Dennis
Aeronautical Research Scientist, Ames Aeronautical Laboratory, NACA, Moffett Field, Calif.

November 27, 1957

W. J. CARTER[1] and I. D. Chang[2] have calculated the shape of the body of revolution of given length and base diameter, having minimum drag in hypervelocity free-molecule flow, assuming specular reflection from a smooth surface. With this assumption, the expression defining surface pressure coefficient is the same as that for Newtonian flow except for a constant factor of 2. Accordingly, the minimum drag body should have the same shape, including a small flat nose, as that derived by Newton.[3] The parametric equations defining this shape are

$$y = (y_1/4)\,[(1 + y'^2)^2/y'^3]$$

$$x = (y_1/4)\,[(3/4y') + (1/y'^2) - (7/4) + \ln y']$$

where y_1 is the nose radius.[4]

The flat nose results from the restriction on body length. If the length is not fixed, the minimum drag shapes have sharp noses. For example, the cone is the minimum drag shape of given surface area and base diameter.[4]

As a final point it may be noted that since the local drag on a body in the flows considered here depends only on local slopes and body radii, the first integral to the Euler equation may be written immediately and the body coordinates in terms of body slopes are easily deduced.

References

[1] Carter, W. J., *Optimum Nose Shapes for Missiles in the Superaerodynamic Region*, Journal of the Aeronautical Sciences, Vol. 24, No. 7, pp. 527–532, July, 1957.

[2] Chang, I. D., *On Optimum Nose Shapes for Missiles in the Superaerodynamic Region*, Journal of the Aeronautical Sciences, Readers' Forum, Vol. 25, No. 1, pp. 57, 58, January, 1958.

[3] Newton, Isaac, *Principia-Motte's Translation Revised*, pp. 333, 657–661; Univ. of California Press, Berkeley, 1946.

[4] Eggers, A. J., Jr., Resnikoff, Meyer M., and Dennis, David H., *Bodies of Revolution Having Minimum Drag at High Supersonic Airspeeds*, NACA Report 1306, 1957 (Supersedes NACA TN 3666).

Structural and Impact Loads for the Flexible Airplane . .

(Continued from page 170)

airplane was obtained from experimental measurements over a range of impact conditions. From these measurements the hydrodynamic force and moment on the airplane were obtained. The most critical parameter in measuring the effects of landing impact was found to be the rate of vertical descent.

A comparison of the experimental impact data with the results of the analysis showed that the analytical results generally were in good agreement with the experimental results. This agreement includes both time variation and magnitude. It is concluded that the hydrodynamic step impact and the dynamic response of the flexible seaplane may be accurately given by the method of analysis presented in this paper.

The response of the flexible airplane was found to be a function of both the magnitude and shape of the forcing function. The maximum inertial loading for some structures was not obtained for the conditions of maximum hydrodynamic loading. In order to obtain the maximum loads for the flexible airplane it was necessary to study a range of landing impacts.

The inclusion of airplane flexibility in the equations of motion tended to reduce the hydrodynamic force obtained for the rigid airplane. In this instance the maximum reduction was of the order of 7 per cent. However, for a more flexible airplane this reduction may be of a large magnitude.

References

[1] Schwab, R. H., and Widmayer, E., Jr., *Martin Model 270 Water Loads Investigation—Structural and Impact Loads Considering Airplane Flexibility*, Martin ER 7515, November, 1955.

[2] King, Douglas A., and Adams, Richard C., *Martin Model 270 Water Loads Investigation: Hull Bottom Pressures and Impact Loads*, Martin ER 7516, July, 1955.

[3] Biot, M. A., and Bisplinghoff, R. L., *Dynamic Loads on Airplane Structures During Landing*, NACA ARR 4H10 (WR-W-92), October, 1944.

[4] Mayo, W. L., *Hydrodynamic Impact of a System with a Single Elastic Mode—I Theory and Generalized Solution with an Application to an Elastic Airframe*, NACA Report 1074, 1952.

[5] Milwitzky, Benjamin, *Generalized Theory for Seaplane Impact*, NACA Report 1103, 1952.

[6] Benscoter, Stanley V., *Effect of Partial Wing Lift in Seaplane Landing Impact*, NACA TN 1563, 1948.